Development of Novel Technologies for Improved Natural Illumination of High Rise Office Buildings

Phillip John Greenup

Centre for Medical, Health and Environmental Physics
School of Physical and Chemical Sciences
Queensland University of Technology

KEYWORDS

Daylighting, Non-imaging Optics, Micro-Light Guiding Shade Panel, RADIANCE, Lighting Simulation, Sub-tropical Climate, High Rise Office Buildings

ABSTRACT

Effective daylighting can substantially reduce the energy use and greenhouse gas emissions of commercial buildings. Daylight is also healthy for building occupants, and contributes to occupant satisfaction. When productivity improvements are considered, effective daylighting is also highly attractive financially. However, successful daylighting of sub-tropical buildings is a very difficult task, due to high direct irradiances and excessive solar shading. A device was created that combined effective solar shading and efficient daylight redirection.

The micro-light guiding shade panel achieves all objectives of an optimal daylighting device placed on the façade of a sub-tropical, high rise office building. Its design is based on the principles of non-imaging optics. This provides highly efficient designs offering control over delivered illumination, within the constraints of the second law of thermodynamics. Micro-light guiding shade panels were constructed and installed on a test building. The tested devices delivered daylight deep into the building under all conditions. Some glare was experienced with a poorly chosen translucent material. Glare was eliminated by replacing this material. Construction of the panels could be improved by application of mass-manufacturing techniques including metal pressing.

For the micro-light guiding shade panel to be utilised to its full potential, building designers must understand its impact on building performance early in the design process. Thus, the device must be modelled with lighting simulation software currently in use by building design firms. The device was successfully modelled by the RADIANCE lighting simulator. RADIANCE predictions compared well with measurements, providing bias generally less than 10%. Simulations greatly aided further development of the micro-light guiding shade panel. Several new RADIANCE algorithms were developed to improve daylight simulation in general.

TABLE OF CONTENTS

Chapter 3 - The Micro-Light Guiding Shade Panel

Chapter 4 - Initial Investigations

Chapter 7 - RADIANCE Algorithms for Improved Daylight Simulation

Chapter 8 - Discussion and Conclusion

Appendices

Bibliography

LIST OF FIGURES

LIST OF TABLES

NOMENCLATURE

Abbreviations

ADELINE	Advanced Daylighting and Electric Lighting Integrated New Environment
CCD	Charge Coupled Device
CEC	Compound Elliptical Concentrator
CHC	Compound Hyperbolic Concentrator
CIE	International Commission on Illumination
CPC	Compound Parabolic Concentrator
DLS	Dynamic Lighting System
HOE	Holographic Optical Element
IEA	International Energy Agency
LCM	Light Channel Module
LCP	Laser Cut Panel
LGS	Light Guiding Shade
RMS	Root Mean Square
SSLD	Standard Sky Luminance Distribution

Mathematical Symbols

a, a'	Aperture widths (m)
amb_r, amb_g, amb_b	Red, green and blue diffuse reflectance components (-)
A, A'	Concentrator aperture widths (m)
A1, A2, A3, A4	RADIANCE user input variables (-)
BRDF	Bi-directional reflectance distribution function (sr^{-1})
BTDF	Bi-directional transmission distribution function (sr^{-1})
C	Concentration factor (-); photopic average of RADIANCE input parameters A1, A2, A3
d	Distance from collector centre to edge of parabolic mirror (m); mkillum controlling parameter
dx, dy, dx', dy'	Infinitesimal lengths (m)
dx1, dy1, dz1, dx2, dy2, dz2	Direction cosines of redirected light rays
dL, dM, dL', dM'	Infinitesimal increments in direction cosines (-)
$d\omega_i$	Solid angular size of incident light source (sr)
dd	Spread specular reflection component (-)
D	Distribution factor (-)
D/W	Cut-spacing to cut-depth ratio (-)

E_1	Illuminance incident upon sample in BTDF assessment (lx)
E_2	Luminous exitance from sample in BTDF assessment (lm/m^2)
f	Lens focal length (m); degree of truncation (-)
fd, fu	Fractions deflected and undeflected (-)
g	Apparent roughness function (-)
G	Geometrical factor (-)
HGI	Horizontal global illuminance (lx)
K	RADIANCE luminous efficacy (lm/W)
m, n	Gensurf input parameters (-)
n, n'	Refractive indices (-)
n_real	Real component of refractive index (-)
L, M	Direction cosines (-)
L_2	Luminance in transmitted direction in BTDF assessment (cd/m^2)
R	Fresnel reflectivity (-)
R_g	Ground brightness ($Wm^{-2}sr^{-1}$)
s	Specular reflection component (-)
S	Shadow function (-)
w	Thickness of micro-light guiding shade panel (m)
β	Tilt from vertical of micro-light guiding shade panel (°)
Δ	Delta function 0 outside, 1 inside (-)
ϕ	Angle subtended by half the parabolic mirror at the collector centre (°)
γ	Lower limit of micro-light guiding shade panel's output angular range (°)
θ	Upper limit of micro-light guiding shade panel's output angular range (°)
θ_I	Angle of incidence (°)
θ_r	Angle of reflection (°)
(θ_1, ϕ_1)	Direction of incident illumination in BTDF assessment (°)
(θ_2, ϕ_2)	Direction of transmitted illumination in BTDF assessment (°)
λ	Wavelength of light (nm)
ρ	Ground reflectance (-)

ρ_{bd}	Bi-directional reflectance distribution function (sr^{-1})
$\rho_{bd,sp}$	Specular component of bi-directional reflectance distribution function (sr^{-1})
$\rho_{bd,ss}$	Spread specular component of bi-directional reflectance distribution function (sr^{-1})
$\rho_{bd,ud}$	Uniform diffuse component of bi-directional reflectance distribution function (sr^{-1})
ρ_d	Diffuse reflectance (-)
ρ_s	Specular reflectivity (-)
σ_0	Standard deviation in surface height (μm)
τ	Autocorrelation length (μm)

STATEMENT OF ORIGINAL AUTHORSHIP

The work contained in this thesis has not been previously submitted for a degree or diploma at any other higher education institution. To the best of my knowledge and belief, the thesis contains no material previously published or written by another person except where due reference is made.

Signed:

Date:

ACKNOWLEDGMENTS

This work was completed in the Centre for Medical, Health and Environmental Physics at the Queensland University of Technology. I am greatly indebted to the staff and students of the centre and the university, for the provision of resources, time, effort, funding, and friendship. Elizabeth Stein and Brian Thomas are thanked for answering my many questions and helping me find my way through the university system.

Some of the work was completed in collaboration with the International Energy Agency Task 31 - Daylighting Buildings in the 21st Century, and the CIE Technical Committee 3.33 - Test Cases for Assessment of Accuracy of Interior Lighting Computer Programs. My communications with these groups were always informative, insightful and enjoyable. I enjoyed discussing the intricacies of RADIANCE with John Mardaljevic, Christoph Reinhart and Haico Schepers. Laser cut panel simulations were performed with Michael Laar, and validations were performed with Marilyne Andersen. The all sky model was developed with Yasuko Koga. Thank you for your patience, and I hope we will publish our work together soon. Mark Luther is always great to talk with; I hope we can continue our work together in the future.

Some support was provided by the Australian Cooperative Research Centre for Renewable Energy. Thanks to Chris Lund, Michelle Bayly, Kat Lyon and John Bell for your enthusiasm, support and fun student conferences.

I am also grateful to Greg Ward, the creator of RADIANCE, and to the RADIANCE online community. Our discussions are always interesting and useful.

I also thank my examiners. I appreciate the time and effort required of you. I hope you will find it interesting, useful, and not too full of mistakes. Thanks also to anyone else who reads my thesis. I hope you enjoy the work too. It will be my great pleasure to discuss it with you.

Thanks are also due to my family and friends who supported me throughout my degree. To my mother and father who made it all possible, but were unable to see the final product, thank you and I miss you both. Nan, Pop, David, Joanne, Nathan and Emily – thanks for your love and support. I will miss you all when we move to Sydney. To Nathan and Reneé, many thanks for your understanding, and I hope your study ordeal does not last too much longer. Team Uni are a great bunch of friends, always

willing to go bowling, play netball, go camping, and put a beer in my hand. The Lerner family has always been there for me, like a second family. Thanks again, and love to you all.

My supervisors Ian Edmonds and Steve Coyne, and workmate John Mabb deserve special thanks. They have all supported me at QUT since before I began this degree. John always put up with me, sharing various rooms for years. It has been a pleasure working with John, and I wish him luck for his future. Steve is an utter professional, a very smart man, friendly, helpful and enthusiastic. Steve developed the Bland and Altman test and spreadsheets. Ian's style is unique, as is his talent and passion for daylighting and solar engineering. It has been exciting, eventful and entertaining to work with Ian for the last seven years. Ian developed the light guiding shade and applied non-imaging optics to sub-tropical daylighting design. Ian also gave me the prior appointment during which I started to learn RADIANCE.

Lastly, the greatest thanks must go to my girlfriend Jaime. She has given me everything throughout the last five years. Soon we will be away in Sydney, starting our new life. I promise I will have more time to spare, and less work for you to do for me. I love you very much, and I appreciate everything that you have done for me.

Brisbane, 3 December 2002

CHAPTER 1 - INTRODUCTION

1.1 BACKGROUND - DAYLIGHTING COMMERCIAL BUILDINGS

Before the days of easily accessible electricity, artificial lighting and air conditioning, daylight was the primary source of building lighting. High ceilings, open spaces and large windows allowed daylight and natural ventilation to penetrate deeply into buildings. Natural lighting and climate control had to be considered carefully in building design. The introduction of cheap and easily accessible electricity allowed the widespread use of artificial lighting and air conditioning. Commercial buildings grew taller and wider, with reduced floor to ceiling heights. This resulted in a large stock of buildings with low daylight access through small windows, on crowded streets, with excessive shading from other buildings. This makes for a particularly difficult daylighting problem.

1.1.1 DAYLIGHT AND ENERGY IN BUILDINGS

Australian office buildings annually consume around 40 PJ (11 million kWh) of energy, with an average energy consumption intensity of around 380 kWh/m^2/annum. The same buildings contribute annually 8.5 million tonnes of greenhouse harming carbon dioxide emissions (Australian Greenhouse Office, 1999; Productivity Commission, 1999). This rate of consumption is growing rapidly, with greenhouse gas emissions expected to almost double between 1990 and 2010 (Institution of Engineers Australia, 2001).

Lighting, ventilation and cooling dominate energy consumption in Australian office buildings. These energy uses contribute roughly 15, 16 and 18%, respectively, of Australian commercial building energy use, and 21, 22 and 24% of greenhouse gas emissions (Australian Greenhouse Office, 1999). These proportions vary greatly between buildings and climates. In many cases, lighting is the single largest user of building energy (Leslie, 1994; Littlefair, Aizlewood & Birtles, 1994; Steemers, 1994).

Greenhouse gas emissions could be greatly reduced by improving the efficiency of lighting systems (Australian Greenhouse Office, 1999). Between 20 and 40% of lighting energy use can be saved (Littlefair *et al.*, 1994; Steemers, 1994).

This is achieved by combining effective daylighting and artificial lighting controls. Savings can be as high as 70 to 90% when daylighting, efficient artificial lighting and effective lighting controls are combined (Kristensen, 1994).

Daylight provides more light for less heat than most forms of artificial lighting. Due to daylight's greater lighting efficiency, displacing artificial lighting by natural lighting also reduces internal heat loads. Thus, daylighting provides high quality lighting and reduces both lighting and cooling costs. Similarly, since peak cooling loads occur on clear, hot days when daylight is abundant, daylighting reduces cooling loads during periods of peak power demand.

The effective use of daylighting can contribute to substantial reductions in the energy use and greenhouse gas emissions of commercial buildings. These savings can be achieved by decreasing both artificial lighting and cooling loads. To attain these goals, effective daylighting designs and devices must be combined with efficient artificial lighting and effective lighting controls.

1.1.2 Effect of Daylighting on Building Occupants

Daylight has numerous physical and psychological effects on people. Effects include increased production of vitamin D3, increased calcium absorption, suppressed secretion of melatonin, effects on the growth and secretion of several endocrine organs, effects on psycho-motor performance, muscular activity, rate of breathing, pulse rate, blood pressure, mood and emotional state (Hughes, 1983). Natural light is perceived as more natural, pleasant, bright and stimulating, and provides greater levels of relaxation and visual comfort, and less fatigue. Daylight can efficiently provide high levels of illumination that, 'can contribute to good health, comfort and productivity' (Leslie, 1994: 5).

Daylight also significantly affects occupant satisfaction. Good lighting, to which daylight contributes, is one of the most important aspects of occupant comfort (Abdou, 1997; Cowling, Coyne & Bradley, 1990; Wotton & Barkow, 1983). Windows provide, 'contact with the outside, an orientation of space and ambience' (Wotton & Barkow, 1983: 405). Such an outside connection is highly desired in buildings, where offices with a view are highly sought after.

1.1.3 ECONOMICS OF DAYLIGHTING

As well as energy savings, daylighting can provide significant operating cost savings. Savings include reduced energy costs for lighting and cooling, and reduced maintenance costs for associated equipment. Effective daylighting can also significantly reduce capital outlays in the construction of new buildings. The efficient use of daylighting can reduce peak cooling loads. This, in turn, reduces the size of required ducts, air handlers, coils, filters, pipes, chillers, boilers, pumps and cooling towers (Randazzo, 1994). This allows substantial savings on capital outlays.

The greatest economic benefit of daylighting is the potential to improve worker productivity. Information received through the eye is essential to shaping moods, reactions and psychological well-being (Abdou, 1997). Natural illumination and a connection to the outside world improve occupant satisfaction and comfort, decrease stress levels, and thereby improve worker morale and motivation (Abdou, 1997; Clanton, 1996). This presents great potential to improve worker productivity. Many research programs have reported increased worker output due to improved interior environmental conditions, including increased natural lighting. Percentage productivity increases range between 5 and 20% (Abdou, 1997; Clanton, 1999; Nicklas & Bailey, 1996; Penney & Althof, 1990; Riegel, Windheim, Davy & Shanus, 1983).

These impressive productivity improvements provide ample financial rewards for improving the lighting of an office building (Abdou, 1997; Cohen-Rosenthal, Schlarb, Thorne, Serchuk & Bradley, 2000; Raiford & Smith, 2000). Consider that an office employee may occupy 10 m^2, and earn $40000 pa (approximate Australian figures). At an energy density of 380 kWh/m^2/annum (section 1.1.1), the energy required to run the office around this worker is 3800 kWh/annum. At an energy cost of 10c/kWh, this energy costs $380 pa. A 5% increase in the output of this worker is worth $2000 pa. These figures demonstrate that the economic impact of increased worker productivity, due to improved working conditions, well exceeds operating cost savings due to energy consumption reductions.

Reduced sickness and absenteeism due to healthier working environments can substantially improve productivity (Abdou, 1997; Nelson, 1997).
Leslie (1994: 4) illustrates this, stating that, 'one hour of salary is equivalent to the cost of one year of lighting energy for that worker'. An absenteeism reduction of one day in a year is then ample to repay a firm for improved lighting.

Effective daylighting also allows building owners to increase rent, demand a higher selling price, or save in worker salaries. This is achieved by the enhanced appeal of the building to tenants, purchasers and workers (Abdou, 1997; Penney & Althof, 1990). Thus, a building with enhanced comfort levels due to daylighting can prove a great financial benefit to its owners. This is beginning to be recognised in the Australian building market. The constructors of a recently completed Brisbane office building have realised the available 'marketing advantages in showcasing building integrated solar and cost effective improvements in building energy consumption' (Wren & Barram, 2000). The building was designed for low environmental impact with prominent building integrated photovoltaics. Their approach was taken, 'partly for life cycle cost benefits and environmental considerations but primarily for marketing benefits, essentially creating a point of difference for the project' (Wren, 2000).

Daylighting design is often considered too costly by building owners and managers. Simple payback periods often range from 3 to 20 years, enough to discourage many owners from daylit options. However, the simple payback period does not consider improvements in worker productivity nor marketing advantages. As shown above, productivity improvements dwarf operating cost savings, making daylighting design a much more attractive option.

1.1.4 THREE REASONS TO CONSIDER DAYLIGHTING WHEN DESIGNING A COMMERCIAL BUILDING

There are three main reasons to carefully consider daylight when designing a commercial building. These are:

1. Daylighting strategies can substantially reduce energy use and associated greenhouse gas emissions.
2. Daylight is healthy for building occupants, and contributes to occupant satisfaction.
3. When productivity improvements are considered, effective daylighting pays for itself time and again.

1.2 IMPROVING THE DAYLIGHTING OF SUB-TROPICAL OFFICE BUILDINGS

The successful daylighting of sub-tropical buildings is very different to that of more temperate buildings. The principal objective of sub-tropical window design is thermal comfort in summer. More sunshine means that windows are commonly shaded by wide eaves, external and internal shades, and reflecting or absorbing glass (Figure 1.1). Daylight entering the windows is severely reduced, to the extent that internal daylight levels in shaded sub-tropical buildings are often well below those achieved in buildings in more temperate climates (Edmonds, Reppel & Jardine, 1997; Rodgers, Ballinger & Dunkerley, 1979).

Figure 1.1 - Heavily Shaded Sub-tropical Office Building

1.2.1 COMBINING SHADING AND LIGHT REDIRECTION

Daylighting technologies employed in the sub-tropics should utilise direct sunlight, while maintaining acceptable visual and thermal comfort for building occupants (Laar, 2001). This can be achieved by adapting the design of an external shade. The adapted shade guides some of the incident sunlight deep into the building. If this is done carefully to avoid glare and to direct light deep into the room, the device could enhance daylighting while still providing direct solar shading.

Discomfort glare from windows is related primarily to visible sky luminance, and secondly to the ratio of sky brightness to room brightness (Boubekri & Boyer, 1992; Chauvel, Collins, Dogniaux & Longmore, 1982; Hopkinson, 1970a, b, 1972). As such, daylighting systems should not redirect bright sky illumination directly into occupants' eyes.

The light guiding shade (LGS) achieves these objectives. The LGS is a daylight redirecting device in the form of a conventional tilted window shade. The device consists of a diffusing input aperture and specially shaped reflectors that are designed to direct light into a specified angular range (Figure 1.2) (Edmonds, 1992). Usually the specified angular range extends from horizontal up to an elevation of around 60°. Thus, to occupants, the LGS output aperture appears dark, reducing the possibility of glare.

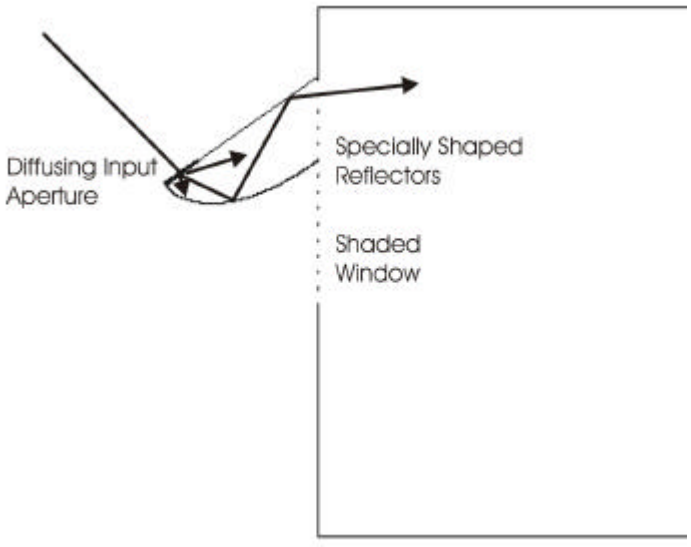

Figure 1.2 - The Light Guiding Shade Combines Shading and Light Redirection

The concept is illustrated in Figure 1.2. The shade protrudes over the window, shading it from sunlight entry. The diffusing input aperture admits a fraction of the sunlight incident on the shade. This illumination is diffused on passing into the device. The transmitted light interacts with the two specially shaped reflectors so that it enters the building within the specified angular range. As the input aperture is diffusing, light transferred into the room remains spatially constant, irrespective of the position of the sun.

The LGS is fixed over the window in the same way as a conventional external shade, acting both to reduce radiant heat gain and to redirect daylight into the building. It has been installed on some large institutional buildings and has been adapted for use on houses (Edmonds, 1998). Thus, the LGS is an intelligent and effective device, and is well suited to the daylighting of sub-tropical office buildings. However, it is a large, bulky device that adds weight to a building's façade. For architects to consider such a technology, it must adhere to the form and proportion of the remainder of the building, both from inside and outside (Hopkinson, 1972). Thus, architects may not find the device attractive to install on their buildings. Similarly, it could be difficult to construct, install and maintain.

1.3 LIGHTING SIMULATION IN THE BUILDING DESIGN PHASE

For daylight to be utilised to its full potential, its effect on building performance must be understood early in the design process. In this phase of building design, crucial decisions are made regarding a building's orientation and main forms (Reinhart, 2001); it would be difficult to add a comprehensive daylighting strategy in any later phase. For effective decisions to be made at this design stage, designers must be confident that a daylighting strategy under consideration would be beneficial. If the designers do not understand the benefit of a novel daylighting strategy, they will not include it in their design.

The design problem is superficially very simple: if we know something of the way in which light behaves, why can't we predict how a building design will look before it is built (Roy, 2000)? However, the behaviour of light in the built environment is exceptionally complex. The interaction of light with the surfaces

of the rooms in which we work and live is so complicated that it would take months of manual work to completely understand the lit environment of a building at one moment in time.

The traditional approaches with which designers have investigated new daylighting designs are hand calculations, rules of thumb, spreadsheet calculations and scale models. The most accurate and robust of these methods, scale modelling, is preferred by many designers. However, scale model validations show that scale models consistently overestimate illuminance levels (Cannon-Brookes, 1997). Errors are often related to imprecise positioning of measuring cells, particularly in regions of high illuminance gradients.

Computational methods are commonly used during building design. Many forms of software are currently available that allow the rapid evaluation of the thermal, energetic, acoustic and luminous performance of design alternatives (Bellia, Cesarano & Sibilio, 1994). Lighting simulation software is a natural inclusion in the computer repertoire of building design firms. Numerous lighting simulation programs have been developed to replace the laborious task of hand-calculating the behaviour of light. Computer lighting simulation is now common-place in building design offices, permitting the swift evaluation of lighting design alternatives (Ubbelohde & Humann, 1998).

Computer lighting simulation tools are used for a spectrum of applications by professionals in architecture, engineering, manufacturing, energy management and scientific research. Applications vary from the investigation of new luminaire designs, through energy modelling of interior environments, to lighting design visualisations by illuminating engineers and architects well before the building project takes form. Such programs can pre-calculate the photometric output of lighting fixtures, visualise new concepts in building lighting, find work surface illuminances at any position, and determine effects on the lit environment of changes in lighting positions, intensities, orientations, frequencies, colours and usage.

Numerous programs are available for lighting simulation, aimed at a range of end-users. The programs are distinguished mainly by the capabilities of their photometric translators, the speed and accuracy of their calculation engines, the way in which data is input to the program and the presentation of calculated results (Alonso, 1998). A program's photometric translator defines how the program identifies and treats different materials and light sources. Photometric translators differ in their abilities to model the diverse range of existing materials. The calculation engine includes the mathematical models, algorithms and assumptions used to compute the lit environment. Calculation engines are commonly based on either radiosity or raytracing methods, or some mixture of both (Ashdown, 1996). Radiosity is faster but considerably less flexible in its modelling capabilities. Raytracing excels in the rendition of point light sources, specular reflections and refraction, and radiosity is best suited for area light sources, diffuse reflections, colour bleeding effects and realistic shadows (Ashdown, 1996).

The performance of these programs varies widely, with some being more effective for artificial illumination and some being very accurate in simulating natural lighting techniques (Apian-Bennewitz, Goller, Herkel, Kovach-Hebling & Wienold, 1998). Most softwares were developed to model artificial illumination of indoor spaces, with relatively few programs able to sufficiently model daylighting (Bellia *et al.*, 1994).

1.3.1 RADIANCE

The RADIANCE lighting simulator is a program of great sophistication and versatility (Jarvis & Donn, 1997; Mardaljevic, 1995; Reinhart, 2001; Ward, 1994; Ward Larson & Shakespeare, 1998). The RADIANCE calculation engine optimises physically based, light-backwards raytracing to achieve the best balance between speed and accuracy. The result is a lighting simulation tool with which no other tool can compare. It is quoted that, 'there are still some things that one cannot do in Radiance but what it can do is more than any other existing lighting tool' (Mardaljevic, 1995: 188).

The RADIANCE photometric translator models diffuse, specular and semispecular reflection and transmission, refraction in dielectrics, patterns and textures, material mixtures, and general bi-directional reflection/transmission functions (Erhlich, 2001; Jarvis & Donn, 1997; Khodulev & Kopylov, 1996; Mardaljevic, 1995; Ward, 1994; Ward Larson & Shakespeare, 1998). Natural and artificial light sources are both easily supplied to the model. RADIANCE has successfully modelled highly advanced glazing materials, in ways that could not be matched by any other lighting simulation package. With such exceptional flexibility, RADIANCE is probably the most capable lighting simulation program currently available.

RADIANCE can import CAD-generated geometry from various CAD platforms, and can produce geometry directly from user-written text files. RADIANCE delivers visualisations, false colour and contour luminance images, and user-selected luminances and illuminances (Ubbelohde & Humann, 1998; Ward Larson & Shakespeare, 1998). It can also detect glare sources and indicate visual comfort levels both qualitatively and quantitatively (Ward, 1994).

RADIANCE is portrayed primarily as a research tool, lacking many of the user-friendly features available with other commercial packages. It is difficult to use and requires a steep learning curve. Regardless, the program has gained considerable acceptance, and is now used by researchers and lighting specialists around the world (Mardaljevic, 1995; Ng, Poh, Wei & Nagakura, 2001; Reinhart, 2001; Ward, 1994). A number of design companies have even, 'abandoned their own in-house software (some of which cost over a million dollars to develop)', in favour of RADIANCE (Ward, 1994: 460).

RADIANCE's material modelling ability makes it ideal to simulate novel daylighting technologies. Such technologies use materials difficult to model by other lighting simulation programs (Mardaljevic, 2001; Ng *et al.*, 2001). For this reason, it was considered the only program capable of modelling the advanced light redirecting devices under investigation.

1.4 SUMMARY - MOTIVATIONS FOR THIS STUDY

The successful daylighting of commercial buildings can provide many benefits for building owners and occupiers. It can also afford important savings in building energy use and related greenhouse gas emissions. The daylighting of sub-tropical office buildings is particularly difficult, due to extensive shading installed to improve thermal comfort. The light guiding shade (LGS) is an intelligent and effective device created to improve the daylighting of sub-tropical office buildings. However, the LGS does not appeal to building designers, and is therefore not an effective solution. A device based on the design of the LGS, with greater appeal to building designers, stands to fill this need. This device is the micro-light guiding shade panel, the subject of this study. The micro-light guiding shade panel is described in detail in Chapter 3.

For the micro-light guiding shade panel to be utilised to its full potential, building designers must understand its impact on building performance early in the design process. Thus, the device must be modelled with lighting simulation software currently in use by building design firms. RADIANCE is the best software with which to model the new device, and has therefore been developed extensively as part of this study. Developments to RADIANCE include the model of the micro-light guiding shade panel, and other improvements in the functional capability of RADIANCE's daylight modelling.

1.5 AIMS

The purpose of this research project was

TO IMPROVE THE DAYLIGHTING OF HIGH RISE SUB-TROPICAL BUILDINGS.

The specific aims of the work performed were:

- Review the literature related to daylighting devices and techniques and identify promising approaches
- Develop an optimal daylighting device for sub-tropical high rise buildings
- Examine the device theoretically to determine optimal design, application and construction
- Construct several devices and examine them experimentally

- Compare experimental findings with the requirements of an optimal daylighting device for high rise sub-tropical buildings
- Review the literature related to daylight simulation and identify promising softwares and algorithms
- Improve the penetration of daylighting technologies by developing computer algorithms useful for improved daylight simulation
- Perform lighting simulations involving the developed device to improve its design, specification and implementation
- Validate simulations against experimental measurements

1.6 THESIS OUTLINE

The structure of this thesis is illustrated in Figure 1.3. This introductory chapter is followed in Chapter 2 by a review of the literature pertaining to daylighting strategies and technologies, and computer lighting simulation. Included is a list of characteristics of an ideal daylighting device for high rise sub-tropical buildings. Non-imaging optics and the micro-light guiding shade panel are detailed in Chapter 3. Initial theoretical, experimental and simulation examinations of the micro-light guiding shade panel are described in Chapter 4. This includes descriptions of the first prototype micro-light guiding shade panels. Chapter 5 details the construction and assessment of two full scale micro-light guiding shade panel designs on the daylighting test building. The constructed panels are compared with the characteristics of an ideal daylighting device for high rise sub-tropical buildings. The constructed panels and the test building are simulated in Chapter 6, and results are compared with experimental measurements. Chapter 7 provides detailed discussion of the various simulation algorithms developed to complete the simulations of Chapter 6. The research findings are summarised and concluded in Chapter 8, followed by suggested directions for future work.

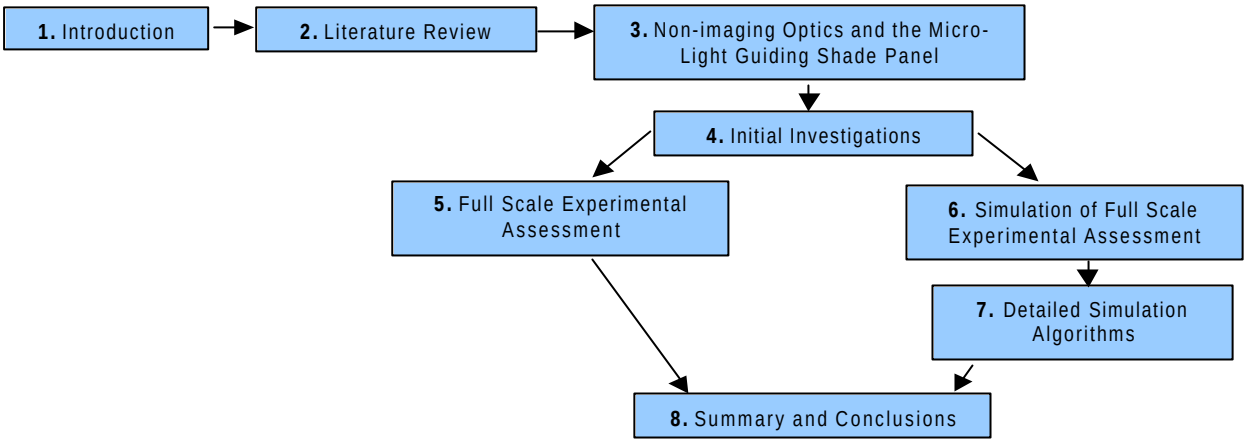

Figure 1.3 - Outline of Thesis

CHAPTER 2 - LITERATURE REVIEW

2.1 DAYLIGHTING STRATEGIES AND TECHNOLOGIES

The environmental, financial and physical benefits of daylighting are best attained by applying effective daylighting design and advanced daylighting systems. Several advanced daylighting systems are commercially available. Many more systems are the focus of international research. The aim of this section is to review the literature pertaining to the daylighting of high rise office buildings. The first section describes the characteristics of an optimal device, against which the following descriptions are compared. Several strategies and technologies are discussed, followed by the basis of development of the micro-light guiding shade panel.

2.1.1 OBJECTIVES OF DAYLIGHTING SYSTEMS FOR SUB-TROPICAL HIGH RISE OFFICE BUILDINGS

The purpose of this research is to improve the daylighting of sub-tropical high rise office buildings. This requires a device capable of the several objectives outlined below.

- Shading must be provided to reduce the transmission of direct sunlight.
- Some sunlight must be effectively utilised without overheating the building.
- Light must be directed deep into the building for uniform illumination.
- The distribution of delivered daylight should remain reasonably constant and not distract occupants.
- Light must be collected from a large exterior region for maximum natural illumination.
- Delivery of illumination through the device must be efficient.
- Light must be directed without causing glare to occupants.
- Continual manual adjustment should not be required.
- The device must be cost effective, easy to install and not space intrusive.
- The device should be suitable for new buildings and for retrofitting existing buildings.
- The external and internal appearance of the building must not be degraded by the device.

2.1.2 APPLICATIONS WITH LARGE IMPACT ON BUILDING DESIGN

2.1.2.1 Atria

Atria place large skylights over multi-storey open volumes adjacent to rooms or public areas (Figure 2.1). Atria can provide a thermal buffer for the parent building, improving its thermal performance, as well as delivering daylight deep inside multi-storey buildings (Kristensen, 1994). However, atria can also be an energy drain, and must be designed with consideration of energy efficiency (Bordenaro, 1993). Atria often become stratified, with cool air collecting at the bottom and hot air rising to the top. This can reduce thermal comfort of building occupants and requires increased use of air conditioning and forced ventilation.

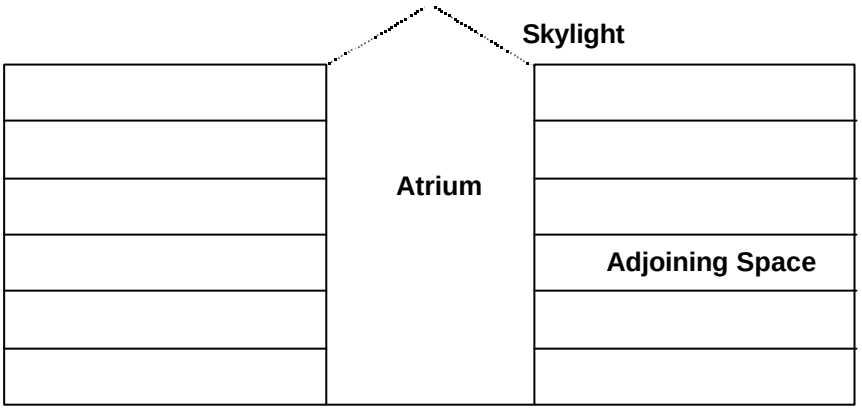

Figure 2.1 - An Atrium

2.1.2.2 Skylights and Vertical Light Piping

In smaller buildings, skylights are an efficient source of daylight (Carter, 2002). Skylight advantages include the delivery of daylight illumination directly onto the work surface from above and the ability to present a larger area for daylight collection. There are numerous forms of skylights available, including domes, pyramids, plastic panels and louvres for heat and glare control (Rea, 1994). Shading is very important for horizontal skylight glazings to avoid overheating in summer.

For larger buildings, skylights can be combined with light pipes to transfer daylight down from the roof into the building (Carter, 2002; Edmonds, Moore, Smith & Swift, 1995; Edmonds, Travers & Reppel, 1997). Many systems consist of sun-tracking mirror devices on the roof, transferring sunlight into light guides for daylight delivery deep inside buildings (CADDET, 1991; Schuman,

Rubinstein, Papamichael, Beltran, Lee & Selkowitz, 1992; York, de Vaal, DesBrisay, Eijadi, Harlow, Lee, Selkowitz & Whitehead, 1990). These systems can provide daylight deep inside buildings, but are very difficult and expensive to install.

2.1.2.3 Light Piping

Light pipes transfer light from a building's roof or façade into the depths of the building (Figure 2.2) (Edmonds, 1994). There are many forms of light pipes presently available. The most common light pipes are mirror reflective guides, prismatic light guides, lens guides, fibre optic guides and other solid state guides (Schuman *et al.*, 1992). Each can be combined with numerous light collecting and distributing systems. Light pipe performance varies with the length of the light pipe, the maintenance condition of the guide, coupling with collecting and distributing apertures, and the direction from which light is incident. Light pipes are generally quite bulky. In order to efficiently transport light, guides are generally enclosed, and room occupants cannot see through them. Thus, the guide appears as a bulky, boxy intrusion into the room.

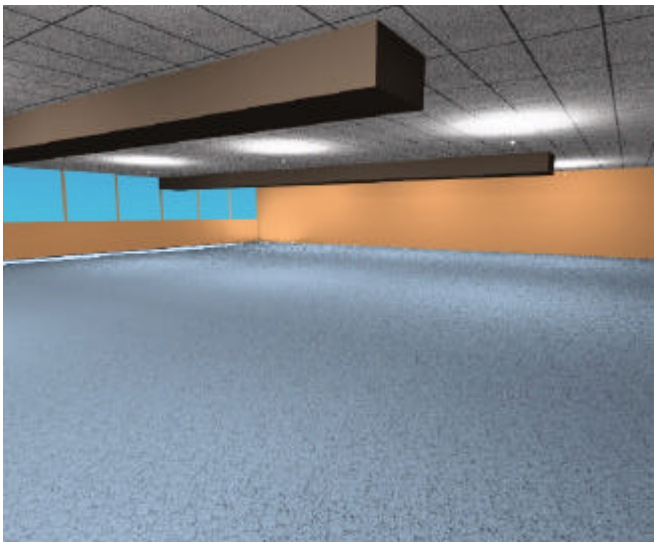

Figure 2.2 - Light Pipes (Shown Above Suspended from the Ceiling) Deliver Light from the Façade into the Depths of the Building

2.1.2.4 Summary - Rejection of Atria, Skylights and Light Pipes for Daylighting High Rise Office Buildings

Atria, skylights and light pipes each significantly intrude on the interior design of buildings. Atria and skylights require roof openings, and space within the building to distribute collected illumination. Light pipes require light collectors

on the building's façade or roof, and also occupy significant volume within the building. As such, they are each considered inappropriate for improving the daylighting of sub-tropical high rise office buildings without excessive expense and space intrusion.

2.1.3 WINDOW SHADING DEVICES

There are a number of devices that can be placed on a building's façade to control the admission of direct sunlight. The simplest of such devices is the fixed window overhang. This sits out over a window and inhibits the penetration of sunlight. This simple and cheap system is useful for sunlight control, but is not preferred for daylighting. Under overcast conditions, the shade obstructs useful daylight from a large portion of the sky.

More typical of Australian buildings is the tilted canopy shade. This shade extends down and out from the window head over the window (Figure 2.3). These shades drastically reduce internal natural light levels (Rodgers, Ballinger & Dunkerley, 1979).

Figure 2.3 - Tilted Canopy Shades Drastically Reduce Internal Natural Illumination

Adjustable sunshades are common in sunny climates. These are beneficial since fixed shades work optimally for only a limited range of solar positions. Mobile external louvre sunshades are suitable for east and west aspects, but require manual or automatic control mechanisms (Department of Employment and Industrial Relations, 1983).

2.1.3.1 Light Shelves

Light shelves are horizontal or near horizontal baffles, placed between view and clerestory windows, used to shield from glare and reflect light onto the ceiling (Ruck, Aschehoug, Aydinli, Christoffersen, Courret, Edmonds, Jakobiak, Kischoweit-Lopin, Klinger, Lee, Michel, Scartezzini & Selkowitz, 2000a: 4.10) (Figure 2.4). A light shelf's upper surface is generally of a light colour that reflects daylight upwards through the clerestory window onto the nearby ceiling. This reflected daylight aids in improving the penetration and uniformity of daylight (Ruck *et al.*, 2000a: 4.11). They can be situated outside or inside a building (or both), and can be horizontal or tilted upwards or downwards. Light shelves require high ceilings and maintenance of external reflective surfaces (Ruck *et al.*, 2000a: 4.12).

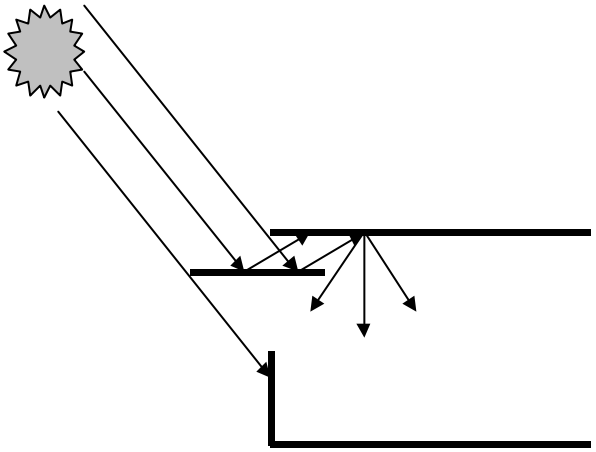

Figure 2.4 - A Light Shelf Shields from Sunlight and Reflects Daylight into the Building

2.1.3.2 Summary - Rejection of Shading Devices and Light Shelves for Daylighting High Rise Office Buildings

Light shelves are large façade devices that must be incorporated into a building's design from its inception. They can be difficult to design and install. This is primarily because they are large façade elements that add considerably to the façade design. As such, their use on high rise office buildings is rare. Therefore, light shelves were not the subject of this study.

Shading devices are useful to control the entry of sunlight into buildings. They also drastically impede the passage of natural light. The subject of this work, the micro-light guiding shade panel, aims to maintain the shading of these devices while concurrently contributing to internal natural illumination.

2.1.4 REFLECTIVE LIGHT REDIRECTING DEVICES

Daylight redirecting devices in the upper façade area can improve interior daylight levels. Sunlight can be reflected onto a lightly coloured ceiling, providing daylight illumination deep inside a room. Light redirecting devices can be mounted outside or inside the building façade.

2.1.4.1 External Reflective Light Redirecting Devices

Rodgers *et al.* (1979) compared the performance of several light redirecting devices. The tested devices included an open window, a shaded window, reflective blinds, tilted exterior reflective shelves and various combinations of each. An adjustable, single, flat reflector, exterior to the façade produced the highest and most uniform levels of interior illuminance. This system needs continual adjustment to achieve the best results.

2.1.4.2 Internal Reflective Light Redirecting Devices

Light directing louvres involve movable elements coated with a specularly reflecting material. These reflective blinds can be placed in windows to redirect incident light upwards toward the ceiling. It is possible that, 'reflecting venetian blinds mounted behind a small clerestory window will reflect sufficient lumens off the ceiling to provide adequate illumination throughout much of the year' (Rosenfeld & Selkowitz, 1977: 50). They are more flexible than light shelves, as well as being somewhat cheaper and easier to install. However, they may require automatic or manual control to work effectively (Ruck *et al.*, 2000a: 4.22).

2.1.4.3 Summary - Consideration of Reflective Light Redirection Devices for Daylighting High Rise Office Buildings

Reflective light redirecting devices have great potential to improve the daylighting of high rise office buildings. The micro-light guiding shade panel is a further development of reflective light redirection. This device combines reflective light redirection with effective solar shading, without causing glare, and without requiring adjustments to follow the sun.

2.1.5 REFRACTIVE AND DIFFRACTIVE LIGHT REDIRECTING DEVICES

Angular selective glazings transmit energy from only a restricted range of directions. These glazings selectively reject sunlight at times when it will cause overheating, while admitting low elevation diffuse light and sunlight as desired. The devices discussed below employ refraction and diffraction to act both as light redirecting devices and angular selective glazings.

2.1.5.1 Prismatic Glazing

Prismatic glazing systems commonly comprise a series of glass or plastic prisms placed within a double glazing unit (Ruck *et al.*, 2000a: 4.38) (Figure 2.5). These panels can selectively reject direct sunlight while accepting and redirecting high elevation light more effectively into the building (Schuman *et al.*, 1992). Prismatic glazing offers efficient passive control of solar heat gain for façades facing within 70 degrees of the equatorial direction (Lorenz, 1998, 2001).

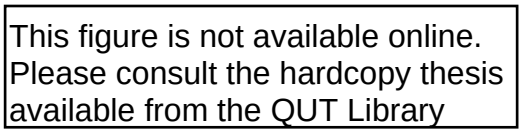

Figure 2.5 - Prismatic Glazing (Ruck *et al.*, 2000a: 4.40)

Prismatic glazing systems also act as light redirecting devices. These systems were compared with mirrored louvres and light shelves by Aizlewood (1993) and Littlefair, Aizlewood and Birtles (1994). With the sun directly facing the windows, the illuminance at the back of the room was more than doubled. However, prismatic glazing performed worse than the other devices under overcast conditions. The prismatic glazing provided the best sunlight control, achieving sharp reductions in window glare. A prismatic film system was also examined in the above tests. This is a much finer version of prismatic glazing, etched onto a thin film that can be coated onto glass. This produced modest increases in light levels throughout the room under clear skies, and performed the best of the examined systems under overcast skies. Some glare control

was provided, but other glare control devices may be required. Prismatic system performance can be significantly improved by employing sun-tracking technology (Moeck, 1998).

2.1.5.2 Laser Cut Panel

The laser cut panel (LCP) is a powerful light redirecting element used to improve the distribution of daylight in rooms, whilst rejecting unwanted solar heat gains. The device is manufactured by making laser cuts in thin sheets of acrylic plastic. Each laser cut acts as a mirror within the acrylic, at which total internal reflection causes a large redirection of incident light (Figure 2.6). Thus, the panel is converted into a powerful light deflecting system (Edmonds, 1988, 1991, 1993a, b). The spacing and tilt of the laser cuts can be altered to change the device's angular selectivity and the strength of redirected illumination. The LCP is similar to conventional glazing in terms of thickness and viewing transparency. The latter is maintained provided that the viewing direction is near normal to the panel's surface.

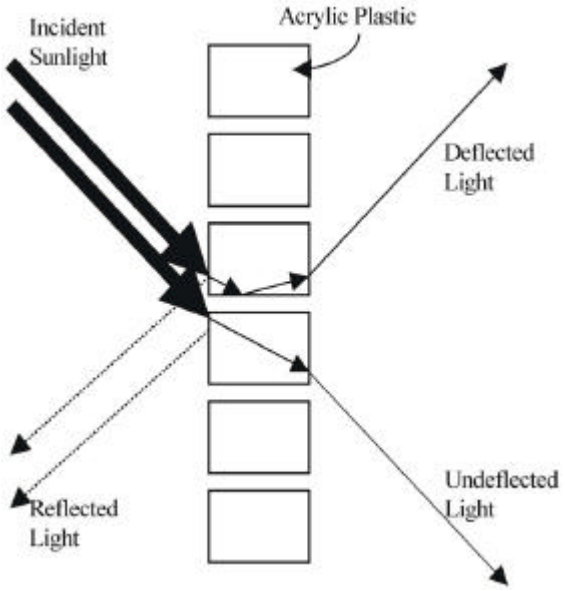

Figure 2.6 - Powerful Light Deflection by the Laser Cut Panel

The material can be combined in numerous configurations to deliver increased natural light into buildings without introducing excessive glare (Edmonds, 1998; Edmonds, 1994; Edmonds *et al.*, 1995; Edmonds *et al.*, 1997). In its primary application, the LCP is mounted in a clerestory window. In this application, it performs similarly to a light shelf, redirecting daylight across the ceiling of the room, pushing daylight illumination deeper into the room while avoiding glare.

Numerous angular selective glazings for sub-tropical buildings are based on various geometric configurations of the LCP (Edmonds, Jardine & Rutledge, 1996; Reppel & Edmonds, 1998).

The effectiveness of the LCP in improving room illumination depends strongly on the window fitting and sky conditions (Edmonds, 1993a). The inclination of panels mounted in the clerestory window should be adjusted in clear sky conditions to avoid direct sunlight penetration (Sit & Aydinli, 1999). Reduced viewing transparency and possible glare due to light spreading in imperfect laser cuts are negative aspects.

Two other products perform the same function as the LCP, but are made in different ways. Serraglaze is manufactured by compression moulding (Milner & Wiggington, 2001). The gaps formed in the process are significantly smaller than those in the LCP. Thus, the gaps are more difficult to observe and the panel appears clearer. The other device, Inglas-Y, is manufactured by extrusion moulding (Inglas, 2002). The gaps in the latter device are similar to those in the LCP. Although direct comparisons have not been completed, little difference is expected in the performance of these three similar devices.

2.1.5.3 Holographic Optical Elements

Holographic optical elements (HOE's) are produced by lasers on thin films that are then laminated between two panes of glass (Muller, 1994). Light is redirected by diffraction between the closely spaced lines. Placing the devices in clerestory windows or skylights improves illuminance uniformity. The diffraction process is wavelength dependent, and disperses incident illumination. The dispersed light must be recombined to white light for daylighting applications. In combination with one-axis tracking systems, HOE's cost around \$2275/m^2 (Australian dollars, 2000) (Laar & Grimme, 2002).

2.1.5.4 Summary - Rejection of Refractive and Diffractive Devices for Daylighting High Rise Office Buildings

Similar to reflective daylight redirecting devices, these devices have great potential to improve the daylighting of high rise office buildings. Their angular selective properties also make them useful for solar shading. However, it is

difficult for these devices to combine both sunlight rejection and effective daylight redirection, without resorting to active optics. This is the objective of the micro-light guiding shade panel. As such, these refractive and diffractive devices were not the subject of further research.

The LCP is an effective daylighting element for buildings other than high rise office buildings. A RADIANCE model of the LCP was developed in parallel with the micro-light guiding shade panel. This model and its application are detailed in Chapter 7.

2.1.6 NON-IMAGING OPTICS

A more novel approach to light redirection is achieved through non-imaging optics. Non-imaging optics is the study of optical systems that maximise the efficiency of light transfer, concentration and deconcentration, without producing images (Compagnon, 1993; Welford & Winston, 1978; Winston, 1991). The second law of thermodynamics and the law of conservation of étendue imply that light concentrated from a large area to a small area can only be achieved for a restricted angular range of accepted light rays. Conversely, light deconcentration directs light rays into a restricted angular range. This property is useful for the collimation of light (Figure 2.7).

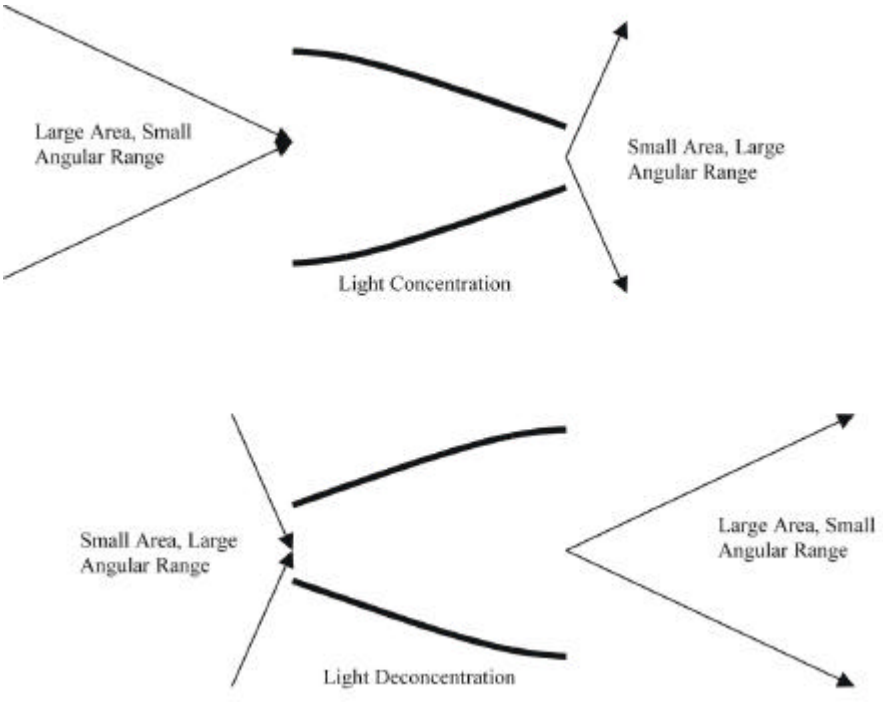

Figure 2.7 - Light Collimation by Deconcentration using Non-imaging Optics

Non-imaging optics was originally developed for solar concentration (Rabl, 1976; Welford & Winston, 1978; Winston, 1991), and has since been applied to the design of artificial luminaires (Elmer, 1980; Gordon & Kashin, 1994; Gordon, Kashin & Rabl, 1992; Gordon & Rabl, 1992; Rabl & Gordon, 1994; Ries & Winston, 1994; Winston & Ries, 1993). Non-imaging optics can also be applied to the design of novel daylighting devices. Several of these devices are described in the following sections.

The science of non-imaging optics is described in greater detail in Section 3.1. This section reviews optical devices with design influenced by non-imaging optical theory.

2.1.6.1 Reflective Light Redirecting Devices Employing Non-Imaging Optics

The Okasolar light redirecting device is a fixed reflective louvre system mounted within a double glazing unit (Kumpers, 1989). Each louvre element has three specially shaped faces. These combine to either redirect sunlight towards the ceiling or to reject it, depending on the solar elevation. Low elevation winter sunlight is admitted while high elevation summer sunlight is rejected (Aizlewood, 1993; Littlefair *et al.*, 1994) (Figure 2.8). However, substantial diffuse illumination was also excluded, such that, 'the mirrored louvres are unable to boost light levels at the back of the room' (Aizlewood, 1993: 151). Additional glare protection devices were required at times. Okasolar devices have been installed in over 120 000m^2 of facades and roofs, with costs ranging from \$600 to \$775/m^2 (Australian dollars, 1999) (Laar & Grimme, 2002).

This figure is not available online. Please consult the hardcopy thesis available from the QUT Library

Figure 2.8 - Angular Selective Transmission by Okasolar (Ruck *et al.*, 2000a: 4.24)

Koster (1994) describes another light redirecting device placed within a double glazing unit. Similar to Okasolar, each element comprises three reflector parts (Figure 2.9). However, Koster's device redirects both daylight and interior artificial lighting, providing unchanging indirect interior lighting. The device provides high interior daylight illuminance levels, well directed toward the rear of the room (Moeck, 1998). However, low angle sunlight penetrated the device during winter. The price of Koster's device starts around $\$450/m^2$ (Australian dollars, 2000) (Laar & Grimme, 2002).

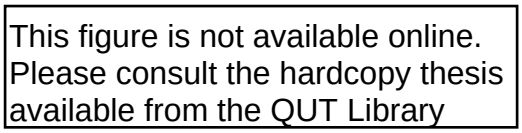

Figure 2.9 - Light Redirection by Koster Louvres (Laar & Grimme, 2002: 290)

The strangely named 'fish' device combines a flat upper reflector with a parabolic lower reflector (Figure 2.10) (Bartenbach, Moeller & Lanzenberger, 1986, 1987). Similar to the LGS (section 1.2.1), upper and lower extremes are defined, beyond which no illumination is directed. Thus the output aperture appears dark to occupants, minimising glare. The devices may be mounted one above another, with their exit apertures forming a continuous plane. A similar device can be added to define a range of acceptance from beyond which no illumination will be transmitted into the room. The elements that comprise the device can be extruded into a form small enough to mount inside a double glazing unit.

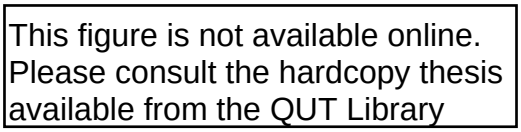

Figure 2.10 - Bartenbach's 'Fish' Louvre System (Ruck *et al.*, 2000a: 4.24)

Digert's 'mini-optical light shelf' system serves the dual purposes of light redirection and shading (Figure 2.11) (Digert, 2001). The system can be mounted within a double glazing unit, or hung similar to venetian blinds, and is placed above the view window. Various forms of the system redirect incident daylight, from a defined range of directions, into the room toward a defined ceiling region, while obstructing the transmission of low altitude sunlight.

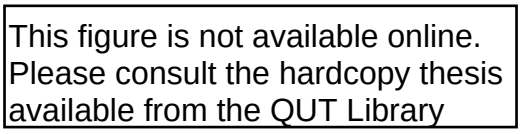

Figure 2.11 – Digert's Mini-optical Light Shelf (Digert, 2001)

2.1.6.2 Refractive Light Redirecting Devices Employing Non-Imaging Optics

The light channel module (LCM) is similar to the LCP (section 2.1.5.2), comprising a transparent acrylic material with regularly spaced air gaps for controlled light redirection (Figure 2.12). Light is accepted from the incident

range 20 to 70° elevation and emerges from the panel in directions between horizontal and 40° above horizontal (Cowling, 1994; Cowling & Veevers, 1990). Light from oblique incidence is bent towards the panel normal, for more effective interior daylighting. Adjustable light blocking elements hung within the panel can be moved into position to reject all or some incident light.

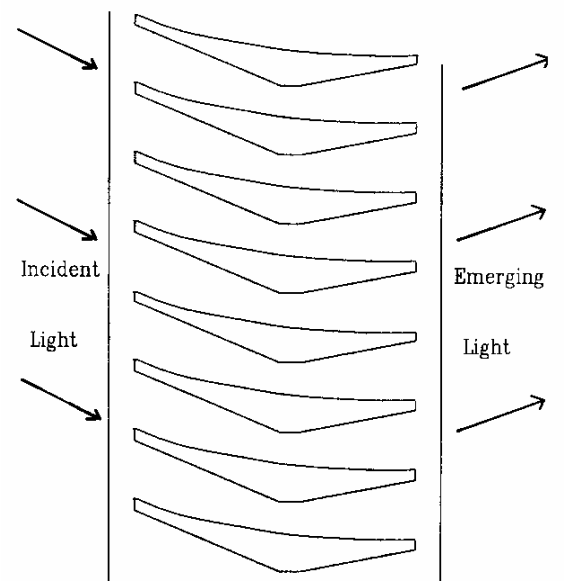

Figure 2.12 - The Light Channel Module

The 'LIF' comprises several specially shaped transparent acrylic blade sections stacked upon each other (Figure 2.13) (Beck, Korner, Gross & Fricke, 1999). The device accepts illumination from a specified sky region and directs light into the room within a specified angular range. No light emerges from the device into directions below horizontal.

This figure is not available online.
Please consult the hardcopy thesis
available from the QUT Library

Figure 2.13 - The LIF (Beck *et al.*, 1999: 217)

2.1.6.3 'Anidolic' Devices

Anidolic solar blinds aim to control daylight penetration into buildings, using a rigid grid of three dimensional hollow reflective elements (Courret & Scartezzini, 1998). The elements consist of three dimensional asymmetrical compound parabolic concentrators (CPCs). An outer CPC defines a radiation admission sector, and an inner CPC directs light into a defined range of directions. The radiation admission sector is designed to provide favourable angular selectivity. The anidolic solar blinds delivered some improvement in deep room illumination, effective seasonal selectivity, good glare protection near the window and poor glare performance at the rear of the room. The devices were difficult to manufacture, introducing many imperfections. As such, their performance was poorer than desired.

The anidolic ceiling device consists of a light duct integrated into a suspended ceiling with non-imaging optical elements placed at either end (Figure 2.14) (Courret, Scartezzini, Francioli & Meyer, 1998). The collector extends from the façade facing upward to collect zenithal illumination. Two more anidolic elements, placed at either end of the light duct, efficiently transport light from the façade and deliver it into the room. The anidolic ceiling enhanced illumination at the rear of the room, and significantly improved illuminance uniformity. A translucent plate over the light duct's exit aperture further improved the daylight distribution and improved its visual appearance. An external shading device, mounted over the collecting aperture, reduced excessive internal brightness in clear sky conditions.

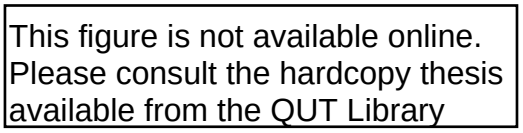

Figure 2.14 - The Anidolic Ceiling (Ruck *et al.*, 2000a: 4.85)

2.1.6.4 Summary - Consideration of Non-imaging Optical Devices for Daylighting High Rise Office Buildings

Non-imaging optics can provide highly efficient devices for light collection and collimation. The preceding sections outline numerous applications of non-imaging optics to daylight design. However, the only described devices known to be based on non-imaging optical design are the 'fish' and anidolic devices.

Those devices that do not rely on non-imaging optical design (viz. Okasolar, Koster's reflective device, Digert's mini-optical light shelf, the LCM, and the LIF) could benefit by consideration of non-imaging optics. All of these devices have defined acceptance ranges for incident illumination. They also contain no diffusing elements. These two characteristics limit their applicability to daylighting sub-tropical buildings. The defined acceptance ranges implies lower interior daylight levels under non-clear skies, as much sky and ground reflected illumination is rejected. The lack of diffusing elements implies that, as the sun moves across the clear sky, the interior illumination pattern changes dramatically.

The anidolic devices are designed for climates dominated by overcast skies. They could, therefore, deliver excessive heat and glare into sub-tropical buildings dominated by clear skies. The anidolic solar blinds proved difficult to construct, limited the sky acceptance region and also contained no diffusing element. The anidolic ceiling's light duct occupies significant volume within the building. As such, the device is considered inappropriate for office buildings without excessive expense and space intrusion.

The 'fish' device also limits the sky acceptance region and contains no diffusing element. The micro-light guiding shade panel, described in Chapter 3, does not limit its sky acceptance region, and will therefore perform better in non-clear skies. As the micro-light guiding shade panel contains a diffusing element, it will also provide a more constant and less distracting interior daylight distribution. The micro-light guiding shade panel can also be mounted exterior to a building’s façade, thus providing shading as well as light redirection.

2.1.7 SUMMARY OF DAYLIGHTING SYSTEMS FOR SUB-TROPICAL HIGH RISE OFFICE BUILDINGS AND SELECTION OF THE MICRO-LIGHT GUIDING SHADE

The daylighting strategies described above are here considered with regard to the objectives outlined in section 2.1.1.

Atria, skylights and light pipes are highly space intrusive, and difficult to install in a building retrofit. Light shelves also must be incorporated into a building's design from its inception, and can be difficult to design and install. Conventional shading devices are useful to control sunlight entry into buildings, but detract from natural lighting. Reflective, refractive and diffractive light redirecting devices are generally useful for either sun control or delivering natural light. However, these devices do not achieve both objectives without manual or automatic adjustment.

Non-imaging optics presents the ability to achieve most of the objectives. The efficient collimation provided by non-imaging optical design directly contributes to objectives relating to deep daylight penetration, large light collection region, low glare and low space intrusion. To deliver a constant interior daylight distribution without user adjustment, a diffusing element should be added at or near the device's input aperture; a diffusing element placed at the device's output aperture will deliver light into all directions, reducing control over the delivery of illumination to the interior space. The optimal device also must meet objectives related to solar shading, ease of installation, suitability to building retrofits, cost effectiveness and pleasing appearance.

Design of the micro-light guiding shade panel is based on non-imaging optics. However, the micro-light guiding shade panel combines the benefits of non-imaging optics with the shading, ease of installation and accepted appearance of conventional shades. The device looks outwardly like a conventional tilted canopy shade (Figure 2.3), and is well suited to both new buildings and existing building retrofits. Cost effectiveness was approached by using cheap and commonly available materials and simple construction techniques.

The micro-light guiding shade panel was the subject of the performed research. It is compared in more detail against each of the objectives of section 2.1.1 in Chapters 3, 4 and 5.

2.2 LIGHTING SIMULATION

Lighting simulation tools are used by many professionals for various applications. There are numerous lighting simulation programs available, intended for many different applications. This section presents a review of the literature related to computer lighting simulation, with emphasis on architectural daylight simulation. Several different softwares are described and compared. This is followed by a review of the literature specifically related to the validation, application and extension of RADIANCE.

2.2.1 LIGHTING SOFTWARES

Lumen Micro is an easy-to-use, radiosity based lighting simulator, able to produce internal illuminance levels and rendered greyscale perspectives (Ubbelohde & Humann, 1998). However, it supports only a limited number of orthogonal surfaces (Ashdown, 1995). The program performs well for simple spaces and calculations, but degrades as the model becomes more complex (Ward, 1998).

Superlite's calculations are executed using a radiosity based computation process (Fontoynont, Laforgue, Mitanchey, Aizlewood, Butt, Carroll, Hitchcock, Erhorn, De Boer, Michel, Paule, Scartezzini, Bodart & Roy, 1999). Simulation results are presented as tabular data, isolux contour plots and illuminance cross-sections (Ubbelohde & Humann, 1998). Superlite is quite accurate for models of simple geometry, such as rectangular rooms with limited furniture, and common materials, such as plastics, paints and clear glass (Fontoynont *et al.*, 1999; Ubbelohde & Humann, 1998). For these simulations, the program is an easy-to-use lighting simulator with effective and useful presentation of results. However, it is limited in the materials and geometry that it can model. For instance, it cannot accurately model mirrors, metals and other materials with specular and semispecular reflections. Limitations are also revealed when introducing complex geometries such as L-shaped rooms and furniture.

ADELINE (Advanced Daylighting and Electric Lighting Integrated New Environment) is a lighting simulation suite containing both Superlite and RADIANCE, as well as a dedicated CAD platform, a library of materials, luminaires and furniture, and links to external thermal simulators (Fontoynont *et al.*, 1999; Ruck, Aschehoug, Aydinli, Christoffersen, Courret, Edmonds, Jakobiak, Kischoweit-Lopin, Klinger, Lee, Michel, Scartezzini & Selkowitz, 2000b: 6.9). The suite provides useful interfaces to both Superlite and RADIANCE. The RADIANCE interface is particularly helpful due to RADIANCE's inherent user-unfriendliness. Unfortunately, the ADELINE interface has 'many minor inconsistencies that make it frustrating to use' (Ashmore & Richens, 2001: 31).

The Lightscape Visualisation System is a professional lighting analysis and rendering program aimed at architectural and entertainment applications (Ashdown, 1996). In contrast to Lumen Micro and Superlite, Lightscape's radiosity calculation is followed by a view-dependent final raytracing to model specular reflections (Ashdown, 1995; Ashmore & Richens, 2001; Maamari, Fontoynont & Mitanchey, 2002). Thus, the program models diffuse, specular and semispecular reflection and transmission, as well as texture maps and imported luminaire photometry. Outputs include visualisations, walk-throughs, false colour luminance and illuminance projections and isolux contour plots (Ashmore & Richens, 2001; Maamari *et al.*, 2002; Ubbelohde & Humann, 1998)[1]. Lightscape's user interface is relatively easy to use (Ashmore & Richens, 2001). However, accurate daylight simulation is hindered by the program's inability to import arbitrary sky luminance distributions, inadequate definition of material specularity and the lack of a glazing database (Close, 1996). Lightscape renderings are high quality and quite convincing, but do not always compare well with reality (Ashdown, 1995; Cuttle, 2001; Khodulev & Kopylov, 1996).

[1] The Lightscape software package has since been redeveloped by AutoDesk. In its new form, Viz, the software no longer provides detailed lighting analysis.

Genelux uses a forward, spectral, ray-tracking process to trace light rays from sources forward toward measurement points (Fontoynont *et al.*, 1999; Mitanchey, Periole & Fontoynont, 1995). This technique is similar to RADIANCE's raytracing process, except that rays are traced in the opposite direction. Genelux can model light interaction with specular, semi-specular and diffuse surfaces. More complex materials with arbitrary light reflection and transmission functions can also be modelled. The program's forward ray-tracking process is generally less efficient than RADIANCE's backward raytracing. However, Genelux is better suited to modelling complex specular reflectors like light pipes, which are very difficult for RADIANCE to model.

Specter combines Genelux's forward ray-tracking and RADIANCE's backward raytracing. Forward ray-tracking provides view-independent illuminance distributions, while backward raytracing creates view-dependent visualisations (Khodulev & Kopylov, 1996). Complex angle-dependent reflection and transmission are supported. Refraction and intensity attenuation in dielectrics are also modelled, as are participating media (eg. rain, fog, haze). Outputs include visualisations, false-colour representations, tables and graphs of luminance and illuminance.

Numerous other lighting simulators are commercially available (Ashdown, 1996; Ashmore & Richens, 2001). Real Light, Strata StudioPro, MicroStation Masterpiece and Accurender provide photorealistic images, and cost up to $A1500 (in 1996). AGI 32, Luminosity, Genesys, RadioRay and Microstation provide lighting analysis tools as well as photorealistic images, with costs rising to $A3000 (in 1996).

2.2.2 SOFTWARE COMPARISONS

Simulations using RADIANCE, Genelux, Superlite, ADELINE (simulations performed by RADIANCE) and LESO-DIAL were compared with scale model experiments by Fontoynont *et al.* (1999). For relatively simple simulations, all softwares compared well with scale model measurements, with errors generally less than 5%. For more complex geometries, RADIANCE provided good agreement with experiment, with errors less than 10%; errors increased to

greater than 20% in other programs. The primary source of disagreement between simulation and experiment was difficulties modelling surface reflections (Roy, 2000).

Ubbelohde and Humann (1998) compared Superlite, Lightscape, RADIANCE and Lumen Micro, in simulating a two-storey daylit office building. RADIANCE offered the greatest input accuracy and made accurate illuminance predictions under all sky conditions. Lightscape underestimated illuminance levels, while Superlite and Lumen Micro significantly overestimated due to limitations in geometrical input. RADIANCE and Lightscape produced the most realistic visualisations, while Superlite and Lumen Micro were incapable of rendering effective images. Lightscape offered walk-through renderings that compared well with the real space. RADIANCE required greater learning and rendering times, but performed well when employed by a skilled user.

Ashmore and Richens (2001) performed a similar comparison of Lightscape, RadioRay, Microstation and ADELINE (simulations performed by RADIANCE). Simulation results were compared with scale model measurements under an artificial sky. Predicted illuminances compared favourably with measurements for all softwares except RadioRay. ADELINE (RADIANCE) provided the most convincing visualisations, with all other softwares displaying 'some mottled and streaky surfaces' (Ashmore & Richens, 2001: 27).

Khodulev and Kopylov (1996) compared Lightscape, Specter and RADIANCE. In terms of accuracy of luminance predictions, Lightscape performed relatively poorly, Specter provided reasonably accurate results, and RADIANCE was the most accurate. Each software provided some rendering errors. Lightscape consistently produced less realistic images than both Specter and RADIANCE. Specter displayed rougher, more noisy visualisations than RADIANCE. However, for more complex scenes, Specter images were smoother than those provided by RADIANCE. This may be due to incorrect setting of RADIANCE control parameters. Overall, Specter was the preferred software, due to its more complete light propagation model and better user interface.

2.2.3 VALIDATION OF RADIANCE

RADIANCE validations have been performed by comparison with scale models and full scale projects. Probably the most extensive validation effort was performed by Mardaljevic (1995, 2000a, 2001). RADIANCE predictions were compared with measurements made in full scale rooms exposed to real sky conditions. Disagreements were more likely to be caused by errors in input parameters than by the simulation process. For highly accurate geometry, material and sky models and high level controlling parameters, mean bias errors were less than 13%. It was concluded that RADIANCE can predict daylight illuminance levels with a high degree of accuracy for a range of realistic sky conditions and glazing strategies.

A similar study was performed by Jarvis and Donn (1997). RADIANCE simulations were compared with measurements made in a full scale room and in scale models. Medium level controlling parameters performed well under cloudy skies, while high level parameters were preferred for clear skies. It was concluded that a high degree of agreement between predictions and measurements could be obtained, although the results were highly dependent on the control parameters. It was demonstrated that it is possible to obtain reasonable results within reasonable times.

In numerous other studies, RADIANCE compared very well with measurement for both simple and complex geometries, providing errors generally less than 10% (Fontoynont *et al.*, 1999; Khodulev & Kopylov, 1996; Roy, 2000). RADIANCE results were very sensitive to control parameter settings. Errors made setting these parameters tended to cause illuminance underestimations.

2.2.4 APPLICATIONS AND DEVELOPMENTS OF RADIANCE

RADIANCE is a popular program used by many lighting designers and researchers around the world. Numerous applications of RADIANCE have been discovered. Some of these applications required the development of new RADIANCE functionalities.

2.2.4.1 Light Redirection

Simulation of strong light redirection by many daylighting devices requires special modelling techniques (Apian-Bennewitz, 1995; Apian-Bennewitz, Goller, Herkel, Kovach-Hebling & Wienold, 1998; Mischler, 2001). Photogoniometers can measure the reflection and transmission properties of various materials and devices. The results of these measurements can then be added into RADIANCE for effective modelling of advanced daylighting materials and devices (Apian-Bennewitz, 1995). Forward raytracing is another effective approach to modelling light redirection. Forward raytracers pre-process light redirection through daylighting devices, and their results are plugged into RADIANCE (Andersen, 2002; Mischler, 2001).

RADIANCE is well suited to the simulation of anidolic devices (section 2.1.6.3) (Compagnon, 1993: 11). Simulations assessed the daylighting performance of anidolic devices, luminous output distributions and visual comfort. Illuminance predictions compared well with measured data, and efficiency results compared favourably with previous studies (Courret *et al.*, 1998; Scartezzini & Courret, 2002). Favourable comparisons were made between measurements and simulations of luminous output distributions, with a maximum relative difference of 12% (Courret, Paule & Scartezzini, 1996; Scartezzini & Courret, 2002).

2.2.4.2 Building and Device Performance Appraisal

RADIANCE can be used to assess daylighting devices against several performance criteria. Criteria include luminous intensity distributions, workplane illuminance levels and uniformity, luminous transfer efficiency, and glare analysis (Moeck, 1998). Photorealistic visualisations allow users to perform quantitative and qualitative comparisons between alternative designs, interactively altering their daylighting design for optimal visual performance (Moeck & Selkowitz, 1996; Sick, 1995; Wienold, Beckinger, Apian-Bennewitz, Reetz & Reinhart, 1998). RADIANCE can also be combined with thermal simulation programs to provide an integrated assessment of daylighting strategies (Clarke, Janak & Ruyssevelt, 1998).

Long term design analysis can be achieved by running annual daylight simulations, similar to those performed by energy and thermal simulation programs (Littlefair, 1992). Three such applications of RADIANCE are DAYSIM (Reinhart, 2001; Reinhart & Herkel, 2000), the Dynamic Lighting System (DLS) (Mardaljevic, 2000a, b) and REVISCOM (van Dijk, 2000, 2001). Each application takes annual hourly (or more frequent) weather data as input, and provides internal daylight levels for each daylit hour (or more frequent) of the year. Each application performs its calculations in a different manner, and each takes a different amount of time to run.

2.2.5 SUMMARY OF LIGHTING SIMULATION AND SELECTION OF RADIANCE

The most attractive lighting simulation programs appear to be RADIANCE, Lightscape and Specter. Each of these softwares can perform advanced lighting simulation and provide convincing visualisations. Of these three programs, Lightscape is probably the least capable, yet has the best user interface. Lightscape, Lumen Micro and Superlite cannot model the specular reflecting surfaces of the micro-light guiding shade panel. ADELINE contains a DOS-based version of RADIANCE, but has a poor user interface. However, ADELINE's version of RADIANCE can be accessed directly from the DOS-prompt. Genelux is a forward raytracer that can model the specular reflections within the micro-light guiding shade panel. However, Genelux is generally less efficient than RADIANCE, requiring longer simulation times.

Lighting software comparisons and validations consistently revealed that RADIANCE is a superior lighting simulator, provided it is used by an experienced user, and sufficient levels of simulation parameters are employed. RADIANCE can predict interior lighting levels within 5 to 15% when exposed to real skies. Such accurate light predictions can be made in reasonable computation times (generally ranging between minutes and hours, depending on complexity, based on current computer technology).

RADIANCE can successfully model complex light redirecting devices. The successful modelling of anidolic devices is particularly encouraging for the micro-light guiding shade panel, as both systems are created using the same principles.

RADIANCE has been widely applied to performance appraisals of novel building designs and devices. Analysis of visual comfort, energy efficiency, device luminous efficiency and annual daylight profiles are all possible using RADIANCE.

RADIANCE was chosen to perform advanced lighting simulations involving the micro-light guiding shade panel. It is a lighting simulator of high quality, high capabilities and high accuracy. Only Specter was rated higher than RADIANCE in one of several software comparisons. However, the numerous validations, applications and extensions of RADIANCE have not been reported for Specter. Importantly, RADIANCE can model complex light redirection through non-imaging optical devices. It can also provide complex performance appraisals of the investigated device.

CHAPTER 3 - THE MICRO-LIGHT GUIDING SHADE PANEL

The micro-light guiding shade panel was developed by applying the theory of non-imaging optics. The necessary theory is demonstrated in the first part of this chapter. The theory is then applied to an optimal daylighting device for sub-tropical high rise office buildings. The micro-light guiding shade panel is then introduced and detailed. Device performance is compared with the theory developed earlier in the chapter. The chapter is completed by a summary and conclusions.

3.1 Non-Imaging Optics

The design of the micro-light guiding shade panel is based on the theory of non-imaging optics. Non-imaging optics is the study of optical systems that maximise the efficiency of light transfer, concentration and deconcentration, without producing images (Compagnon, 1993; Welford & Winston, 1978; Winston, 1991). Non-imaging optical devices dispense with the need to form optical images. This allows them to approach the maximum possible concentration. Solar concentrators and artificial luminaires both employ non-imaging optical design (Elmer, 1980; Gordon & Kashin, 1994; Gordon, Kashin & Rabl, 1992; Gordon & Rabl, 1992; Rabl, 1976; Rabl & Gordon, 1994; Ries & Winston, 1994; Winston & Ries, 1993). The theory was then easily applied to daylighting design.

3.1.1 LAW OF CONSERVATION OF ÉTENDUE

To examine the theory of non-imaging optics, and thence the design of the micro-light guiding shade panel, it is necessary to explain the concept of 'conservation of étendue'.

In any optical system, there is a quantity known as étendue. This is defined as follows. At position 1 in an optical system, a set of light rays are incident on a cross-section of area $dx.dy$. These rays are incident from a range of directions with corresponding direction cosines ranges dL and dM (Figure 3.1) (L and M are the direction cosines of each ray projected onto the x- and y-directions respectively). The refractive index of the optical medium at this position is n. At position 2 in the same optical system, the same set of rays passes through a

cross-sectional area *dx'.dy'*, with direction cosines ranges *dL'* and *dM'*. The refractive index of the optical medium at this location is *n'*. This set of rays maintains an infinitesimal étendue at each of the two positions, as shown below.

$$Etendue_1 = n^2 dx.dy.dL.dM$$
$$Etendue_2 = n'^2\, dx'.dy'.dL'.dM' \qquad \textbf{Equation 3.1}$$

The law of conservation of étendue simply states that, for a given set of rays in an optical system, étendue is conserved throughout the system (Welford & Winston, 1978),

$$n^2 dx.dy.dL.dM = n'^2\, dx'.dy'.dL'.dM' \qquad \textbf{Equation 3.2}$$

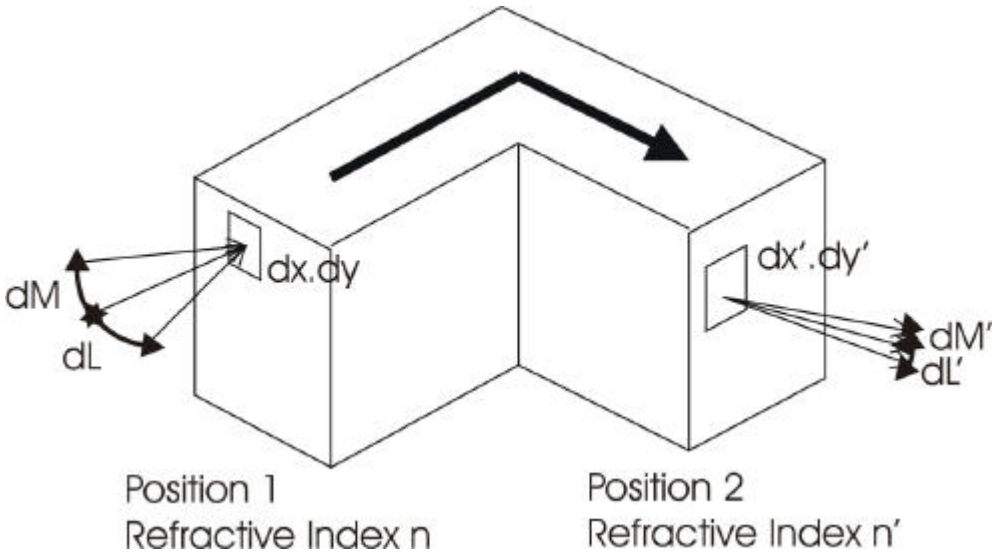

Figure 3.1 - Light Rays Passing Through an Optical System

This is a physical law, applicable to any optical system through which rays may pass. This includes systems with any or no symmetry and any structure (Welford & Winston, 1978: 21). It is independent of the type of optical system, the direction of travel of rays and the choice of coordinate system.

If one considers several individual light rays passing through an optical system, the law can be stated as, 'all light rays that enter the system must exit the system'. The law can also be used to calculate changes in the cross-sectional

area and angular extent of a ray-packet as it passes through an optical system. Thus, the law has direct application to both concentrators and collimators of radiation. The micro-light guiding shade panel is essentially a light collimator. Therefore, its design is directly dictated by the law of conservation of étendue.

3.1.2 APPLICATION TO A SIMPLE TWO-DIMENSIONAL CONCENTRATOR

To illustrate the application of the law of conservation of étendue, it is applied below to a simple two-dimensional concentrator (Figure 3.2). This involves an input aperture of width *2a* uniformly accepting radiation incident from directional range *2q*. The device concentrates this collected radiation onto an output aperture of width *2a'*. Radiation uniformly exits the output aperture into the directional range *2q'*. For the sake of simplicity, the system is considered to be in air, with a uniform refractive index of *n=n'=1*. For the present, only the relationship between *a*, *a'*, *q* and *q'* is considered; the form of the optical system between the input and output apertures is not considered. To obtain this relationship, the law of conservation of étendue is integrated across both apertures.

$$\int_{-q}^{q}\int_{L_1}^{L_2}\int_{-a}^{a}\int_{x_1}^{x_2} dx.dy.dL.dM = \int_{-q'}^{q'}\int_{L_1}^{L_2}\int_{-a'}^{a'}\int_{x_1}^{x_2} dx'.dy'.dL'.dM' \qquad \textbf{Equation 3.3}$$

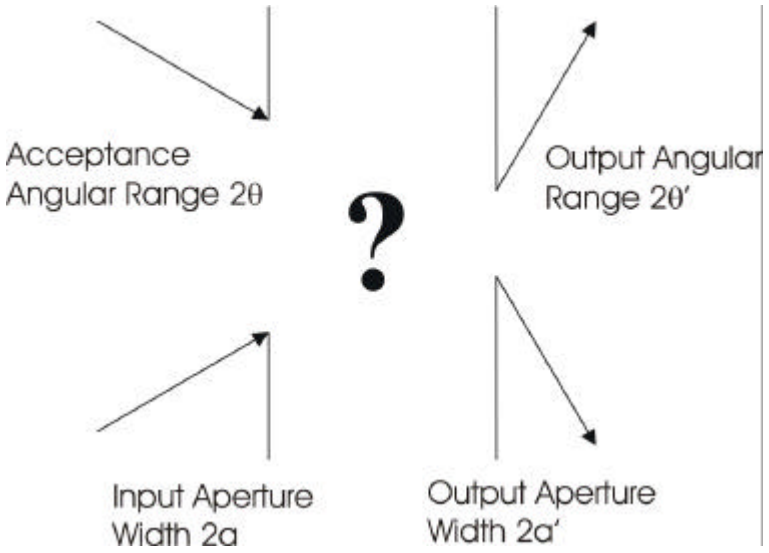

Figure 3.2 - A Simple Two-Dimensional Concentrator

The device is two-dimensional in form (trough-like), containing no reflectors with normal components in the x-direction (into the page on Figure 3.2). Hence, no x-direction ray cosines will be affected while traversing the system. The extents of the system in the x-direction, x_1 and x_2, are the same at both apertures. The x-direction cosines, L_1 to L_2, are also the same at both apertures. Thus, the dx, dx', dL and dL' terms in Equation 3.3 cancel, leaving

$$\int_{-q}^{q}\int_{-a}^{a} dy.dM = \int_{-q'}^{q'}\int_{-a'}^{a'} dy'.dM' \qquad \textbf{Equation 3.4}$$

The y-direction (up the page on Figure 3.2) ray cosines, M, are found as

$$\begin{aligned} M &= \sin q \\ dM &= \cos q.dq \\ M' &= \sin q' \\ dM' &= \cos q'.dq' \end{aligned} \qquad \textbf{Equation 3.5}$$

The double integral Equation 3.4 is then simply solved (Welford & Winston, 1978: 24) as

$$4a\sin q = 4a'\sin q' \qquad \textbf{Equation 3.6}$$

Thus, $4a.\sin q$ represents the two-dimensional étendue associated with a two-dimensional aperture of width $2a$ with rays uniformly incident from a range of directions $\pm q$. Likewise, $4a'\sin q'$ represents the two-dimensional étendue associated with a two-dimensional aperture of width $2a'$ with rays uniformly exiting into a range of directions $\pm q'$.

Equation 3.6 can be rearranged to express the relationship between the aperture widths and the incident and exiting range of directions.

$$\frac{a}{a'} = \frac{\sin q'}{\sin q}$$ **Equation 3.7**

Equation 3.7 represents the theoretical maximum concentration, *a/a'*, that may be attained by a trough-like concentrator. It implies that the greater the concentration, *a/a'*, the greater the de-collimation of light rays, *q'/q*. Alternatively, the larger the output aperture, the greater the collimation of exiting light rays.

The above analysis applied to rays uniformly spaced over both apertures. If, for instance, there was some compression of rays within the exit aperture, *dx'.dy'* decreases, and *dL'.dM'*. necessarily increases. Overall, the integrated étendue will be conserved. This allows for rays exiting the system beyond the directions $\pm q'$, reducing the effective collimation. Thus, Equation 3.7 represents the maximum possible concentration achieved by a trough-like concentrator. A device satisfying Equation 3.7 is known as an 'ideal concentrator' (for a system of uniform refractive index). The form of the optical device will determine the extent to which it deviates from ideality.

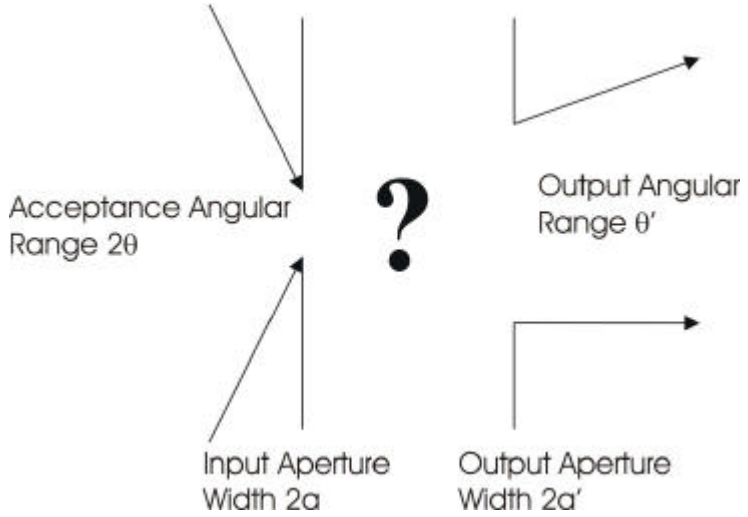

Figure 3.3 - A Two-Dimensional Collimator

3.1.3 APPLICATION TO A TWO-DIMENSIONAL COLLIMATOR

The micro-light guiding shade panel is more similar to the collimator illustrated in Figure 3.3. This device collects light uniformly at the input aperture of width *2a* from incident directions $\pm q$. Light exits the optical system through an

aperture of width *2a'*. Light is not allowed to exit the system in directions below the horizontal, but is allowed to pass into directions up to q' above the horizontal.

Following the same procedure as shown in Equations 3.3 to 3.6, the law of conservation of étendue is expressed as

$$4a\sin q = 2a'\sin q' \qquad \textbf{Equation 3.8}$$

For this system, if light is collected from all directions, $q=p/2$, and Equation 3.8 reduces to

$$2a = a'\sin q' \qquad \textbf{Equation 3.9}$$

The micro-light guiding shade panel contains optical systems with a function very similar to this device. Each system is placed adjacent to the others, with exit apertures meeting at their extremes (Figure 3.4). Greater unused space between adjacent input apertures implies less incident illumination collected by the device. Where it is desired to collect maximum incident illumination, this unused space must be minimised. This is achieved by minimising the ratio of exit and input apertures, a'/a. Applying Equation 3.9, this is achieved by setting $q'=p/2$. By setting q' to this value, Equation 3.9 further reduces to

$$a' = 2a \qquad \textbf{Equation 3.10}$$

Thus, if the output aperture is twice the width of the input aperture, all light incident upon the input aperture can be collected ($q=p/2$), and this light can exit the device in all directions above horizontal ($q'=p/2$). Collimation from all incident directions to half the possible exiting directions can be achieved with an exit aperture twice the width of the input aperture.

Equation 3.9 demonstrates the necessary compromise between light collection and light collimation. To deliver daylight deep into a building, collected light must be well collimated. At the same time, maximum incident light must be collected. These two requirements are in direct conflict. Thus, a compromise must be reached for optimal daylighting of deep rooms.

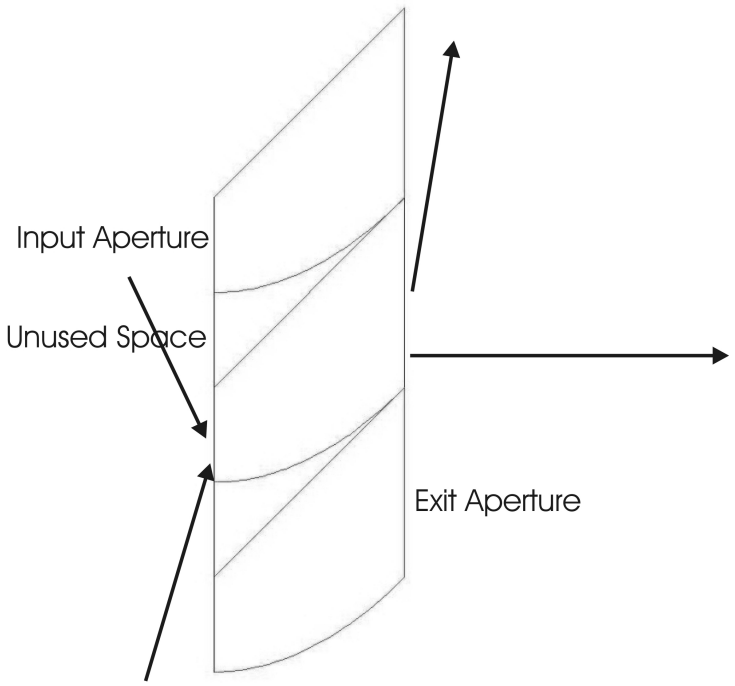

Figure 3.4 - Maximising Light Collection by the Micro-Light Guiding Shade Panel

If the ratio of exit to input aperture width, a'/a, is increased, q' can be decreased, providing greater collimation. However, this comes at the cost of less collecting area. Alternatively, if the ratio of apertures is decreased, light collecting area will be increased. This will, however, have one of two effects. Firstly, collimation could be reduced and light rays could exit the system below the horizontal direction. Otherwise, rays that would have exited the system through the exit aperture will be returned to the input aperture. The net étendue passing through the input and exit apertures is thereby reduced. This effectively decreases the width of the input aperture, or the input acceptance region, or both. Finally, this negates the expected benefit of increasing the light collecting area. For the micro-light guiding shade panel, it is more important to have total control over the direction of exiting illumination. Thus, for this system, it is best to set a'/a to at least two.

Similar to the concentrator described in section 3.1.2, the collimator shown in Figure 3.3 is described by Equation 3.8 only where light is uniformly distributed over the entire input and output apertures. Where there is a greater density of ray throughput, the range of directions into which rays are directed is necessarily increased, and collimation is effectively decreased. Thus, for the system shown in Figure 3.3, Equation 3.8 describes a device of maximum collimation, an 'ideal collimator'.

These two examples have shown that the law of conservation of étendue provides expressions describing ideal concentrators and collimators. Optical systems satisfying these expressions will provide the maximum possible concentration or collimation of incident radiation. Section 3.3.3 shows that the micro-light guiding shade panel is an ideal collimator.

Thus far, it has been demonstrated that if one wishes to collect illumination from a wide exterior angular range and deliver it into a building in a controlled manner, the device's output aperture must be larger than its collecting aperture. The ratio of aperture widths depends on the desired collimation of exiting illumination. To deliver daylight deep into buildings, a compromise must be reached between light collimation and collecting area. The form of the optical system between the apertures has not yet been determined.

3.1.4 IMAGING OPTICS

As a first attempt to create a suitable optical system, the well-known principles of imaging optics will be applied to the concentrator described above (section 3.1.2). An example of such a system is shown in Figure 3.5. This system involves an open output aperture and an input aperture in which an imaging lens is placed. The two apertures are separated by the lens' focal length *f*.

The lens focuses rays from the extremes of the acceptance angular range onto the edges of the output aperture. Rays from within the acceptance angular range are directed by the lens between the edges of the output aperture (i.e. passing through the output aperture).

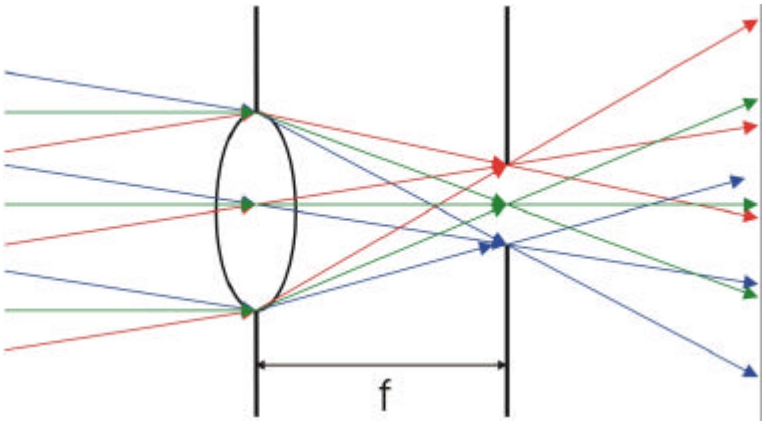

Figure 3.5 - Concentrator Employing Imaging Optics

The focal length and aperture widths can be set to satisfy Equation 3.7. Thus, the device should achieve the desired concentration. However, in reality, the device will not work as desired. In this example, spherical aberration will ensure that rays passing through the extremes of the input aperture will not focus on the edges of the output aperture (Welford & Winston, 1978: 16). Some rays will not reach the output aperture, and the desired concentration is lost. For imaging devices in general, aberrations including spherical and chromatic aberration, coma and astigmatism cause all similar designs to fail in some manner (Welford & Winston, 1978: 45; Winston, 1991). This applies to imaging devices employing either refractive or reflective elements. As such, no imaging system can satisfy Equation 3.7, or any other similar expression. All imaging concentrators will reject rays within their nominal collection range, and all imaging collimators will send rays beyond their nominal extreme directions.

3.1.5 NON-IMAGING OPTICS

No imaging optical devices achieve maximum possible concentration or collimation because aberrations break the basic assumption that all light can be focused to a point. Thus, the requirement for image formation must be dispensed with to achieve maximum concentration and collimation (Winston, 1991). This is the basis of the theory of non-imaging optics.

The first non-imaging optical device described was the compound parabolic concentrator (CPC) (Rabl, 1976: 99; Welford & Winston, 1978: 49; Winston, 1991). The two-dimensional form of this device is shown in Figure 3.6. Two parabolic sections join the input and output apertures. The

upper parabolic section has its focus at the lower edge of the output aperture, and its axis parallel to the lower extreme of the acceptance angular region. The lower parabolic section is a mirror image of the upper parabolic section. All light entering the device from the lower extreme direction is reflected off the upper parabolic section and focused onto the lower edge of the output aperture. All light entering the device from the upper extreme direction is reflected off the lower parabolic section and focused on the upper edge of the output aperture. All light entering the device from within the acceptance angular range will either reach the output aperture directly, or will reach it after reflecting off one parabolic section. All rays entering the device from outside the acceptance angular range will be rejected (Rabl, 1976: 99; Welford & Winston, 1978: 54). This device satisfies Equation 3.7, thus providing the maximum possible concentration (Rabl, 1976: 99; Welford & Winston, 1978: 52).

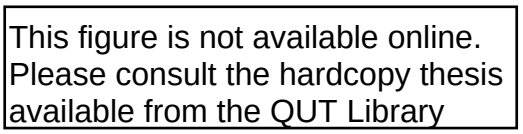

Figure 3.6 - The Two-Dimensional Compound Parabolic Concentrator (Welford & Winston, 1978: 53)

This is just one of many non-imaging optical devices. Other examples include compound elliptical concentrators (CECs) and compound hyperbolic concentrators (CHCs) (Winston & Ries, 1993). Applications of non-imaging optics range from high-energy physics to fluorescent luminaire design (Elmer, 1980; Gordon & Kashin, 1994; Gordon *et al.*, 1992; Rabl & Gordon, 1994; Ries & Winston, 1994; Winston, 1991; Winston & Ries, 1993). Even vision itself appears to rely on non-imaging optics. The cone cells of the retina resemble the CPC, and are sized to concentrate light from approximately the size of the dark adapted pupil (Welford & Winston, 1978: 6; Winston, 1991).

3.1.6 COMPARISON OF IMAGING AND NON-IMAGING CONCENTRATORS

All imaging concentrators fall well short of the maximum allowable concentration limit (by factor of at least two) (Rabl, 1976; Welford & Winston, 1978: 45; Winston, 1991). Non-imaging concentrators, however, reach the limit of concentration in two dimensions, and approach the limit in three dimensions. This is demonstrated below by comparison of two classical concentrators, one image-forming and the other non-imaging.

A two-dimensional image-forming parabolic mirror concentrator and a two dimensional non-imaging CPC are shown in Figure 3.7. Both have an opening aperture width A and a collector width A'. Both also collect radiation over the range $\pm q$ from vertical.

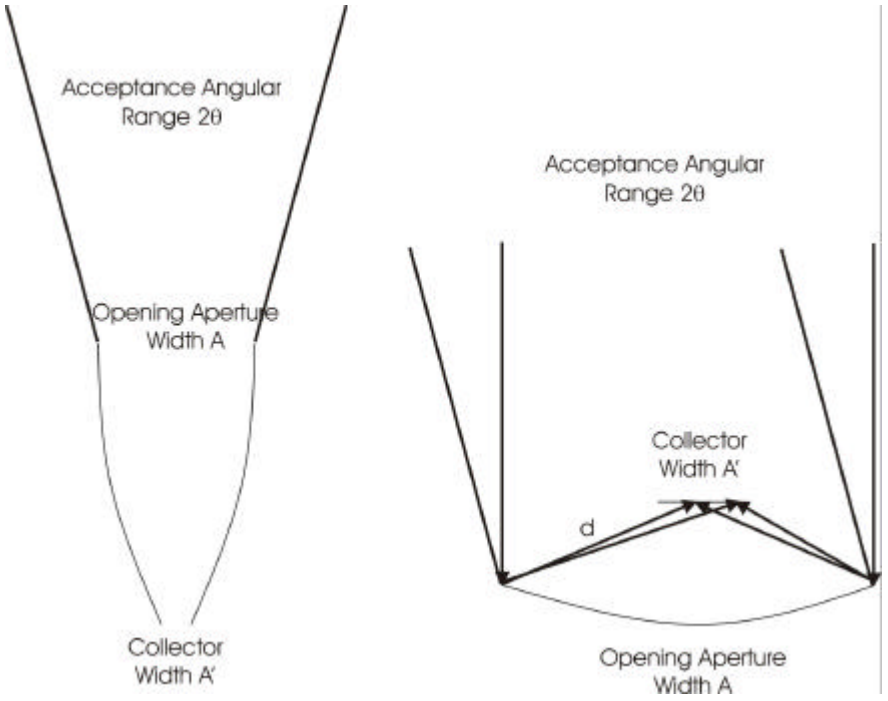

Figure 3.7 - Comparing Concentrations of a Non-imaging CPC and an Image-forming Parabolic Mirror

The two-dimensional CPC is an ideal concentrator that satisfies Equation 3.7. If the collector A' were removed, light would exit the device in all directions, $q'=p/2$. Thus, the concentration ratio C of the two-dimensional CPC is (Rabl, 1976; Welford & Winston, 1978: 51)

$$C_{CPC} = A/A' = \frac{1}{\sin q} \qquad \text{Equation 3.11}$$

The concentration of the parabolic mirror is found by calculating its necessary collector width, *A'*. Rays incident from the vertical direction focus on the centre of the collector. The collector must be sufficiently large that all rays incident within the acceptance angular range are reflected by the parabola to hit the collector. The collector width *A'* is found as

$$A' = \frac{2d \sin q}{\cos(f + q)} \qquad \textbf{Equation 3.12}$$

where *d* is the distance from the collector centre to the edge of the parabolic mirror and f is the angle subtended by half the parabolic mirror at the collector centre. The total width of the parabolic mirror is

$$A = 2d \sin f \qquad \textbf{Equation 3.13}$$

Since the collector obscures part of the parabolic mirror, the device's concentration *C* is found as

$$C_{parabolic} = \frac{A - A'}{A'} = \frac{\sin f \cos(f + q) - \sin q}{\sin q} = \frac{\sin(2f + q) - 3\sin q}{2\sin q} \qquad \textbf{Equation 3.14}$$

This is a more complex expression for concentration, but can be considered as follows. The first term on the numerator is less than one. The second term is greater than zero. Thus, for any real concentrator, the numerator must be less than one. This implies that

$$C_{parabolic} < \frac{1}{2\sin q}, \qquad C_{parabolic} < \frac{1}{2} C_{CPC} \qquad \textbf{Equation 3.15}$$

Thus, for any real trough-like concentrator, the CPC provides greater concentration than the parabolic mirror, by more than a factor of two (Rabl, 1976: 106; Welford & Winston, 1978: 44). As explained in section 3.1.4, the failure of the parabolic mirror to achieve maximum concentration is caused by failure of the assumption that all incident radiation can be focused to a point. The aberration in this example is coma, where rays incident from directions other than the vertical meet the focal plane at different distances from the parabolic axis (Welford & Winston, 1978: 43).

3.1.7 THE EDGE-RAY PRINCIPLE

For maximum control over exiting illumination, the micro-light guiding shade panel must strive to attain the maximum collimation allowed by the law of conservation of étendue. The best way to approach this goal is to apply the principles of non-imaging optics. How is this device designed?

The idea behind the lens design of section 3.1.4 contained the best starting point. The fundamental idea is: all rays entering the device from the extremes of the acceptance angular range should exit the device from the edges of the exit aperture. In this way, all rays incident within the acceptance angular range should pass through the exit aperture. This basic premise is the 'edge-ray principle' (Rabl, 1994; Welford & Winston, 1978: 48; Winston, 1991).

The CPC follows this principle (Welford & Winston, 1978: 50). In contrast to the lens based device, rays incident upon the CPC from extremes of the acceptance angular range are focused on the same edge of the output aperture (Figure 3.6). The image-forming device of Figure 3.5 focuses extreme direction rays on the opposite edge of the output aperture. This is *not*, however, a fundamental difference between imaging and non-imaging optical devices (Winston & Ries, 1993).

Another process by which to design non-imaging devices is the 'geometric vector-flux approach' (Greenman, 1981; Winston, 1991). This involves designing optical systems that do not disturb the 'geometric vector-flux field'. It is conceptually more difficult than the edge-ray principle.

Since the edge-ray principle is, 'well suited to sketch daylighting systems' (Compagnon, Scartezzini & Paule, 1993: 2), it forms the basis of the design of the micro-light guiding shade panel.

3.2 Requirements of a Daylighting Device on the Façade of a High-Rise Office Building

The objective of this research is to improve the daylighting of sub-tropical high rise office buildings. This requires a device capable of the several objectives outlined in section 2.1.1.

To achieve the requirements for a solar shading, passive, easily installed and visually acceptable device, the micro-light guiding shade panel outwardly assumes the form of a conventional tilted window shade. The device's optical system must achieve the remaining objectives relating to efficient sunlight utilisation, deep, constant and non-glaring daylight penetration, and maximum light collection and throughput. As an optical system, its required optical characteristics are:

1. Maximum light collection angular range
2. Efficient transfer of light between apertures
3. High degree of output light collimation
4. Well controlled light output distribution

All of these objectives are related to the law of conservation of étendue. An ideal system would satisfy an expression derived directly from this law (similar to Equation 3.8), without providing glare.

3.2.1 The Law of Conservation of Étendue and the Micro-Light Guiding Shade Panel

Figure 3.8 displays a simplified cross section of the micro-light guiding shade panel. The optical system between input and output surfaces is not shown. The device has the outward form of a conventional tilted window shade, tilted through angle b from vertical. It is trough-like, having translational symmetry along the axis running out of the page. Thus, it is treated as a two-dimensional system.

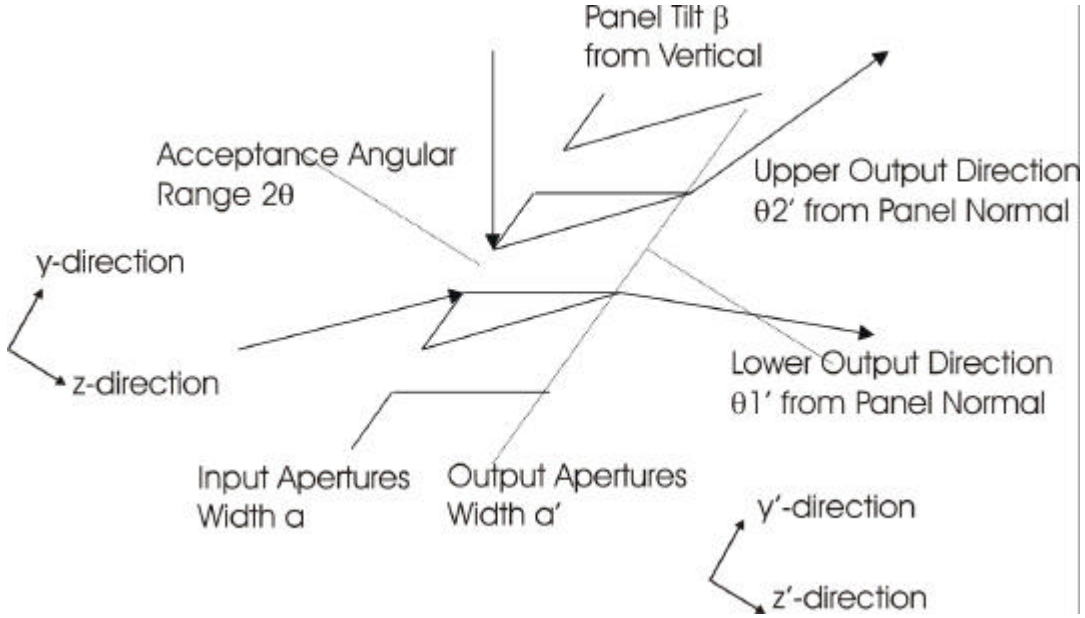

Figure 3.8 - Simplified Cross-Section of the Micro-Light Guiding Shade Panel. The Actual Optical System between Input and Output Apertures is not Shown

Several input apertures (of width *a*) uniformly collect external illumination from a collection region of angular size *2q* (*q* is measured relative to the outward panel normal). Each input aperture combines with an output aperture (of width *a'*) that uniformly distributes exiting illumination into the region between q_1' and q_2' (relative to the inward panel normal).

Integrating the infinitesimal étendue (Equation 3.2) across the input aperture gives the two-dimensional input étendue as

$$\int_{-q}^{q}\int_{-a/2}^{a/2} dy.dM = 2a\sin q \qquad \textbf{Equation 3.16}$$

The two-dimensional output étendue is

$$\int_{q_1'}^{q_2'}\int_{-a'/2}^{a'/2} dy'.dM' = a'\left(\sin q_2' - \sin q_1'\right) \qquad \textbf{Equation 3.17}$$

Finally, the input and output étendues are equated to provide the ratio of input to output aperture widths.

$$\frac{a}{a'} = \frac{\sin q_2' - \sin q_1'}{2\sin q}$$ **Equation 3.18**

This analysis has assumed that light is uniformly incident and uniformly output over all allowed directions at all positions within the two apertures. As described in section 3.1.2, this condition provides maximum control over exiting illumination. A device satisfying Equation 3.18 will be an ideal two-dimensional collimator, simultaneously satisfying requirements 2, 3 and 4 above. To achieve maximum light collection, q is set to $p/2$, providing the final expression for the ratio of aperture widths,

$$\frac{a}{a'} = \frac{1}{2}\left(\sin q_2' - \sin q_1'\right)$$ **Equation 3.19**

If $q_1'=0$ and $q_2'=p/2$, Equation 3.19 reduces to Equation 3.10, and the device is the same as that illustrated in Figure 3.3. Section 3.3.3 shows that the micro-light guiding shade panel satisfies Equation 3.19, and all of the requirements set out above.

3.3 The Micro-Light Guiding Shade Panel

The micro-light guiding shade panel comprises several 'micro-light guiding shade' elements contained in one thin panel (Figure 3.9).

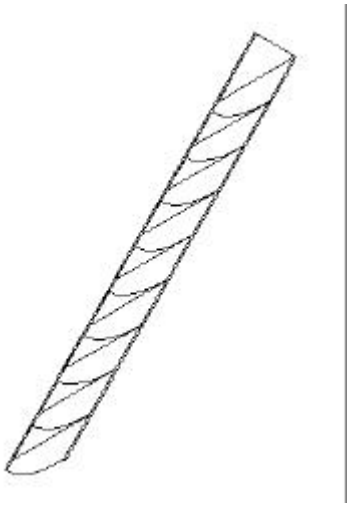

Figure 3.9 - The Micro-Light Guiding Shade Panel Comprises Several Micro-Reflecting Elements

3.3.1 DESIGN

The design of the micro-light guiding shade elements is based on the edge-ray principle of non-imaging optics (section 3.1.7). In order to achieve ideal concentration or collimation, all rays incident from extreme input directions must pass through the edges of the opposite aperture.

The elements of the micro-light guiding shade panel are essentially two-dimensional (trough-like) light collimators. Since an ideal collimator is an ideal concentrator in reverse, the micro-light guiding shade elements are designed as ideal concentrators. The collimator's output aperture then forms the concentrator's collection aperture, and *vice-versa*.

The design of a micro-light guiding shade element is described below and illustrated in Figure 3.10. The panel is tilted through angle b from vertical. Light is collected by the concentrator (output by the collimator) in the angular range from g to q above horizontal (negative angles imply below horizontal). The collimator's collection aperture (concentrator's output aperture) forms a plane OA of width a tilted at angle b from vertical. Rays incident from the lower extreme g of the concentrator's acceptance region (lower extreme of the collimator's output region) focus on the lower edge A of the aperture OA. This requires a parabolic section OD passing through O, with focus A, and axis parallel to the direction g. Similarly, rays incident from the upper extreme q of the concentrator's acceptance region (upper extreme of the collimator's output region) focus on the upper edge O of the aperture OA. This requires a parabolic section AB passing through A, with focus O, and axis parallel to the direction q.

For maximum control over delivered illumination, the collimator's output aperture must be sufficiently large (section 3.1.3). This is achieved by setting the extents of the parabolic sections OD and AB. The parabolic section OD extends to D, located in direction q from A. The parabolic section AB extends to B, located in direction g from O.

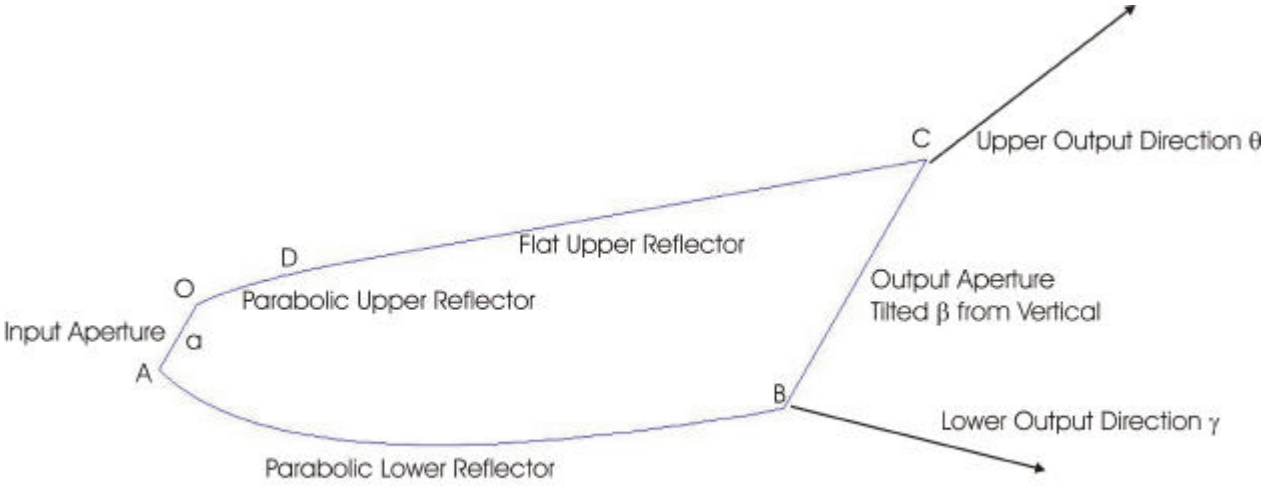

Figure 3.10 - Design of the Micro-Light Guiding Shade Element, $q+b<p/2$

There are two further constraints on this design. The first of these is concerned with rays entering the collimator at grazing incidence near to O. It is possible for these rays to be reflected back out of the aperture OA by the reflector AB. This can happen where $q+b>p/2$. To avoid this, a circular arc reflector AE is inserted, with centre O, radius of curvature a, extending through angle $q+b-p/2$ (Figure 3.11). The lower parabolic section EB passes through E, with focus O, and axis parallel to the direction q.

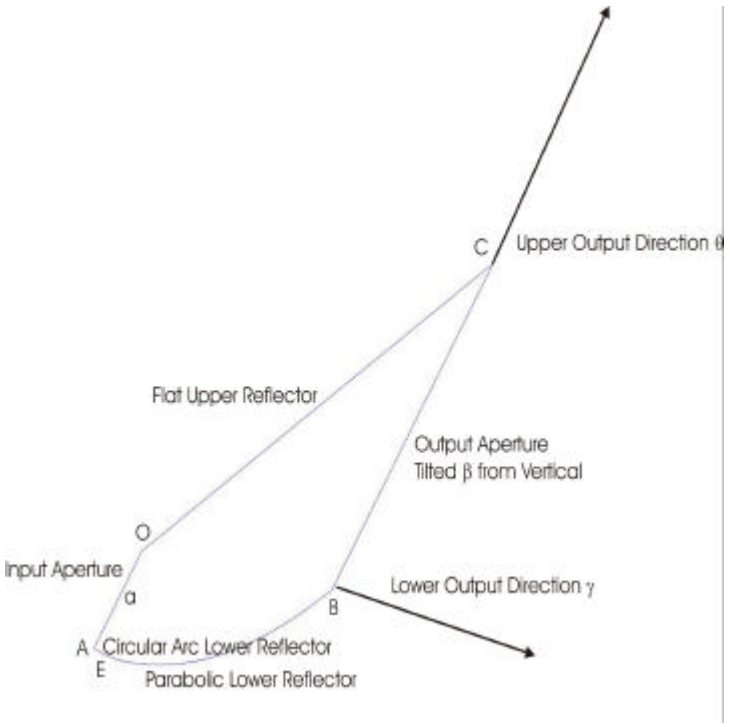

Figure 3.11 - Micro-Light Guiding Shade Element with Circular Arc Lower Reflector, $q+b>p/2$

The second constraint involves the upper parabolic reflector OD. As shown in Figure 3.11, where $q+b>p/2$, point D is located outside the panel. For this design, no parabolic section OD is required.

The micro-light guiding shade panel comprises several of these micro-reflecting elements, assuming the form of a conventional tilted shading panel. To make this possible, the output apertures BC of the micro-reflecting elements must be parallel to the input apertures OA. Thus, a flat upper surface DC (or OC) is introduced. Point C is located above point B, in the direction b from vertical. This surface DC (or OC) is a flat sheet at angle $(q+g)/2$ above horizontal. Any rays intercepting DC (OC) travelling in direction q are reflected into the direction g. All other rays hitting DC (OC) are reflected into directions between g and q. Thus, adding this flat sheet to the micro-light guiding shade element does not violate its nominal output range g to q. Since the parabolic section AB (or EB) also has the slope $(q+g)/2$ at B, adjacent elements fit together in an ideal packing arrangement (Figure 3.9).

There are three versions of the micro-light guiding shade elements. These three forms are distinguished by the sum $q+b$, as shown in Figures 3.10 to 3.12. The three designs are described below.

The first case is shown in Figure 3.10, and occurs where $q+b<p/2$. The input aperture OA has width a and is tilted b from vertical. The lower parabolic section AB passes through A, with focus O, axis parallel to direction q, extending to B at direction g from O. The upper parabolic section OD passes through O, with focus A, axis parallel to direction g, extending to D at direction q from A. The upper flat reflector DC passes through D in direction parallel to $(q+g)/2$, extending to C at direction b from vertical above B.

The second case occurs where $q+b>p/2$ (Figure 3.11). As above, the input aperture OA has width a and is tilted b from vertical. A circular arc AE passes through A, with centre O and included angle $q+b-p/2$. The lower parabolic

section EB passes through E, with focus O, vertex E, axis parallel to direction q, extending to B at direction g from O. No upper parabolic section is required. The upper flat reflector OC passes through O in direction parallel to $(q+g)/2$, extending to C at direction b from vertical above B.

The final special case occurs where $q+b=p/2$ (Figure 3.12). Again, the input aperture OA has width a and is tilted b from vertical. No circular arc nor upper parabolic section are required. The lower parabolic section AB passes through A, with focus O, vertex A, axis parallel to direction q, extending to B at direction g from O. The upper flat reflector OC passes through O in direction parallel to $(q+g)/2$, extending to C at direction b from vertical above B.

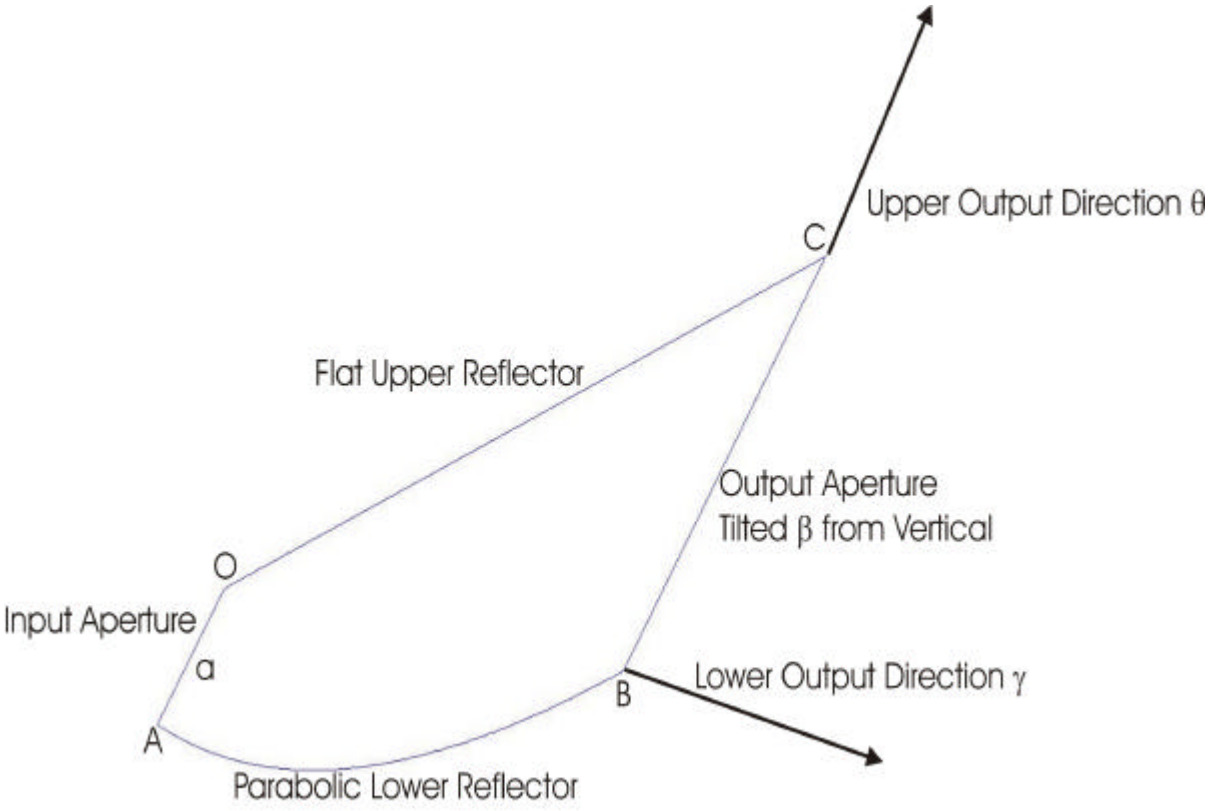

Figure 3.12 - Micro-Light Guiding Shade Element, $q+b=p/2$

3.3.2 RAYTRACING THROUGH THE DEVICE

To show that device works as required, the following section describes some basic raytracing through a micro-light guiding shade element. The rays are illustrated in Figure 3.13 (colour coded, for the special case $q+b=p/2$). All rays shown in Figure 3.13 are in the plane of the diagram. However, as the micro-

reflecting elements are trough-like in form, there are no reflector elements with normal components in directions orthogonal to the plane of the diagram. Therefore, components of any incident rays orthogonal to the plane of the diagram will not be affected by interaction with the reflector elements. Thus, the two-dimensional raytracing described below includes all three-dimensional incident rays.

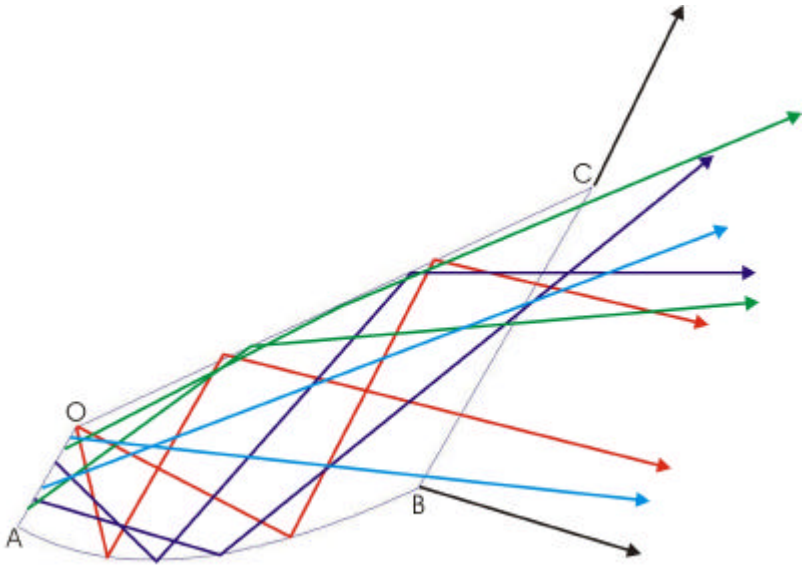

Figure 3.13 - Raytracing within a Micro-Light Guiding Shade Element

Rays from point O incident upon the circular arc AE are reflected directly back to O. From there they are reflected in other directions that are discussed below.

Rays from point O incident upon the parabolic section AB (or EB) (red in Figure 3.13) are reflected parallel to the q direction. None of these rays will subsequently hit OA, AE, OD nor AB. Some of these rays (all rays where $q+b^3p/2$) may hit DC (or OC) . The remaining rays will exit the aperture BC in direction q. All rays that hit DC (OC) will be reflected parallel to the g direction. None of these rays will again hit any other surface, and all will exit BC in direction g.

Rays from point A incident upon the upper parabolic section OD reflect parallel to the g direction. None of these rays will subsequently hit any other surface, and all will exit BC in direction g.

Rays from aperture OA (excluding point O) incident upon the circular arc AE reflect into directions between $p/2-q$ below horizontal and q above horizontal. These rays pass through the imaginary surface OE. Their further progression is covered below.

Rays from aperture OA or imaginary surface OE (excluding point O) incident upon the lower parabolic section AB (purple in Figure 3.13) reflect into directions below q. These rays cannot then hit OA, OD nor AE. Some reflected rays may hit AB again. Some reflected rays may also hit the flat upper reflector OC (or DC). All rays reflected off AB and OC (DC) reflect into directions between g and q. Thus, all rays exit aperture BC in directions between g and q.

Rays from aperture OA (excluding point A) incident upon the upper parabolic reflector OD reflect into directions above g. These rays cannot then hit OA nor AB. Some rays may hit OD again, or DC. No ray can reflect into directions below g. Thus, all rays exit aperture BC in directions between g and q.

Rays from aperture OA or imaginary surface OE incident upon the flat upper reflector OC (or DC) (green in Figure 3.13) reflect into directions between g and q. These rays cannot subsequently hit any other surface, and all exit aperture BC in directions between g and q.

Rays from aperture OA directly incident upon aperture BC (blue in Figure 3.13) will exit into directions between g and q.

This simple raytracing exercise shows that all rays passing into the micro-light guiding shade elements exit the device within the nominal output range of directions g to q. This is valid for rays incident from all three-dimensional directions.

3.3.3 AN IDEAL DEVICE

When several elements stack upon each other in the micro-light guiding shade panel, adjacent points B and C become coincident (Figure 3.14). Thus, the separation of adjacent elements, along the length of the panel, is the width BC. No light incident upon the panel between adjacent input apertures can enter the device. Thus, the fraction of light accepted by the device is the ratio of lengths AO and BC,

$$Accepted\_Fraction = \frac{|AO|}{|BC|} \qquad \textbf{Equation 3.20}$$

This fraction is equivalent to the ratio of input and output apertures a/a' discussed in section 3.1.3. If this ratio is equal to that shown in Equation 3.19, the micro-light guiding shade elements are ideal light collimators, giving maximum light throughput and control over exiting illumination.
Given the geometrical descriptions of the micro-light guiding shade elements above, it is possible to calculate this ratio. Where $q+b \le p/2$, the ratio of aperture widths is

$$\frac{a}{a'} = \frac{1}{2}\left[\sin(b+q) - \sin(b+g)\right] \qquad \textbf{Equation 3.21}$$

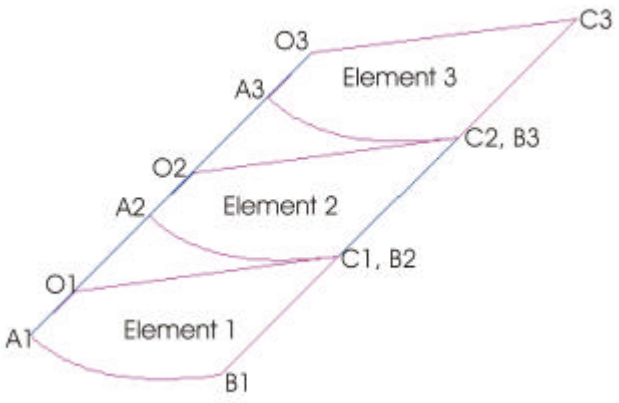

Figure 3.14 - Stacking Adjacent Micro-Light Guiding Shade Elements

A comparison of Figures 3.8, 3.11 and 3.12 shows that $q_2'=b+q$ and $q_1'=b+g$. Thus, Equation 3.21 is identical to Equation 3.19. Thus, these micro-light guiding shade elements are ideal trough-like collimators. The ratio of aperture widths for a design in which $q+b<p/2$ is always less than that shown above. Thus, these designs are not ideal, but can be close to ideal. It should be noted that it is not meaningful for a panel to be created for which $q+b>p/2$. Since the panel is tilted through angle b from vertical, the highest direction into which it can cast illumination is $p/2-b$ above the horizontal. Thus, the most efficient form of device is that for which $q+b=p/2$. This is further demonstrated in the next chapter.

3.3.4 IMPLEMENTATION

Sections of two micro-light guiding shade panels are illustrated in Figure 3.15. Figure 3.15a's panel is tilted through 45° (b=45°), with light exiting the device between directions 30° below and 45° above horizontal (g=-30°, q=45°). Figure 3.15b shows a vertical panel (b=0) with light output from horizontal up to 90° above horizontal (g=0, q=90°). This latter design can be incorporated into clerestory windows and combined with light shelves. This combination substantially improves luminous throughput and provides shading and an unimpeded view through the lower window. This latter design formed the first full-scale implementation of the micro-light guiding shade panel, and is discussed further in Chapter 5.

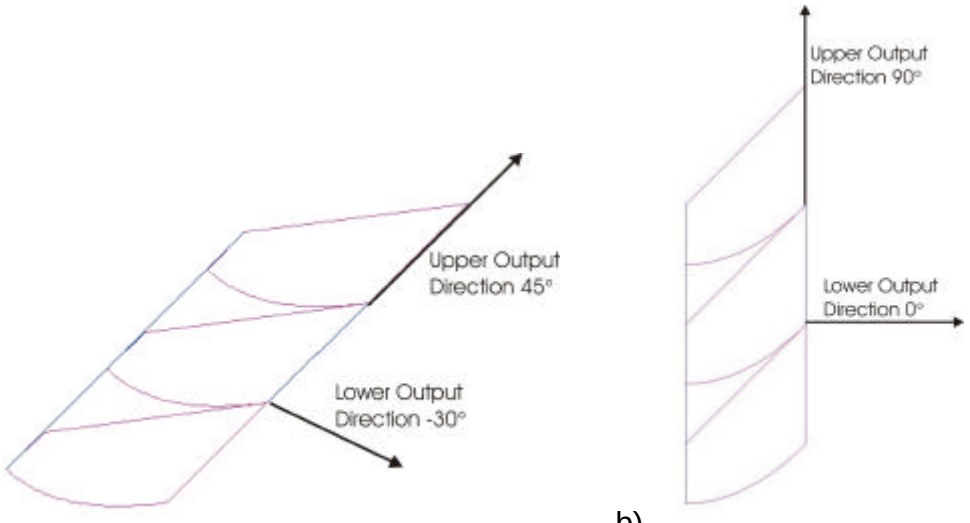

a) b)

Figure 3.15 - Sections of Two Micro-Light Guiding Shade Panels: a) Tilted through 45°; b) Vertical Orientation

The outer surface of the micro-light guiding shade panel comprises a large sheet of translucent material, diffusing all light transmitted into the device. In this way, the spatial light output distribution of the panel does not vary with external conditions. The inner surface is covered by transparent sheeting to avoid degradation of the reflecting surfaces by rain and insects.

The action of the micro-light guiding shade panel is shown in Figure 3.16. Sunlight is incident from the left. The diffusing input aperture admits a fraction of the incident sunlight. This illumination is diffused upon transmission and passes into the device. The diffused light interacts with the reflectors to exit the device within the specified output angular range. Transmitted light is distributed across the ceiling, and from there reflected as comfortable diffuse illumination. Since the device's output angular range is controlled by its design, no light is directed downwards into the eyes of occupants. This evades the possibility of disability or discomfort glare caused by the device. The lower limit of the output angular range should generally be the horizontal direction.

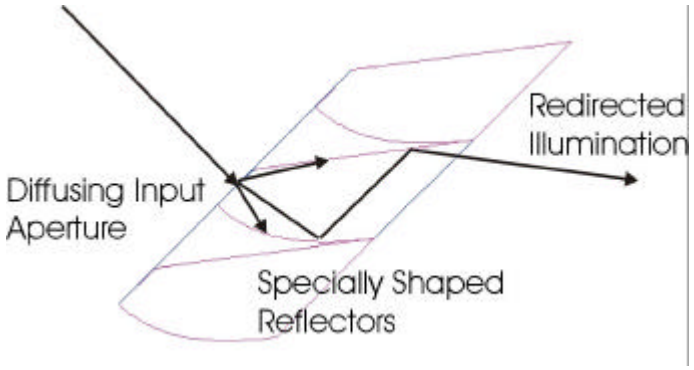

Figure 3.16 - Action of the Micro-Light Guiding Shade Panel

Figure 3.9 shows a section through a complete panel, comprised of several micro-light guiding shade elements. The panel may be installed onto buildings in the same manner as conventional shade panels, having similar size, thickness and outward appearance. The micro-light guiding shade panel, however, both shades the façade and distributes daylight deep into the building. As the device looks outwardly the same as existing shades, it will not cause the same concern to architects as the conventional light guiding shade. It will also be more easily installed and maintained. The micro-light guiding shade panel can also be adjusted to suit particular climates and orientations, without drastically changing its outward appearance. Specification of a micro-light

guiding shade panel requires only the panel's thickness, height and tilt from the façade, and the extreme directions g and q. All of these parameters are determined by the building's function and orientation.

3.4 Summary

This chapter began with an introduction to non-imaging optics and the law of conservation of étendue. It was shown that ideal concentrators and collimators have aperture ratios that satisfy equations directly derived from the law of conservation of étendue. An ideal concentrator achieves maximum possible concentration and accepts radiation from all of its nominal acceptance angular range. An ideal collimator achieves maximum control over delivered illumination, and transmits incident illumination from all of its nominal acceptance angular range. Image-forming and non-imaging devices were compared, and it was shown that non-imaging optical devices far better approach ideality. Finally, the edge-ray principle was introduced as a principle by which to design ideal non-imaging optical devices.

The following section outlined the several requirements of a daylighting device mounted on the façade of a sub-tropical high rise office building. It was shown that, if the micro-light guiding shade panel could achieve ideality, it would satisfy all of the listed requirements. An equation was derived against which the micro-light guiding shade panel could be compared.

Finally, the micro-light guiding shade panel was introduced. The edge-ray principle was applied to its design, and a raytracing exercise demonstrated the resulting device working as desired. The ratio of its input and output apertures was then shown to be equal to that derived in section 3.2.1. This revealed that the version of the micro-light guiding shade panel where $q+b=p/2$ is indeed an ideal collimator. Thus, the micro-light guiding shade panel achieves all of the requirements set out for a daylighting device installed on the façade of a high rise sub-tropical office building. Implementation of the micro-light guiding shade panel was then discussed, with some examples.

3.5 Conclusions

- Application of non-imaging optics to daylighting provides highly efficient devices with optimal control over delivered illumination.
- The micro-light guiding shade panel is an ideal collimator, theoretically meeting all the requirements of a daylighting device for sub-tropical high rise office buildings.

CHAPTER 4 - INITIAL INVESTIGATIONS

At the early stages of investigating the micro-light guiding shade panel, it was important to gain a better understanding of its performance. This involved ensuring that the devices direct light into the desired output angular range. Once this was established, further investigations aimed to specify the most appropriate design for each project. RADIANCE simulations aimed to validate the simulation program and to optimise the design.

4.1 SCALE MODEL MEASUREMENTS

The micro-light guiding shade panel is designed to direct light between two nominal output directions. The lower of these directions is horizontal so that light passed into the room is not directed into the eyes of occupants. To ensure that the devices work as desired, three early prototype devices were constructed and their luminous output distributions measured.

4.1.1 MEASURED DEVICES

The first device measured was a light guiding shade. As described in Chapter 1, this was the predecessor of the micro-light guiding shade panel. It is essentially a larger version of a single micro-light guiding shade element (Figure 1.2). A scale model of the device was created, a fluorescent light tube was fixed over the input aperture, and the assembly was mounted in a photogoniometer. The light source (Mirabella F15 T8 cool white fluorescent tube, 18 inches long) was well covered so that any light delivered by the combination passed through the light guiding shade. The device was rotated in the photogoniometer and its output luminous intensity was measured. The nominal range of luminous output directions for this device was 0 to 70°, where 0° represents horizontal.

The two other measured prototypes were micro-light guiding shade panels. The two devices differed in design, with intended luminous output ranges of 0 to 90° and -30 to 45° (Figure 3.15). These represent quite distinct design variations, with one mounted vertically within the window and the other tilted 45° out from the window. The former device (0 to 90°) is described in more detail in

Chapter 5. The latter device (-30 to 45°) delivers illumination into directions below horizontal. Measurement of light directed below the horizontal could assess the possibility of glare caused by this design.

The initial prototype micro-light guiding shade panels were constructed from several reflecting elements, joined with frame elements, contained within acrylic sheeting and an outer wood frame (Figure 4.1). The reflecting elements comprised shaped polystyrene, coated with reflective sisallation (aluminium coated paper used in the building trade) (Figure 4.2). The desired shape of the polystyrene elements was obtained by computer-controlled, hot-wire cutting. Frame elements were created in the same fashion. The translucent input sheets were created by sanding down the clear acrylic sheets with an orbital sander. The translucent sheets were created in this way as opalescent sheeting was judged to be less transmissive than desired.

Figure 4.1 - Initial Prototype Micro-Light Guiding Shade Panel

Figure 4.2 - Polystyrene Reflecting Element

The constructed devices were attached to a radiography light box (of diffuse light output distribution) and placed on a rotating table marked with angular measurements (Figure 4.3). The edges of the light source were shielded so that all measured illumination passed through the micro-light guiding shade panels. An illuminance meter was placed at a distance from the rotating table, with a black cardboard collimating cone in front of its measuring head (Figure 4.4). The collimator excluded light reflected off nearby surfaces and measured only the light delivered by the micro-light guiding shade panel. The rotating table was turned through various angles and the device's luminous output was measured at each angle (at 5° increments).

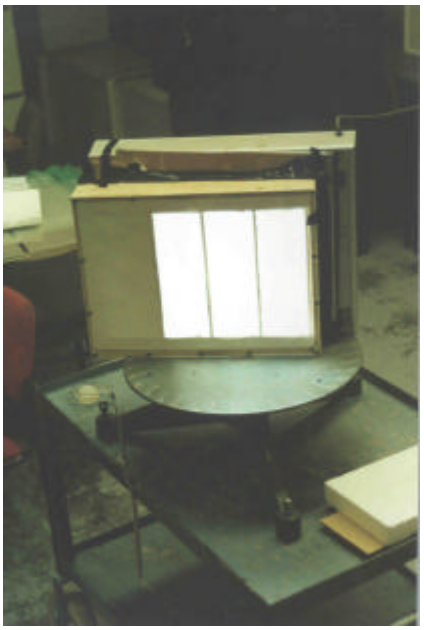

Figure 4.3 - Micro-Light Guiding Shade Panel Mounted on Rotating Table

Figure 4.4 - Measuring the Light Output of a Micro-Light Guiding Shade Panel

4.1.2 MEASUREMENT RESULTS

Figure 4.5 shows the luminous output distribution of the photogoniometer mounted light guiding shade. This presents the distribution of luminous intensity (units: candela) exiting the light guiding shade, within the vertical plane containing the normal to the output aperture. Recall that the design range of this device's luminous output was horizontal to 70°. Nearly uniform luminance (units: candela/m^2) is delivered to the range 10 to 70°. Very little illumination exits the device in directions below horizontal or above 70°. Luminous intensity distributions in lateral planes reveal equal luminance sent in all lateral directions.

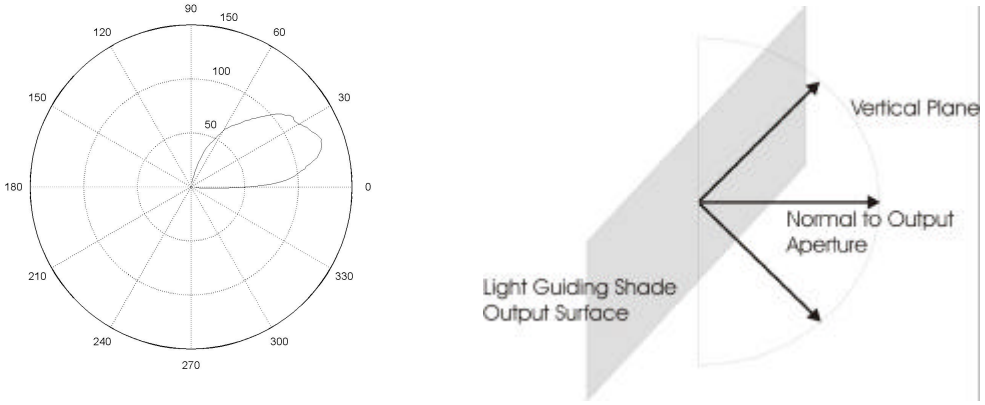

Figure 4.5 - Vertical Light Output Distribution of the Light Guiding Shade

The vertical luminous intensity output distributions of the two prototype micro-light guiding shade panels are shown in Figure 4.6. Both devices distributed illumination largely within their nominal output angular ranges. For both devices, however, there was some light spillage below the lower nominal direction. Both devices also displayed near uniform luminance output in lateral directions. The 45° tilted panel could not be used on a building's façade, as too much illumination would be redirected into the eyes of occupants, causing excessive glare.

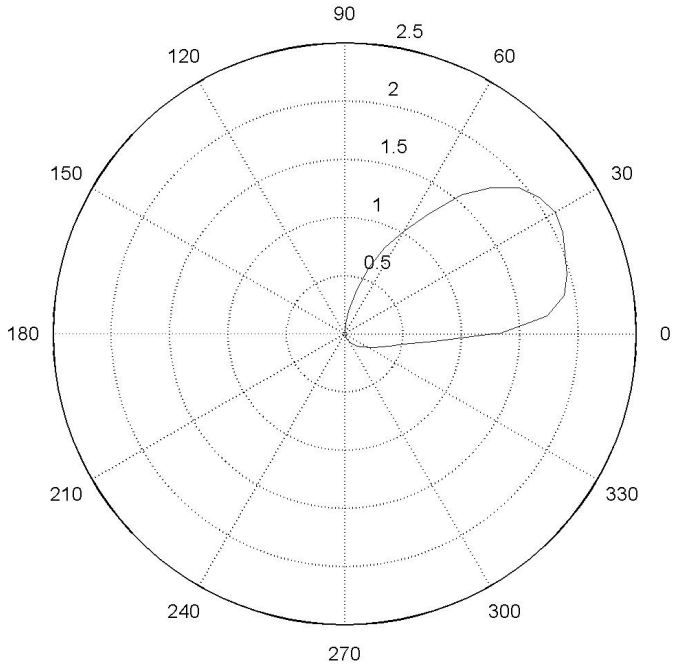

a)

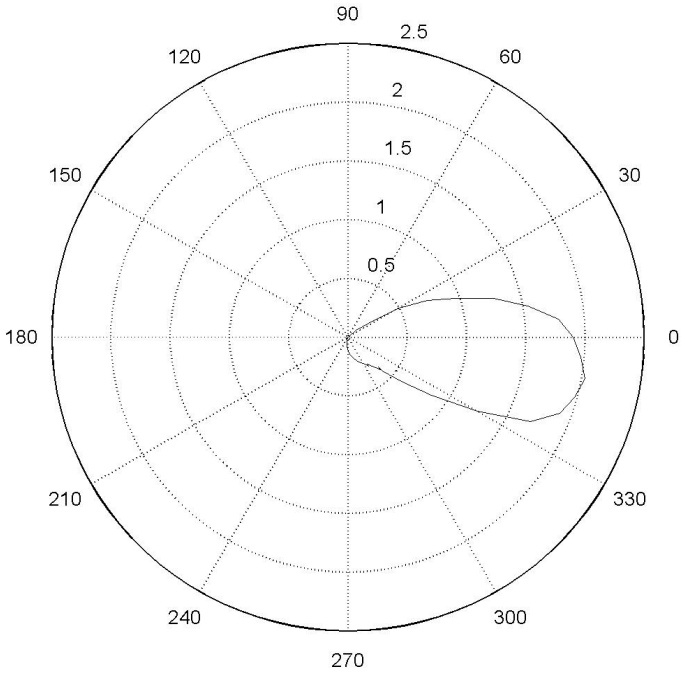

b)

Figure 4.6 - Luminous Intensity Outputs of Micro-Light Guiding Shade Panels: a) Vertical Panel; b) 45° Tilted Panel

4.1.3 SUMMARY

The constructed devices provide luminous output distributions that agree closely with expectation. Some light was spilt below the devices' nominal lower boundaries. This could be caused by imperfect manufacture of the devices, or imperfect specular reflection off the sisallation. However, at this early stage, the agreement between theory and measurement was satisfactory.

4.2 AUTOMATING AND INVESTIGATING DIFFERENT DESIGNS

Scale model measurements revealed the micro-light guiding shade panel performing as expected. Theoretical examinations followed to improve design and optimise devices for each situation. Examinations were completed using Matlab. Some of the developed scripts are displayed in Appendix 1.

4.2.1 GEOMETRY GENERATION

The creation of panel geometry was automated by script *lgs2.m* (Appendix 1). Panel thickness *w*, tilt b and nominal output directions g and q (Figure 3.10) are entered into the program, and a section of a panel is displayed. Numerous parameters of interest are also calculated for each design. These include the portion of panel surface available to collect illumination, calculated using Equation 3.20. The length of reflecting material required to manufacture a micro-light guiding shade element is also calculated. Coordinates generated by this program could be exported to dxf-format models, where these are required for manufacturing purposes.

4.2.2 PANEL PERFORMANCE PARAMETERS

The ability of the micro-light guiding shade panel to naturally illuminate an office space is largely determined by the area presented for light collection. Matlab script *lgs3.m* (Appendix 1) examined variations in panel throughput with input parameters b, g and q. Figure 4.7 shows panel throughput variation for a panel tilt b=30°. The script also calculates the total length of reflective material required to manufacture a micro-light guiding shade panel. Numerous applications of this script provided the following findings:

- For each panel tilt b, there is an upper direction q that provides maximum throughput. This optimal q is independent of the lower direction g.
- Throughput increases as the lower direction g gets lower (becomes more negative).
- The length of material required per micro-light guiding shade element is greater for larger q and more negative g. However, the total length of reflecting material required is less for larger q and more negative g.

- The previous result occurs because fewer micro-light guiding shade elements are required for larger q and more negative g.
- Changes in g do not strongly affect reflecting material requirements and the number of required elements in a panel.

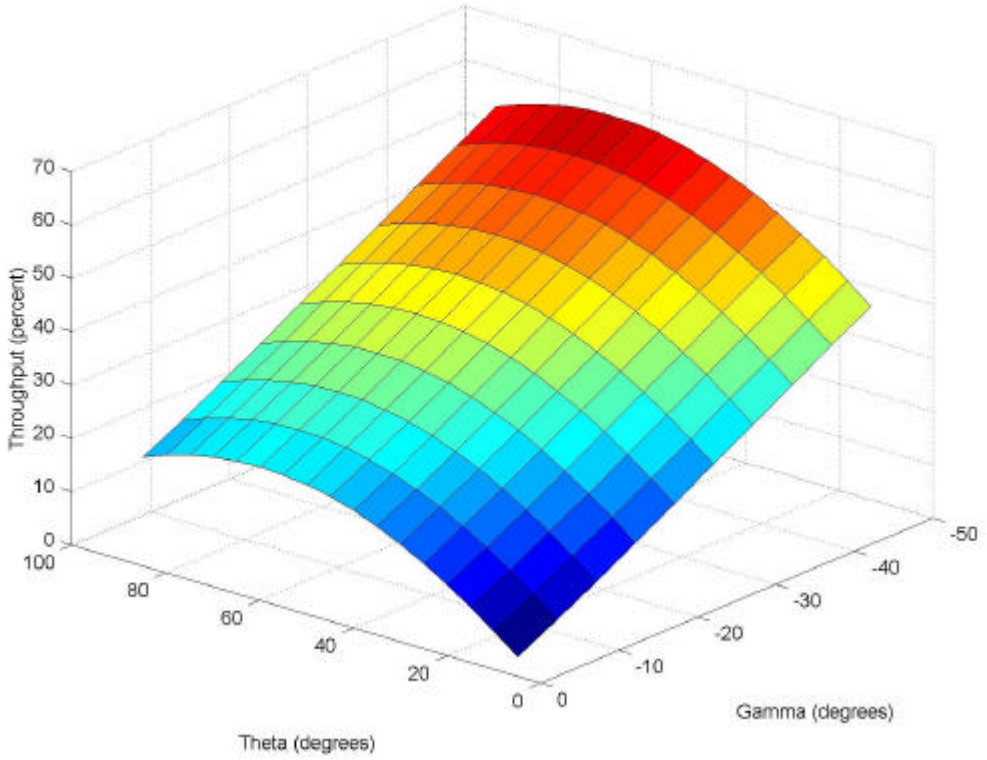

Figure 4.7 - Percentage Throughput for a Micro-Light Guiding Shade Panel of Tilt 30°

The optimum upper limit q is equal to the complement of the panel tilt angle b,

$$q_{optimum} = 90° - b \qquad \textbf{Equation 4.1}$$

If q takes this value, panel throughput is maximised, fewer micro-light guiding shade elements are required, and the total length of reflecting material is reduced. This design also requires no upper parabola and no lower circular arc (Figure 3.12), simplifying manufacture. This value of q is its greatest realistic setting. Light leaving the panel in this direction travels parallel to the panel's output surface. It is not possible for light to leave the panel at a greater vertical angle. The Matlab script *lgs4.m* (Appendix 1) designs this optimal panel, given parameters b, g and w.

4.2.3 PANEL TILT

For any panel tilt b, the upper limit q is optimised using Equation 4.1. However, what is the optimal panel tilt? As tilt decreases, panel throughput increases. However, as panel tilt decreases, so does solar shading ability. Also, the panel presents a greater incidence angle to high elevation sunlight, thus collecting less illumination. Therefore, optimal panel tilt is a complex function of geographic location, orientation, climate, time of day and time of year. Scripts *lgs6.m* and *lgs7.m* (Appendix 1) investigate this problem.

The former script performs calculations over the course of a working day. The program calculates hourly averaged luminous throughput (units: klm) and daily integrated luminous throughput (units: klm hr). This is performed and presented for a range of panel tilts. The program assumes direct sunlight incidence only, and does not account for clouds or sky light.

The latter script, *lgs7.m*, performs calculations over the course of the year, and considers both sunlight attenuation and cloudiness (using sunshine probability factors). Results are presented as a function of panel tilt b, for any combination of g and orientation. The peak of this function reveals the panel tilt that provides maximum luminous throughput throughout the working year.
Two conclusions were drawn from these investigations:

- Luminous throughput is generally improved for panel tilts less than 30°. This depends on orientation and lower direction g.
- Maximum luminous throughput over working hours is achieved for façades oriented between north and west (sub-tropical, southern hemisphere).

4.2.4 APPLICATION

The above findings were applied to the design of the prototype micro-light guiding shade panels of section 4.1.1. It was determined to test one vertical device (b=0) and one panel tilted through b=45°. One device was to be given a horizontal lower limit (g=0). The other panel was given g=-30°. Four design options were entered into script *lgs4.m* (Appendix 1). Results are displayed in Table 4.1. The panels have thickness w=80mm, and length 1200mm.

Table 4.1: Four Design Alternatives for Prototype Micro-Light Guiding Shade Panels

Tilt b (degrees)	0	0	45	45
Upper limit q (degrees)	90	90	45	45
Lower limit g (degrees)	0	-30	0	-30
Aperture width *a* (mm)	40	69	16.6	30.7
Percentage throughput	50	75	15	37
Number of elements	15	13	10.6	14.5
Total material length (mm)	3074	2294	3610	3337

The first and last of these design options were selected. These designs displayed similar percentage throughputs, making their measured luminous output distributions easier to compare. Displays of the panels' designs showed that the third option was somewhat awkward to create for a first prototype panel.

4.3 RADIANCE SIMULATION OF THE MICRO-LIGHT GUIDING SHADE PANEL

Intending to accelerate optimisation of the micro-light guiding shade panel, it was desired to perform accurate lighting simulations of the device. If simulations could achieve repeatable and realistic predictions of parameters of interest (eg. illuminance, luminance, luminous intensity), the need for time- and cost-consuming experimental work could be reduced substantially. The first step in this process was to ensure that simulation results compare well with experimental data.

In the first set of validations, RADIANCE simulated luminous output distributions were compared with the measurements described in section 4.1.2 above. Comparisons were only made of the *relative* light output distributions of the micro-light guiding shade panel prototypes, and not of their magnitude. Direct comparisons between experiment and simulation were completed for the light guiding shade measured in the photogoniometer.

4.3.1 LIGHT GUIDING SHADE IN THE PHOTOGONIOMETER

A RADIANCE model was created of the light guiding shade measured in the photogoniometer. This involved a flat upper reflector, a curved lower reflector, a flat translucent input aperture and a light source. The material properties of the light guiding shade components were measured as described in Chapter 6. RADIANCE materials were created to match these measured properties. The geometry of the light guiding shade surfaces were modelled in a similar fashion to that of the micro-light guiding shade panels, described in Appendix 3. A simulated 18 inch fluorescent tube light source matched that in the measured device.

Angular profiles of luminous throughput were created by determining the luminance (units: candela/m^2) seen by a set of rays aimed at the device's output from a variety of directions. The process by which this was performed is detailed Chapter 7.

These simulations provided the luminance output from the light guiding shade due to the simulated fluorescent light source at an arbitrary distance from the input aperture. Accordingly, this output distribution was scaled for direct comparison with experimental data. Scaling was applied according to luminous flux incident upon the device's input aperture. The experimental light source was coupled to the light guiding shade's input surface with a highly reflective enclosure. Thus, it was assumed that all light flux leaving the source reached the measured device's input aperture. The luminous flux output of the fluorescent tube was obtained by contacting the lamp manufacturer and comparing with standard tables, giving F_m=960 lm. The simulated luminous flux incident on the input aperture was F_s=23.9 lm. Scaled, simulated luminances were converted to luminous intensity (units: candela) for comparison with experimental measurements. This was performed by multiplying the predicted area-averaged luminance by the projected area of the output surface.

The results of this scaling process are displayed in Figure 4.8, along with the corresponding measurements (from Figure 4.5). This presents luminous intensities exiting the light guiding shade in the vertical plane containing the

normal to the output aperture (Figure 4.5). Luminance is almost constant in the range 13 to 60°. Some light is spilt below horizontal (to around -13°), and some is spilt above 70° (to around 78 degrees). That light spilt below horizontal accounts for the reduced luminous intensity in the angular range 0 to 13° above horizontal. Thus, light spilt beyond the boundaries of the light guiding shade's output angular range (0 to 70°) is that which is missing from within the boundaries. This is caused by the simulated roughness added to the reflector material. This roughness was added to account for imperfections in reflector material and geometry. Further description of simulated roughness is found in section 4.3.4.

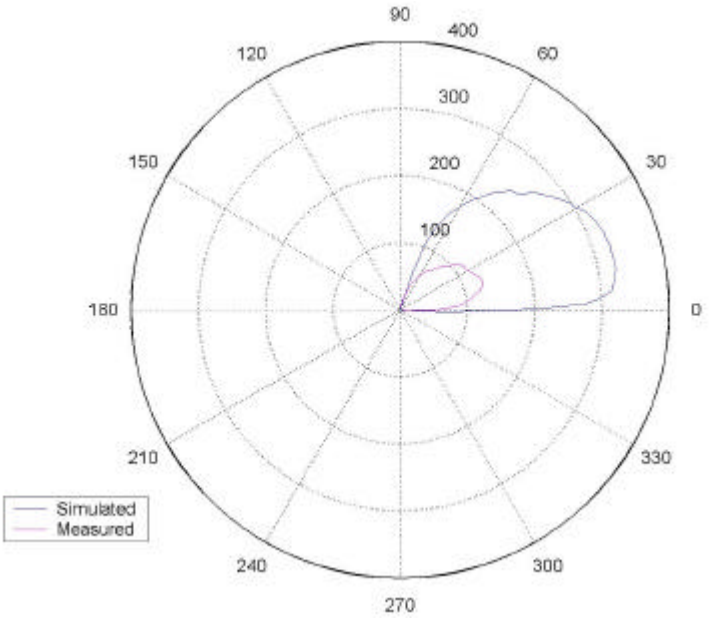

Figure 4.8 - Simulated Light Output Distribution of the Light Guiding Shade

It is clear in Figure 4.8 that the simulated luminous output severely over-estimates the measured distribution. What is the cause of this large discrepancy? Recall that it was assumed that all light emitted by the experimental light source was incident on the input of the light guiding shade. The simulated luminous intensity output was thus scaled up as though 960 lm, the total lamp light output, were incident. If losses were allowed between the lamp and the input aperture, this scaling factor would be significantly reduced. The overestimation of luminous intensity by the simulation indicates that this assumption was incorrect. A ratio of the measured and simulated distributions could provide an estimate of the efficiency of luminous transfer between the lamp and the aperture. This ratio is shown in Figure 4.9. This reveals a near

constant 30-40% ratio between measurement and simulation in the region 0 to 70°. This indicates around 35% efficiency in luminous flux transfer between the light source and the input of the light guiding shade. Investigation of the measured light guiding shade reveals that this is a plausible figure.

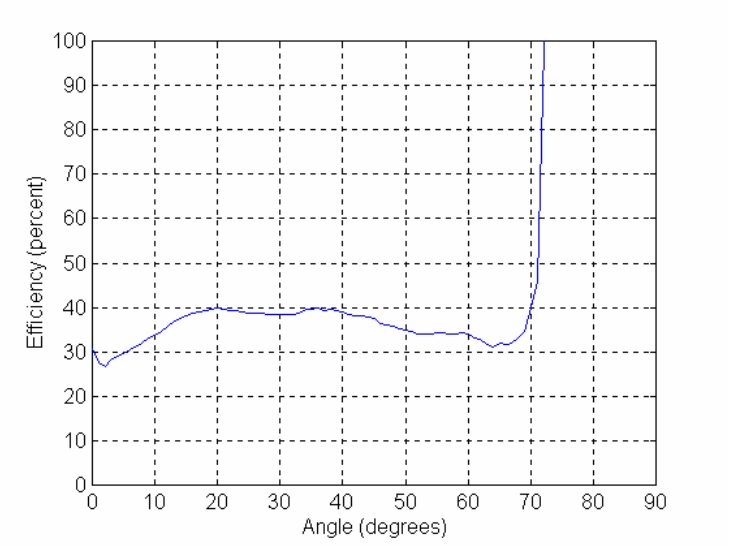

Figure 4.9 - Efficiency of Luminous Transfer between Light Guiding Shade Lamp and Input Aperture

When this factor is considered, the resulting comparison between measurement and simulation is shown in Figure 4.10. This diagram shows excellent agreement, both in magnitude and distribution. A more thorough comparison between the two distributions, using a developed statistical technique, is presented in section 4.3.3.

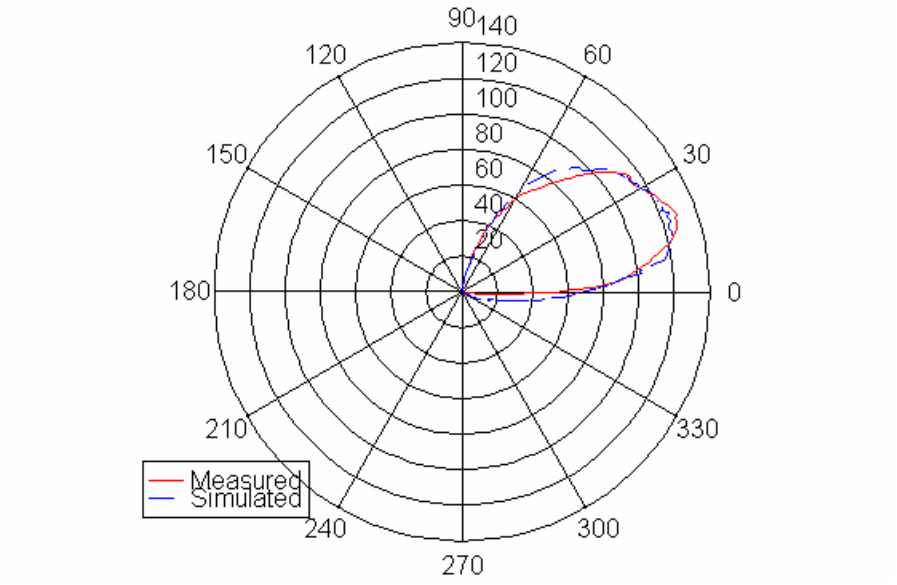

Figure 4.10 - Measured and Simulated Light Output Distribution of the Light Guiding Shade, Considering Efficiency of Luminous Transfer between Light Source and Input Aperture

4.3.2 PROTOTYPE MICRO-LIGHT GUIDING SHADE PANELS

RADIANCE models were also created for the prototype micro-light guiding shade panels. Direct comparisons between experimental and simulated results could not be completed for these panels, due to complex experimental conditions (due to the relatively large size of the prototype panels, their luminous output distributions could not be measured directly in the photogoniometer). However, the *relative* distributions of luminous intensity output could be compared. This was achieved by simply scaling for identical maxima of measured and simulated distributions.

The modelled materials and light source were the same as for the light guiding shade. Only one micro-light guiding shade element was modelled for each panel. As each element within a panel is identical, the total panel output distribution was assumed to be proportional to that from one element. The specially shaped reflecting surfaces were created in RADIANCE using *gensurf*. RADIANCE's *mkillum* pre-processor pre-calculated the devices' luminous outputs. This provided a surface of pre-calculated, area-averaged luminance output distribution. Predictions of luminous output were found using *rlux*. Luminance output distributions were converted to luminous intensities to compare with experimental measurements.

Figure 4.11 displays the scaled comparisons between measurement and simulation for the two prototype micro-light guiding shade panels. Some light was leaked beyond the lower output boundary, with corresponding deficiency in luminous intensity in directions above but near to this direction. This light spillage was largely caused by simulated reflector roughness. Further description of this roughness property is given in section 4.3.4. However, the measured and simulated distributions were very similar. In terms of relative luminous intensity output, there appears to be good agreement between measurement and simulation.

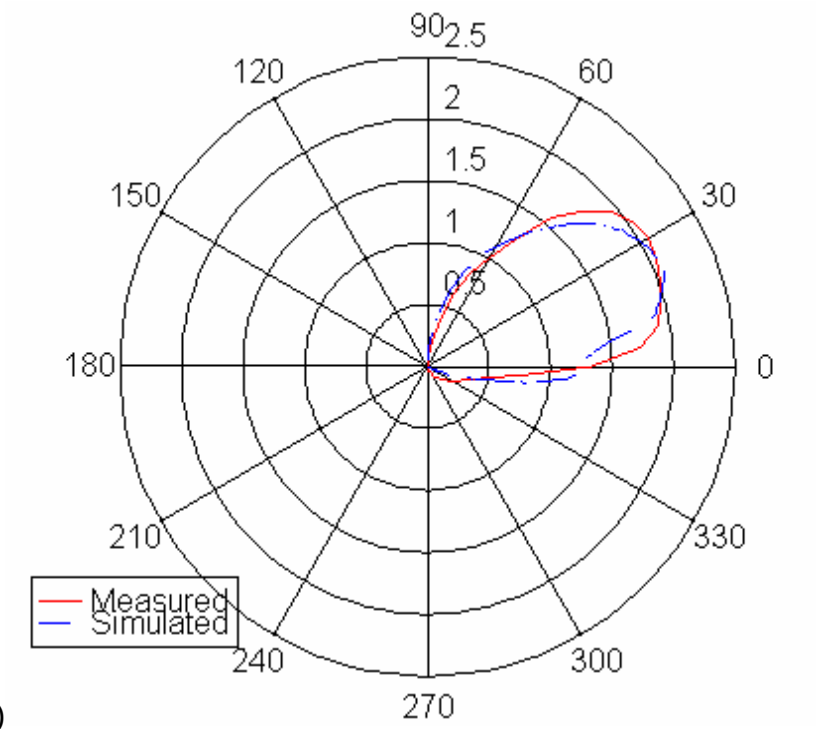

a)

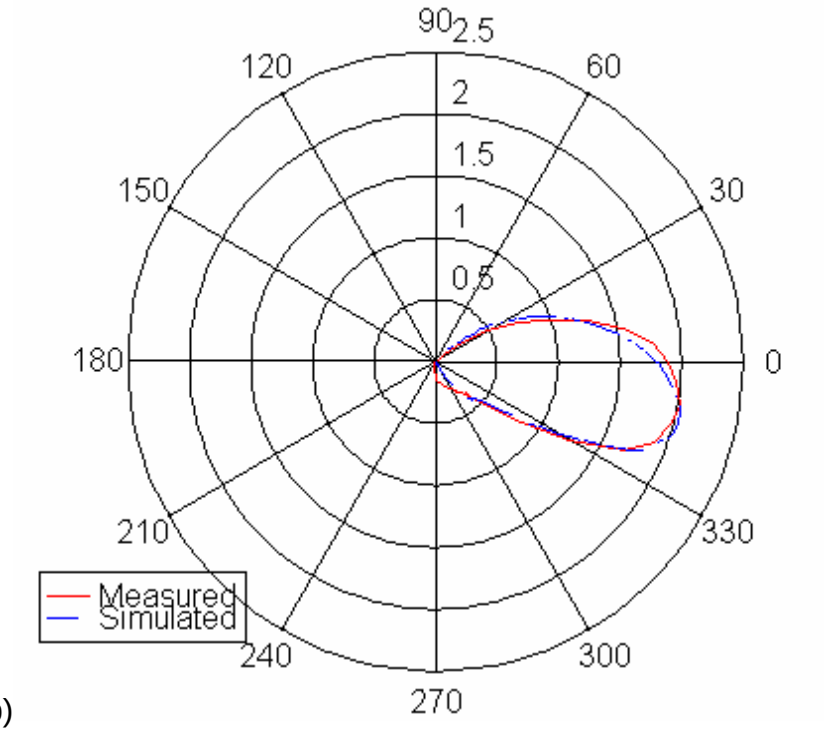

b)

Figure 4.11 - Simulated Light Output Distributions of the Prototype Micro-Light Guiding Shade Panels: a) Vertical Panel; b) Panel Tilt 45°

4.3.3 STATISTICAL COMPARISON OF MEASUREMENT AND SIMULATION

Statistical comparison between measurement and simulation was performed using the test of Bland and Altman (1986). This test graphically displays differences between measured and simulated results. 95% confidence intervals

for the difference and bias (mean difference) are also displayed. Thus, the resulting plot is a graphical representation of bias between experiment and simulation, and clearly demonstrates any disagreement between simulations and measurements. This test can be applied to either absolute or percentage differences between measurement and simulation. The test is further described in Chapter 7.

The Bland and Altman test was applied to the comparison of measured and simulated luminous intensities for the light guiding shade measured in the photogoniometer. The compared data are displayed in Figure 4.8. Measured luminous intensities were rounded to the nearest integer. In the region of vertical output directions below -9° and above 80°, measured luminous intensities were less than or equal to 4 cd. Significant rounding errors can occur in these regions, so these data were disregarded in the comparison. The plot of percentage differences, produced by the Bland and Altman test, is displayed in Figure 4.12. Absolute differences were not examined as the percentage variation better indicated agreement or disagreement. Displayed differences are positive where simulated intensities exceed measured intensities. The data displayed in this chart belongs to one data series, with each point representing the device's luminous output at one angle of output.

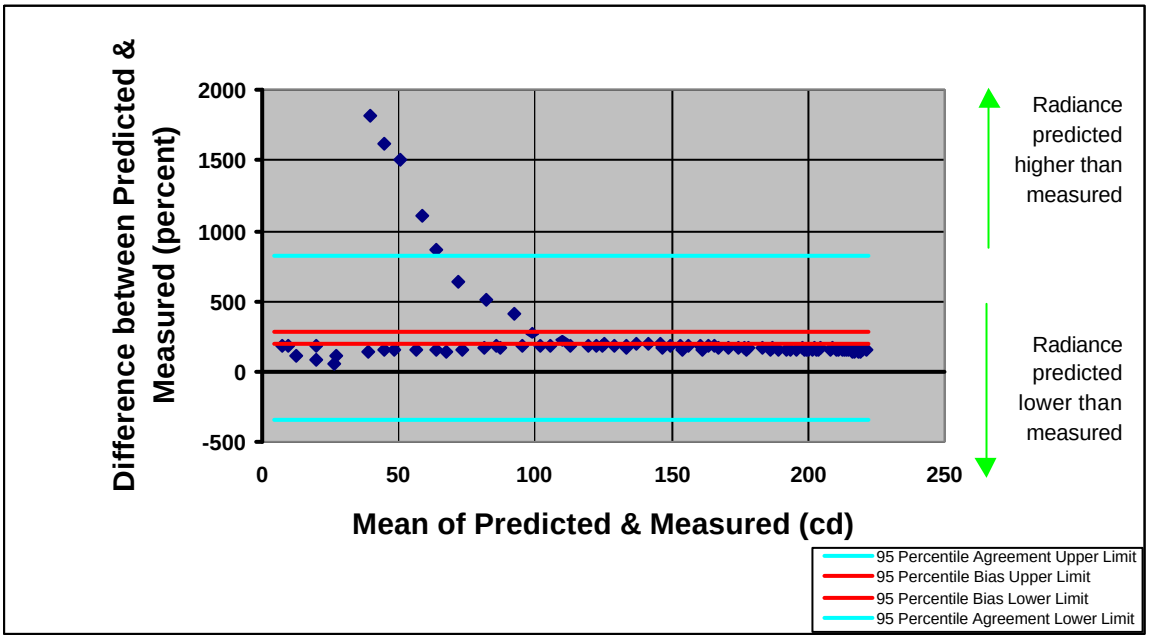

Figure 4.12 - Percentage Differences between Measured and Simulated Luminous Output Distributions for the Light Guiding Shade

The major feature of the percentage difference plot is some very high percentage differences. This range corresponds to vertical output directions between -9 and 0 degrees. Figure 4.13 presents a re-scaled percentage difference plot, showing more clearly the remainder of the data. This shows that the remainder of the data display more uniform percentage differences, varying mainly between 150 and 200%. The vertical output region between 70 and 80° provided more varied percentage differences, ranging between 50 and 190%. The reported bias and range are heavily influenced by the very high differences shown in Figure 4.12.

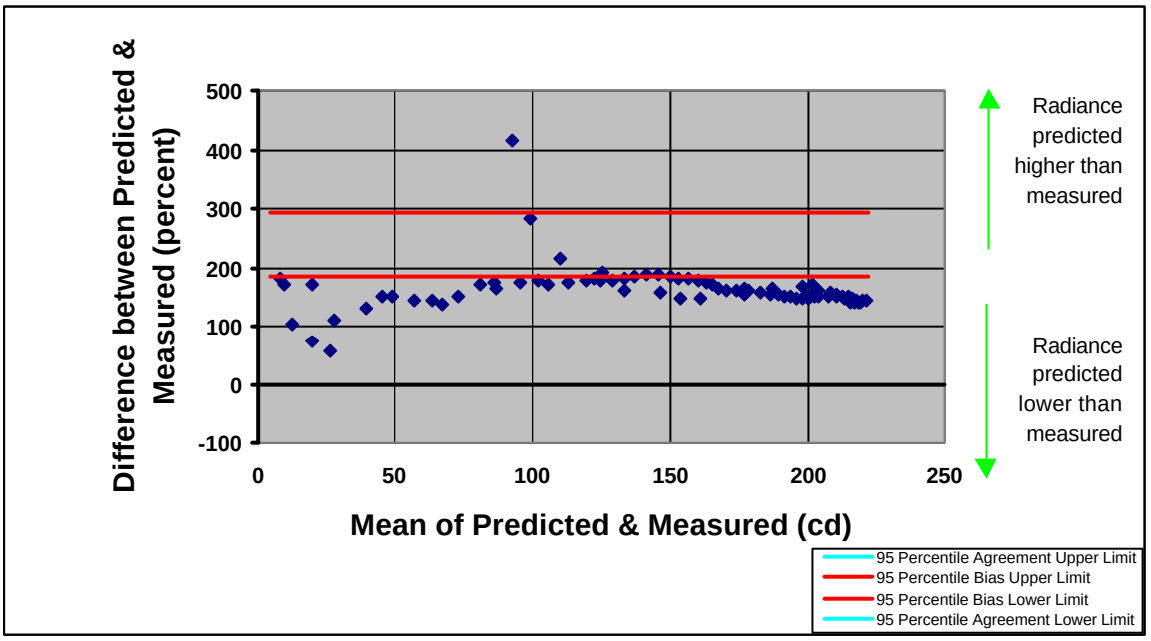

Figure 4.13 - Re-scaled Percentage Difference Plot for Light Guiding Shade

Clearly, there is major disagreement between measurement and simulation in the output region near horizontal. Referring to section 4.3.1, illumination is redirected from the region above the horizontal to the region below the horizontal. This is caused by roughness of the reflector material. If the roughness is overestimated, more illumination is redirected to the region below horizontal, and differences between measurement and simulation in this region are excessive. This roughness specification is revisited in section 4.3.4.

Reported differences in the output angular range 70 to 80° are lower than those in other regions. This indicates either that simulated intensities in this region are reduced, or measured intensities are increased, or both. This contrasts the region below horizontal, where measured intensities were well overestimated.

Light sent into these upper directions is reflected off the lower, curved surface. Thus, unexpected results in this region indicate potential problems with the lower reflector. If the curve was not manufactured as required, more light would be spread into regions above the nominal upper boundary (70°).
Reinvestigation of the measured light guiding shade revealed some bowing of the lower reflector. The centre region of the lower reflector sent light further up than expected. When the bowing was removed, no light was sent into the upper directions. Thus, the reason for the unexpected differences in the range 70 to 80° was the imperfectly formed curved surface.

In the output angular range 0 to 70°, percentage differences were relatively consistent. Simulations clearly overestimated measurements. However, most of the overestimation was by a relatively constant percentage. This supports the argument outlined above regarding efficiency of transfer between the lamp and the light guiding shade's input aperture. In comparing Figures 4.9 and 4.13, an efficiency of luminous transfer between 33 and 40% corresponds to percentage differences between 150 and 200%. When this efficiency is considered, agreement between measurement and simulation in this region is excellent, as shown in Figure 4.10.

4.3.4 REFLECTOR ROUGHNESS

The previous sections have revealed that simulations of the light guiding shade compare favourably with measurements. However, some concern was raised regarding performance in the important region near the lower boundary of output angular range. Incorrectly modelled reflector roughness was suggested as the cause of variation. Roughness is a material parameter that can be added to most material primitives in RADIANCE. Roughness is defined as the RMS slope of surface facets (Ward, 1996; Ward Larson & Shakespeare, 1998). For the material primitive used to model the reflectors (*metal*), suggested roughness values vary from 0 (polished) to 0.5 (roughened).

The simulated light output distributions described in sections 4.3.1 and 4.3.2 were generated with a roughness of 0.1. Increasing roughness to 0.2 introduced excessive noise to the simulated distribution and caused greater

unwanted spillage of illumination. Decreasing reflector roughness to 0 provided sharply peaked luminous output distributions. However, the latter simulated distributions displayed poor agreement with measurement.

A sensitivity study was performed concerning the reflector roughness. Firstly, which RADIANCE roughness was the correct value to use in future simulations? Secondly, how sensitive were output distributions to material roughness? Two new luminous output distributions were simulated for the light guiding shade, with roughnesses 0.05 and 0.02. The resulting luminous intensity distributions were examined using the test of Bland and Altman.

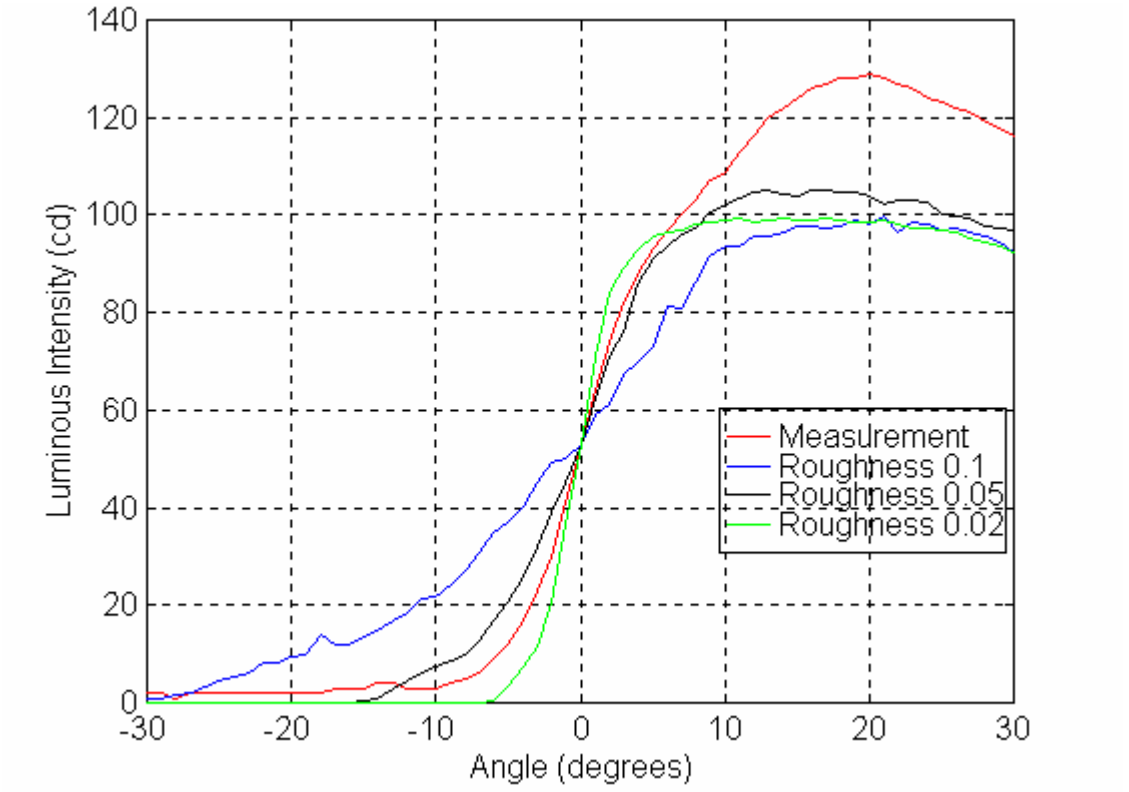

Figure 4.14 - Effect of Reflector Roughness on Luminous Performance around Horizontal

Figure 4.14 displays the effect of reflector roughness on luminous output in the region near horizontal. Luminous intensity distributions are shown for three values of material roughness (0.1, 0.05 and 0.02), along with the corresponding measured distribution. For ease of comparison, the plots were scaled for agreement in the horizontal direction. In this way, where simulation underestimates measurements in the region above horizontal, and overestimates measurements in the region below horizontal, the simulated reflectors are too rough. If the opposite is the case, the reflectors are not rough

enough. Roughness 0.1 is clearly too rough. Both roughnesses 0.05 and 0.02 provide better agreement with measurement. Roughness 0.05 is too great, and roughness 0.02 is too little.

The test of Bland and Altman was applied to the new simulated distributions. Figure 4.15 displays the resulting plot of percentage differences for roughness 0.05. This shows relatively constant percentage differences, between 150 and 200%, at higher intensities. For lesser intensities, one trend leads up to differences of 580%, and another trend leads down to differences around -50% (where measurement exceeds simulation). The upper trend corresponds to the output angular range -9 to 0°. The lower trend corresponds to the output angular range 66 to 80°.

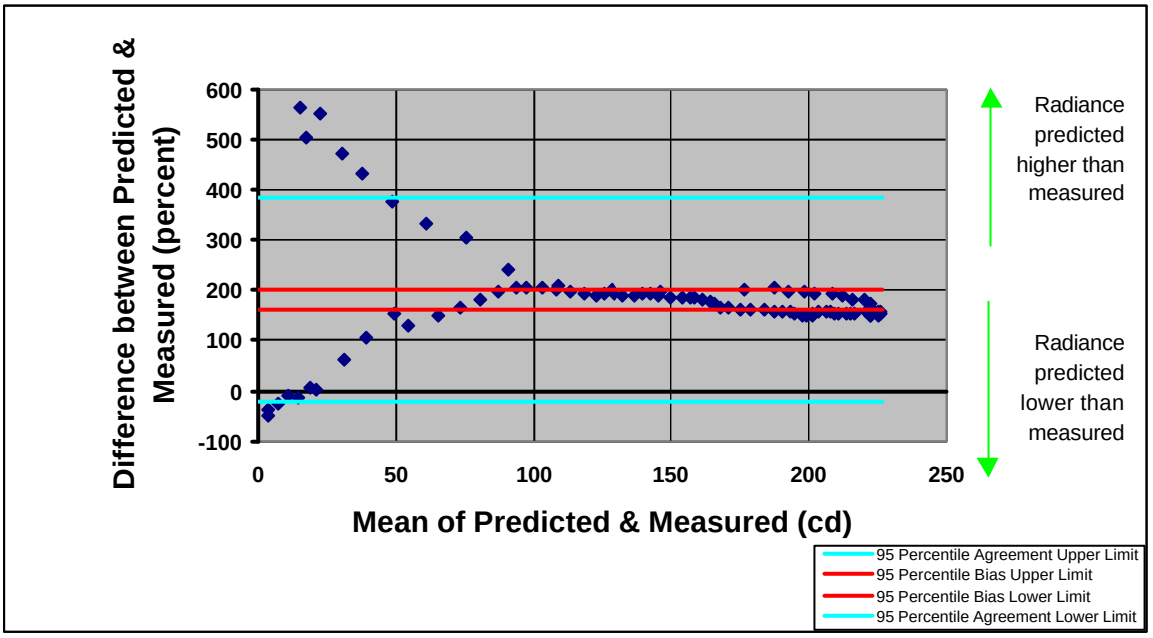

Figure 4.15 - Percentage Differences between Measurement and Simulation for Light Guiding Shade, Roughness 0.05

Roughness 0.05 is an obvious improvement over roughness 0.1. However, there is too much spreading of illumination. This implies that, in the region -9 to 0°, measurements drop more rapidly than the simulations. As a result, percentage differences in this region rise substantially. Thus, the rise in percentage differences at low intensities indicates too great a material roughness. The lower trend is similar to that displayed in Figure 4.13, and was caused by the bowed lower reflector of the light guiding shade.

Percentage differences for roughness 0.02 are displayed in Figure 4.16. This plot is different to those for roughnesses 0.1 and 0.05. There is no rise in differences at low intensities, and differences at larger intensities are not as stable. In the higher intensity region, one trend shows differences falling steadily from 220 to 150%, and the other trend displays differences up to 270%. The latter trend corresponds to the output angular range 0 to 15°. At lower intensities, differences fall from 220 to -100%.

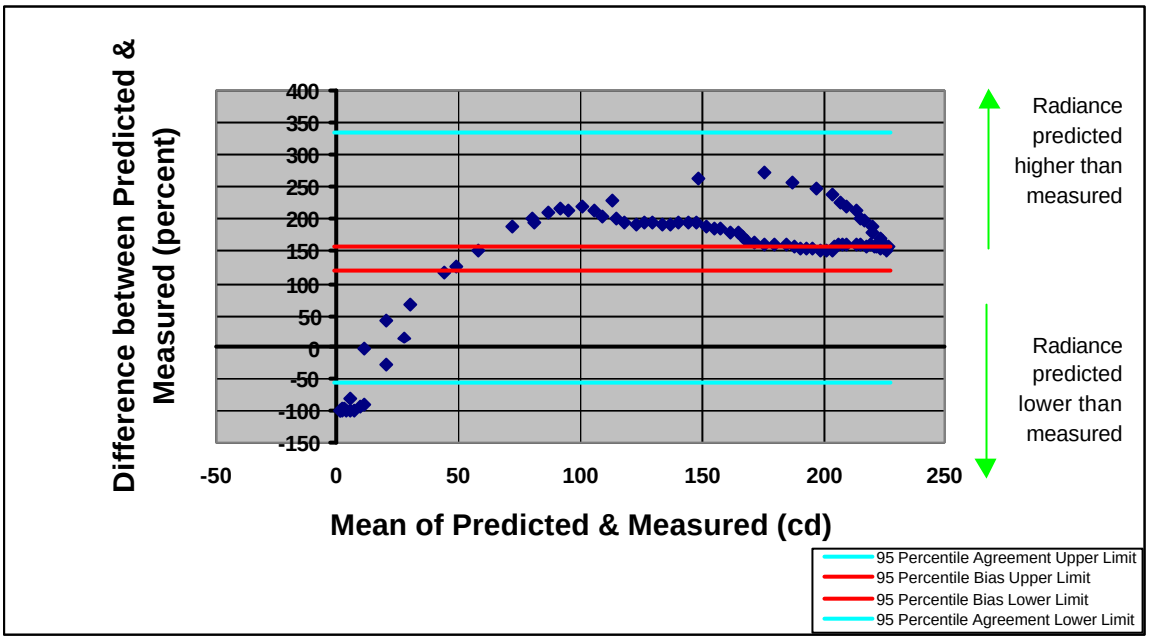

Figure 4.16 - Percentage Differences between Measurement and Simulation for Light Guiding Shade, Roughness 0.02

Following previous arguments, the lower percentage differences in the range -9 to 0° indicate too low a roughness. By the same reasoning, simulations in the range 0 to 15° were too high, providing large percentage differences in this region. The bowed lower surface of the light guiding shade caused the lower percentage differences in the output angular range 70 to 80°. The bowed surface redirected light into this region from the expected output angular range below 70°. Thus, measurements in the region below 70° are less than expected, and percentage differences rise. This is shown in the lower trend in the higher intensity region.

This sensitivity study revealed the importance of specifying appropriately smooth reflector material. Comparison between measurement and simulation was improved for reflector roughnesses closer to 0.05. This is still a little too

rough, but a roughness of 0.02 is too smooth. A roughness of 0.04 was considered most appropriate for further simulations of the micro-light guiding shade panel.

4.3.5 SENSITIVITY TO CONSTRUCTION TECHNIQUES - REFLECTOR SHAPE

With confidence that RADIANCE simulations closely model the performance of the micro-light guiding shade panel, further simulations were performed to optimise the device's construction. Studies were performed to analyse the sensitivity of micro-light guiding shade panel performance to variations in design and construction. The aim was to determine how accurate the device's construction must be to achieve the desired performance under real conditions.

The first sensitivity study involved the geometric form of the micro-light guiding shade elements. The curved surface of the lower reflector is a parabolic section. The manufacture of such a shape can be difficult. It was desired to determine how the substitution of a circular arc or several flat sections would affect the device's light output distribution.

The curved reflector was created using the RADIANCE program *gensurf*. This generates parametric surfaces defined in terms of two dummy variables. These variables take m and n values respectively. Smoothing may be applied, based on surface normal interpolation. If smoothing is not applied, adjacent vertices are joined with flat polygons.

Several vertical micro-light guiding shade elements were created by varying n and not applying smoothing. The modelled panel was described by its tilt b=0 and output angular range g=0 to q=90° (Figure 3.15b). Surfaces were created comprising one, two, four, six and ten flat sections. A smooth circular arc approximation was also created by defining a different parametric curve. The circular arc shared the same endpoints as the parabolic section and had the same tangent at the input aperture. The defined approximations are illustrated in Figure 4.17. It is quite difficult to discern any difference between the four, six and ten flat section profiles and the parabolic section.

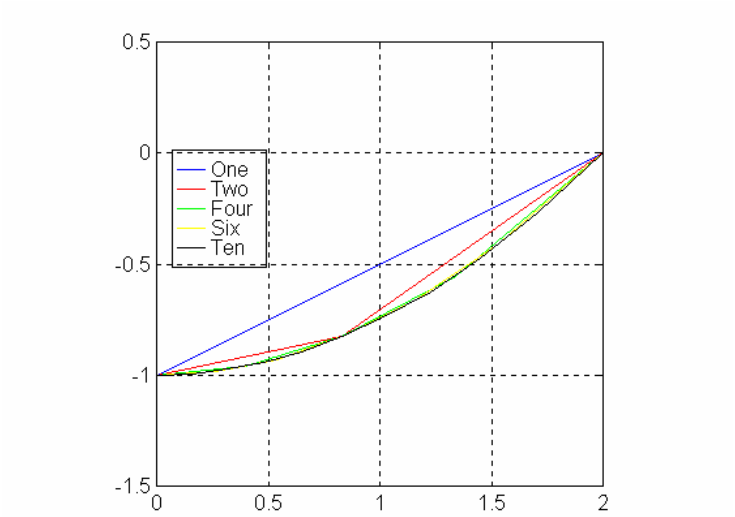

a)

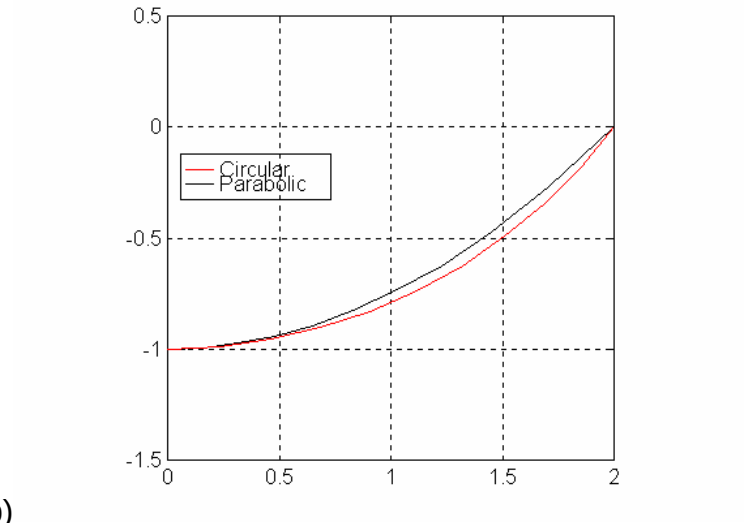

b)

Figure 4.17 - Approximations to the Parabolic Section: a) Flat Sections; b) Circular Arc. The Parabolic Sections are Black

Luminous output distributions were generated for each device as outlined in Chapter 7. A reflector roughness of 0.1 was assumed for each simulation. The resulting luminance profiles (unit: cd/m^2) are shown in Figure 4.18. There is large variation amongst the luminance output distributions of the numerous flat sections. This is most evident in the output angular range higher than 60°. For lower segment numbers, luminance is substantially decreased at larger angles. Luminance is reduced at high elevations as a more steeply sloping reflector is required near the output aperture to deliver light into these directions. The luminance output from the circular arc design is very similar to that from the parabolic section.

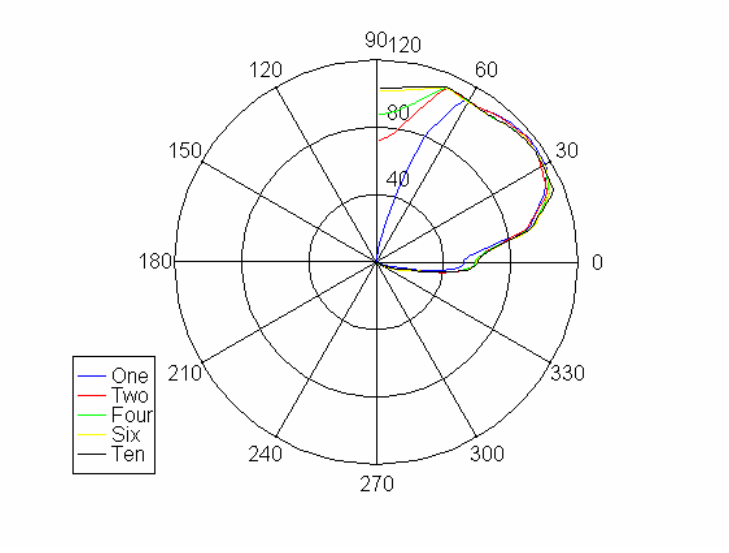

a)

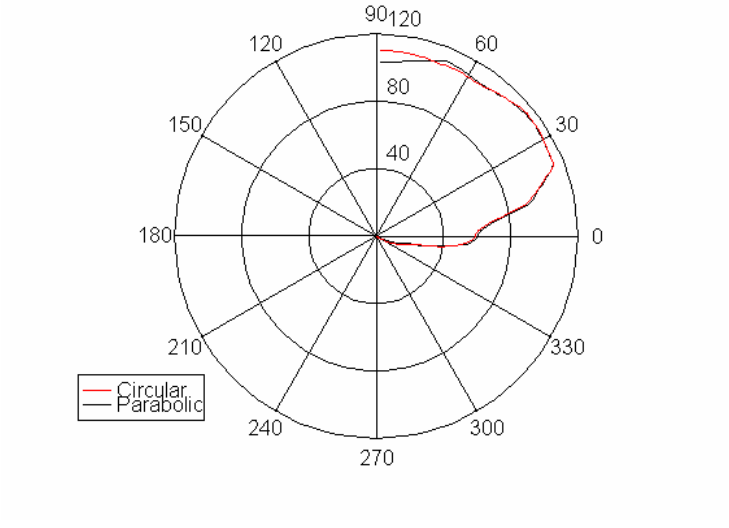

b)

Figure 4.18 - Luminance Output Distributions from Approximations to the Parabolic Section: a) Flat Sections; b) Circular Arc. Parabolic Section Light Output Distributions are Black

Luminous intensity profiles (unit: cd) were estimated by multiplying the luminance profiles by the cosine of the incidence angle (Figure 4.19). There was very little variation amongst the distributions. The luminance differences at high angles were reduced by the cosine factor.

For the vertical micro-light guiding shade panel, replacing the parabolic surface with flat surfaces or a circular arc makes little change to the luminous intensity output distribution. Thus, this device can be constructed with ease by replacing the parabolic reflector with a few flat sections. However, the altered reflectors spilt more light below horizontal than the parabolic reflectors. Thus, if the manufacture can be easily implemented, parabolic shaped reflectors are

preferred. These conclusions apply only to the investigated vertical micro-light guiding shade panel. Further investigations into reflector shape are described in Chapter 5.

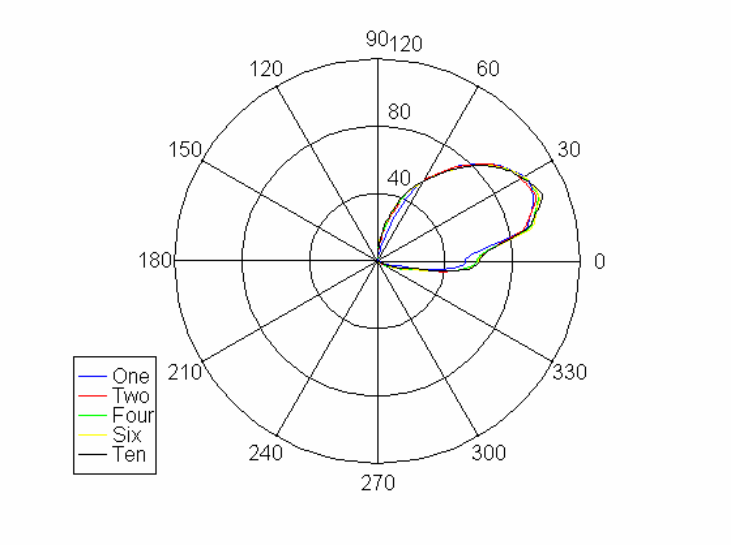

a)

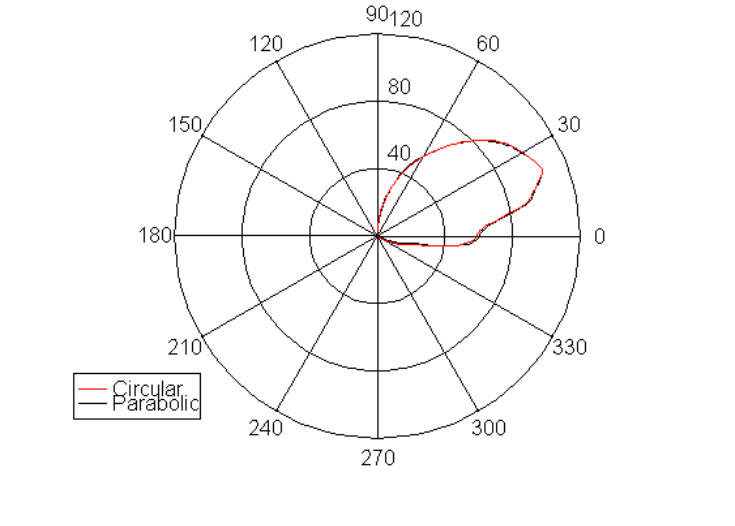

b)

Figure 4.19 - Luminous Intensity Output Distributions from Approximations to the Parabolic Section: a) Flat Sections; b) Circular Arc. Parabolic Section Light Output Distributions are Black

4.3.6 SENSITIVITY TO CONSTRUCTION TECHNIQUES - TRUNCATION

Solar concentrators are often truncated to save reflector material and reduce collector depth (Carvalho, Collares-Pereira, Gordon & Rabl, 1985). Some concentration is lost, but the truncated device can accept radiation from a broader range of directions (Zacharopolous, Eames, McLarnon & Norton, 2000). Wishing to reduce reflector requirements and simplify production the effect of truncation on light output distribution was examined by simulation.

The basis of this investigation was the vertical micro-light guiding shade panel described above. The truncation process is illustrated in Figure 4.20. The output aperture BC is pulled back toward the input aperture OA, keeping the two parallel. The thickness of the panel is thus reduced to a fraction *f* of its full thickness (*f*=1 for untruncated, *f*=0 for no thickness). Six different designs were simulated for which *f*=0.1, 0.3, 0.5, 0.7, 0.9 and 1.0. Reflector roughness was set at 0.1.

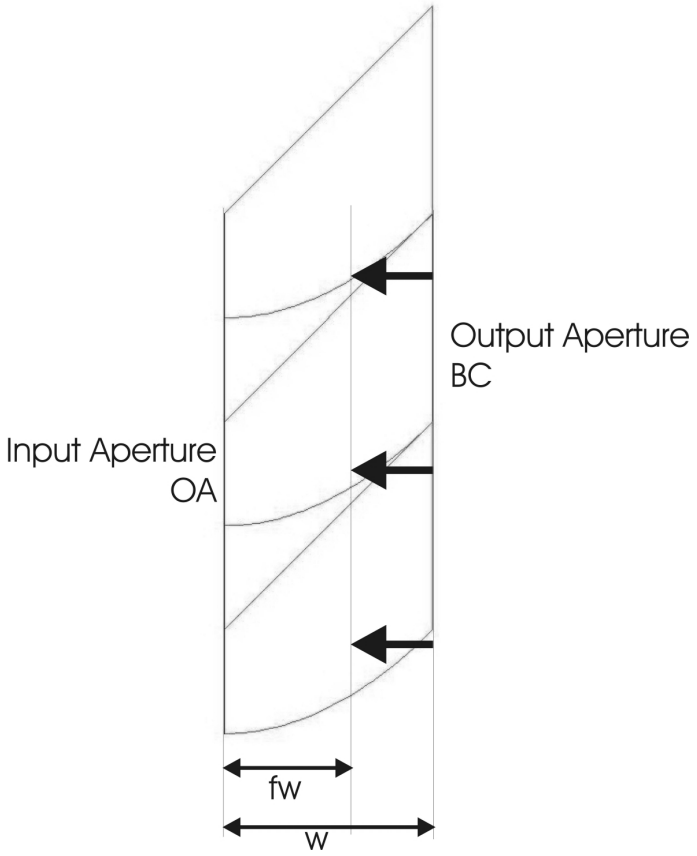

Figure 4.20 - Truncating a Vertical Micro-Light Guiding Shade Panel

The luminous intensity outputs for different degrees of truncation are displayed in Figure 4.21. Greater light spillage below horizontal is observed for greater degrees of truncation, as expected. The *f*=0.9 profile is quite similar to the untruncated profile. The *f*=0.7 profile is also similar. For $f \leq 0.5$, significant light is spilt below horizontal. This level of light spillage is unacceptable in terms of glare performance.

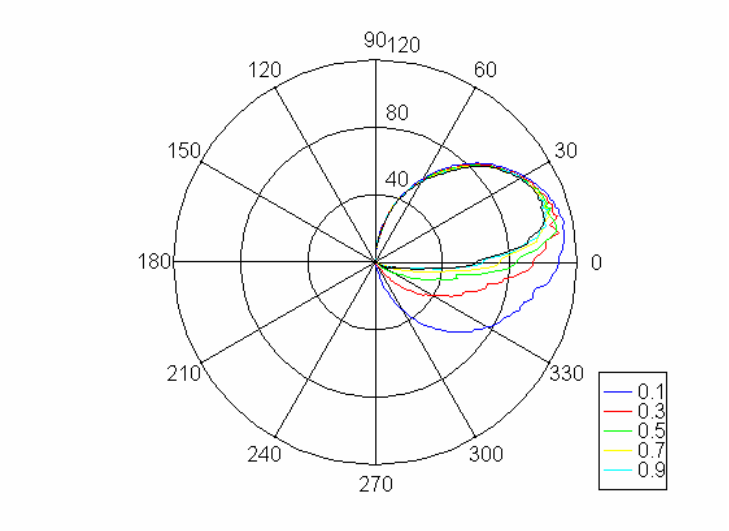

Figure 4.21 - Luminous Intensity Output Distributions of Truncated Vertical Micro-Light Guiding Shade Elements

The visual performance of the micro-light guiding shade panel in directions near horizontal is very important. It is undesirable to deliver any illumination into directions below horizontal. Thus, any truncation producing f<0.7 would be counter-productive. This provides little advantage in terms of reflector requirements, manufacture and panel width (Carvalho *et al.*, 1985). Therefore, truncation was not applied to further designs of the micro-light guiding shade panel.

4.3.7 SUMMARY OF SIMULATIONS

RADIANCE simulations of the micro-light guiding shade panel have qualitatively compared favourably with measurements. When consideration is made of the efficiency of luminous transfer between the lamp and the input aperture of the light guiding shade, simulated and measured luminous intensities agreed very well. This applies to both the relative distribution and magnitude of luminous intensity. Similar agreement was observed in relative luminous output distributions of the prototype micro-light guiding shade panels.

The Bland and Altman statistical test provided useful quantitative comparison of measured and simulated profiles. The test confirmed agreement between measurement and simulation for the light guiding shade, but revealed problems with the specified surface roughness. This problem was further investigated and an optimal roughness value for these simulations was determined.

Sensitivity studies assisted in choosing appropriate materials and manufacturing techniques. The vertical micro-light guiding shade panel displayed a large tolerance to manufacture of the specially shaped surfaces. The same device revealed low tolerance to truncation of the micro-light guiding shade elements.

4.4 SUMMARY

A better understanding of the performance of the micro-light guiding shade panel has been developed. Measurements of three early devices revealed luminous output distributions that agreed closely with expectation. Some light was spilt below the devices' nominal lower boundaries, likely indicating problems either with material properties or manufacturing techniques. This problem is discussed further in Chapter 5.

The design of the micro-light guiding shade panel was further investigated using Matlab scripts. Panel geometry was automatically generated by several scripts. Numerous important conclusions were reached regarding the panels' design. The most important of these concerned the relationship between panel tilt and the upper limit of the output angular range, Equation 4.1. Other important findings affected the panel's optimal tilt on the façade.

RADIANCE simulations were performed of the measured light guiding shade and two micro-light guiding shade panels. The simulations validated RADIANCE's predictions. Further simulations helped to improve further simulations of the micro-light guiding shade panel by correctly specifying material roughness. This involved a statistical technique found useful to compare measured and simulated data.

With validated RADIANCE models of the micro-light guiding shade panel, sensitivity studies assisted in choosing appropriate manufacturing techniques. Some applications of these simulations were demonstrated, and more are shown in Chapter 5. RADIANCE is then applied to modelling micro-light guiding shade panels on a complete building.

4.5 CONCLUSIONS

- Measurements show the micro-light guiding shade panel performing as desired.
- Maximum luminous throughput is provided where $q+b=p/2$.
- Panel tilts close to 30° provide maximum annual luminous throughput for sub-tropical climates.
- RADIANCE simulations of luminous throughput distributions agree closely with measurements.
- RADIANCE simulations aided development of micro-light guiding shade panel design, manufacture and specification.

CHAPTER 5 - FULL SCALE MICRO-LIGHT GUIDING SHADE PANELS - TEST BUILDING EXPERIMENTS

Two full-scale micro-light guiding shade panels were constructed and installed on the façade of a test building. Light distribution measurements were collected within the test building, and observations of visual comfort were made.

This chapter commences with a description of the test building facility. The two micro-light guiding shades are then introduced, and their construction described. Measurement procedures are then explained, followed by presentation of the results. A final summary of results and discussion concludes the chapter.

5.1 THE TEST BUILDING

The daylighting test building measures 3m wide, 3m high and 8m deep (Figure 5.1). The room's long axis is oriented north-south. A single unshaded window is set in the north facing wall, with dimensions 2.4 by 1.5m. The room is located on an open expanse of ground and has largely unobstructed views of the horizon. The interior walls and ceiling are cream and white Colorbond steel (diffuse reflectances 66.4% and 71.5% respectively (Section 6.2.2.1)). The floor is covered with blue carpet (diffuse reflectance 9.6% (Section 6.2.2.1)).

Figure 5.1 - Daylighting Test Building with Vertical Micro-Light Guiding Shade Panel Configuration

5.2 THE TESTED MICRO-LIGHT GUIDING SHADE PANELS

The first full-scale micro-light guiding shade panel had a vertical orientation. It was a larger version of the first prototype device described in section 4.1.1. The test building installation is illustrated in Figure 5.2.

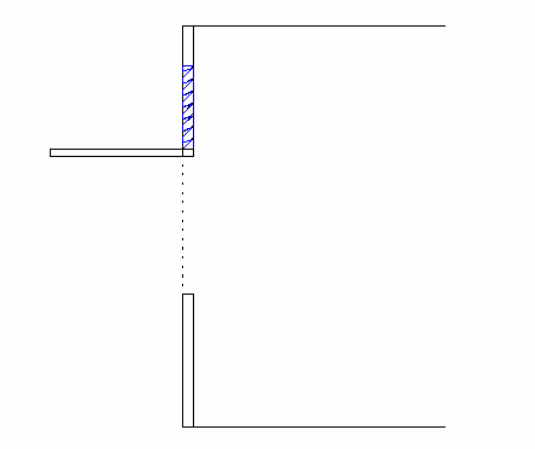

Figure 5.2 - Vertical Micro-Light Guiding Shade Panel Configuration

In this configuration, the vertical micro-light guiding shade panel was placed in a clerestory window and combined with an external light shelf. The light shelf provided extra shading not provided by the vertical panel. Its upper surface was lightly coloured, such that incident light was reflected onto the outer face of the vertical panel. This effectively increased the light passing into the room through the panel. The panel had thickness 80mm, suitable to fit into a conventional window mullion. This design achieved a substantial improvement in luminous throughput, combined with shading and an unimpeded view through the lower window.

This vertical configuration is not the generic form of the micro-light guiding shade panel. Generally, the device is intended to form a shading panel tilted out from the building façade. In this way, the device is easily installed on high rise commercial buildings. Thus, a tilted micro-light guiding shade panel was constructed and installed on the test building.

A panel tilt of b=30° was determined by considering percentage throughput, annual luminous throughput and shading (section 4.2.3). This provides total shading in summer, sufficient shading in autumn and spring, and useful solar gains in winter. This tilt also delivers near maximum luminous throughput over

the working year. For maximum percentage throughput, the upper boundary of the output angular range was set at q=60° (Equation 4.1). The lower boundary was set at g=0. The tilted panel is illustrated in Figure 5.3. Similar to the vertical panel, the tilted panel had thickness 80mm.

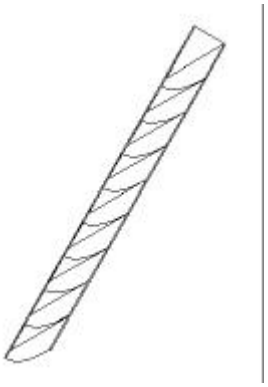

Figure 5.3 - Tilted Micro-Light Guiding Shade Panel

5.3 PANEL CONSTRUCTION

The vertical micro-light guiding shade panel was constructed soon after the prototype panels described in Chapter 4, using similar construction techniques. The tilted panel employed a different approach to construction. Each design required the construction of two panels to fit the total window width of 2.4m.

5.3.1 CONSTRUCTING THE VERTICAL PANEL

5.3.1.1 Interior Elements

The micro-light guiding shade elements of the vertical panel comprised shaped polystyrene elements, shown to the right in Figure 5.4. The elements were shaped by computer controlled hot-wire cutting. The top and bottom surfaces were coated with sisallation (an aluminium coated reflective insulation product).

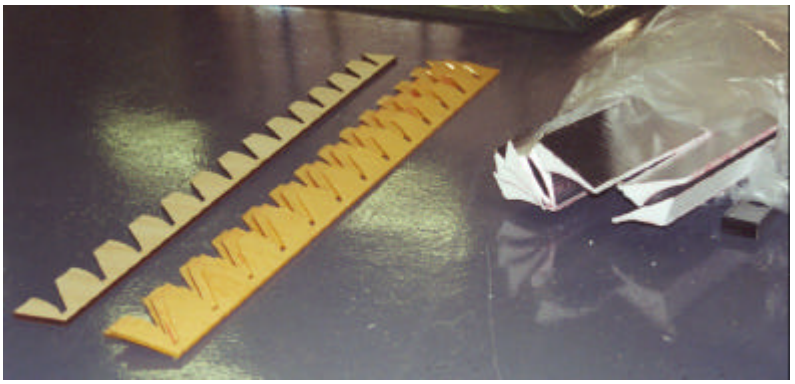

Figure 5.4 - Polystyrene Micro-Light Guiding Shade Elements and Wood and Acrylic Frame Sections

Frame sections were created from laser cut wood and acrylic (to the left in Figure 5.4). One vertical panel contained wood frame sections, coated with adhesive reflecting material. The other panel contained frame sections of clear acrylic. By putting the two different types of frame section in the two panels, their appearance could be compared *in-situ*.

To fit the micro-light guiding shade elements to the frame sections, small cuts were made in the upper edges of the reflecting elements. The elements and frames then locked together, one into the other (Figure 5.5).

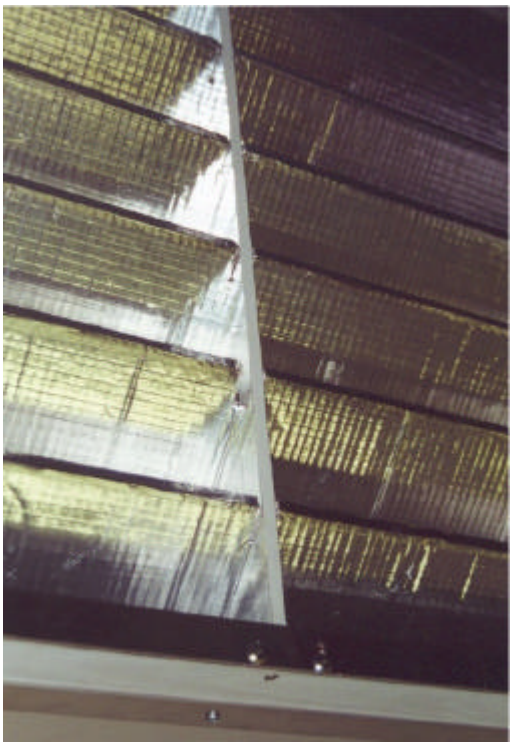

Figure 5.5 - Connecting the Reflectors to the Frame Sections

5.3.1.2 Containing the Interior Elements and Mounting the Panels

The reflecting elements and frame sections were contained in white painted, wooden outer frames (Figure 5.6). The transparent output and translucent input surfaces were sheets of clear acrylic. The latter was made translucent by sanding down a clear acrylic sheet with an orbital sander. In this way, the input surfaces were more transmissive than opalescent sheeting, but more diffusing than clear acrylic. The panels had outer dimensions 86mm thick, 630mm high and 1140mm wide. Each panel contained seven micro-light guiding shade elements and three frame sections.

Figure 5.6 - Vertical Micro-Light Guiding Shade Panel

The panels were attached to the window frame using L-section aluminium and masking tape. The external light shelf was constructed of aluminium L-sections and corrugated polycarbonate sheeting (Figure 5.1). The tilt of the shelf created effective shading without excessively restricting view. Wood side shade sections obstructed sunlight incident with large relative azimuth. The light shelf construction was firmly attached to the building by bolts through the wall.

5.3.1.3 Construction Problems

The polystyrene micro-light guiding shade elements were coated with adhesive sisallation. Although the sisallation remained attached to the polystyrene, often the polystyrene itself deformed. This polystyrene deformation caused similar deformations in the surface of the curved reflectors. This allowed light to be deflected into undesirable directions. The sisallation material was also quite rough. The amount and specularity of its reflectance were not as great as desired. For future panels, it was determined to attempt another approach to the creation of the micro-light guiding shade elements.

The laser cut wood and acrylic frame sections performed much better than the polystyrene sections used in the early prototypes. It was clear that the acrylic frame sections had a better appearance than the wood frame sections. Thus, the clear acrylic frame sections were applied in future panels.

5.3.2 CONSTRUCTING THE TILTED PANEL

5.3.2.1 Micro-Light Guiding Shade Elements

The micro-light guiding shade elements of the tilted panels were created from a readily available, highly reflective, aluminium material. The curved reflectors of the micro-light guiding shade panel are parabolic sections. This shape is difficult to manufacture. It was necessary to discover a reliable method of forming parabolic sections from aluminium. Several construction techniques were investigated. These are discussed below:

- Rolling to shape in a roller (Figure 5.7): cheap and relatively easy to perform; difficult to obtain a parabolic section; problems with reproducibility
- Pressing in metal pressing machine (Figure 5.8): industrially available; provide accurate shapes with excellent material; very expensive in the short term
- Bending to several flat sections (Figure 5.9): cheap and relatively easy to perform; unable to produce exact parabolic sections; can create blemishes on the reflecting surface; questionable reproducibility

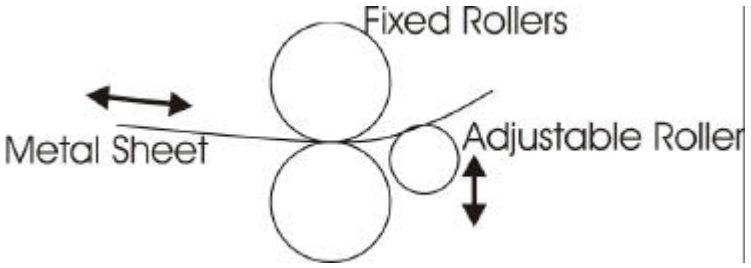

Figure 5.7 - Bending Metal Sheet in a Roller

Figure 5.8 - Creating Curved Metal in a Metal Press

Figure 5.9 - Creating Flat Section Reflectors in a Bending Machine

Metal pressing (Figure 5.8) presents the most accurate and reproducible manufacture technique. A mould can be created for around $A2000. This mould is used to manufacture shaped reflectors at great speed. A few manufacturers were contacted, but the initial cost was considered excessive for this first device.

Metal rolling could easily create circular sections (Figure 5.7), while bending easily approximates a parabolic section with several flat sections (Figure 5.9). If one of these methods was chosen for manufacturing the curved surfaces of the micro-light guiding shade panel, these approximations must not adversely affect the panels' light output distribution.

5.3.2.2 Sensitivity to Construction Techniques - Shape of Reflectors

To determine the best manner in which to manufacture the micro-light guiding shade elements, a sensitivity study was performed on the tilted micro-light guiding shade panel. The sensitivity study was similar to that described in section 4.3.5. The objective was to test the sensitivity of the panel's vertical output distribution to variations in construction techniques. In particular, it was desired to examine the effect on the panel's output of construction using flat section and circular arc approximations to the parabolic section.

The testing technique is described in sections 4.3.5 and 7.3. Sections through three of the tested reflector shapes are shown in Figure 5.10. The five flat section approximation closely fits the parabolic section, while the circular arc approximation is quite different. A reflector roughness of 0.04 was assumed for each simulation, following the findings of section 4.3.4.

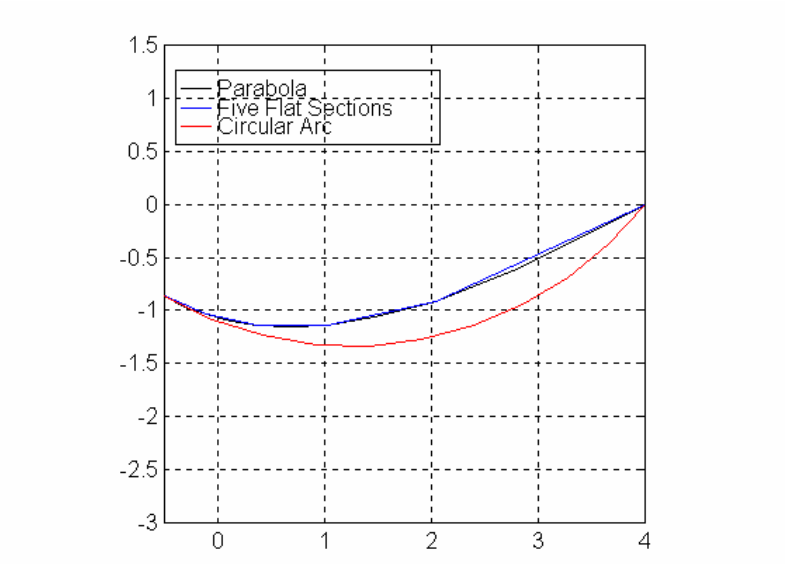

Figure 5.10 - Approximations to Parabolic Section of Tilted Micro-Light Guiding Shade Panel

Luminous intensity output profiles (unit: cd) are shown in Figure 5.11. In all cases, significant illumination exited the panel in directions below horizontal. This was the case even for the perfectly manufactured parabolic section. Illumination was sent into directions as far as 60° below horizontal. Associated with this unexpected illumination below horizontal, there was an unexpected drop in luminance in directions above 30° above horizontal. Unexpected luminances in directions below horizontal present a problem for the tilted micro-light guiding shade panel. The cause of this discrepancy was reflections of light rays at the inner surface of the transparent output sheet, described in detail in Appendix 2.

The five flat surface and circular arc approximation luminous output profiles were both different to that for the parabolic section. More flat sections provide less deviation in output profiles. Flat section output profiles agree better with the profile provided by the parabolic section.

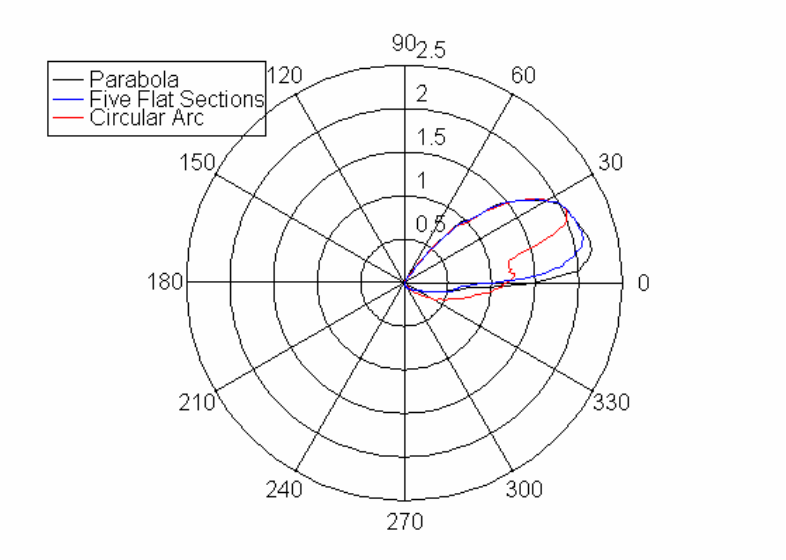

Figure 5.11 - Luminous Intensity Output of the Tilted Micro-Light Guiding Shade Panel

It is clear that the tilted panel's output distribution is more sensitive to construction variations than the vertical panel (section 4.3.5). For both panels, replacing the parabolic surface with flat surface approximations makes little change to the luminous intensity output distribution. Replacing the parabolic surface with a circular arc makes little difference to the output of the vertical panel, but significantly alters that of the tilted panel. Thus, the circular arc approximation was considered unsuitable for the micro-light guiding shade elements of the tilted micro-light guiding shade panel. A high number of flat surface reflectors may be used to approximate the parabolic section, with little degradation of the panel's luminous output distribution.

5.3.2.3 Constructing the Micro-Reflecting Elements

Following the findings of the sensitivity study, the method chosen to create the micro-light guiding shade elements was bending to several flat sections (Figure 5.9). Seven flat sections were created to approximate the parabolic section.

The flat section reflectors were bent to shape in a bending machine. Bends were located in such a way as to maintain bends of equal angle between adjacent flat sections. This was achieved by setting a stop to which the bending machine handle was pulled each time (Figure 5.9). This ensured repeatability between bends and between elements.

The flat section reflectors were combined with two other reflector sections to create the required micro-light guiding shade elements (Figure 5.12). Connecting sections were created by bending two lips to which the other reflector sections were attached. The three components of the micro-light guiding shade elements were bonded together with five minute epoxy adhesive and a construction assembly (Figure 5.12).

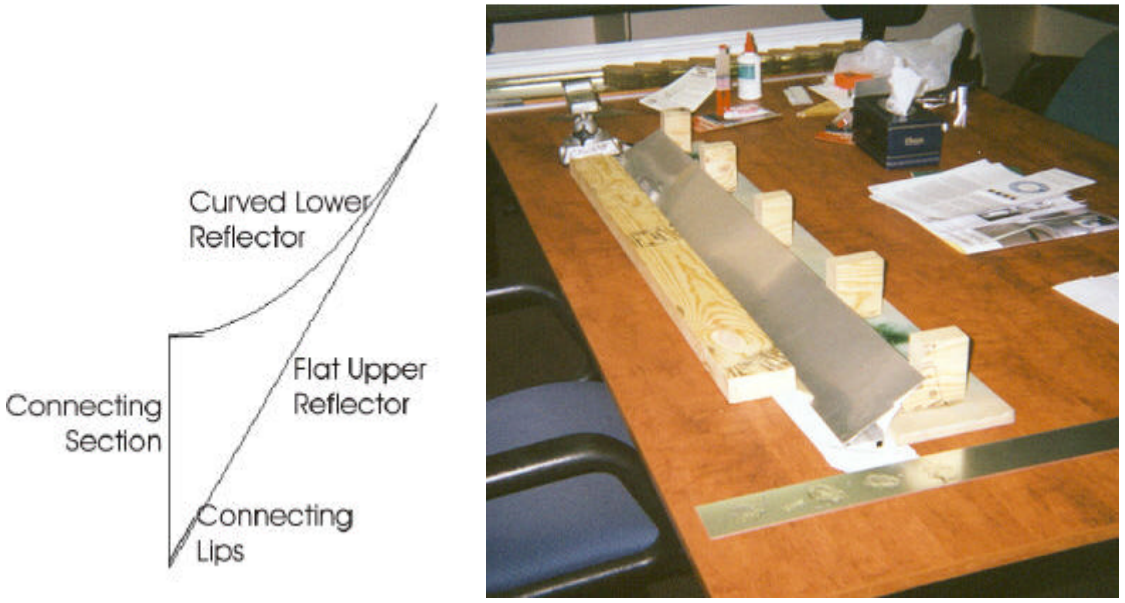

Figure 5.12 - Connecting the Components of Micro-Light Guiding Shade Elements

5.3.2.4 Constructing the Panels

Clear laser cut acrylic frame sections held the micro-light guiding shade elements in place. The frame sections and micro-light guiding shade elements slotted together as shown in Figure 5.5. The micro-light guiding shade elements and frame sections had thickness 64mm.

The sides of the panels comprised aluminium channel. These were connected to the frame sections and front and back panels through intermediate square section aluminium bars. The square bars and screws held the sheeting, frame sections and channel together.

The size of the panels was determined by considering shading and view. The panels needed to provide effective shading, without excessively obstructing view through the window. The lower edge of the panels was located 1770mm above floor level. The panels each contained ten micro-light guiding shade

elements. The two panels had a total width of 2416mm, sufficient to extend across the window of the test building. A total of 2.4 by 3.2m of aluminium reflector was purchased for the tilted micro-light guiding shade panels.

Clear plastic sheeting formed the transparent cover on the output side of the panels (Figure 5.13). The panels' input sides were covered with sheets of anti-reflective coated translucent plastic. These were held in place by the side channels, square mounting bars and fasteners (Figure 5.14). The cover at the top of the panel was formed from excess reflector material. The material's reverse side, a white diffuse surface, was exposed to the exterior (Figure 5.13).

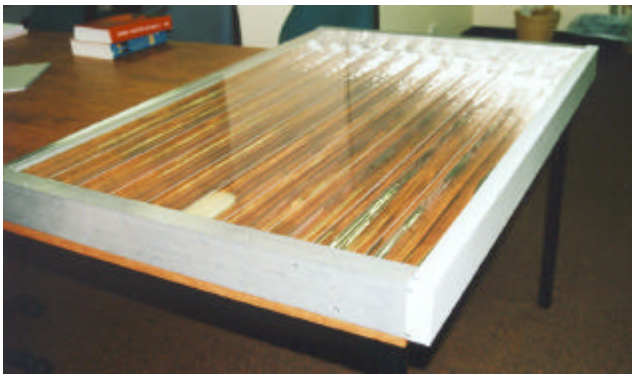

Figure 5.13 - Creation of a Tilted Micro-Light Guiding Shade Panel, Viewed from the Output Side

For reasons discussed in section 5.5.1.4, an alternative design was required for the cover at the bottom of the panel. The bottom cover was constructed of thicker (1.6mm) aluminium sheeting, bent into shape as shown in Figure 5.14. Its attachment to the side channels is also illustrated in Figure 5.14. This required that the bottom end of the side channels be further cut to a matching profile.

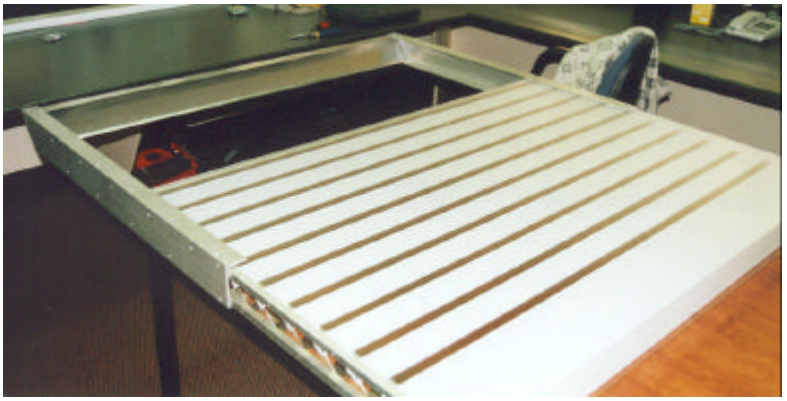

Figure 5.14 - Shaped Bottom Cover of the Tilted Micro-Light Guiding Shade Panel, Viewed from the Input Side

5.3.2.5 Mounting the Panels

Three triangular braces were constructed to mount the panels (Figure 5.15). Two side braces were bolted through the wall to hold the panels firm on the building. The centre brace comprised two aluminium T-sections, joined to the outer window sash. The panels were simply dropped into and attached at various points to the braces. For improved weather proofing, to stop sunlight penetrating over the top of the panels, and for improved appearance, a top cover was manufactured and attached over the top of the panels (Figure 5.15).

Figure 5.15 - Tilted Micro-Light Guiding Shade Panels Mounted on the Test Building

5.3.2.6 Construction Problems

The manual construction of the micro-light guiding shade elements was difficult and time-consuming. Some of the machines used for this process were not performing perfectly. This was particularly the case for the bending machine. Despite correct use of the bending machine, bends were not consistent along their length. This caused some imperfections in the shape of all micro-light guiding shade elements.

5.3.3 COST ANALYSIS

The cost of manufacture of the two panels was calculated and compared (on a basis of cost per unit area of device ($/m^2)). Material costs were allocated to the reflectors, framing the reflectors in panels, and mounting the panels (Table 5.1). Additional estimates of the cost of labour were also made (Table 5.2).

Table 5.1 - Material Costs and Areal Cost for Constructed Micro-Light Guiding Shade Panels

	Vertical Panel	**Tilted Panel**
Area	1.44 m^2	2.03 m^2
Reflectors	\$146.60 (\$102/m^2)	\$351.30 (\$173/m^2)
Framing	\$260.40 (\$181/m^2)	\$482.35 (\$238/m^2)
Mounting	\$185.15 (\$129/m^2)	\$198.95 (\$98/m^2)
Total materials	\$592.15 (\$411/m^2)	\$1032.60 (\$509/m^2)

Table 5.2 - Labour Costs and Areal Cost for Constructed Micro-Light Guiding Shade Panels

	Vertical Panel	**Tilted Panel**
Hours	60 hrs	75 hrs
Cost per hour	\$15/hr	\$15/hr
Total labour cost	\$900	\$1125
Labour cost per square metre	\$625/m^2	\$554/m^2

The figures shown above are basic estimates of the cost of production. Clearly, lessons learnt while constructing these panels can be more easily, quickly and cheaply applied to future construction efforts. Thus, these costs should be viewed as worst case scenarios.

The tilted panel was more expensive in terms of material requirements. The costs of the reflectors and framing were more expensive for the tilted panel, while the cost of mounting was reduced (in terms of cost per square metre). Reflector costs could have been reduced by using cheaper rolled aluminium sheeting. However, the rolling process produces unidirectional grooves in the

reflector that scatter light in preferential directions (Ronnelid, Adsten, Lindstrom, Nostell & Wackelgard, 2001). Also, this cheaper aluminium is not as highly reflective as the employed reflector materials.

The major material cost component was framing the micro-light guiding shade elements into a panel. The frames containing the tilted panels were of higher quality than those containing the vertical panels. The vertical panels were surrounded by inexpensive wood, while the tilted panels were sealed in aluminium channel and other cladding. These different materials account for most of the difference in framing material costs. The laser cut frame sections were more economical than the polystyrene frame sections used in the prototype panels described in Chapter 4.

The cost (per square metre) of mounting the vertical panels was greater than that of mounting the tilted panels. The vertical panels were mounted inside the window, with an additional light shelf outside the window (Figure 5.1). The light shelf was included in the mounting costs for the vertical panel. Only one set of mounting materials was required for the tilted panels.

The estimated costs of labour were greater than the material costs for both panels. Total labour costs were greater for the tilted panels, but less on a cost per square metre basis. For the tilted panels it was necessary to manually create the micro-light guiding shade elements. This was greatly time-consuming, accounting for more than half of the estimated cost of labour. The micro-light guiding shade elements in the vertical panels were provided by industrial polystyrene cutters. These elements were cheaper in both material and labour costs. However, the quality of these elements was unsatisfactory, as described in section 5.3.1.3.

If an industrial process could quickly and easily produce satisfactory micro-light guiding shade elements, the labour cost of construction would be significantly reduced. The metal pressing technique described in section 5.3.2.1 is the best alternative known by which to achieve this. For significant volumes of reflector elements, the total cost of panel construction would likely be reduced.

It should again be stated that the costs displayed in Tables 5.1 and 5.2 should be viewed as worst case scenarios. Once the manufacturing process has been further developed, the cost of construction should be significantly reduced. Larger volumes of construction will produce smaller unit costs through the advantages of economies of scale.

5.4 MEASUREMENTS IN THE TEST BUILDING

Several forms of measurement were completed with the two micro-light guiding shade systems on the test building. Completed measurements include monitoring of internal and external light levels, measurement of illuminance profiles, visual observations and visual comfort surveys. The measurement processes are described in this section. The results of measurements are displayed in section 5.5.

5.4.1 MONITORING INTERNAL LIGHT LEVELS

Internal light levels and external irradiances were simultaneously logged on a portable computer. Irradiances were measured by two calibrated pyranometers (Middleton EP-08) separately measuring global and diffuse horizontal irradiance. Internal light levels were measured by a basic photo-diode light sensor. Power was supplied to the sensor by two nine volt batteries. The light sensor device was placed on a table, six metres from the window.

The light sensor was calibrated by simultaneously measuring the circuit's output voltage (Beckman Tech 300 multimeter) and incident illuminance (calibrated illuminance meter, Topcon IM-5). The sensors were exposed to various levels of illumination. The resulting data was examined to form the sensor's calibration.

Internal light levels and external irradiance data were logged (Picolog ADC-16) together, at 30 second intervals, for a total period of six weeks between 14 September and 4 December. This corresponded roughly to the period between spring equinox and summer solstice, and included periods of very clear and very cloudy skies.

5.4.2 MANUAL ILLUMINANCE MEASUREMENT

With the micro-light guiding shade panels installed on the test building, internal illuminance profiles were measured under different sky conditions. Internal horizontal illuminance measurements were completed by a tripod mounted illuminance meter (Topcon IM-5) at 0.8m above floor level. External illuminances and internal vertical illuminances were measured by the hand-held Topcon illuminance meter.

5.4.2.1 Vertical Micro-Light Guiding Shade Panels

Under a very clear sky with direct sun (around 11.15am on 14 September), illuminance profiles were firstly measured with the view window and vertical micro-light guiding shade panels open, and secondly with the panels covered over with black sheeting. Measurements were made at regular intervals through the room's centre, extending from the window to the southern wall (Figure 5.16). Horizontal global illuminances were measured exterior to the room. Measurements completed with the panels covered over were attributed to illumination passing through the view window and roof vent. The contribution of the vertical panels to interior illuminance levels was determined by taking the difference between the two measured profiles, after scaling for similar external illuminances.

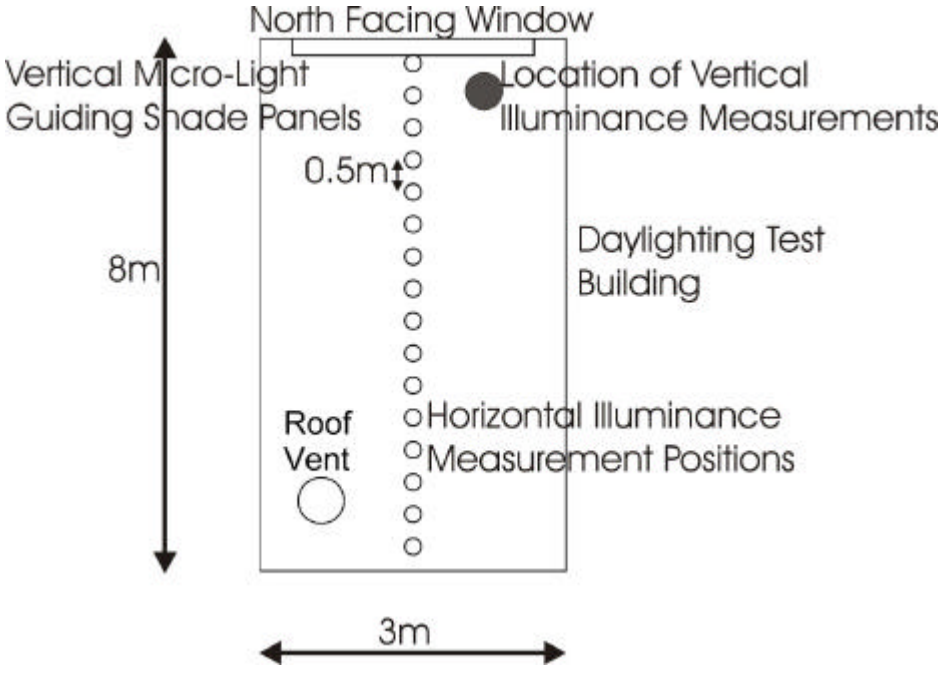

Figure 5.16 - Measurements of Horizontal and Vertical Illuminance in Test Building with Vertical Micro-Light Guiding Shade Panels

Internal vertical illuminances were measured on the same day, under the same sky conditions. This was intended as a method by which to assess possible glare caused by the vertical panels. As the panels were designed to direct light into directions above horizontal, and the panels were mounted above eye height, low luminance was expected when looking into the panels. This would correspond to low vertical illuminances. However, light passing through the panels directly illuminates the upper wall and ceiling. Thus, all vertical illuminances were non-zero. Therefore, the shape of the vertical illuminance distribution, and the height at which it dropped to low levels, were of particular interest. The lower window was covered over to assess only light passing through the panels. Measurements were completed on a vertical line 1.0m from the eastern wall and 1.2m from the window (Figure 5.16).

Internal horizontal illuminances were measured in the room under an uneven but overcast sky, with clear brightening toward the sun (around 1.15pm on 24 October). For these measurements, the view window was covered over with black sheeting, such that measured illuminances were entirely attributed to the vertical micro-light guiding shade panels. Apart from this change, horizontal internal illuminance measurements were completed as described above (Figure 5.16). Horizontal global and vertical north illuminance exterior to the room were also measured.

5.4.2.2 Tilted Micro-Light Guiding Shade Panels

Following installation of the tilted micro-light guiding shade panels, more extensive testing took place. These panels were tested more extensively as these are the intended form of the micro-light guiding shade panel. The measurement process adopted closely followed the recommendations of Ruck, Aschehoug, Aydinli, Christoffersen, Courret, Edmonds, Jakobiak, Kischoweit-Lopin, Klinger, Lee, Michel, Scartezzini and Selkowitz (2000c). For each of three different sky conditions, two measurement sets were completed. The first set involved the tilted panels as installed. The second set involved the panels acting as conventional shading devices. This was achieved by covering the panels with thick black plastic sheeting. This separated the internal illuminance components due to the view window and the panels.

For each measurement set, several illuminance measurements were completed. Horizontal illuminance measurements were made with the tripod mounted Topcon illuminance meter at 0.8m height. 41 measurements were made on a grid pattern (Figure 5.17). Seven measurements on the eastern side could not be completed as foam panels placed against the eastern wall obstructed these positions. Vertical illuminance measurements were completed at head height against the walls, at the centre of the window and rear wall and at three locations along the east and west walls (Figure 5.17). Horizontal global, vertical north and direct normal illuminances were also measured externally. Illuminance incident normally on the tilted panels was also measured.

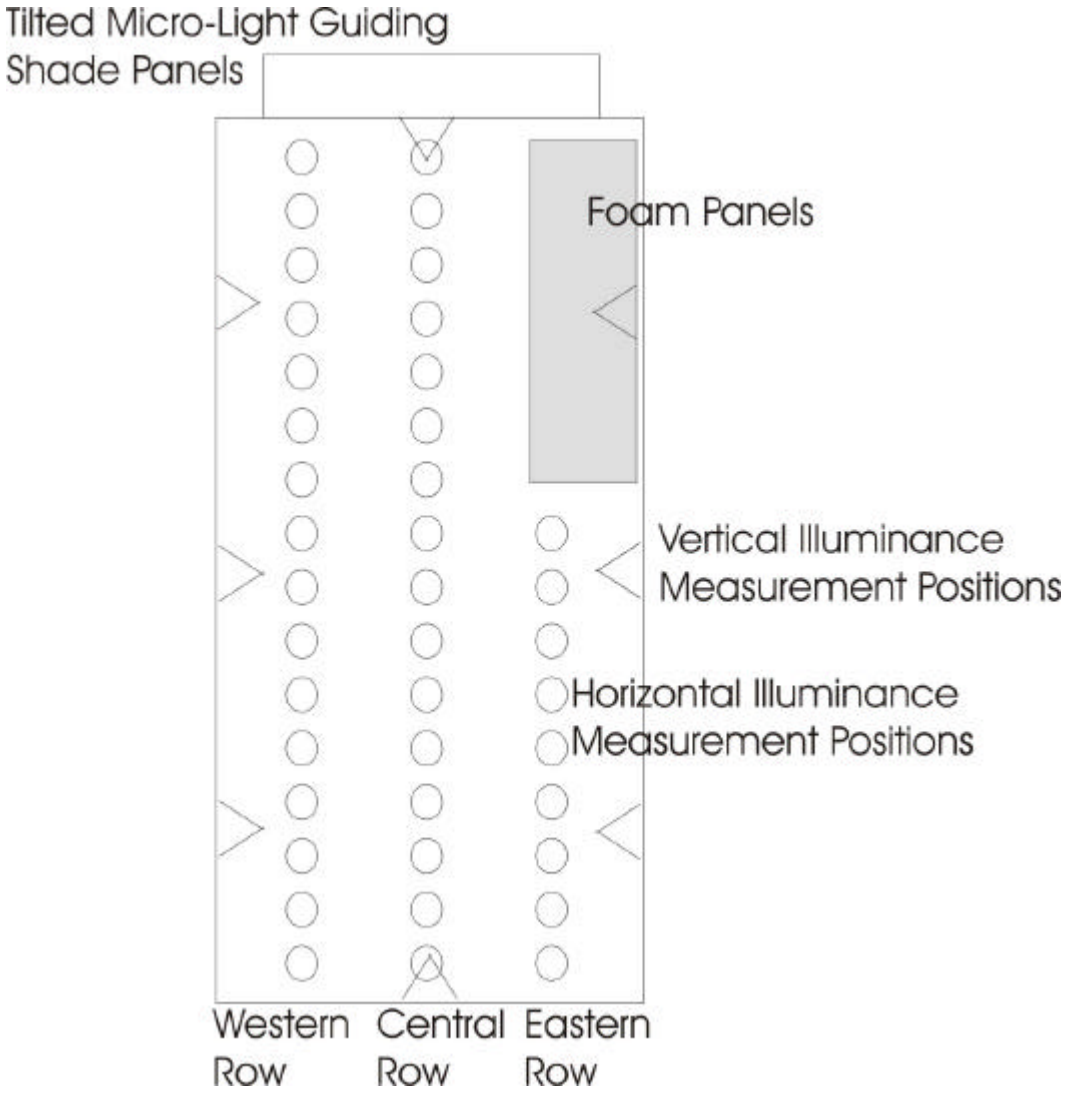

Figure 5.17 - Measurements of Horizontal and Vertical Illuminances in Test Building with Tilted Micro-Light Guiding Shade Panels

Measurements were completed under a very clear, cloudless sky on 2 August. All measurements were completed between 11am and 12.15pm. A smaller set of internal measurements was completed with the window completely covered, to examine the illuminance contribution of light passing through the roof vent.

Further measurements with the tilted panels were completed under a varying overcast sky on 9 August. External conditions varied considerably through the measurement period, requiring extra measurements of internal illuminances. All measurements were completed between 10.30am and 12pm. Another small set of internal measurements was completed with the windows covered over.

Due to problems with the translucent material, described in section 5.5.2, further measurements were completed under a clear sky with few clouds on 29 August. All measurements were completed between 9 and 10am.

Two final measurement sets were completed on 19 and 24 September. Both sets of measurements were made around midday on clear sunny days. It was desired to assess the effect on visual comfort and room illumination of replacing the installed translucent material (specular transmittance 36%, diffuse transmittance 53% (Section 6.2.1.2)) with opalescent sheeting (diffuse transmittance 27% (Section 6.2.1.2)). Visual comfort was assessed by measuring vertical illuminance on the rear wall of the building, facing the window. These measurements revealed different directional transmittances between the installed translucent and the opalescent sheeting. Room illumination was assessed by horizontal and vertical illuminance measurements as shown in Figure 5.17.

The purchased opalescent material had relatively low transmittance, but was highly diffusing in transmission. The view window was covered with thick black sheeting, extending from the bottom of the micro-light guiding shade panels to the bottom of the window. Thus, all light entering the room must pass through the panels. This provided a visual adaptation level unaffected by ground reflected light passing through the view window.

Vertical illuminances were measured up and across the rear wall of the building (Figure 5.18). Solar noon had passed before measurements began on 19 September, so measurements were made up the east part of the rear wall. Measurements were made up the centre of the wall on 24 September at solar noon. Vertical illuminances were also measured across the wall, above eye height, on 19 September. All measurements were completed with and without the opalescent sheeting.

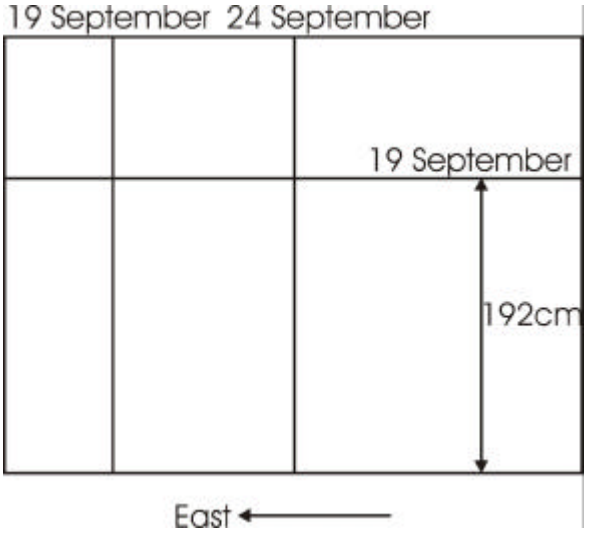

Figure 5.18 - Vertical Illuminance Measurements on Rear Wall of Test Building with Tilted Micro-Light Guiding Shade Panels

Room illumination was assessed by horizontal and vertical illuminance measurements on 24 September. The employed measuring process was described previously and illustrated in Figure 5.17. The view window was still covered by black sheeting as described above. These measurements were completed between 12 and 12.20pm.

5.4.3 VISUAL COMFORT ASSESSMENT

Whilst performing these measurements in the test building, visual comfort assessments were made. Basic glare measurements were performed in the building with the vertical panels installed. These were the vertical illuminance measurements described in section 5.4.2.1.

More stringent visual comfort assessments were completed with the tilted panels installed. Based on daylight measurement protocols of the International Energy Agency (Ruck *et al.*, 2000c), visual comfort surveys were completed under each sky condition. As the daylighting test building was located a large

distance from the city, and the required sky conditions were difficult to predict, it was not possible to obtain a representative sample of subjects. Therefore, the surveys were completed only by those two people present during measurements. Conclusions drawn from the surveys are not intended to be complete and true. However, they were useful indicators of the visual performance of the tilted panels.

The utilised survey was specifically designed for, "the assessment of users' opinions on daylighting systems and lighting control systems installed in full scale test rooms" (Ruck *et al.*, 2000c: 42). Surveys were completed under both measurement conditions (panels covered and uncovered). Following completion of Parts 2 (Impression of the Light and the Room) and 3 (The Light and the Room as a Workplace) under both measurement conditions, Part 6 (Comparison of Rooms) was completed in which participants compared their impressions of the two measurement conditions.

5.5 RESULTS OF MEASUREMENTS

The results of measurements are revealed in this section. Results are presented and summarised separately for the vertical and tilted micro-light guiding shade panels.

5.5.1 VERTICAL PANELS

5.5.1.1 Clear Sky

Horizontal illuminance distributions measured in the test building with the vertical micro-light guiding shade panel, under a clear sky, are displayed in Figure 5.19. To allow direct comparison, both measured profiles were scaled for a horizontal global illuminance of 100klx. The displayed 'panels only' profile was calculated as the difference between the other two profiles.

The view window provided excessive illumination near the window. Illuminance then fell off sharply toward the rear of the room. The micro-light guiding shade panels provided more reasonable light levels near the window. The maximum illuminance provided by the micro-light guiding shade panels occurred between 0.5 and 1.0m depth. This position of maximum is provided by the dispersion of

light over the ceiling. In the rear of the room, the micro-light guiding shade panels provided more than twice as much light as the view window. Thus, the vertical micro-light guiding shade panels in the clerestory window raised illuminances at 8m depth three-fold over what would have been achieved with a shaded view window.

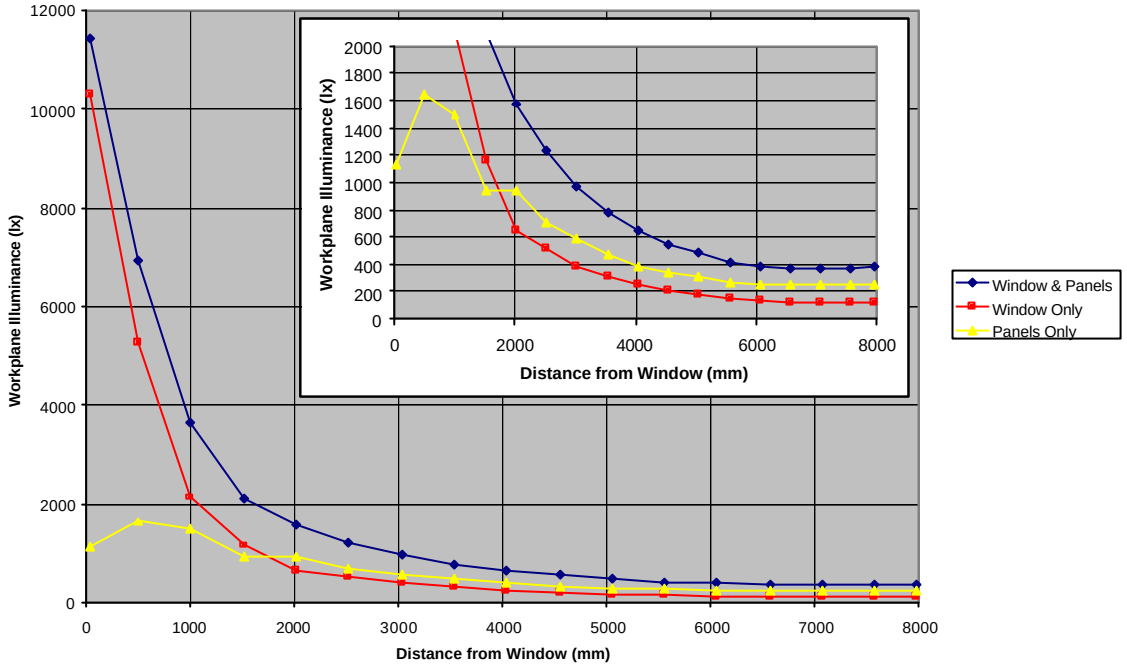

Figure 5.19 - Horizontal Illuminances in Test Building with Vertical Micro-Light Guiding Shade Panels, Clear Sky (Insert Shows Scaled Up Version of Same Figure)

Illuminance uniformity was improved by the micro-light guiding shade panels. Ratios of maximum to mean and mean to minimum illuminances were both reduced. These ratios were between 7 and 12 for the view window only. These were reduced to between 5 and 6 by the vertical micro-light guiding shade panels. Illuminances ratios due to the panels only lay between 2.5 and 2.7.

Some glare was observed at standing height, while looking directly at the panels. Some illumination must have been directed below horizontal. This was confirmed by measurements of vertical illuminance (Figure 5.20). Note on Figure 5.20 that heights are displayed up the vertical axis and vertical illuminances are marked along the horizontal axis. The heights of the top and bottom of the micro-light guiding shade panels are also marked. These results indicate that the panels directed light upward and into the room as desired, with a little light spilt below horizontal.

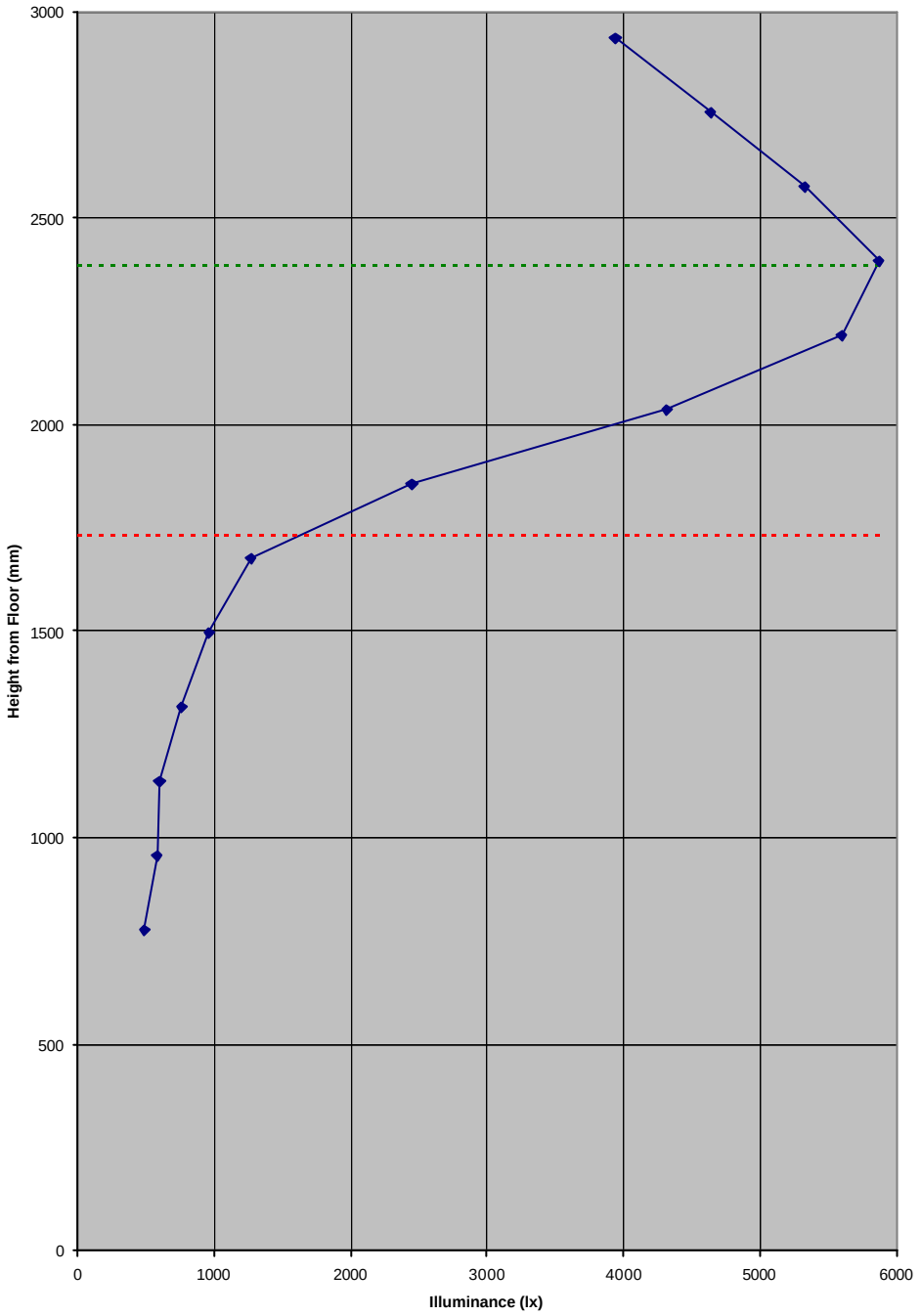

Figure 5.20 - Vertical Illuminances in the Test Building with Vertical Micro-Light Guiding Shade Panels, Clear Sky

The degree of glare delivered by the panels was not excessive. The remainder of the room was very comfortably lit. Figure 5.21 displays a photograph looking into the room from near the window (without a flash). This photograph shows clearly the uniform illumination within the room, and conveys the observed perception of comfortable illumination.

Figure 5.21 - Uniform Illumination of Test Building with Vertical Micro-Light Guiding Shade Panels under Clear Sky

5.5.1.2 Overcast Sky

Measured horizontal illuminance profiles under an uneven but overcast sky are shown in Figure 5.22. Two sets of measurements are presented, with light passing only through the vertical micro-light guiding shade panels. The overcast sky displayed clear brightening toward the sun. External measurements revealed an average horizontal global illuminance of 70klx and an average vertical illuminance of 40klx on the panels' input surfaces.

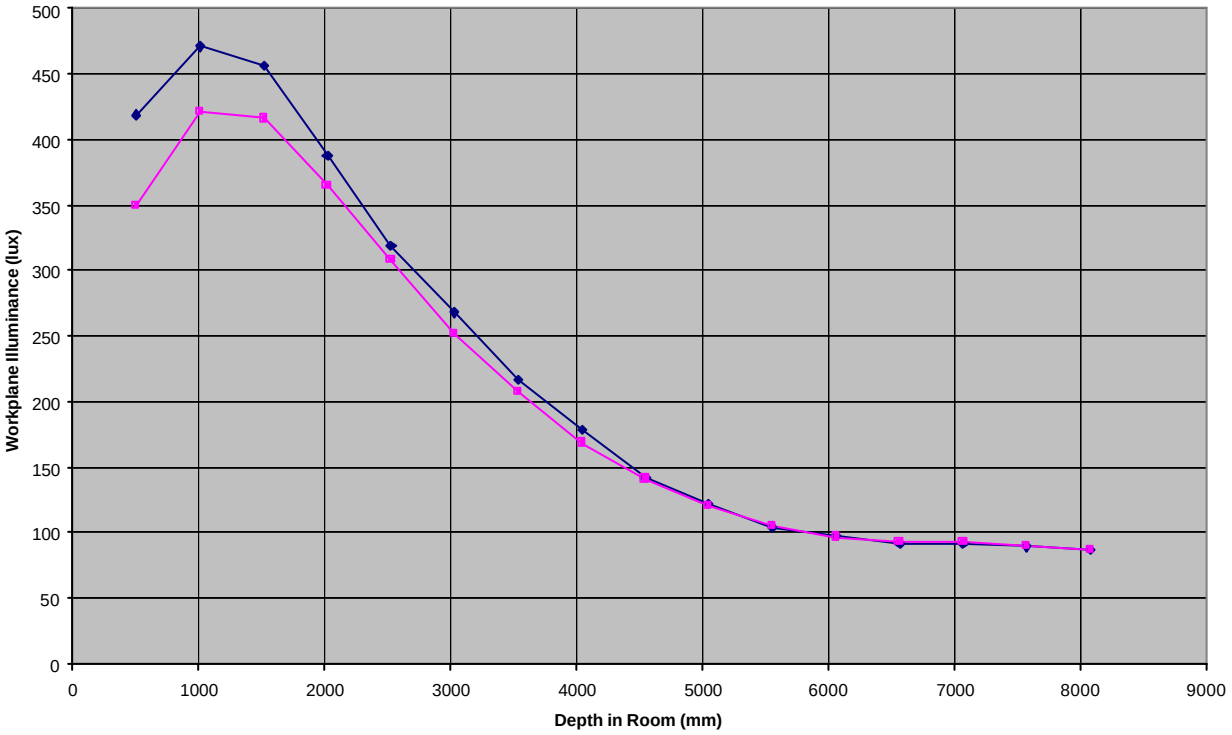

Figure 5.22 - Horizontal Illuminances in Test Building with Vertical Micro-Light Guiding Shade Panels, Overcast Sky

The position of maximum illumination was shifted between 1.0 and 1.5m into the room, due to illumination dispersed across the ceiling. Beyond this depth there was a steady decline to the back of the room. Illuminance uniformity was acceptable, with ratios between maximum, mean and minimum illuminances between 2.0 and 2.6.

Internal light levels provided by the panels depend mainly upon the illuminance incident upon the panel. This implies independence on external conditions, including sun position. This is provided by the diffusing nature of the panels' input sheets. This independence on external conditions was important in the design of the micro-light guiding shade panel (section 3.3.4). Figure 5.22 displays the results of scaling the two measurement sets to an average vertical illuminance of 40klx.

5.5.1.3 Monitored Light Levels

Internal light levels six metres back from the window were logged for a total period of six weeks, along with external global and diffuse irradiance. Figures 5.23 to 5.25 display typical daily profiles of global irradiance, diffuse irradiance and interior illuminance for clear, partially cloudy and cloudy days. Under each sky condition, interior illuminance followed global irradiance fairly closely. To examine the relationship between room illuminance and global irradiance, the two were plotted against each other (Figure 5.26). This plot displays data measured from 14 to 22 September. A clear positive correlation is suggested between global irradiance and internal illuminance.

Six metres back from the window, natural illuminance exceeded 200 lx where the global irradiance exceeded 550W/m^2. In clear skies at this time of year, this occurs around three hours either side of midday. This demonstrates the effectiveness of the micro-light guiding shade panels in consistently providing natural illumination deep inside a room.

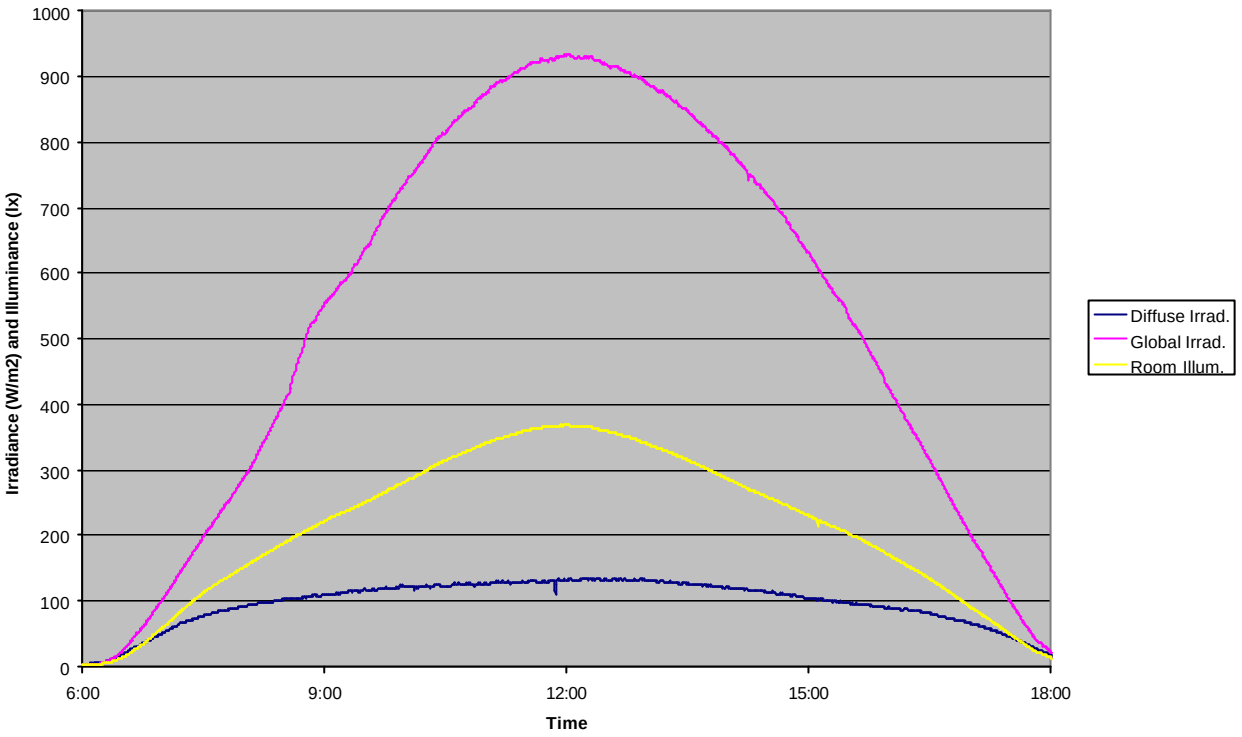

Figure 5.23 - Global and Diffuse Irradiance and Room Illuminance in Test Building with Vertical Micro-Light Guiding Shade Panels, Clear Day

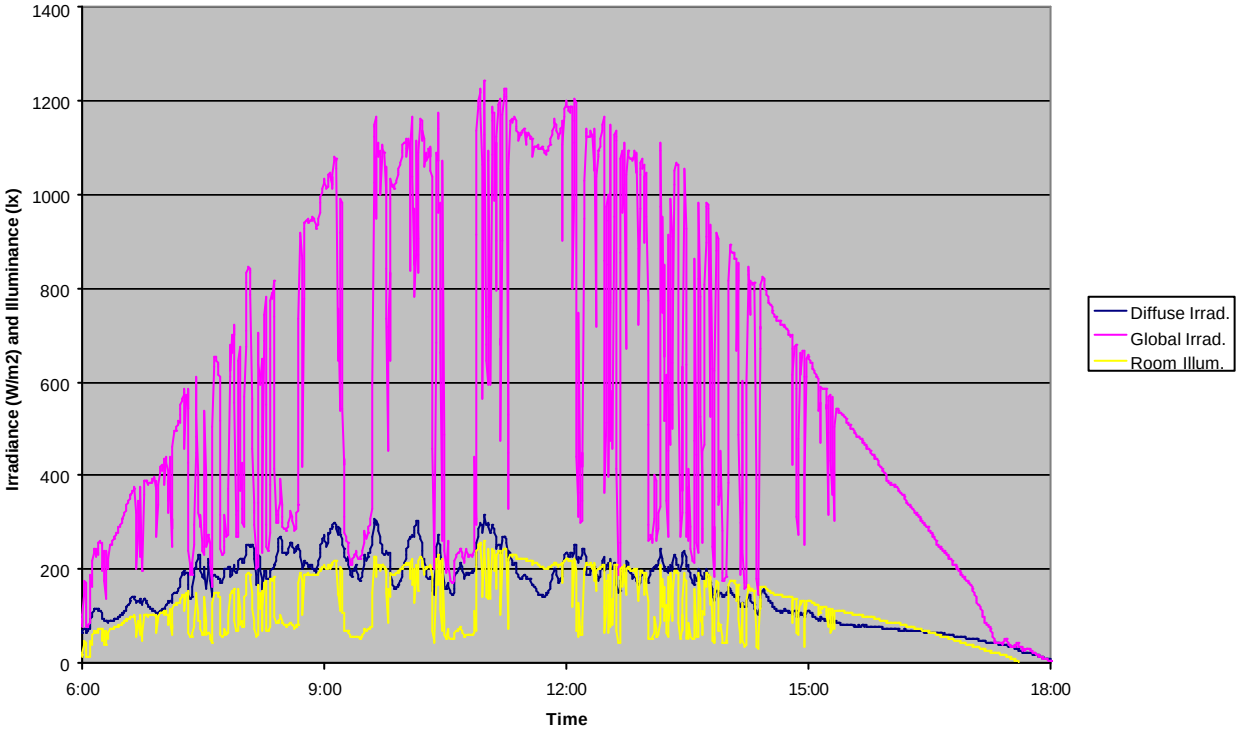

Figure 5.24 - Global and Diffuse Irradiance and Room Illuminance in Test Building with Vertical Micro-Light Guiding Shade Panels, Partially Cloudy Day

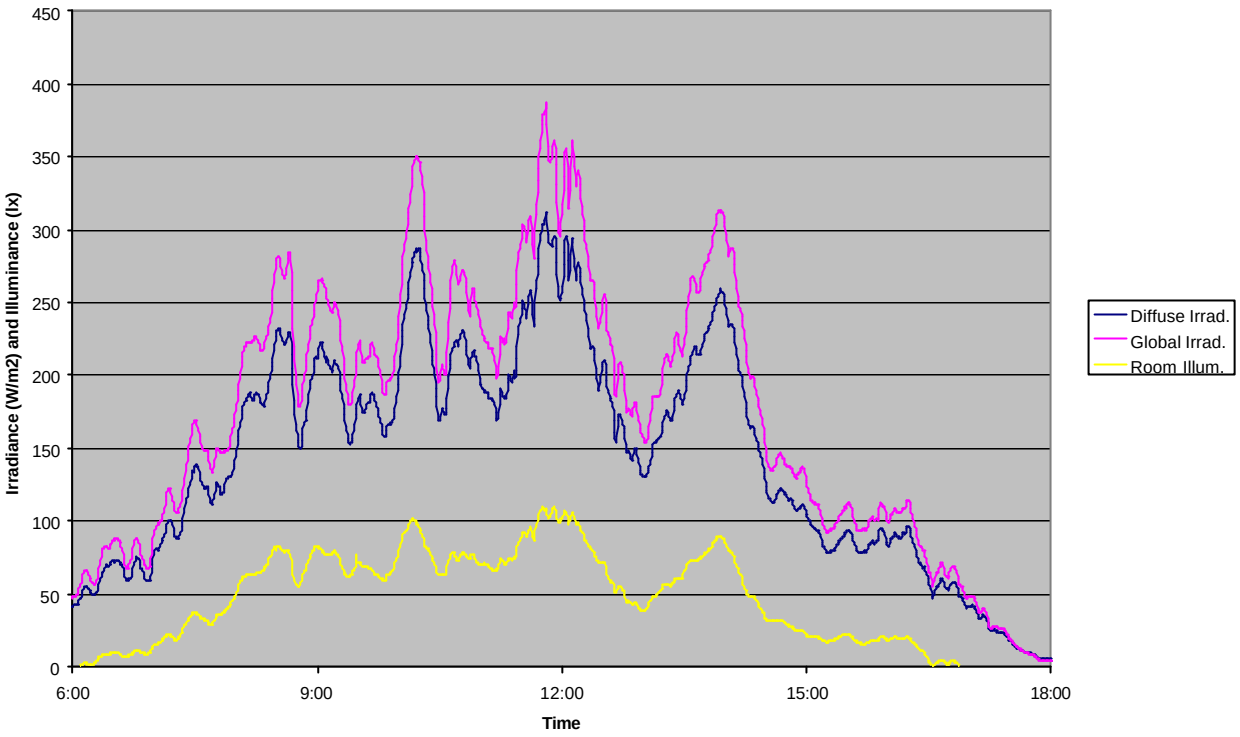

Figure 5.25 - Global and Diffuse Irradiance and Room Illuminance in Test Building with Vertical Micro-Light Guiding Shade Panels, Cloudy Day

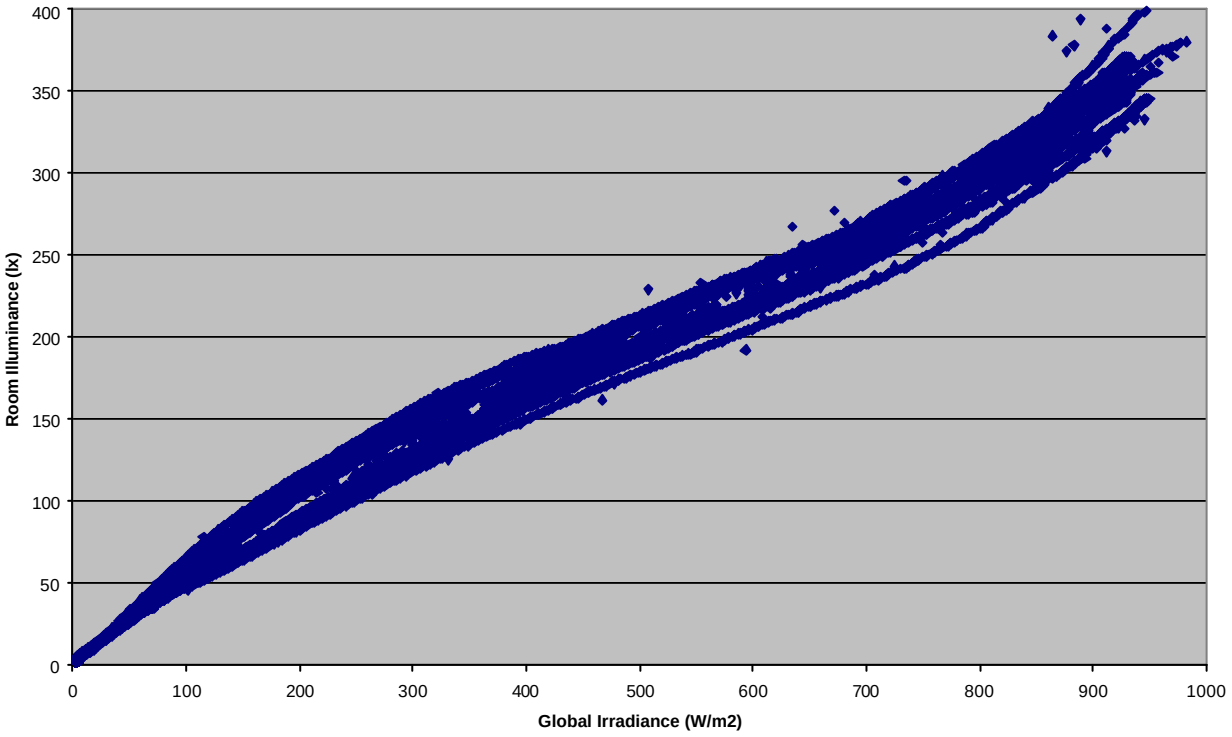

Figure 5.26 - Relationship between Global Irradiance and Room Illuminance, Vertical Micro-Light Guiding Shade Panels on Test Building

5.5.1.4 Summary

Measured illuminance profiles (Figures 5.19 and 5.22) showed the vertical micro-light guiding shade panels working as expected, distributing light deep into the room while reducing excessive illumination near the window. Comfortable illumination was supplied throughout the room (Figure 5.21). A small degree of glare was observed when looking directly at the device, indicating some light spilt into directions below horizontal (Figure 5.20). This was likely caused by reflector roughness and difficulties in manufacture (section 5.3.1.3). Internal illuminances supplied by the micro-light guiding shade panel were largely independent of the solar position, depending only on the illuminance incident upon the panels.

The efficiency of the micro-light guiding shade panels was further supported by monitored internal illuminances. A light sensor six metres from the window measured natural illuminances exceeding 200 lx from 8.30am to 3pm on a string of clear spring days (Figures 5.23 and 5.26).

It should be noted that the vertical device is not the intended form of the micro-light guiding shade panel. Generally, the device is intended to form a shading panel tilted out from the building façade, as shown in Figure 5.15. The device is also intended to be installed on high rise commercial buildings. Under these circumstances, the high illuminances passing through the view window would be reduced, and more uniform illumination would be supplied.

Finally, the space beneath the lowest micro-light guiding shade output apertures appeared quite dark when installed (Figure 5.27). This dark lower border created excessive contrast between the view window and the micro-light guiding shade panels. As visual discomfort may be increased by the presence of this dark region, this should be avoided for future panels. For this reason, the bottom cover of the tilted micro-light guiding shade panel was created as shown in Figure 5.14.

Figure 5.27 - Contrasting Dark Band at Bottom of Vertical Micro-Light Guiding Shade Panels

5.5.2 TILTED PANELS

5.5.2.1 Clear Sky, Midday

Figures 5.28 and 5.29 display averaged horizontal illuminances measured without and with the panels covered, respectively. Average external illuminances were: horizontal global 81klx, vertical north 90klx, direct normal 115klx, panel incident 113klx. Measurements exposed to direct sunlight are not shown.

Measurements were completed around solar noon. At this time, the sun directly faced the test building window. With the sun in this position, significant glare was perceived when looking toward the window. The main cause of this glare was the installed translucent panels. These were not as diffusing as desired. A significant amount of spread specular transmission occurred, and sunlight was directed into the eyes of standing observers (Figure 5.30). This also resulted in a bright patch of redirected sunlight incident upon the rear wall (Figure 5.31).

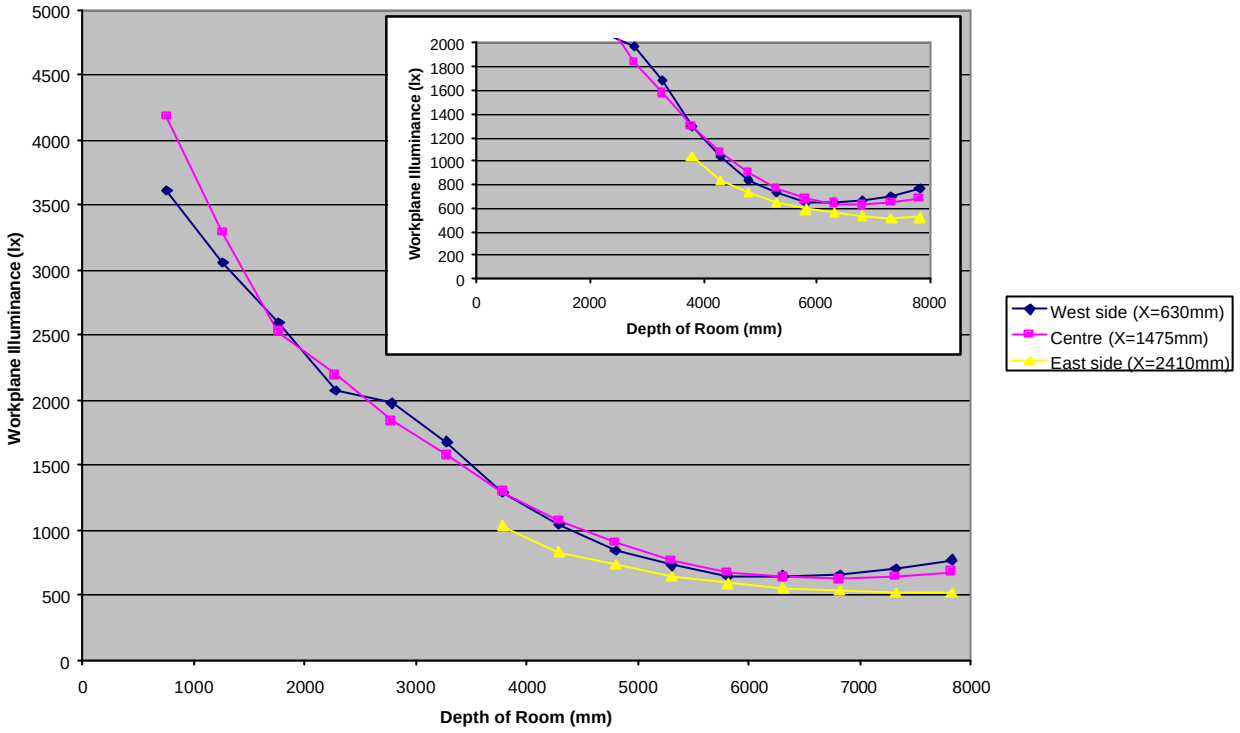

Figure 5.28 - Measured Illuminances in Test Building with Tilted Micro-Light Guiding Shade Panels, Clear Sky Midday, Panels Uncovered (Insert Shows Scaled Up Version of Same Figure)

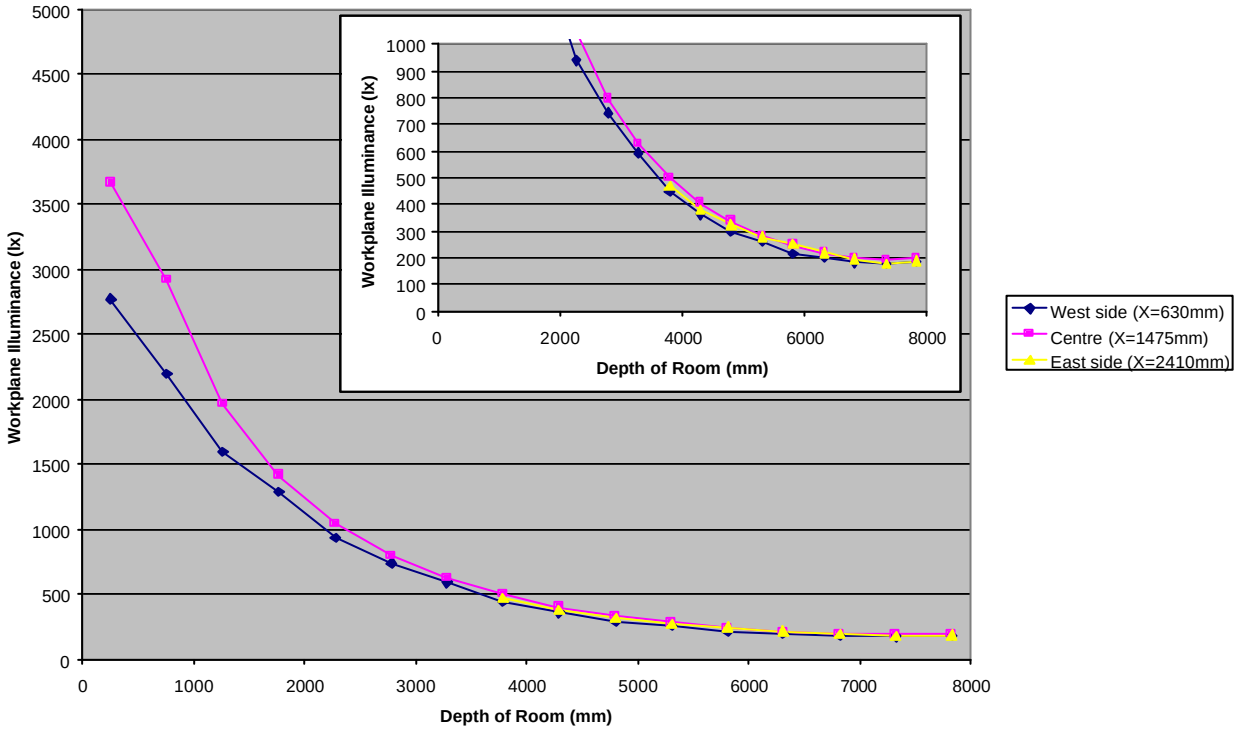

Figure 5.29 - Measured Illuminances in Test Building with Tilted Micro-Light Guiding Shade Panels, Clear Sky Midday, Panels Covered (Insert Shows Scaled Up Version of Same Figure)

Figure 5.30 - Sunlight Directed into the Eyes of Observers at Solar Noon by the Tilted Micro-Light Guiding Shade Panels

Figure 5.31 - Bright Patch of Redirected Sunlight on the Rear Wall of the Test Building with Tilted Micro-Light Guiding Shade Panels

The bright patch of redirected sunlight provided a large vertical illuminance on the rear wall. Light reflected off this bright patch raised horizontal illuminances in the rear of the room (Figure 5.28).

The illuminance contribution of the tilted panels was calculated as the difference between the scaled averaged profiles without and with the panels covered (Figure 5.32). Illuminances were greater on the west than on the east. During

measurements, the sun was slightly to the east of north. Directionally transmitted sunlight was then spread over the west and rear walls. This raised illuminances on the west and in the rear of the room.

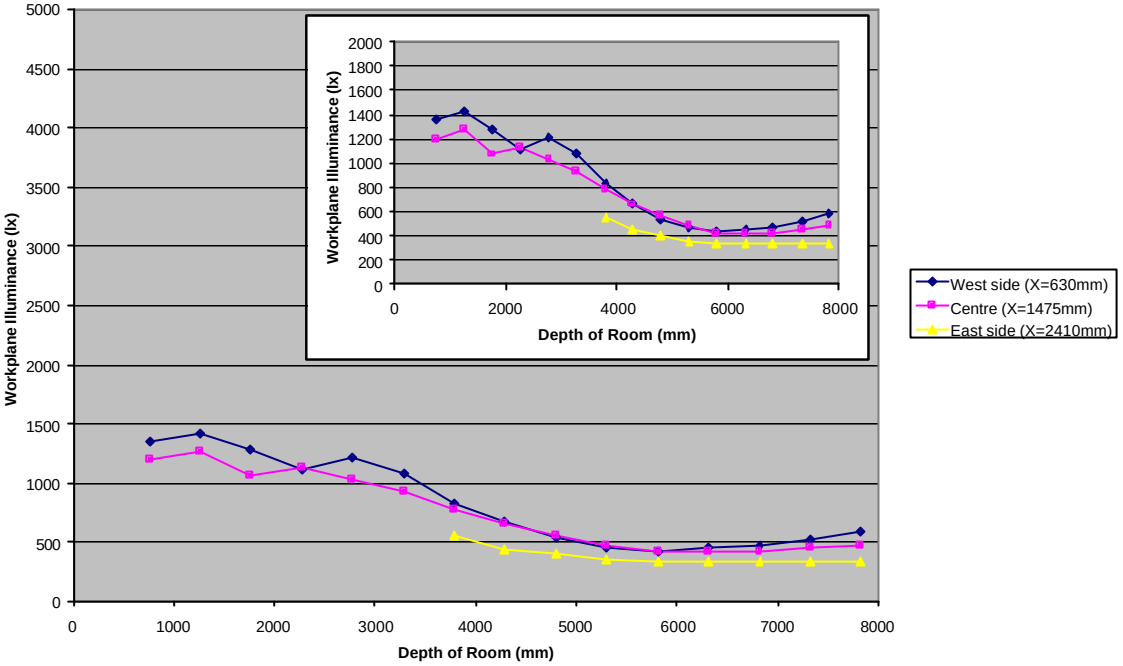

Figure 5.32 - Calculated Illuminances in Test Building with Tilted Micro-Light Guiding Shade Panels, Clear Sky Midday, Panels Only (Insert Shows Scaled Up Version of Same Figure)

The scaled averaged central profiles of each measurement set are displayed in Figure 5.33. The view window provided most illumination within two metres of the window. Beyond this depth, the tilted panels provided more illumination. In the rear of the room, the panels provided 2.4 times the illuminance provided by the view window.

Illuminance uniformity was improved by the tilted micro-light guiding shade panels. The ratios of maximum, mean and minimum illuminances ranged between 2.0 and 2.4 for total illumination, between 3.0 and 3.6 for illumination provided by the view window, and between 1.60 and 1.65 for illumination provided by the panels.

Internal illuminances provided by the roof vent were quite low, with a maximum of 12 lx on the work surface.

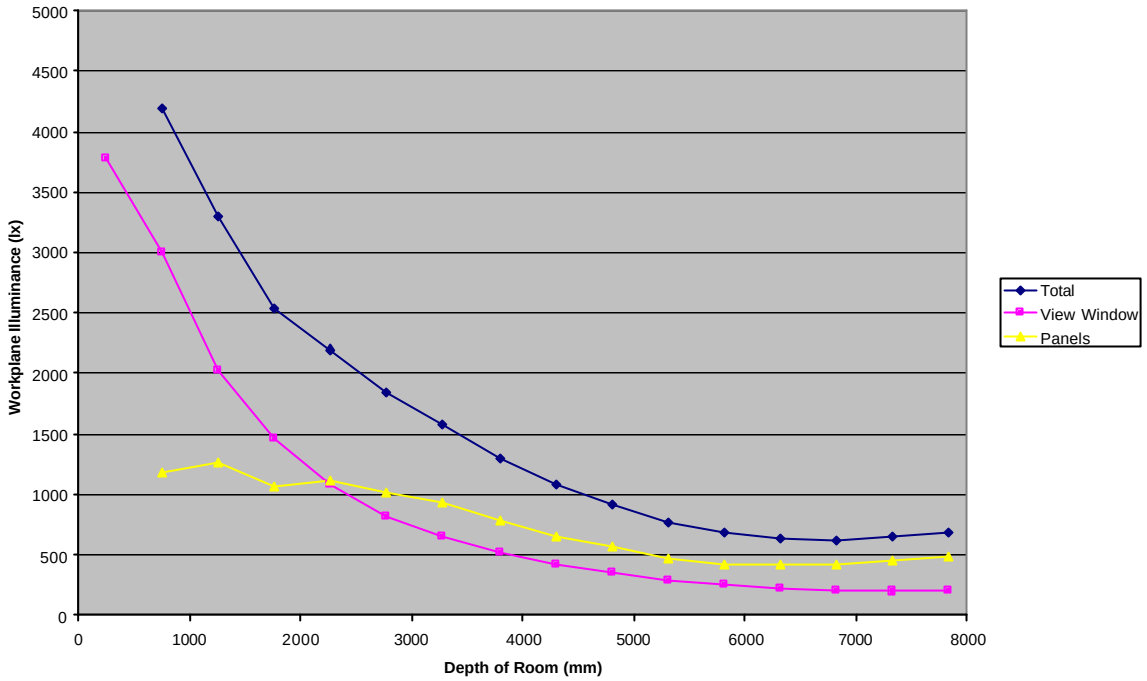

Figure 5.33 - Illuminance Contributions along the Central Profile of the Test Building with Tilted Micro-Light Guiding Shade Panels, Clear Sky Midday

As described above and shown in Figures 5.30 and 5.31, there was a glare problem with these panels under these conditions. When in line with the sun, significant glare was experienced at standing height. This was likely caused by four factors:

- The installed translucent was not as diffusing as desired. Strong directional transmission was evident.
- The parabolic section reflectors were approximated by seven flat sections. This could cause light to be directed up to 15° below horizontal (section 5.3.2.2).
- The flat section reflectors were manufactured on an imperfect bending machine (section 5.3.2.6). This could cause varying reflection properties within the panels.
- Interior reflections off the transparent surface can cause low level luminances up to 60° below horizontal (section 5.3.2.2, Appendix 2).

Occupant surveys revealed that the room illuminated by the micro-light guiding shade panels was perceived as light, even, pleasant, not gloomy, and with some bright areas. This compared well with the shaded room (with the panels

covered over). The latter was perceived as dark, uneven, unpleasant, gloomy, dim, dull and disliked. Occupants preferred the unshaded room (with the panels uncovered) generally and for its light distribution, but not for view out. Neither surveyed occupant would have turned on task lighting in the unshaded room.

5.5.2.2 Overcast Sky

External conditions during overcast sky measurement were somewhat variable, with the horizontal global illuminance varying between 10 and 35klx. Due to the highly variable exterior conditions, internal illuminances were also quite varied. To compare measurement sets, measured internal illuminances were scaled to an average horizontal global illuminance of 30klx. This was achieved by interpolating external illuminances for each row (centre, west, east) in each measurement set. External illuminances were assumed to vary linearly with time in between measurements. Scaled measurement sets were analysed to obtain average internal illuminance distributions under a 30klx overcast sky. This corresponds to an average vertical north illuminance of 16klx and a panel incident illuminance of 21klx. The resulting scaled average internal illuminances are displayed in Figures 5.34 and 5.35.

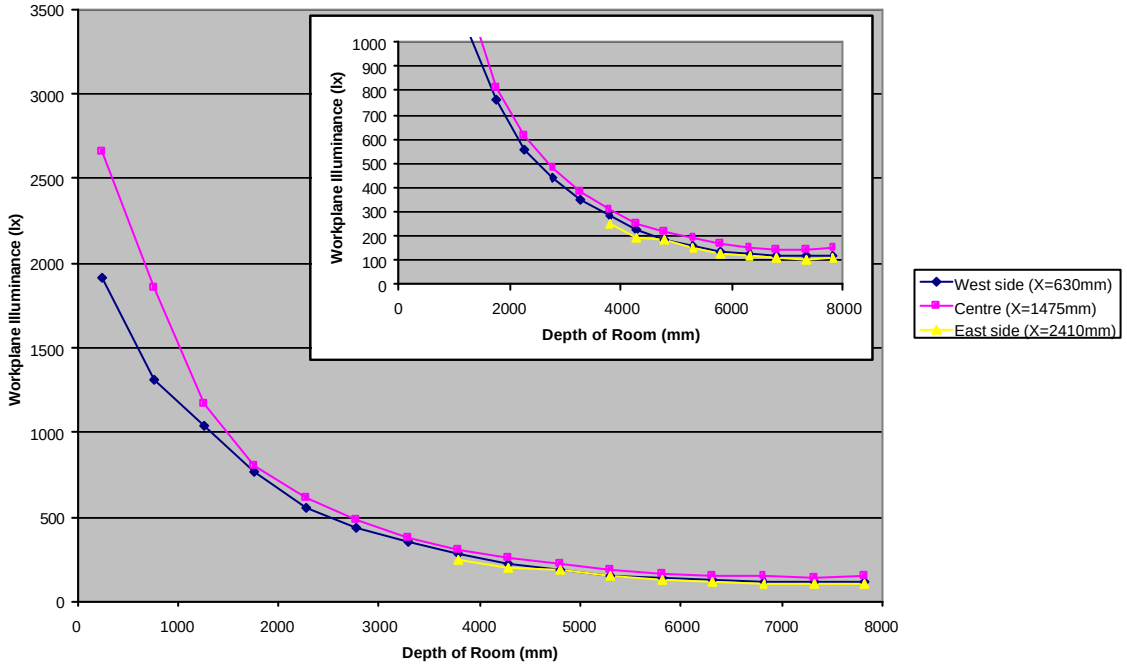

Figure 5.34 - Measured Illuminances in Test Building with Tilted Micro-Light Guiding Shade Panels, Overcast Sky, Panels Uncovered (Insert Shows Scaled Up Version of Same Figure)

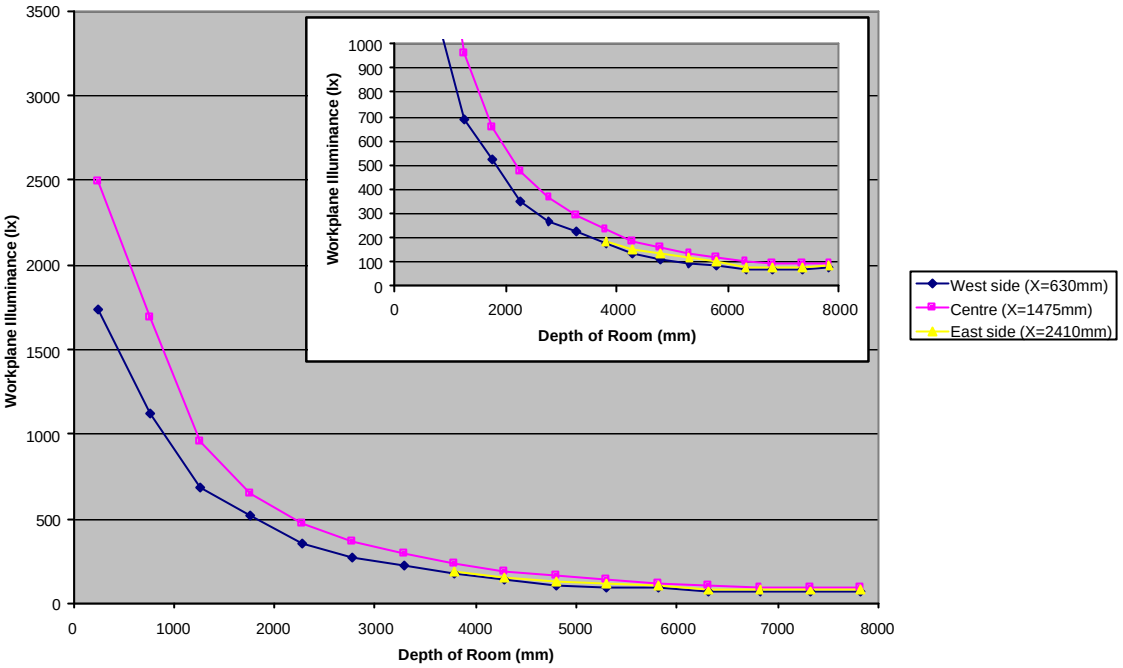

Figure 5.35 - Measured Illuminances in Test Building with Tilted Micro-Light Guiding Shade Panels, Overcast Sky, Panels Covered (Insert Shows Scaled Up Version of Same Figure)

Both horizontal illuminance distributions decayed with depth up to six metres. With the micro-light guiding shade panels uncovered, interior illuminances levelled out somewhat in the rear of the room. The panels did not deliver as much illumination to the rear of the room as they did under sunny conditions. The calculated illuminance contribution of the micro-light guiding shade panels is shown in Figure 5.36. This distribution is quite rough. This may be due to the complex way in which measured data were scaled and averaged in order to calculate this contribution.

Figure 5.37 displays the components of horizontal illuminance along the centre row. The panels provided little illumination throughout the room. In the rear of the room, the panel contribution exceeded 50% of the illumination provided by the view window.

This result appears discouraging for the panels. Recall that the panel incident illuminance was around 21klx. This compares with 113klx under the clear sky condition, and 40klx under a bright overcast sky with the vertical panels. Since the panels' contribution to internal illumination varies with panel incident illuminance, it is not surprising that these illuminance contributions are relatively

low. Internal natural light levels are still improved at all depths by the panels. The panels also improved illuminance uniformity. The ratios of maximum, mean and minimum illuminances improved from between 3.7 and 4.1 for the view window to between 3.25 and 3.35 for total illumination. The panels only contribution displayed excellent uniformity, between 2.15 and 2.20.

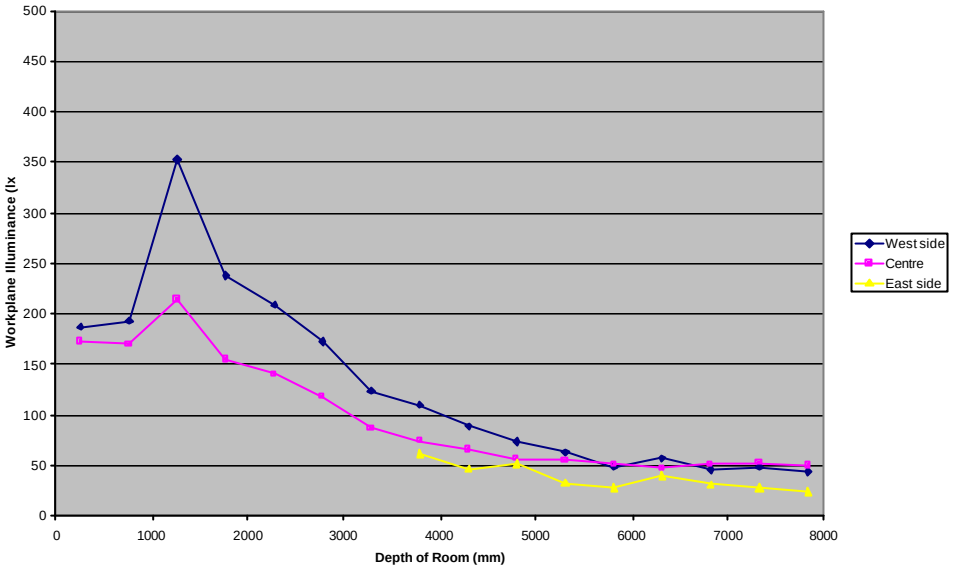

Figure 5.36 - Measured Illuminances in Test Building with Tilted Micro-Light Guiding Shade Panels, Overcast Sky, Panels Only

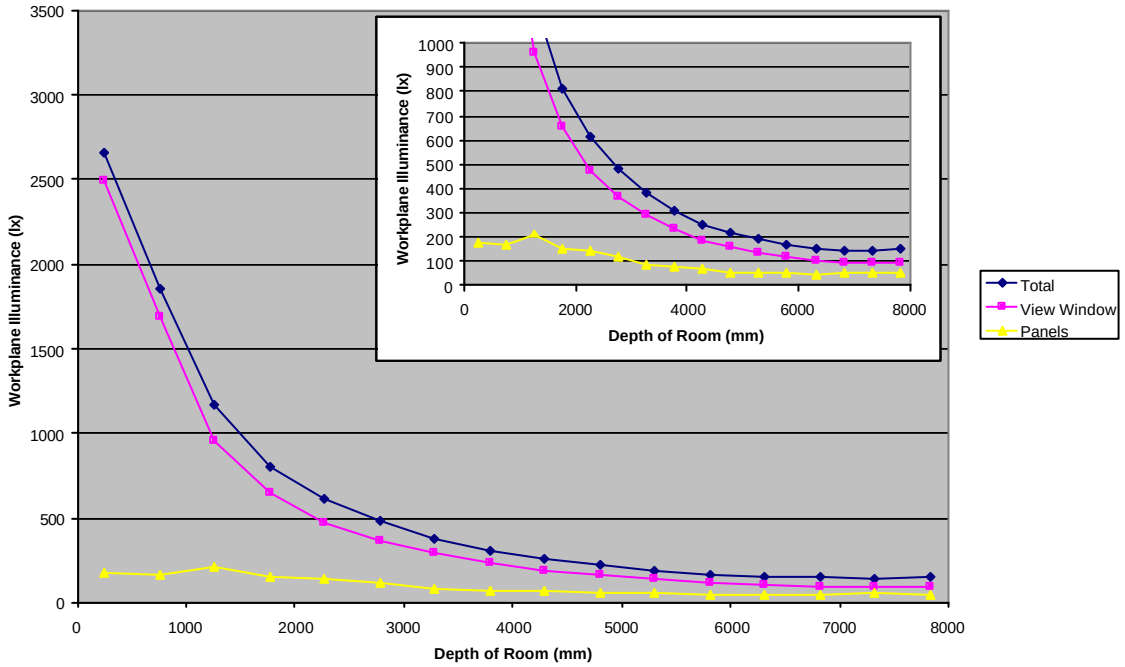

Figure 5.37 - Illuminance Contributions along the Central Profile of the Test Building with Tilted Micro-Light Guiding Shade Panels, Overcast Sky (Insert Shows Scaled Up Version of Same Figure)

Internal illuminances provided by the roof vent were measured under a horizontal global illuminance of 26klx. Delivered illuminances were very small, with a maximum of 4 lx under the vent.

The room was somewhat darker and gloomier under overcast skies than under clear skies. However, no glare problem was apparent. It actually appeared glarier in the room with the panels covered over. In this situation, the panels were darker to look at, producing greater contrast on looking out the window.

Both survey participants preferred the room with the panels uncovered. The shaded room was perceived to have a fairly low light level, with gloomy regions and little bright regions. It was perceived as unpleasant, disliked, dark, uneven and dim. Some glare was perceived when looking toward the window, and there was difficulty reading in the low light levels. General artificial lighting would have been turned on by both participants. The unshaded room was perceived to be a little gloomy with little bright regions, but illumination was more even. Glare in the window direction was reduced, as was reading difficulty. Both occupants were less likely to turn on general artificial lighting.

5.5.2.3 Clear Sky, High Relative Solar Azimuth

The installed translucent material displays directional transmittance of illumination. This directional transmittance destroys the independence of interior illumination on external conditions. To examine the dependence on solar position, measurements in the test building were repeated with the sun at greater relative azimuth. These measurements were completed around 9.30am on 29 August. The sun was approximately north-east of the building, with a relative azimuth close to 45°. Average external illuminances were: horizontal global 75klx, vertical north 75klx, direct normal 116klx and panel incident 96klx. Figures 5.38 and 5.39 display averaged horizontal illuminances for measurements completed without and with the panels covered.

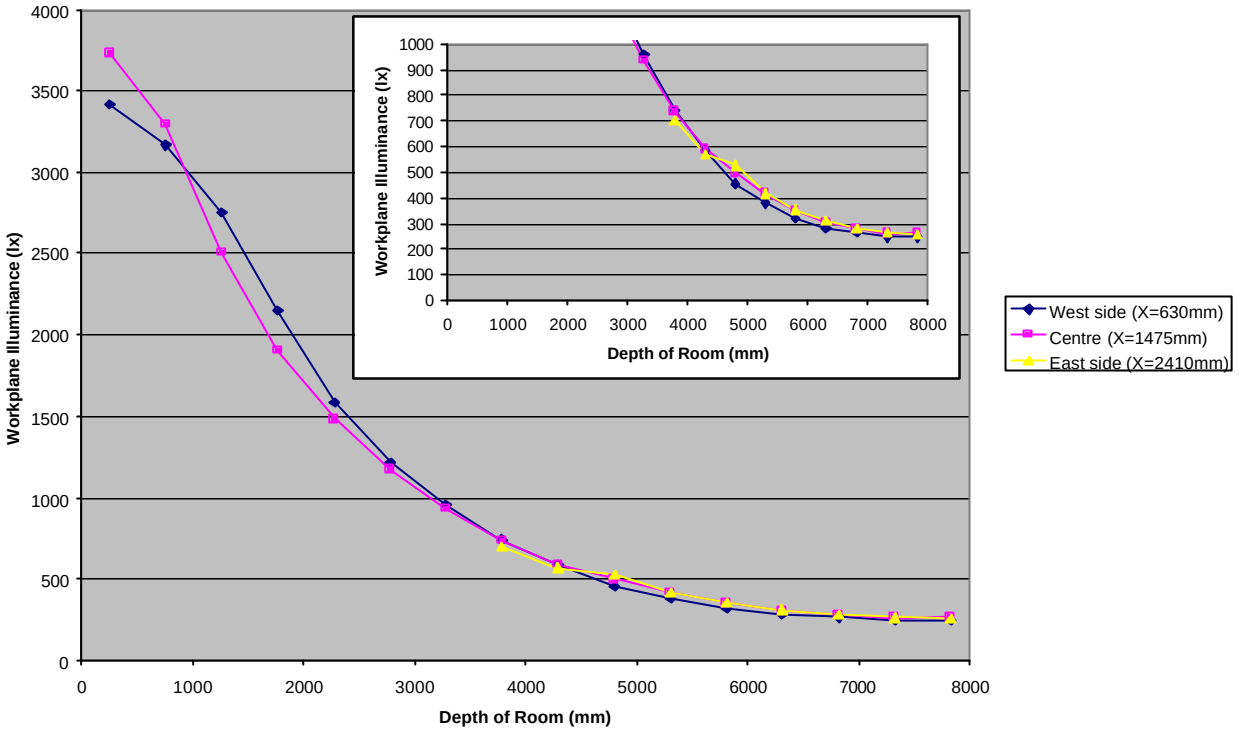

Figure 5.38 - Measured Illuminances in Test Building with Tilted Micro-Light Guiding Shade Panels, Clear Sky, High Relative Azimuth, Panels Uncovered (Insert Shows Scaled Up Version of Same Figure)

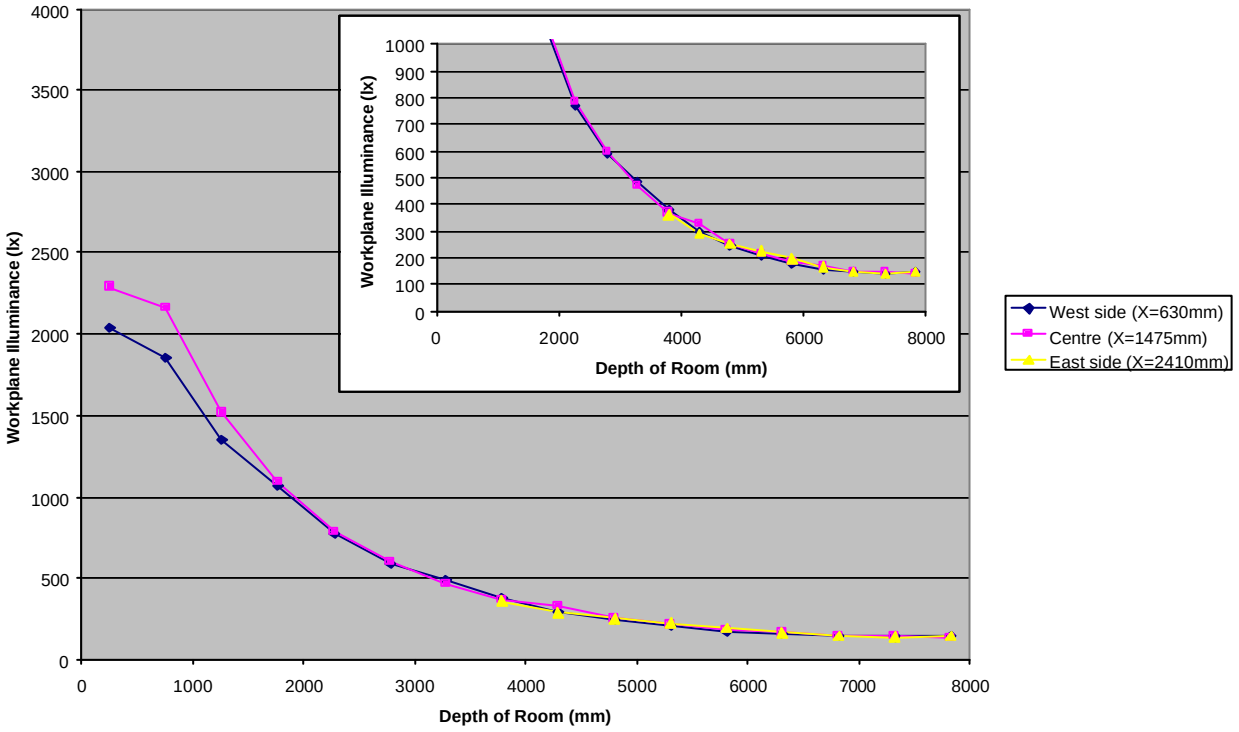

Figure 5.39 - Measured Illuminances in Test Building with Tilted Micro-Light Guiding Shade Panels, Clear Sky, High Relative Azimuth, Panels Covered (Insert Shows Scaled Up Version of Same Figure)

Figure 5.38 displays interior illuminances in the room with the panels uncovered. Interior illuminances fell from around 3.7klx near the window to around 260 lx in the rear of the room. Some difference was apparent between east, centre and west profiles. Western illuminances were less than central illuminances up to around one metre depth. Western illuminances were then higher for the next two metres. At greater room depths, eastern illuminances were around the same as those in the centre, and western illuminances were lower. These profiles indicate the directional transmittance of the panels. With the sun in the north-east, a redirected sun patch struck the west wall near the window. This provided higher western illuminances in this region. The bright patch effectively illuminated central and eastern positions in the depth of the room. However, it was ineffective in illuminating western positions deep inside the room. Thus, deep west illuminances were lower than those in the east and centre. Vertical illuminances displayed a similar trend. Light was not delivered into the rear of the room as much as it was at midday (Figure 5.28).

The illuminance contribution of the panels was calculated as the difference between the previous profiles (Figure 5.40). Interior illuminances delivered by the panels ranged from around 1.7klx down to 120 lx. Directional transmittance is clear as western illuminances peak at 1.25m depth. In the rear of the room, western illuminances were slightly lower than both eastern and central illuminances.

The components of illumination provided by the view window and the panels are shown, for the central profile, in Figure 5.41. Illuminances were provided almost equally by the panels and the view window. The latter provided greater illumination within two metres of the window. The panels provided slightly more illumination between two and four metres depth. Beyond this depth, their contributions were almost equal. Thus, the illumination performance of the panels under these conditions was worse than their performance at midday. The cause of this discrepancy is the directional transmittance of the panels.

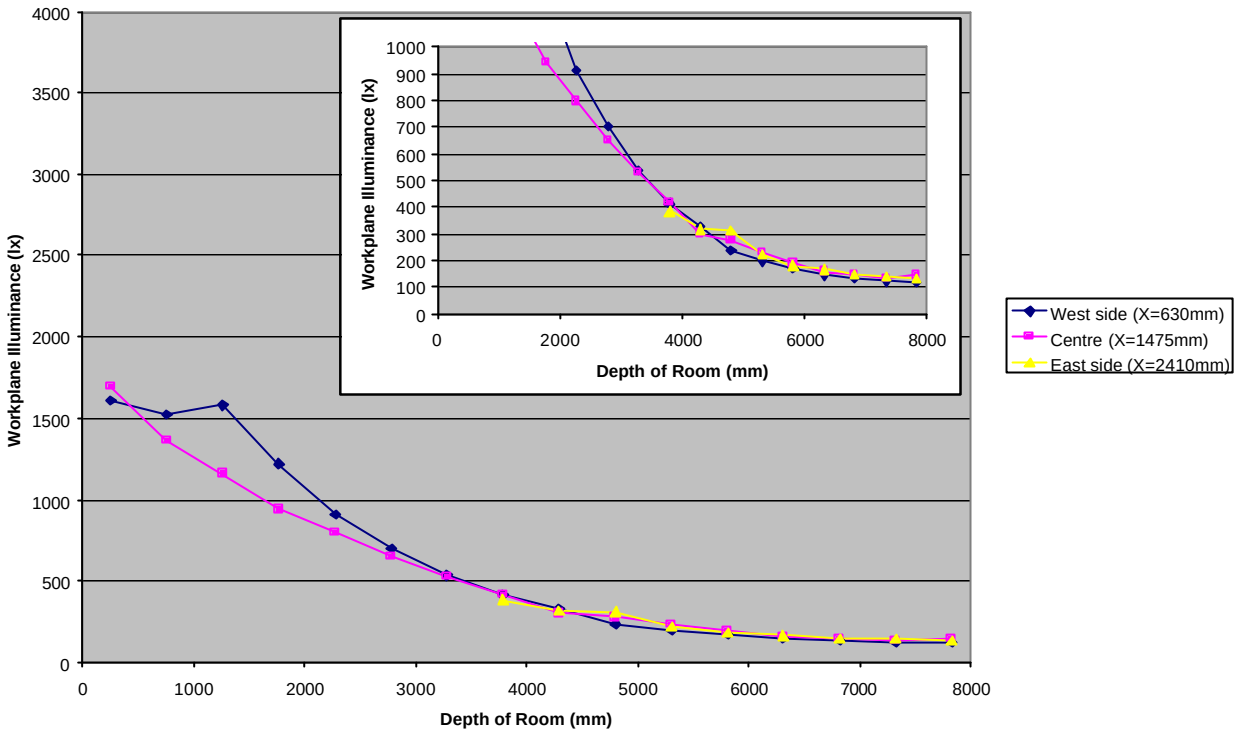

Figure 5.40 - Measured Illuminances in Test Building with Tilted Micro-Light Guiding Shade Panels, Clear Sky, High Relative Azimuth, Panels Only (Insert Shows Scaled Up Version of Same Figure)

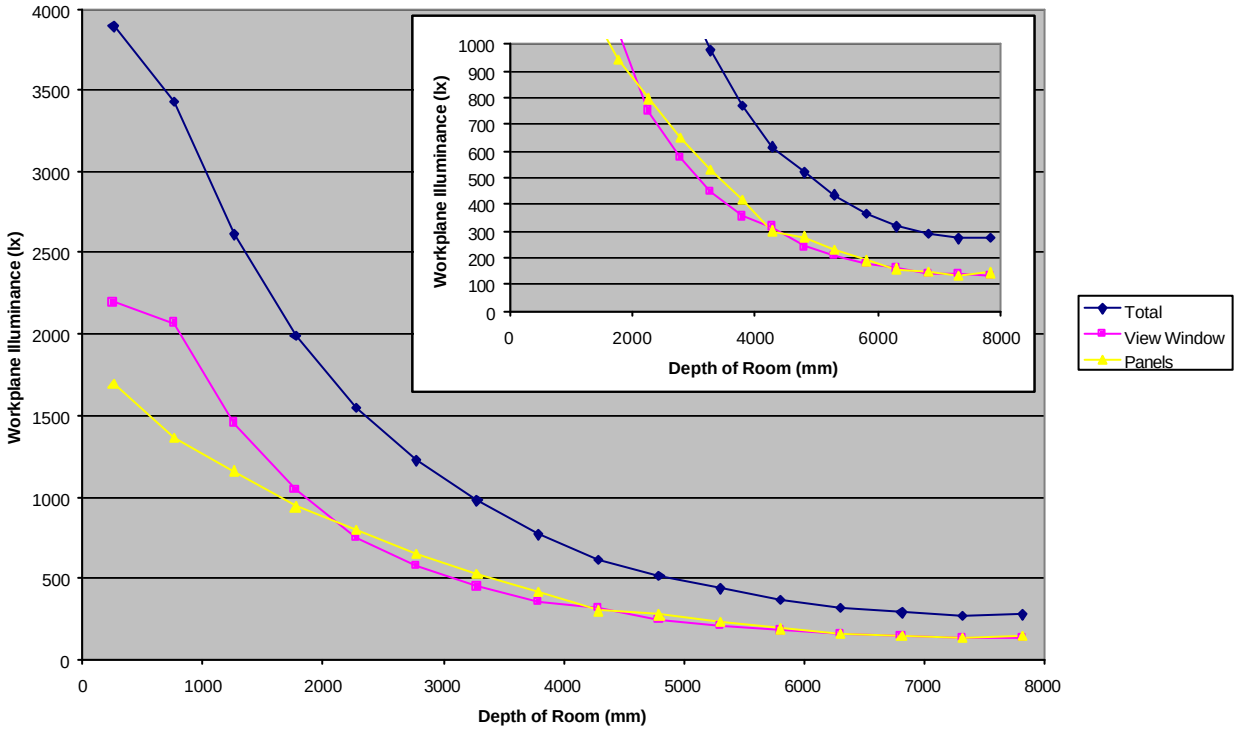

Figure 5.41 - Illuminance Contributions along the Central Profile of the Test Building with Tilted Micro-Light Guiding Shade Panels, Clear Sky, High Relative Azimuth (Insert Shows Scaled Up Version of Same Figure)

Illuminance uniformity was not improved by the micro-light guiding shade panels. The illuminance peak in the western profile increased the mean illuminance and provided a large ratio of mean to minimum illuminance. However, the ratio of maximum to mean illuminance was improved.

Visual comfort conditions were improved. Glare from the panels was not obvious unless you were positioned within the bright patch on the western wall. The bright wall patch wasn't as obvious as that at midday. The room was generally perceived as fairly light and non-glary.

The unshaded room was again preferred in all respects by both survey subjects. The shaded room was perceived to have a fairly low light level with no bright patches. The unshaded room was more liked and evenly lit. Artificial lighting was less likely to be switched on in the unshaded room. One subject found the unshaded room 'much brighter and less patchy', and described 'less need for electric lights'.

5.5.2.4 Opalescent Translucent

The tilted micro-light guiding shade panels displayed problematic directional transmittance. It was wished to examine the effect on glare and room illumination of replacing the installed translucent material with a highly diffusing opalescent. A 3mm sheet of opalescent diffusing acrylic was placed on top of the installed translucent sheeting. This effectively created a highly diffusing material with transmittance equal to the product of the transmittances of the two individual materials.

Figures 5.42 to 5.44 display vertical illuminance measured up and across the rear wall of the building. Note that, for Figures 5.42 and 5.43, illuminances are presented along the horizontal axes and height is presented up the vertical axis. Also note that illuminances with and without the opalescent sheeting are presented on separate axes above and below the plots respectively. Figure 5.44 shows vertical illuminances measured across the rear wall. Vertical illuminances with and without the opalescent sheeting are displayed on axes to the right and left of the chart, respectively.

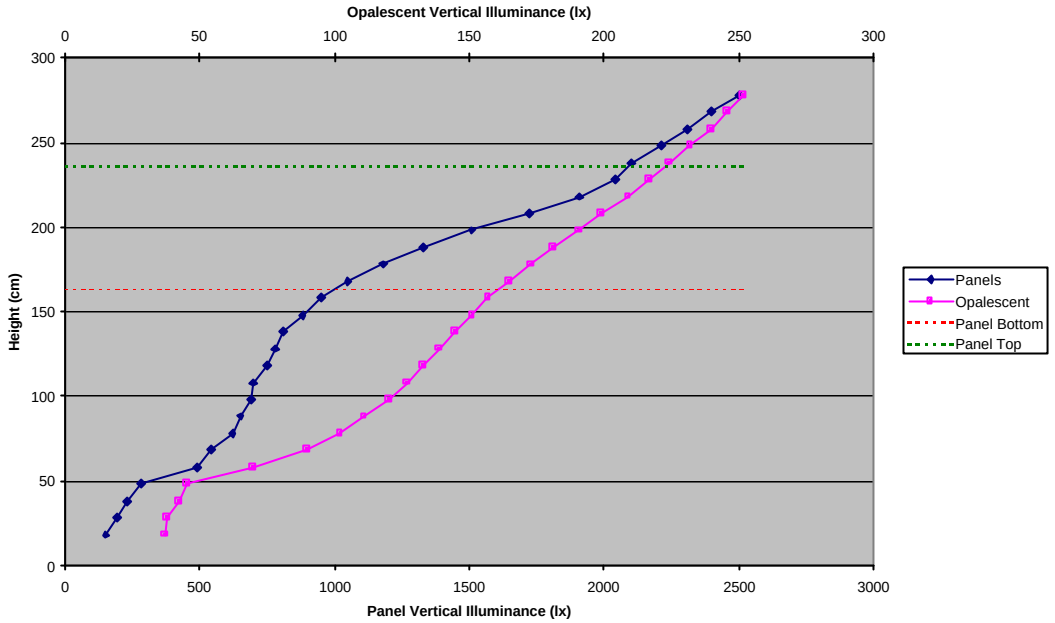

Figure 5.42 - Vertical Illuminances Up the Rear Wall of the Test Building with Tilted Micro-Light Guiding Shade Panels, 19 September

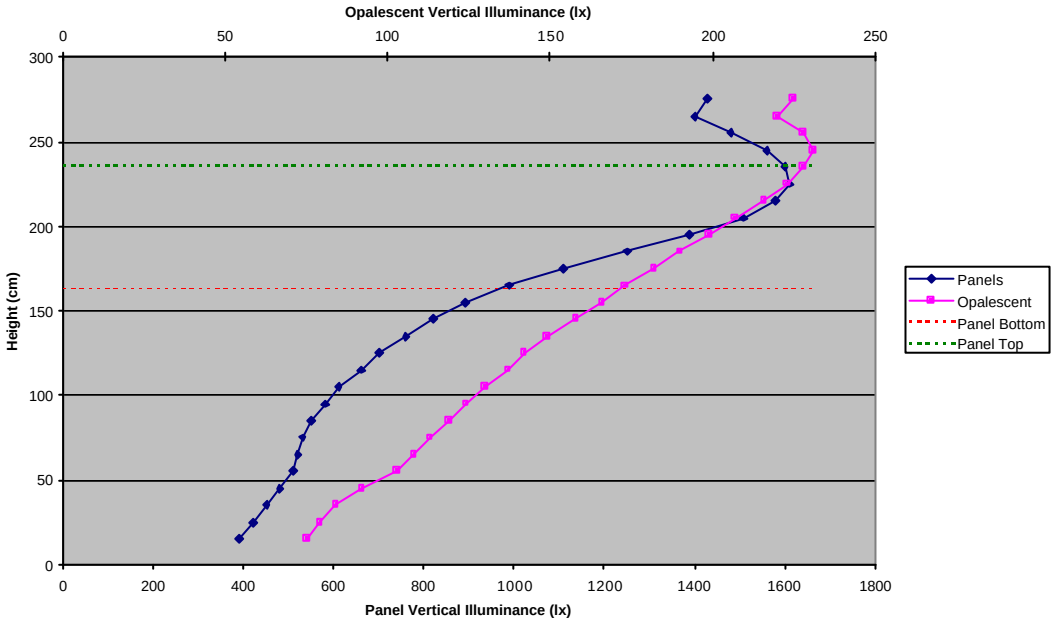

Figure 5.43 - Vertical Illuminances Up the Rear Wall of the Test Building with Tilted Micro-Light Guiding Shade Panels, 24 September

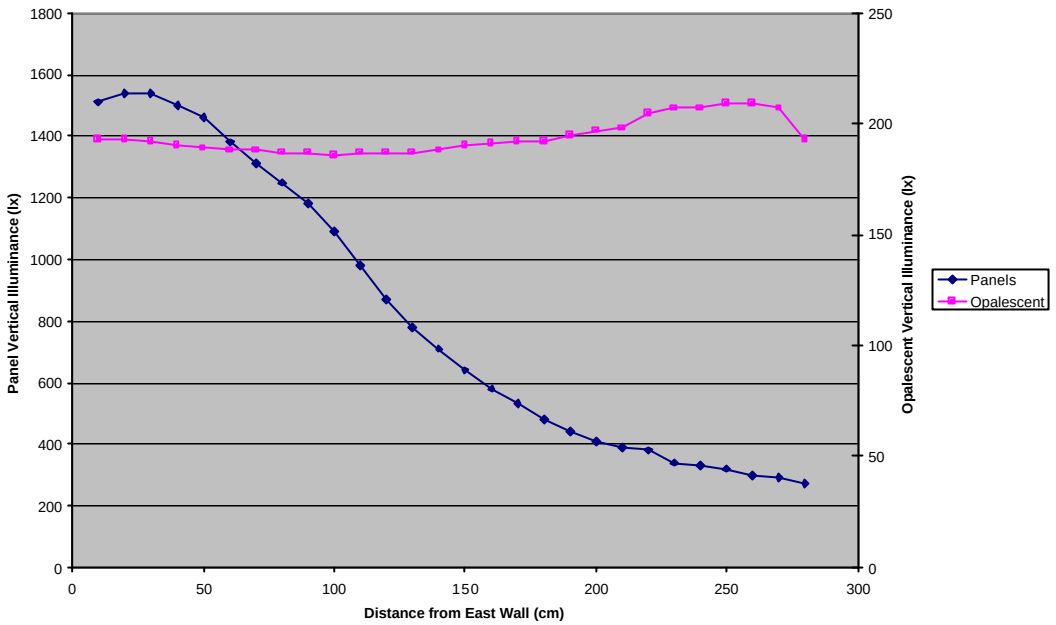

Figure 5.44 - Vertical Illuminances Across the Rear Wall of the Test Building with Tilted Micro-Light Guiding Shade Panels, 19 September

The panels' directional transmittance without the opalescent sheeting is clear in each chart. Figures 5.42 and 5.43 display a sharp rise in vertical illuminance above the bottom of the panels. Figure 5.44 shows vertical illuminances much greater (more than five times) within the bright patch than outside of it. Vertical illuminances due to the opalescent sheeting displayed a more steady rise up the wall, and were almost constant across the wall. The opalescent sheeting delivered little direct component to the rear wall.

Illuminances were much lower with the opalescent sheeting installed. In regions not within the redirected sun patches, the ratio of illuminances measured with and without the opalescent sheet approached the opalescent sheet's transmittance, approximately 30%.

Vertical illuminances dropped dramatically toward floor level in Figure 5.42. These measurements were made in the east of the room. A table is located near this corner of the room. Thus, vertical illuminances fell where the measuring instrument was shaded by the table. No such dramatic drop is seen in Figure 5.43, as these measurements were completed up the centre of the rear wall. Raised illuminances toward the west in Figure 5.44 were provided by light passing through the roof vent.

Room illumination was also assessed by horizontal and vertical illuminance measurements. All illumination was provided by the tilted micro-light guiding shade panels covered by opalescent sheeting. Averaged measurements are shown in Figure 5.45. Horizontal illuminances were quite low, varying between 430 and 90 lx. Illuminances rose to maximum at depth around 0.75m, followed by a steady decline to the rear of the room. This distribution is very similar to those shown in Figures 5.19, 5.22 and 5.36. Illuminances rose slightly near the rear wall, indicating light directed deep inside the room. The panels with the opalescent sheeting provided excellent illuminance uniformity, with ratios of maximum, mean and minimum illuminances varying between 1.8 and 1.9.

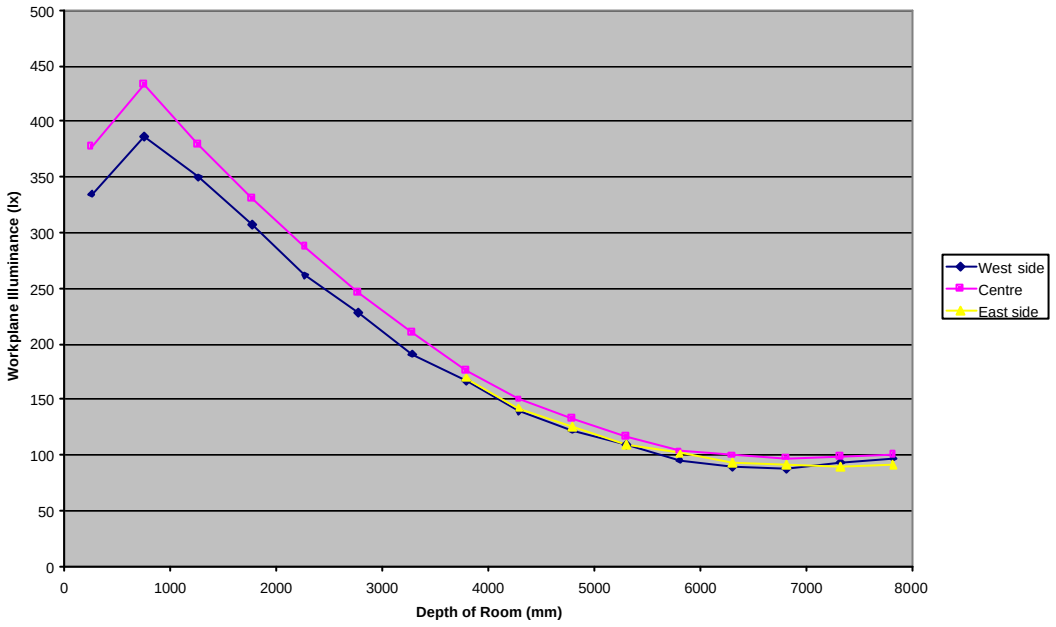

Figure 5.45 - Measured Illuminances in Test Building with Tilted Micro-Light Guiding Shade Panels and Opalescent Sheeting, Panels Only

5.5.2.5 Summary

The installed tilted micro-light guiding shade panels had some glare problems. These were largely caused by the directionally transmitting translucent sheet used at the input. Glare was not always apparent, but was particularly problematic when sunlight was directed deep in the room into the eyes of occupants. Apart from this glare problem, the micro-light guiding shade panels provided excellent room illumination.

With the sun nearly directly north, illumination was pushed back to the rear wall, raising illuminances in the rear two metres. The panels improved daylight uniformity, and the panels alone provided excellent uniformity. Under a clear winter sky, illuminances exceeded 500 lx at all depths. Minimum illuminances in the shaded room were around 180 lx. In the rear of the room, the panels provided more than twice the illumination provided by the view window. The unshaded room was preferred over the shaded room, except for the glare problem. It was also more likely that artificial lighting would be switched on in the shaded room, with little chance of turning on lights in the unshaded room (based on occupant surveys).

With low incident illuminance, the panels provided little illumination to the room under overcast skies. Despite this, natural illuminances within the room were greater and more uniform with the panels. The panels alone again provided excellent illuminance uniformity. No glare problem was apparent, with glare more likely in the shaded room. The unshaded room was preferred over the shaded room, with the unshaded room more evenly lit and a little brighter. Artificial lighting was less likely to be switched on in the unshaded room.

Directional transmittance was again observed with the sun at higher relative azimuth. A redirected sunlight patch on the wall near the window degraded illuminance uniformity. The panels provided roughly the same illumination provided by the view window. Glare was improved over midday conditions, but was still present when the observer was aligned with the panels and the sun. The unshaded room was perceived as brighter and more even, and was preferred over the shaded room. Again, artificial lighting was less likely to be switched on in the unshaded room.

Replacing the installed translucent with opalescent sheeting improved visual comfort and illuminance uniformity. However, natural light level contributions of the panels were significantly reduced. The performance of the system would be greatly improved if a translucent material with similar light spreading ability as opalescent acrylic, but higher transmittance was available.

The internal illuminance distribution measured with the opalescent sheeting and the view window covered displayed a characteristic depth distribution. Horizontal illuminances peaked at depth around 0.75m as natural illumination was dispersed across the ceiling. Beyond this depth, illumination declined slowly until rising near the rear wall. This measured distribution should be easily scalable for other opalescent diffusers of higher transmittances.

5.6 SUMMARY

Two micro-light guiding shade panels were designed, constructed, installed and assessed for performance. The daylighting test building and the selected micro-light guiding shades were described and illustrated in Figures 5.1 to 5.3. Construction proved difficult and time-consuming. The micro-light guiding shade elements of the vertical panels were sisallation coated, hot-wire cut polystyrene. While construction of these elements was relatively quick and easy, problems were discovered with adhesion to and roughness of the sisallation. Highly reflective silver coated aluminium formed the micro-light guiding shade elements of the tilted panels. Reflectors were created by bending the aluminium to seven flat sections to approximate the required parabolic sections. This process was time-consuming and imperfect. Future constructions may require greater initial cost outlay for an industrial pressing technique.

Construction costs outlined in section 5.3.3 should be considered worst-case scenarios. Material costs increased as accuracy of construction and aesthetic considerations were improved. Construction costs would be reduced, for significant volumes of panels, by introducing an industrial manufacturing process such as metal pressing.

Problems with light output distributions may be caused by interior reflections off the transparent output surface. These reflections deliver low level luminances in directions up to 60° below horizontal. The problem is worse for panels of greater tilt. This problem is not easily rectified. Simply raising the lower limit of the output angular range will not solve the problem. If the output surface were

removed, dirt, water and insects would penetrate the device and ruin reflector performance. An anti-reflective coating on the interior surface adds expense and may provide coloured transmission into the room.

The panels were installed on the test building, and measurements of light distributions within the building were completed, along with assessments of visual comfort. The vertical panels worked as expected, delivering daylight deep into the room while reducing excessive illumination near the window. Comfortable illumination was supplied throughout the room. The bottom edge of the panels was too dark, requiring a different design for the bottom of the tilted panels.

Some glare was provided by the tilted panels, due to the poorly diffusing translucent sheeting. This was particularly a problem under clear skies when the observer was aligned with the sun and the panels. Besides this problem of glare, the tilted micro-light guiding shade panels performed exceptionally. Interior illuminance levels were increased throughout the room, illuminance uniformity was improved and the unshaded room was consistently preferred over the shaded room. Importantly, artificial lighting was less likely to be switched on, under each sky condition, due to installation of the panels.

Replacing the installed translucent material with opalescent sheeting further improved visual comfort and illuminance uniformity. However, a translucent material with greater light spreading ability yet higher transmittance would improve the panels' performance.

The device is intended to be installed on high rise commercial buildings. Ground reflections would likely be reduced and the high illuminances provided by the view window would be diminished. This would provide more comfortable and uniform room illumination, and should also improve thermal performance. It would also make the contribution of the micro-light guiding shade panels to internal illumination more important.

5.7 CONCLUSIONS

- Manual construction of micro-light guiding shade panels is time- and cost-consuming. Alternative industrial manufacturing techniques are required.
- Low level light output may be delivered outside the device's output angular range by interior reflections off the output transparent surface.
- Constructed micro-light guiding shade panels delivered comfortable, natural illumination deep into the test building, improved illuminance uniformity, were preferred by occupants and reduced the chances of turning on artificial lighting.
- Some glare was delivered by the directionally transmitting translucent. A translucent material with large light spreading ability and high transmittance would improve panel performance.

CHAPTER 6 - SIMULATION OF THE MICRO-LIGHT GUIDING SHADE PANELS ON THE TEST BUILDING

For the micro-light guiding shade panel to be installed on buildings, designers must be confident that the device performs as desired. This must be determined early in the design process. Computer lighting simulation permits swift evaluation of lighting design alternatives, and is common in building design firms (Ubbelohde & Humann, 1998). Thus, computer algorithms were developed to effectively model the micro-light guiding shade panel.

If simulations could accurately predict real parameters of interest (eg. illuminance, luminance, luminous intensity), the device could be more commonly adopted. This would occur as designers could assess device performance, early in the design process, with confidence in their results. Simulations of the micro-light guiding shade panel must agree closely with measurements. The purpose of this chapter is to demonstrate agreement between measurement and simulation of the micro-light guiding shade panels installed on the test building.

This chapter begins with the basis of all simulations. This is followed by the models of the room and panels. Simulation results are then presented and compared with measurements. The chapter is concluded by a summary of the results and their implications.

6.1 SIMULATION BASIS

Lighting simulations were performed using RADIANCE. RADIANCE was selected following the literature survey presented in Chapter 2. It is a lighting simulator of high quality, high capabilities and high accuracy (Fontoynont, Laforgue, Mitanchey, Aizlewood, Butt, Carroll, Hitchcock, Erhorn, De Boer, Michel, Paule, Scartezzini, Bodart & Roy, 1999; Jarvis & Donn, 1997; Khodulev & Kopylov, 1996; Mardaljevic, 1995, 2000a, 2001; Roy, 2000). Importantly, it is capable of modelling advanced light redirecting devices, including those based on non-imaging optics (Compagnon, 1993; Courret, Paule & Scartezzini, 1996; Courret, Scartezzini, Francioli & Meyer, 1998).

Numerous algorithms were developed to ensure the accuracy of daylight simulations. Simulations of the micro-light guiding shade panel required the development of new materials and geometries within RADIANCE. To test that these models worked as desired, methods were developed to test their angular luminous throughput. Simulated luminous throughput distributions were validated against measurement (Chapter 4), demonstrating that the models worked as required. Sensitivity tests aided the manufacture of the installed devices (Chapters 4 and 5). New sky luminance models were created, based on the Standard Sky Luminance Distributions (SSLD) (Kittler, Perez & Darula, 1997). New material models were also developed to better simulate the test building.

Applications of the developed algorithms to the micro-light guiding shade panels on the test building are described in the following sections. More detailed descriptions of the algorithms are provided in Chapter 7.

RADIANCE simulation parameters can significantly impact the accuracy of simulation results (Fontoynont *et al.*, 1999; Jarvis & Donn, 1997; Khodulev & Kopylov, 1996; Mardaljevic, 1995, 2000a, 2001; Roy, 2000). These were set to very high levels to ensure accurate simulations.

6.2 MODELLING THE PANELS, THE BUILDING AND THE SKY

RADIANCE models were created of the micro-light guiding shade panels, based on the materials and constructions described in Chapter 5. All materials and geometry in the test building were measured and carefully reproduced. This required new material models for the coloured steel walls and ceiling. A new sky model algorithm was applied for more accurate modelling of external conditions.

6.2.1 MODELLING THE MICRO-LIGHT GUIDING SHADE PANELS

RADIANCE simulation of the micro-light guiding shade panel proceeds in four parts. First, the reflective surfaces of a micro-light guiding shade element are created. Second, the reflecting elements are arrayed and surrounded by a supporting frame and translucent input panel. Thirdly, the created panels are

placed into a RADIANCE model. With all geometry and materials defined, the RADIANCE simulation finally proceeds. Several 'scene files' are created, each containing different parts of the model.

A brief description of the model creation and application are given in this section, followed by details specific to each of the modelled panels. A detailed, step-by-step description of model creation and application is provided in Appendix 3.

The specially shaped micro-light guiding shade elements are created by *gensurf*. The flat, upper reflectors are defined as *polygons*. One pair of reflector surfaces are created and placed in a scene file. Panel materials are defined in a second scene file. This latter file also contains the remaining panel geometry. It contains a reference to the first scene file, creating an array of several micro-light guiding shade elements within the panel. The panel is covered with a translucent panel and a supporting frame. A third scene file refers to the second scene file, moving the completed panel into position. Several similar panels can be placed on a building in this third scene file.

The output of a micro-light guiding shade element is an important source of natural illumination. Therefore, the luminous output of each element is pre-calculated using *mkillum*. This program directs a large number of rays at each defined output surface and pre-calculates its luminous output distribution. Light passing through the device enters through the diffusing input sheet. Thus, light reflection within the panel is part of RADIANCE's indirect calculation. Since *mkillum* pre-calculates indirect illumination, this is the most efficient manner of performing RADIANCE simulations of the micro-light guiding shade panel.

A new scene file contains a single surface representing the output of a micro-light guiding shade element. This surface comprises the transparent material that forms the panel's output surface. A final scene file refers to this scene file, creating an array of output surfaces and moving them into position. Options for the *mkillum* program are placed at the beginning of this final scene file, controlling the accuracy of pre-calculated luminous output distributions.

Simulation of the created micro-light guiding shade panel proceeds as follows. A base *octree* is created that contains all surfaces except the panel output surfaces. The panel output surfaces are then added to the previous octree, creating a new octree. Mkillum pre-calculates the required luminous output distributions, taking the new octree as input. This creates a new scene file containing the output surfaces and their luminous output distributions. Finally, this new scene file is added to the base octree, creating a final octree. This final octree contains the complete RADIANCE model, with pre-calculated light output distributions. RADIANCE simulation processes, including *rpict*, *rillum*, *rtrace* and *rview*, can then continue as usual.

6.2.1.1 Vertical Micro-Light Guiding Shade Panels

Two vertical micro-light guiding shade panels were created, each of a different length, to fit into the window of the test building (Figure 5.1). Two scene files contained the micro-light guiding shade elements (two different lengths). Each contained three surfaces: the upper and lower reflectors and a spacer (due to the required thickness of the polystyrene reflector elements). The completed panels were contained in two more scene files. These each contained the arrayed micro-light guiding shade elements, a wood frame, a translucent input panel and three frame elements. Separate scene files contained the output surfaces of the micro-light guiding shade elements.

Material definitions were added, based on measured reflectances and transmittances of all important materials. Material property measurement procedures are described in section 6.2.2.1. Material properties are shown in Table 6.1.

Table 6.1: Material Properties for the Vertical Micro-Light Guiding Shade Panels

Material	Colour	Diffuse Refl. (%)	Specular Refl. (%)	Diffuse Trans. (%)	Specular Trans. (%)	Roughness
Reflector	Grey	0	95	0	0	0.04
Translucent	White	14.4	0	79.7	0	0
Transparent	Clear	0	Fresnel[1]	0	91.5[2]	0
Wood frame	Pine	45.6	0	0	0	0

Notes:
1. Specular reflectance varies according to Fresnel's equations, refractive index 1.52
2. Specular transmittance defined at normal incidence

The exterior light shelf was modelled in AutoCAD, translated into RADIANCE and transformed into position. The corrugated metal light shelf was modelled as a flat sheet. Its corrugation was modelled by functionally modifying its surface normal. Thus, the shelf was a flat rectangular sheet, but its surface normal varied smoothly and periodically across the sheet, affecting the directions into which specular reflections were directed. The sheet comprised galvanised sheet metal with diffuse reflectance 12.1%, specular reflectance 28.2% and roughness 0.2. The size of the corrugations were modelled as measured.

6.2.1.2 Tilted Micro-Light Guiding Shade Panels

The flat surface approximation to the parabolic section was created by gensurf. Gensurf parameters were altered to create seven flat sections (n=7, no smoothing (section 4.3.5)). Ten micro-light guiding shade elements were arrayed within the panel. The panels were then moved into place on the test building, matching their installation.

Material properties are displayed in Table 6.2. The reflector material was significantly smoother than that in the vertical panels. Reflector roughness was reduced accordingly to zero. The anisotropic specular reflections of the extruded aluminium framing material was modelled by applying a functional texture.

Table 6.2: Material Properties for the Tilted Micro-Light Guiding Shade Panels

Material	Colour	Diffuse Refl. (%)	Specular Refl. (%)	Diffuse Trans. (%)	Specular Trans. (%)	Roughness
Reflector	Grey	0	95	0	0	0
Translucent	White	6	4	53.4	35.6	0.02
Opalescent	White	10	0	30.3	0	0
Transparent	Clear	0	Fresnel[1]	0	91.5[2]	0
Framing	Grey	33.5	14.4	0	0	0.2
Acrylic	Clear	0	Fresnel[3]	0	99.7[4]	0
Top cover	White	79.3	4.2	0	0	0.01

Notes:
1. Specular reflectance varies according to Fresnel's equations, refractive index 1.52
2. Specular transmittance defined at normal incidence
3. Specular reflectance varies according to Fresnel's equations, refractive index 1.5, Hartmann's constant 0 (no dispersion)
4. Transmissivity per millimetre, equivalent to 92% per inch (Ward, 1996: 7)

The directionally transmitting translucent material was particularly difficult to model. The measured transmittance and reflectance was partitioned into diffuse and specular components. Total transmittance and reflectance of the translucent material were measured as 89% and 10% respectively. 40% of each of these were assumed to be specular or spread specular. A roughness of 0.02 allowed for spread specular transmission and reflection. The material roughness transferred transmitted sunlight into RADIANCE's indirect calculation. Thus, the pre-processed light output distributions, provided by mkillum, include all transmitted illumination.

The opalescent material was given a purely diffuse transmittance equal to the product of the transmittances of the two translucent sheets. The reflectance was assumed equal to that of the inner sheet. These properties are listed in Table 6.2.

Panel mounting brackets were contained in separate scene files. Two side braces and a central brace were created and moved into position. The braces comprised the aluminium framing material described above, without texture applied. A top cover was added above the panels on the building (Figure 5.15). The top cover comprised the same material as that of the panels' top cover. The side shade sections comprised off-white painted wood of diffuse reflectance 67.5%.

6.2.2 MODELLING THE TEST BUILDING

A detailed RADIANCE model of the test building was created. All materials and geometry in the room were carefully measured and reproduced. Details of the room can be seen in the photographs presented in Chapter 5.

Internal furnishings were added as shown in Figure 6.1. The geometry of the roof vent (Figure 5.16) was quite complex, so a simplified model was constructed (Figure 6.2). The vent's indirect contribution to room illumination was pre-calculated by mkillum.

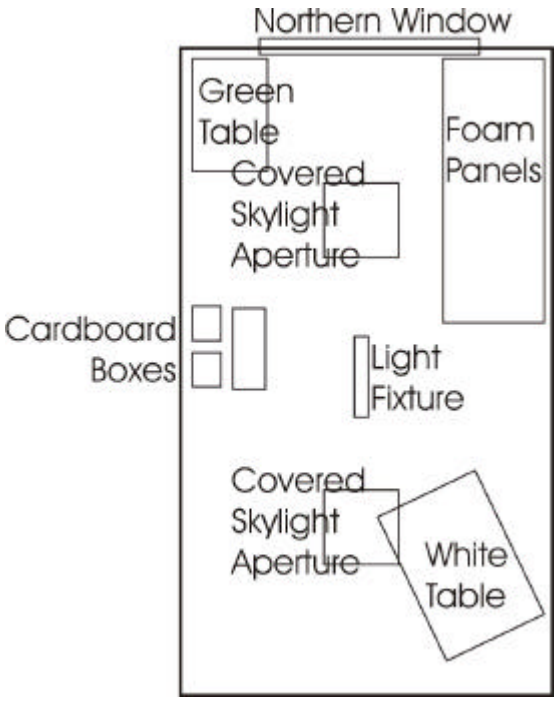

Figure 6.1 - Modelled Internal Furnishings

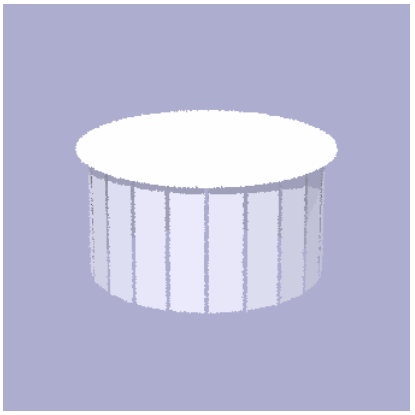

Figure 6.2 - Simplified Model of Roof Vent

6.2.2.1 Material Property Measurement

Material properties of relatively unimportant materials were measured as shown in Figure 6.3. The material of interest was placed under a steady artificial light. Incident illuminance was measured by an illuminance meter placed on the sample. Reflected illuminance was measured by turning over the meter and placing it over the sample such that shadowing was minimised. The material's reflectance was calculated as the ratio of reflected and incident illuminances. Measurements were repeated several times to find a mean reflectance and level of uncertainty. A similar procedure was employed to determine material transmittances. Material properties measured in this fashion are listed in Table 6.3.

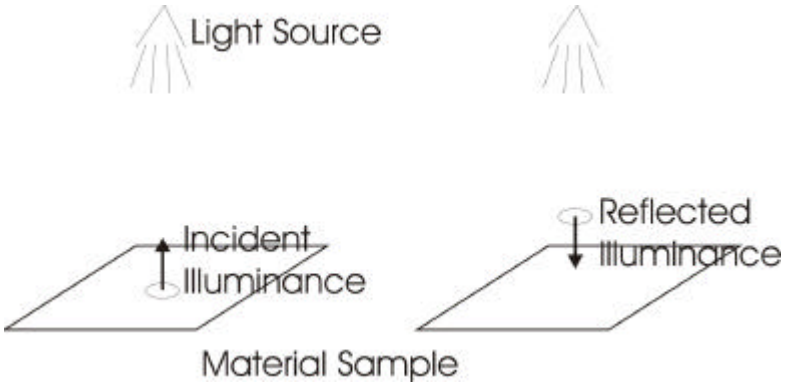

Figure 6.3 - Simple Measurement of Material Reflectance

Table 6.3: Relatively Unimportant Material Properties

Material	Colour	Diffuse Refl. (%)	Specular Refl. (%)	Diffuse Trans. (%)	Specular Trans. (%)	Roughness
Carpet	Blue-grey	9.6	0	0	0	0
Glazing	Clear	0	Fresnel[1]	0	84[2]	0
Black sheeting	Black	4.5	0.24	0	0	0.05
Skylight covers	Grey	19.0	8.1	0	0	0.2
Green table	Green-blue	42.2	0	0	0	0
White table	White	73.5	1.5	0	0	0.03
Table legs	Black	0.15	0.35	0	0	0.05
Cardboard boxes	Brown	37.5	0	0	0	0.1
Door handle	Chrome	8.0	72.0	0	0	0.1
Light fixture	White	2.1	67.9	0	0	0.05
External walls	White	67.0	0	0	0	0

Notes:
1. Specular reflectance varies according to Fresnel's equations, refractive index 1.52
2. Specular transmittance defined at normal incidence

Materials properties of the walls, ceiling and foam panels (Figure 6.1) were measured with greater precision. Diffuse reflectance, specular reflectance and colour were measured separately. The methods of measurement are illustrated in Figures 6.4 to 6.6, and described below.

Diffuse reflectances were measured using an integrating sphere (Figure 6.4). Collimated light entering the integrating sphere illuminated samples placed flush against the sample aperture. Specularly reflected light was directed out the sphere's input aperture. In this way, specular components were removed from the measurement of diffuse reflectance. Diffusely reflected light was distributed over the interior of the sphere. The sphere's interior was painted with highly reflective barium sulphate, of reflectance close to 100%. A diffusing glass sheet was placed over the sphere's measurement aperture. This sheet collected illumination from all parts of the integrating sphere, avoiding errors introduced by localised bright or dark patches within the sphere. A luminance meter aimed at the glass sheet then measured luminance directly related to the diffuse reflectance of the sample. Other lights in the measurement room were extinguished during measurement.

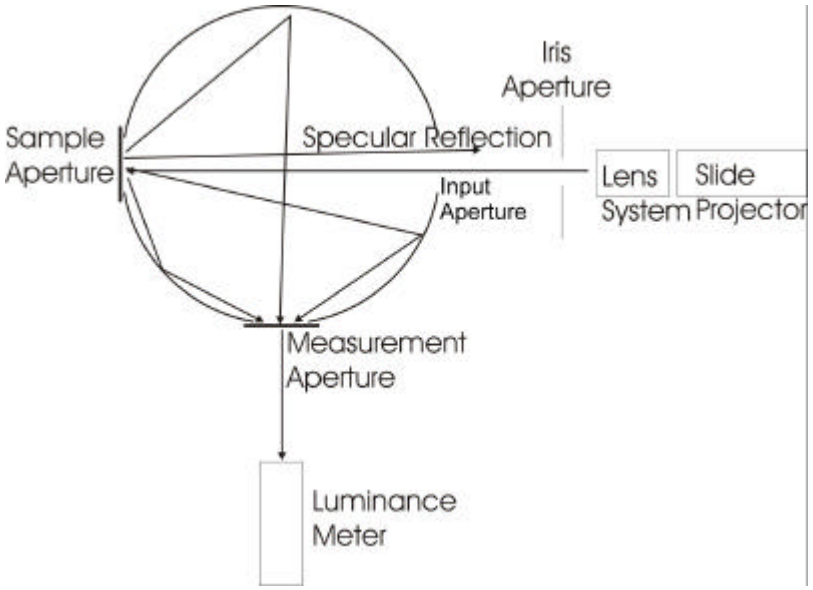

Figure 6.4 - Measuring Diffuse Reflectance with an Integrating Sphere

A black cloth was placed over the sample aperture, and baseline luminance was measured. A mirror was then placed over the sample aperture to measure the effect of specular reflections. A reference tile coated with barium sulphate was next placed over the sample aperture, and a luminance, corresponding to 100% diffuse reflectance, was measured. The material samples were finally placed over the sample aperture, and luminance due to their reflected light was measured. The measurement process was repeated several times over for each sample. Sample reflectances were then found using Equation 6.1, and are displayed in Table 6.4.

$$r = \frac{\overline{L} - \overline{L_b}}{\overline{L_r} - \overline{L_b}} \qquad \textbf{Equation 6.1}$$

where r = diffuse reflectance of sample

$\overline{L}$ = average sample luminance

$\overline{L}_b$ = average baseline luminance

$\overline{L}_r$ = average reference tile luminance

Table 6.4: Diffuse Reflectances Measured with Integrating Sphere

Material	Diffuse Reflectance (%)	Uncertainty (absolute %)
Ceiling	71.5	0.4
Walls	66.4	0.6
Foam	93	2

Specular reflectances were measured at 45° incidence (Figure 6.5). An incandescent light source provided broad spectrum illumination. A back-silvered mirror placed on the sample surface assisted alignment of the luminance meter. The meter focused on the image of the light source, and the measuring spot size was enlarged to encompass all of the visible filament. The mirror was then removed, and the luminance reflected off the sample measured. The sample was rotated and moved between measurements to reduce bias. The light source and luminance meter were then adjusted to measure direct luminances. The total path between source and meter was kept the same as it was for reflected luminance measurements. The light source was rotated so that the meter saw the same aspect of the source as seen at the sample surface. Direct and reflected luminances were averaged over several measurements. Specular reflectances were then found as the ratio of averaged reflected and direct luminances (Table 6.5).

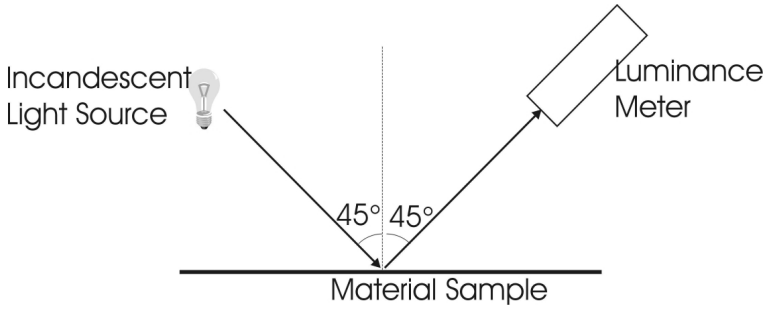

Figure 6.5 - Measuring Specular Reflectance at 45° Incidence

Table 6.5: Specular Reflectances at 45° Incidence

Material	Specular Reflectance (%)	Uncertainty (absolute %)
Ceiling	0.53	0.03
Walls	1.75	0.11
Foam	0.053	0.002

Sample colours were measured using fibre optic sensors, a spectrometer, a stable light source and a reference tile (Figure 6.6). Three fibre optic sensors obtained reflectance in three different wavelength bandwidths. The reference tile was coated with highly reflective barium sulphate, of known spectral reflectance. The light source was located directly above the sample surface. The three fibre optic sensors were aimed at the measurement point at 45° incidence. Light reflected off the reference tile was measured first. Light reflected off the sample surface was then measured at the same location. The fibre optics fed into the spectrometer, driven and powered by software on the connected computer.

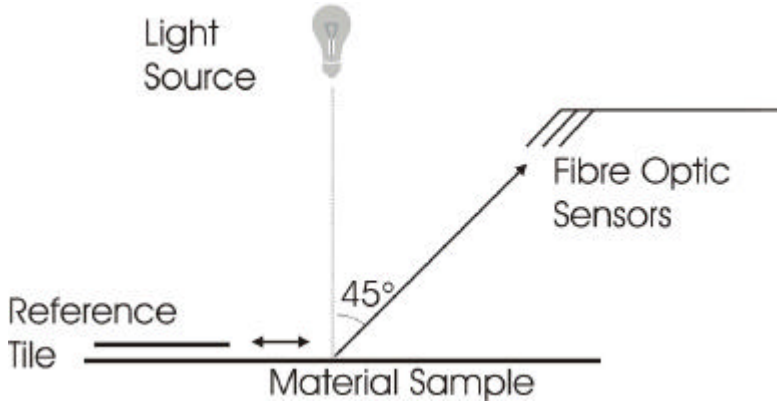

Figure 6.6 - Measuring Sample Colour with Fibre Optic Sensors

Measured spectral reflectance data were analysed to calculate CIE chromaticity coordinates. Spectral reflectances were averaged over 5nm intervals. 5nm interval spectral reflectances were averaged between measurement sets for each material. The (X, Y, Z) chromaticity coordinates of each material were then found as the weighted average of spectral reflectances, according to the tri-stimulus coordinates of the CIE standard observer with a two degree field of view (Table 6.6).

Table 6.6: CIE Chromaticity Coordinates of Ceiling and Wall Materials

Material	X	Y	Z
Ceiling	0.339	0.342	0.320
Walls	0.352	0.358	0.290

6.2.2.2 Material Modelling

For added reality, patterns were applied to the floor and foam materials. A dirt-type pattern was applied to the floor material and a speckle pattern was applied to the foam material. The defined reflectance of each base material was adjusted such that the average surface reflectance, after pattern application, conformed with measurements.

Figures 5.30 and 5.31 display well-defined specular reflections in the test building walls and ceiling. Modelling this specular reflection was a difficult task. These specular reflections must be correctly modelled as they may contribute to increased light levels in the rear of the room. They should also be clear in created visualisations.

Complex light reflection off metal and other surfaces is difficult to model. Reflected components are commonly divided into ideal specular, spread specular and uniform diffuse components (Figure 6.7) (He, Torrance, Sillion & Greenberg, 1991). Ideal and spread specular components vary with the direction of incident illumination. Uniform diffuse reflection is well modelled by RADIANCE. Unfortunately, angular dependent specular reflection was removed from RADIANCE due to problems modelling reflections of light sources (Ward, 1997). In most cases, this will not cause significant errors in results. However, errors may appear in simulations involving materials with large specular components, such as large metal surfaces. The walls and ceiling of the test building comprised such materials. Therefore, particular attention was paid to the correct modelling of specular reflection off these surfaces.

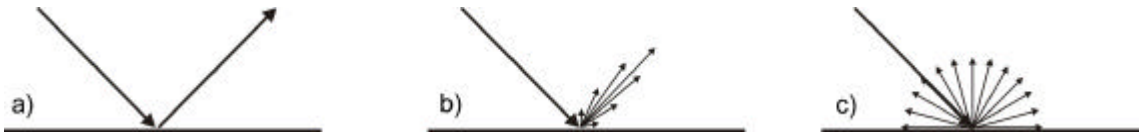

Figure 6.7 - Components of Surface Reflection: a) Ideal Specular; b) Spread Specular; c) Uniform Diffuse

The colours and diffuse reflectances of the walls and ceiling are displayed in Tables 6.4 and 6.6. Measured specular reflectances at 45° incidence are displayed in Table 6.5. There was some difficulty determining the most appropriate RADIANCE specular reflectances. Two approaches were taken, both involving a complex, but physically meaningful model of angular dependent light reflection (He *et al.*, 1991).

In the first approach to modelling specular reflectance, the default angle-independent RADIANCE model was applied. Averaged specular reflectances were calculated as follows, and provided to RADIANCE as the angle-independent specular reflectance. The measured 45° incidence specular reflectances were fitted to the He *et al*. model of angle-dependent specular reflectance. This provided the remaining angular dependence of specular reflectance. These angular distributions were then averaged over projected solid angles. This form of averaging most closely represented the average light flux reflection over all angles of incidence. The resulting material parameters and averaged specular reflectances are given in Table 6.7. Further details of this calculation procedure and material parameters are given in Chapter 7.

Table 6.7: Material Parameters and Averaged Specular Reflectances for the Walls and Ceiling

Material Parameter	Ceiling	Walls
Surface height standard deviation (μm)	0.0928	0.0635
Autocorrelation length (μm)	212	53.5
Averaged specular reflectance (%)	4.28	5.76

The second approach to modelling specular reflectance involved a new RADIANCE material model. A RADIANCE calculation file and modelling algorithm provided angle-dependent reflection according to the model of He *et al.* (1991). The algorithm is detailed in Chapter 7. Several combinations of material parameters (surface height standard deviation, autocorrelation length) were assessed, each providing the measured specular reflectances at 45° incidence. The different employed parameters made little difference to room illumination. The final parameters were determined by qualitative investigations of visualisations. The selected parameters are displayed in Table 6.8.

Table 6.8: Material Parameters in the He *et al.* (1991) Reflectance Model

Material Parameter	Ceiling	Walls
Surface height standard deviation (μm)	0.085	0.05
Autocorrelation length (μm)	0.215	0.116

6.2.3 MODELLING THE SKY

Accurate sky models were necessary for accurate simulations. The standard distribution of RADIANCE provides a uniform sky, and CIE standard clear, intermediate and overcast skies (with and without suns as appropriate). This range of skies did not present sufficient scope to match the range of skies under which measurements were performed (Igawa & Nakamura, 2001; Kittler *et al.*, 1997). For this reason, a new sky modelling algorithm was developed and implemented in RADIANCE, based on the Standard Sky Luminance Distribution (SSLD) of Kittler *et al.* (1997).

Following commencement of the International Daylight Measurement Programme, more than a hundred sky luminance distributions from Berkeley, Tokyo and Sydney were collated (Kittler *et al.*, 1997). These distributions were analysed and 15 new sky types determined. These are known as the Standard Sky Luminance Distributions (SSLD). The SSLD may soon be implemented as the new CIE standard general sky. A RADIANCE calculation file generates each of these skies, based on five model coefficients. The algorithm is applied using the *brightfunc* pattern modifier. The new sky modelling algorithm is detailed in Chapter 7.

Five sky models were created for the five simulations presented in section 6.4. One overcast sky was created for simulation of the vertical micro-light guiding shade panels. Three clear skies and one overcast sky were created for simulation of the tilted panels. Each sky was generated by the SSLD algorithm, and each is described and illustrated below.

The vertical micro-light guiding shade panels were modelled under a bright, uneven but overcast sky, with some brightening toward the sun. The overcast sky was modelled as SSLD type II.2 - overcast, moderately gradated and slightly brightening toward the sun. Figure 6.8 displays the created sky

luminance distribution as a hemispherical fish-eye view, overlaid with iso-luminance contours. This shows an overcast sky with steady brightening in the direction of the sun and darkening toward the horizon.

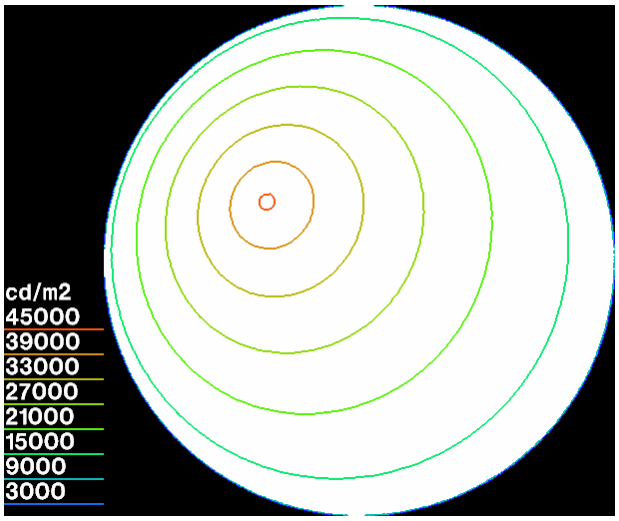

Figure 6.8 - Overcast Sky for Simulation of Vertical Micro-Light Guiding Shade Panels

The tilted micro-light guiding shade panels were first measured under a very clear, cloudless sky with some smoke haze toward the horizon. This sky was modelled as SSLD type VI.5 - cloudless turbid with a broader solar corona. Figure 6.9 shows the sun in the northern sky, slightly to the east. The solar corona (sky brightening around the sun) is clear. Some brightening is also seen around the horizon.

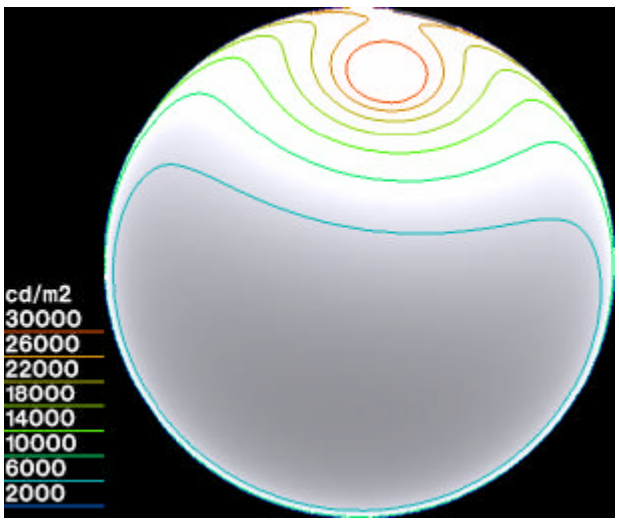

Figure 6.9 - Clear Sky for Simulation of Tilted Micro-Light Guiding Shade Panels

Sky conditions were highly variable when the tilted panels were measured under overcast skies. Several sky types were investigated. The sky type giving greatest agreement with averaged external illuminance measurements was

sky type II.1 - overcast, moderately gradated, azimuthally uniform. The created sky luminance distribution is displayed in Figure 6.10. Azimuthal uniformity is shown by the circular iso-luminance contours. The sky is moderately gradated, with the zenith approximately twice as bright as the horizon.

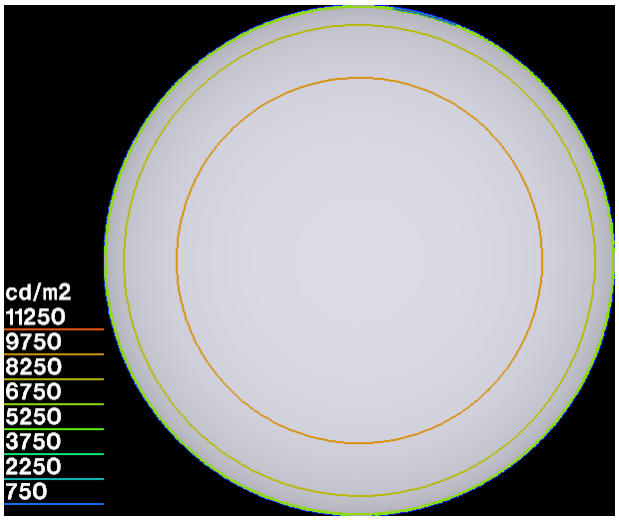

Figure 6.10 - Overcast Sky for Simulation of Tilted Micro-Light Guiding Shade Panels

The second clear sky model contained a sun at high relative azimuth to the window. This sky was clear with few or no clouds and low turbidity. Sky type VI.5 - cloudless turbid with a broader solar corona, was again employed. Figure 6.11 shows the sun in the north-east region of the sky. A solar corona and some horizon brightening are visible.

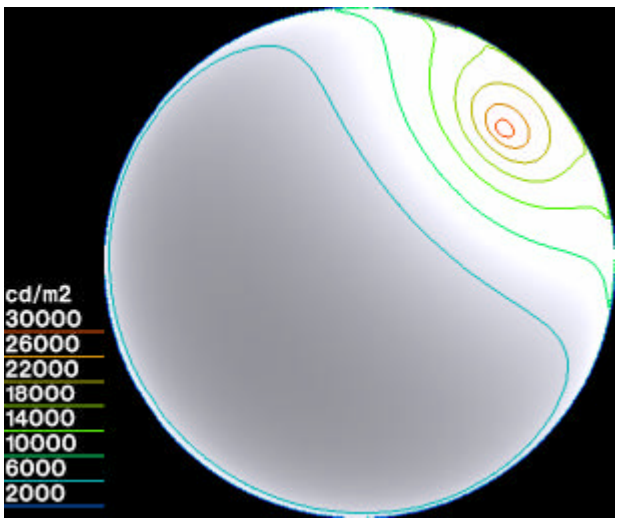

Figure 6.11 - Clear Sky with High Relative Solar Azimuth for Simulation of Tilted Micro-Light Guiding Shade Panels

The opalescent sheeting was also modelled under a clear sky of type VI.5. Figure 6.12 shows the sun a little higher in the sky, and slightly to the west of north. The solar corona is clear, and some horizon brightening is apparent.

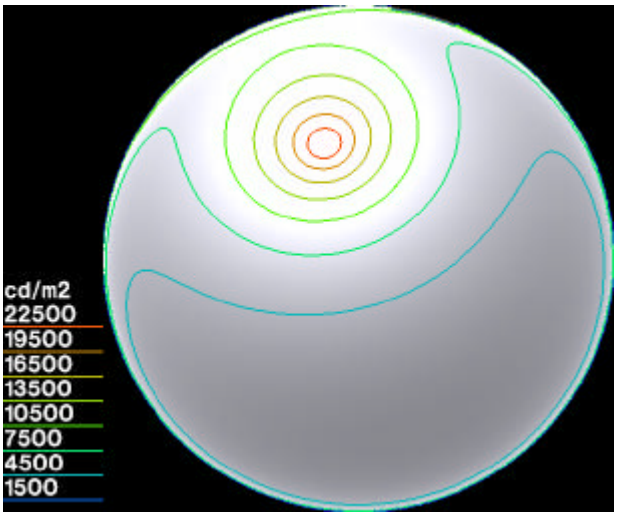

Figure 6.12 - Clear Sky for Simulation of Opalescent Sheeting on Tilted Micro-Light Guiding Shade Panels

Table 6.9 compares external illuminances provided by the modelled skies with the corresponding averaged measurements. These comparisons are made only for simulations of the tilted micro-light guiding shade panels. The overcast sky created for simulation of the vertical panels was treated by scaling according to vertical north illuminances, as explained in section 6.4.1. Excellent agreement is displayed in Table 6.9, with only the clear sky with high relative solar azimuth showing significant differences between simulation and measurement.

External surfaces including the ground and external obstructions were also modelled. The condition of the grass surrounding the test building changed between measurements of the vertical and tilted panels. The ground plane reflectance was altered accordingly. In the same time period, a concrete footpath was constructed around the north and west sides of the building. This footpath was added to the external model. The façade of the nearby Bureau of Meteorology building was added in simplified form as a rectangle of angular size (from the window) and average reflectance resembling that of the real building. Modelled external reflectances are listed in Table 6.10.

Table 6.9: Generated External Illuminances for Tilted Micro-Light Guiding Shade Panels

Sky Model	External Illuminance	Measured (klx)	Simulated (klx)
Overcast	Horizontal global	30	29.8
	Vertical north	15.6	15.7
	Panel incident	21.4	22.4
	Direct normal[1]		25.3
Clear	Horizontal global	80.6	80.4
	Vertical north	90	90.4
	Panel incident	112.5	114.1
	Direct normal[1]	115.1	115.4
Clear, high relative azimuth	Horizontal global	75.2	74.8
	Vertical north	75	66.3
	Panel incident	96.3	90.6
	Direct normal[1]	115.7	113.1
Clear, opalescent	Horizontal global	107.7	107.7
	Vertical north	65.3	67.3
	Panel incident	105.0	107.1
	Direct normal[1]	123.0	122.4

Note:
1. Direct normal illuminance included sky and ground reflected components, giving non-zero result for overcast sky.

Table 6.10: Material Properties of External Objects

Material	Colour	Reflectance (%)
Grass (vertical panels)	Green	20
Grass (tilted panels)	Green	11.5
Foundation concrete	Grey	31
Footpath concrete	Grey	40.5
Façade of Bureau building	Grey	31

6.3 DEMONSTRATION OF THE MICRO-LIGHT GUIDING SHADE PANELS BY SIMULATION

To demonstrate the performance of the micro-light guiding shade panel, four visualisations were created, as shown in Figure 6.13. This shows fish-eye views of the test building with and without the vertical micro-light guiding shade panels and external light shelf (Figure 5.1). Some basic furniture was added for realism, and iso-luminance contours reveal the distribution of light within the building. The visualisations were created for a clear winter afternoon, with the sun in the low north-west.

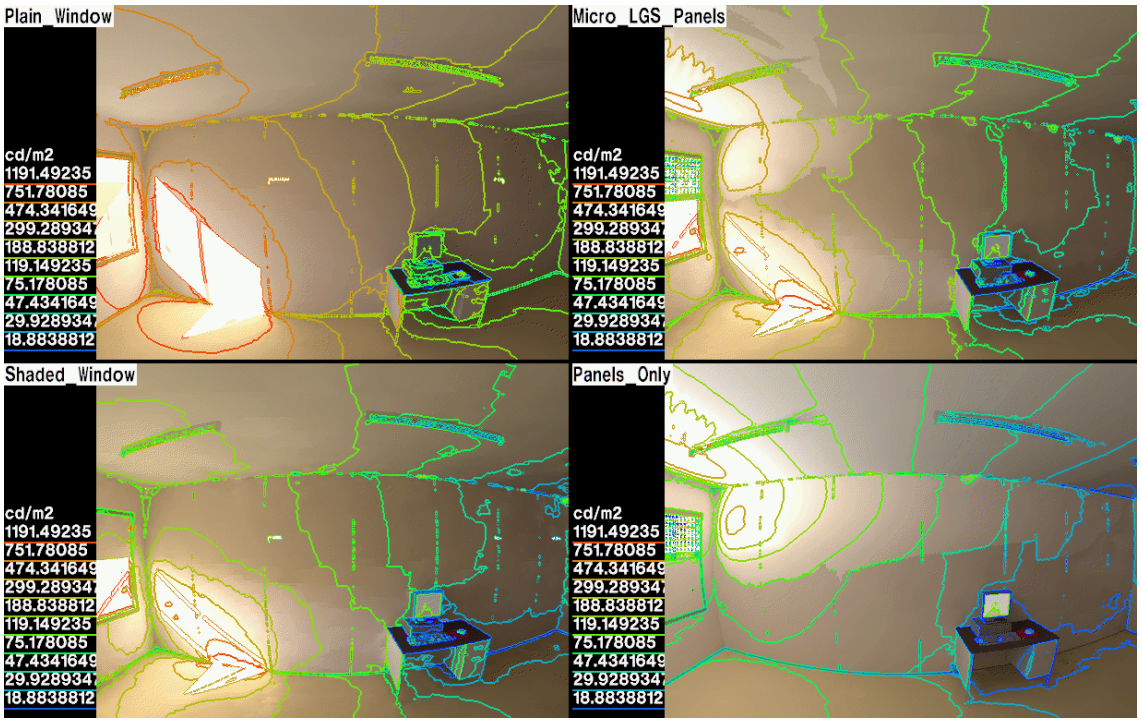

Figure 6.13 - Demonstration of Vertical Micro-Light Guiding Shade Panels on Test Building

The upper left image shows a large open, north facing window. A large transmitted sun patch is clear on the eastern wall. The upper right image shows the micro-light guiding shade panels and external light shelf installed over the window. The lower left and right images show the building with the upper and lower sections of the window blocked respectively. These latter images show the contributions to interior illumination of the lower window and the micro-light guiding shade panels respectively.

The exterior light shelf blocked most of the incident sunlight. The micro-light guiding shade panels clearly distributed light across the upper wall and ceiling. Luminance levels toward the rear of the building in the upper right image were comparable with those in the building with the completely open window (upper left image). However, the bright direct sun patch was severely diminished. Thus, the micro-light guiding shade panels maintained light levels within the room, while significantly reducing direct solar penetration and the possibility of occupant glare.

6.4 SIMULATING THE MICRO-LIGHT GUIDING SHADE PANELS ON THE TEST BUILDING

The micro-light guiding shade panels on the test building were extensively simulated. Models of the panels, the building and the sky were described in the preceding sections. The vertical panels were simulated under the overcast sky conditions of section 5.5.1.2. The tilted panels were simulated under the three clear and one overcast sky conditions of section 5.5.2. Simulated illuminance profiles were created in the same locations as measurements. Visualisations within the test building were also created.

6.4.1 VERTICAL MICRO-LIGHT GUIDING SHADE PANELS UNDER OVERCAST SKY

Simulations were performed using both models of specular reflectance described in section 6.2.2.2. Figure 6.14 shows visualisations completed using both models. These compare with photographs taken standing in the room (Figure 6.15). The visualisations were post-processed to mimic the perception of the human eye in a similar lit environment (Ward, 1994).

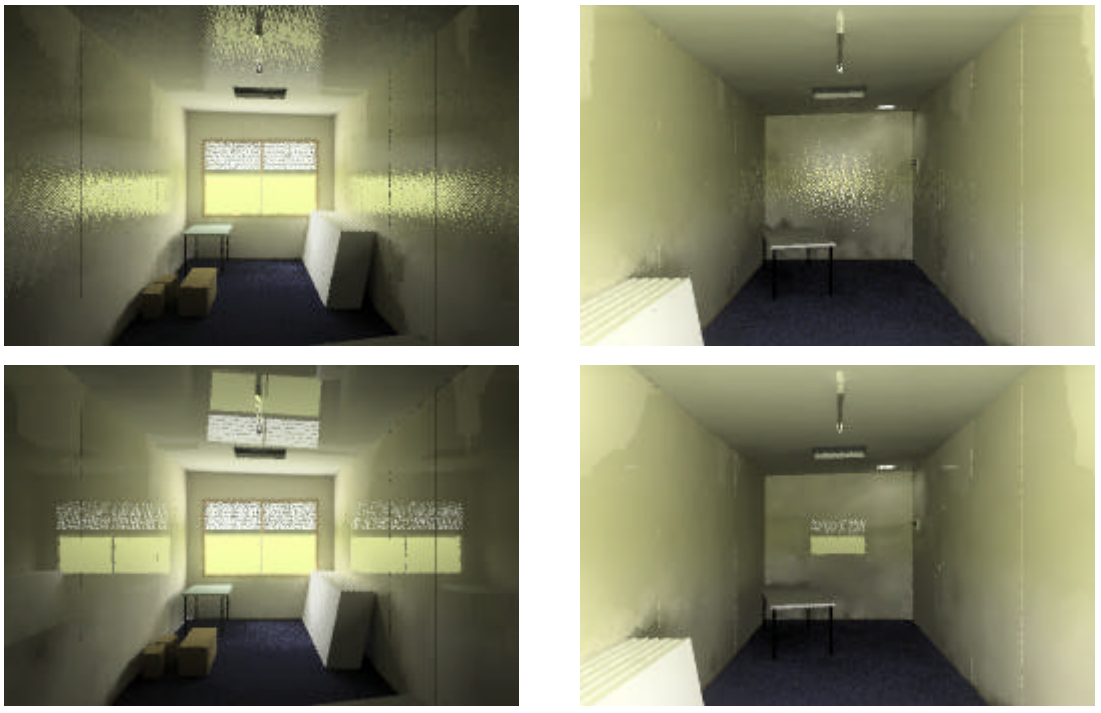

Figure 6.14 - Visualisations of the Test Building with Vertical Micro-Light Guiding Shade Panels: Top) Default Angle-Independent Specular Reflectance Model; Bottom) He *et al*. Angle-Dependent Specular Reflectance Model

a)  b) 

Figure 6.15 - Photographs of the Test Building with Vertical Micro-Light Guiding Shade Panels: a) From Rear of Room; b) From Window

The photographs of Figure 6.15 do not mimic human perception. Within a single photographic exposure, it is impossible to convey the dynamic range perceived by the human eye. Thus, regions of a photograph generally appear either brighter or darker than seen by the human observer. For Figure 6.15a, the photograph generally appears darker than would be seen by the human observer. All images display clear reflections of the window and panels in the walls and ceiling. Some material roughness is revealed in the apparent smudging of the edges of the window and panel reflections. Some reflections are also seen of interior objects such as the foam panels and tables.

Visualisations created using the He *et al*. material model display clear reflections of the window and panels in the walls and ceiling. Some mirror-like reflections of the foam panels and table near the window appear in both the walls and the ceiling. Considering the limitations of photographic exposures, these visualisations agree well with photographs. The reflections of the window, panels and interior objects are perhaps too sharp, indicating lack of roughness in the material model.

Visualisations created using the default material model also agree quite well with photographs. The reflections are still quite clear, as observed in the photographs. Some smudging of reflection edges is also observed. Reflections of internal objects are not apparent.

Similar to measurements described in section 5.4.2.1, when predicting internal illuminances, the view window was covered over with black plastic sheeting. Thus, the distribution of illumination within the test building was attributed

entirely to the vertical micro-light guiding shade panels in the upper window (Figure 6.13). Simulated internal illuminances were scaled for comparison with measurements, according to the vertical illuminance incident upon the panels (section 5.5.1.2).

Predicted interior illuminance profiles are shown in Figure 6.16. Excellent agreement is displayed between simulation and measurement. The default material model provided slightly higher illuminances at most depths. This is most clear in the depth region between five and seven metres.

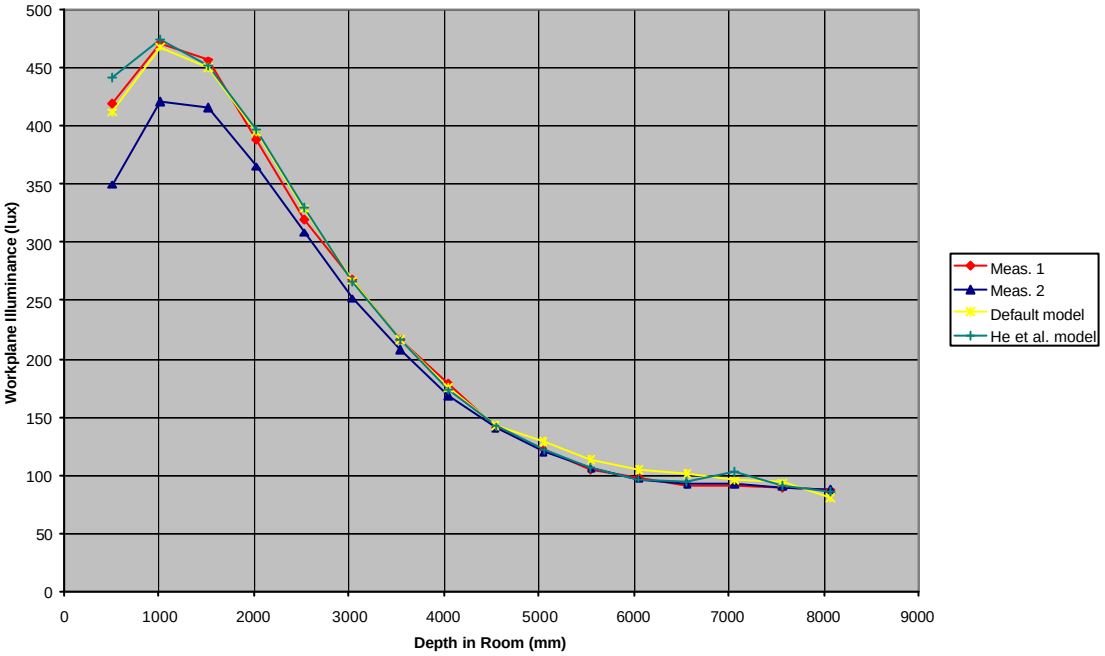

Figure 6.16 - Comparison of Predicted and Measured Illuminances in the Test Building with Vertical Micro-Light Guiding Shade Panels

The statistical test of Bland and Altman (1986), described in section 4.3.3, was applied to comparisons between measurement and simulation. The test was applied to profiles displayed in Figure 6.16, for both material models. The resulting percentage difference plots are shown in Figure 6.17.

The He *et al*. material model displayed a mean percentage difference of 3.4%. This positive mean difference implies that simulations overestimate measurements. Differences were reasonably consistent throughout the room, and mainly ranged between -5 and 12%. Two outliers were apparent, corresponding to depths 0.5 and 7.0m. The bias between simulation and measurement was between 1.4 and 5.3%.

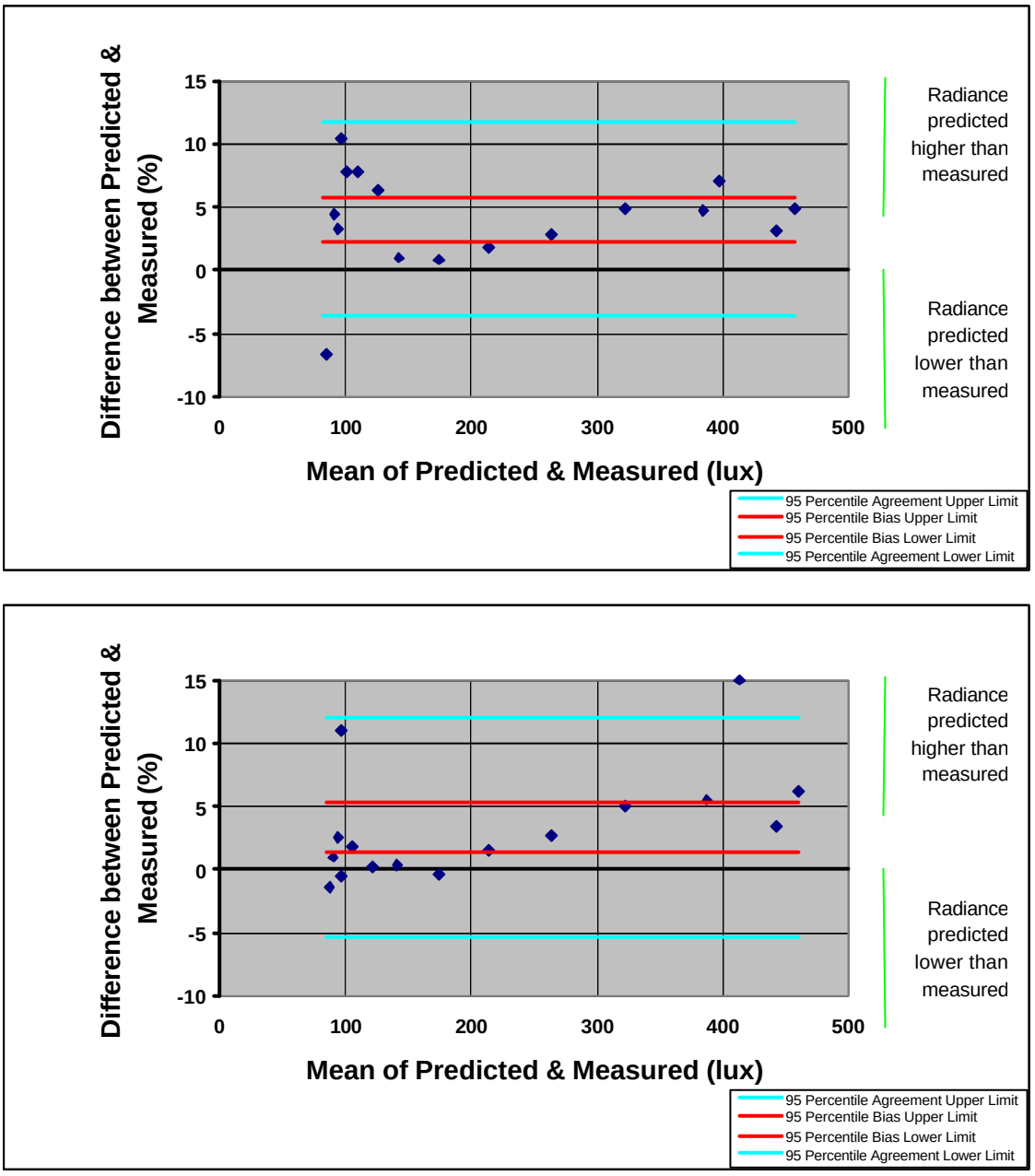

Figure 6.17 - Percentage Differences between Measurement and Simulation of Test Building with Vertical Micro-Light Guiding Shade Panels: a) Default Angle-Independent Specular Reflectance Model; b) He *et al*. Angle-Dependent Specular Reflectance Model

The default material model provided a mean percentage difference of 4.1%. As for the He *et al*. model, simulations generally overestimated measurements. Percentage differences were again reasonably consistent throughout the room, with some greater variation in regions of low illuminance. Differences were slightly less spread than those above, mainly ranging between -4 and 12%. The bias between simulation and measurement lay between 2.4 and 5.8%, slightly higher than that for the He *et al*. material model.

Visualisations and illuminance predictions display excellent agreement with measurement for both material models. Differences were generally less than 10%. Qualitative comparison of visualisations with photographs also showed good agreement.

The He *et al*. material model provided excellent agreement with measurements and photographs, and with the default angle-independent material model. The former model displayed slightly lower bias and more agreements around zero percent. The default material model better replicated apparent surface roughness in smearing of reflections. The He *et al*. model provided more realistic reflections of interior objects. The He *et al*. material model was selected for further modelling of the test building. This selection was based on slightly better interior illuminance predictions, more realistic reflections of interior objects, and its more fundamentally correct formulation.

6.4.2 TILTED MICRO-LIGHT GUIDING SHADE PANELS UNDER VARIOUS SKIES

Test building measurements with the tilted micro-light guiding shade panels were completed with the panels covered and uncovered (section 5.4.2.2). Simulations were performed in a similar manner. As predicted external illuminances agreed well with measurements (Table 6.9), no scaling was applied to simulated internal illuminances. Visualisations were also created, similar to those in Figure 6.14. These were post-processed to mimic human perception. Simulations were performed using the He *et al*. specular reflectance model, based on the findings of section 6.4.1. The mkillum pre-processor created luminous output surfaces for the panels, the view window and the roof vent. This added time to pre-processing, but improved accuracy.

6.4.2.1 Clear Sky, Midday

Figures 6.18 to 6.20 compare measured and simulated illuminances in the test building under a clear sky at midday. Figure 6.18 shows the room with the panels covered over. Figure 6.18 shows internal illuminances with the panels uncovered. The difference between these is delivered by the panels (Figure 6.19).

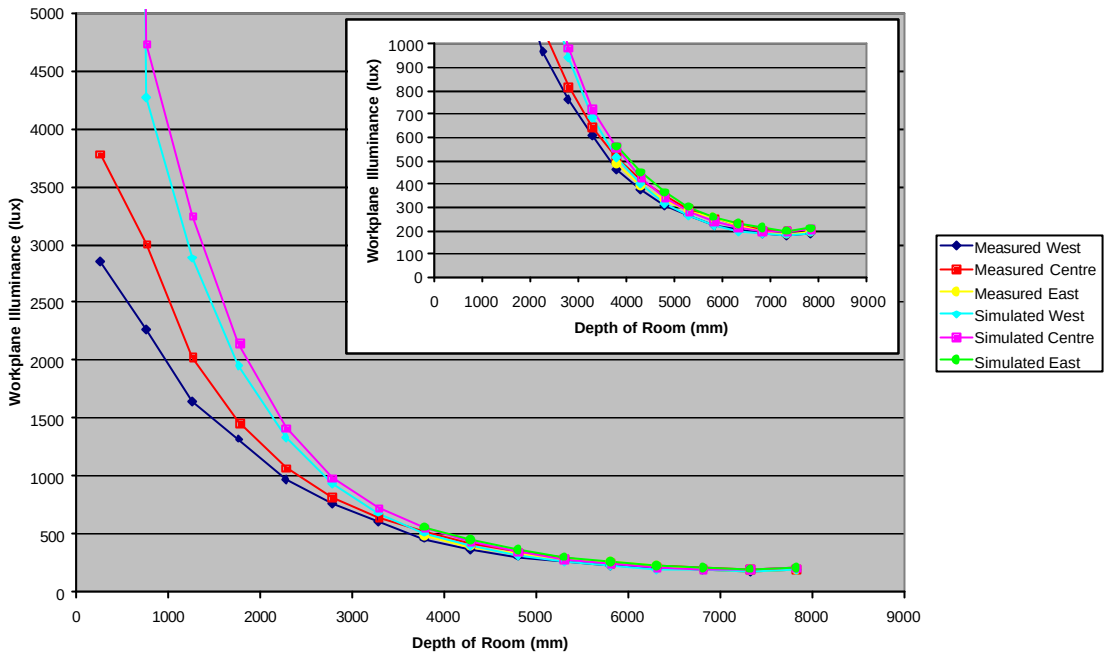

Figure 6.18 - Comparison of Predicted and Measured Illuminances in the Test Building with Tilted Micro-Light Guiding Shade Panels, Clear Sky, Panels Covered (Insert Shows Scaled Up Version of Same Figure)

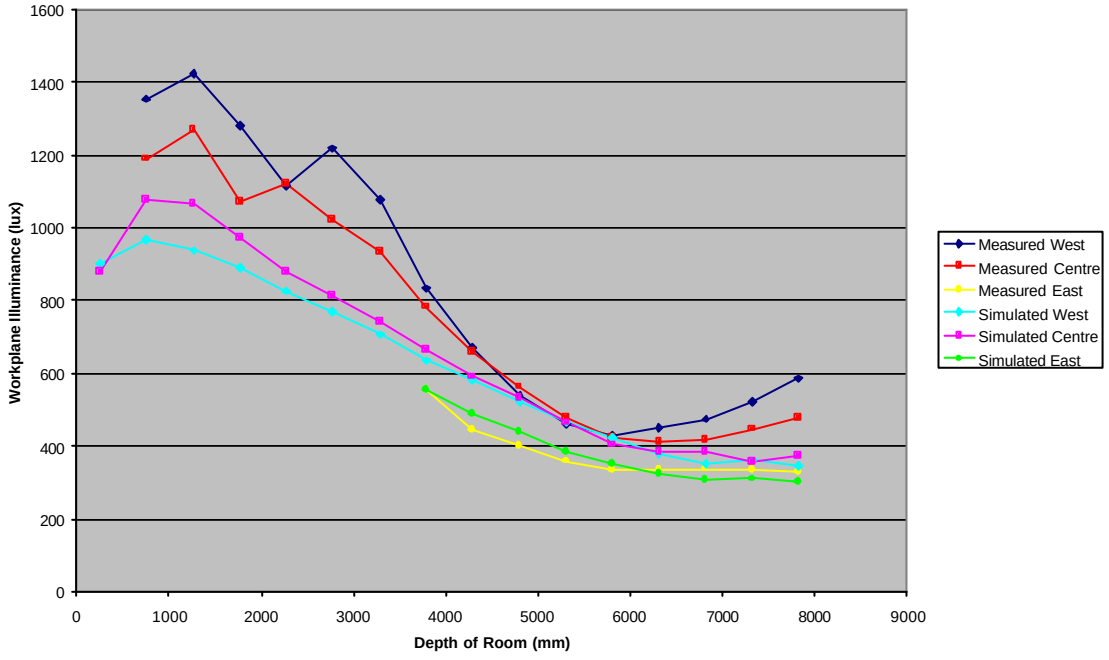

Figure 6.19 - Comparison of Predicted and Measured Illuminances in the Test Building with Tilted Micro-Light Guiding Shade Panels, Clear Sky, Panels Only

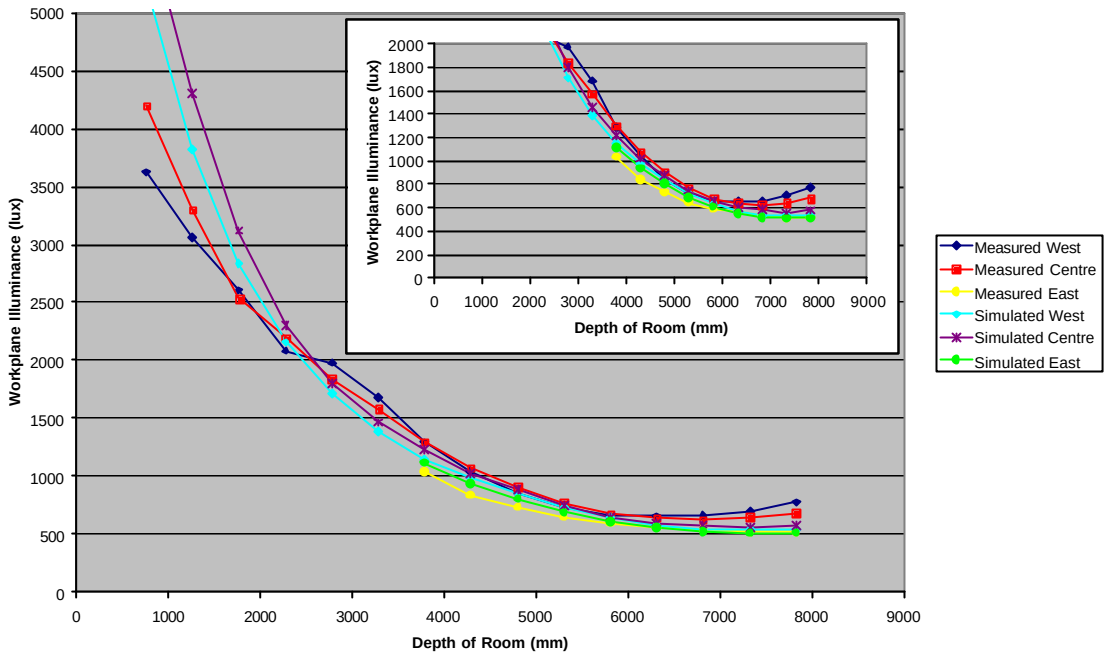

Figure 6.20 - Comparison of Predicted and Measured Illuminances in the Test Building with Tilted Micro-Light Guiding Shade Panels, Clear Sky, Panels Uncovered (Insert Shows Scaled Up Version of Same Figure)

Simulation clearly overestimated measurement in the window half of the room with the panels covered (Figure 6.18). Beyond this depth, good agreement was displayed between measurement and simulation.

In contrast, simulated panel contributions underestimated most measurements (Figure 6.19). Predicted illuminances on the eastern side of the room agreed well with measurements, while those on the west performed worst. Measurements showed a significant rise in illuminance toward the rear of the western side of the room. This was caused by the bright patch on the western side of the rear wall. These raised illuminances were not reflected in the simulations, implying difficulty modelling the translucent sheeting's directional transmittance.

Better agreement between measurement and simulation was displayed in total room illuminances (Figure 6.20). The overestimated view window component combined with the underestimated panel component to produce better overall agreement. The rise in illuminance near the rear on the west is still absent.

Most vertical illuminances were significantly overestimated. With the panels uncovered, overestimations were greatest on the side walls toward the window. The implies that the directional transmittance of the translucent sheeting was not sufficiently modelled. This would spread transmitted light closer to the window than was measured. This is further evidenced by an underestimated vertical illuminance on the rear wall.

Room visualisations are shown in Figure 6.21. These should be compared with the photos of Figures 5.30 and 5.31. Both visualisations display clear reflections of the window and panels in the walls and ceiling. These reflections appear somewhat clearer than are seen in the corresponding photos. Some reflections are also seen of interior objects such as the foam panels. The sun patch on the floor near the window agrees very well with the photo.

a) 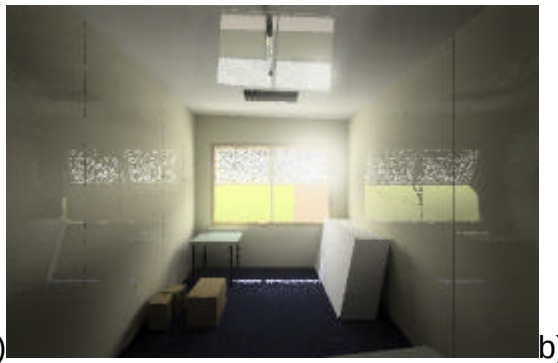 b) 

Figure 6.21 - Visualisations of the Test Building with Tilted Micro-Light Guiding Shade Panels, Clear Sky: a) From Rear of Room; b) From Window

From the back of the room, veiling glare appears to the right of the panels, agreeing well with perceived glare. Seen from the window, the translucent sheeting's directional transmittance appears as bright strips on the west wall and ceiling, and as brightening of the upper right quarter of the rear wall. This bright patch is not as clear as in the photo. This concurs with the lack of raised illuminances in the rear of the room. These visualisations compare quite well with photographs and perception. The reflections of the window and panels are perhaps too sharp, indicating lack of roughness in the material model.

The Bland and Altman statistical test was applied to comparisons between measurement and simulation. Analysis was applied only to total illuminances within the room, as displayed in Figure 6.20. The resulting percentage

difference plot is displayed in Figure 6.22. Percentage differences were fairly inconsistent, with higher differences near the window and greater variation in differences in the rear of the room. A bias between -4.2 and +4.3% was reported, indicating little difference between measurement and simulation, on average. Near to the window, simulation overestimated measurement by 20 to 50%. The west profile beyond 6m depth was underestimated by up to 30%. These results again indicate incorrectly modelled, directionally transmitting, translucent sheeting.

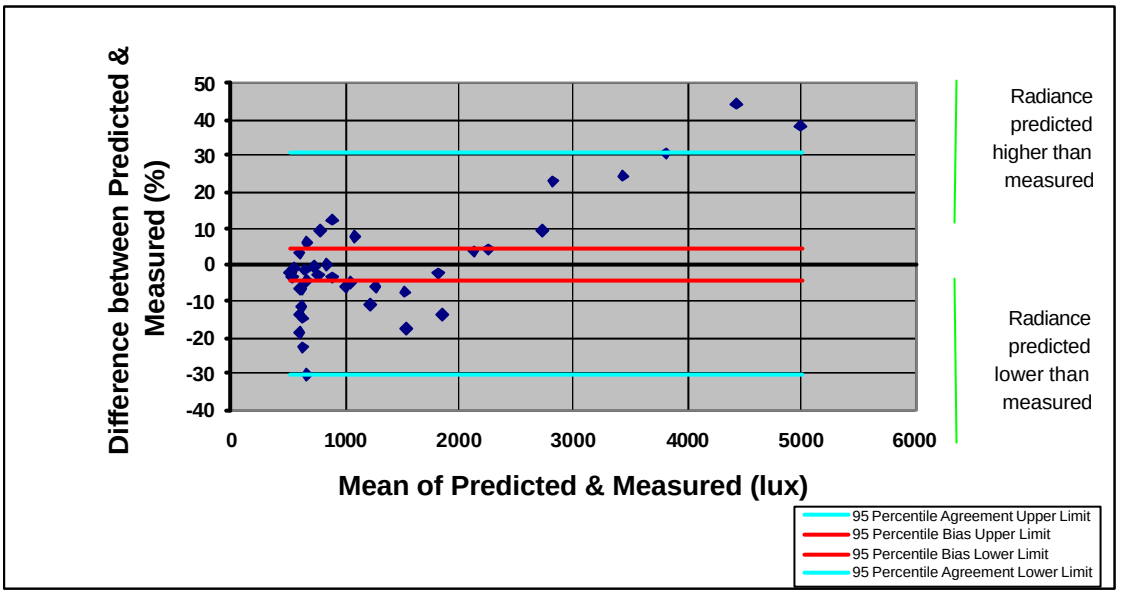

Figure 6.22 - Percentage Differences between Measurement and Simulation of Test Building with Tilted Micro-Light Guiding Shade Panels, Clear Sky

Fairly good agreement was revealed between measurement, perception and simulation. The bias in illuminance predictions was very low, providing confidence in simulation results. The primary cause of discrepancy was the directionally transmitting translucent material. This proved difficult to model. Visualisations also showed clearer reflections of the window and the panels. Simulations were performed under several sky models, and results were quite sensitive to the selected sky luminance distribution.

6.4.2.2 Overcast Sky

Measured and simulated internal illuminances in the test building under overcast sky are displayed in Figures 6.23 to 6.25.

With the panels covered over, east and west illuminance profiles agreed well with measurements beyond depth 3m (Figure 6.23). West illuminances were overestimated nearer to the window. Central room illuminances were underestimated through most of the room.

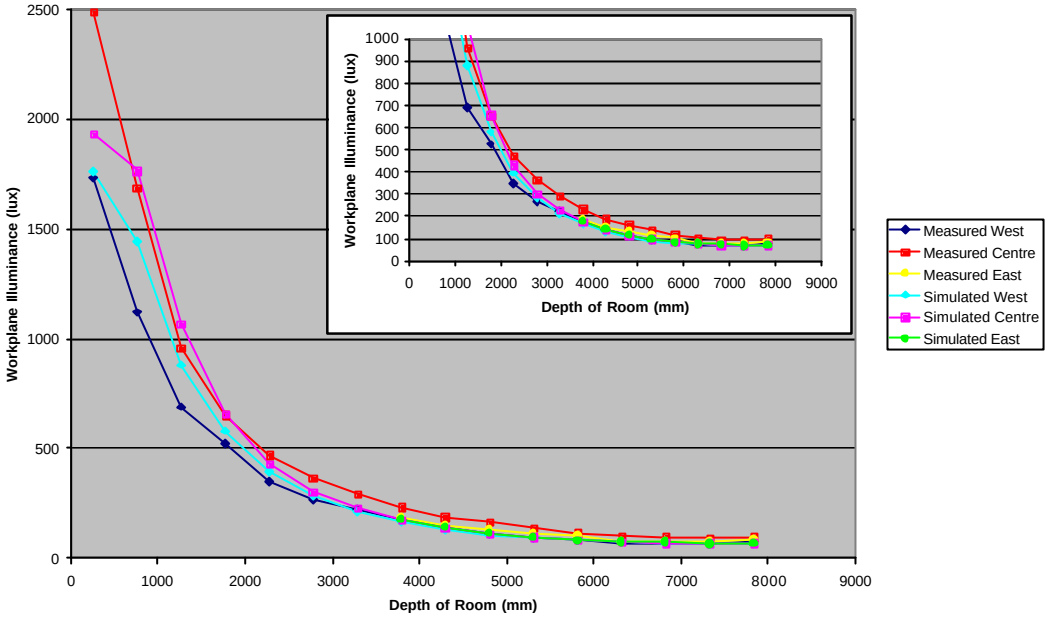

Figure 6.23 - Comparison of Predicted and Measured Illuminances in the Test Building with Tilted Micro-Light Guiding Shade Panels, Overcast Sky, Panels Covered (Insert Shows Scaled Up Version of Same Figure)

Agreement between measurement and simulation was also variable for the panel contribution (Figure 6.24). Central room illuminances were overestimated through most of the room. East room illuminances were significantly overestimated. Better agreement was displayed for western illuminance levels.

Some better agreement was displayed for total room illuminances (Figure 6.25). West and east room profiles agreed well with measurement. Central room total illuminances were mainly underestimated.

No clear trend was displayed between measured and simulated illuminances. Comparisons appear quite different for the east, west and central profiles. This could indicate problems with the scaling of measurements described in section 5.5.2.2. Thus, the variable sky conditions during measurement made it difficult to perform meaningful comparisons between measurement and simulation.

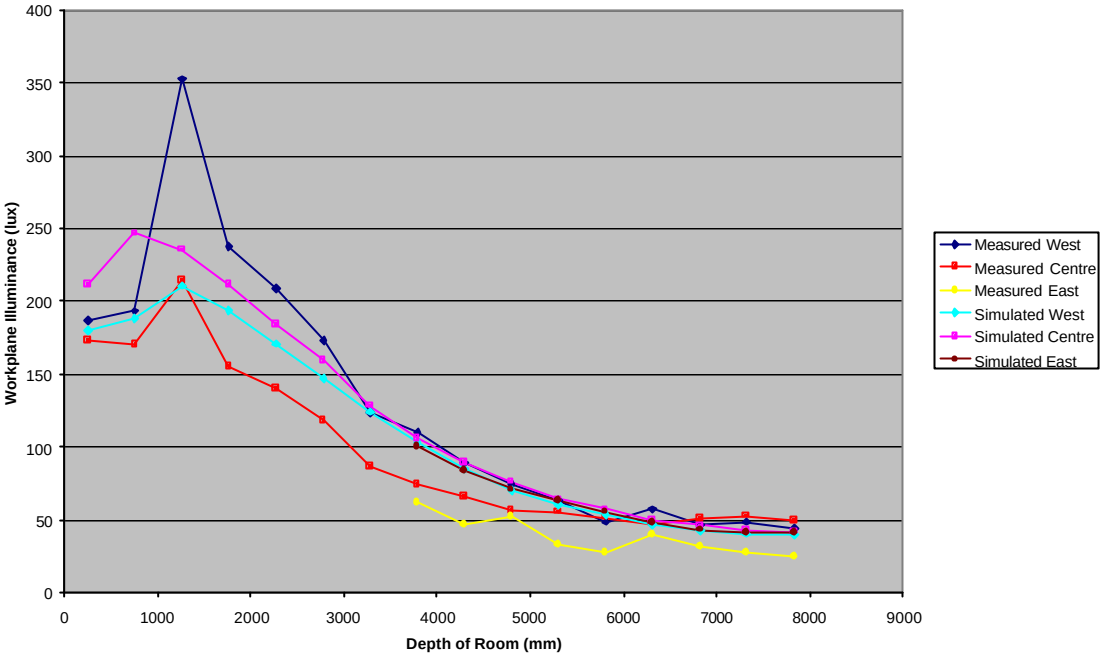

Figure 6.24 - Comparison of Predicted and Measured Illuminances in the Test Building with Tilted Micro-Light Guiding Shade Panels, Overcast Sky, Panels Only

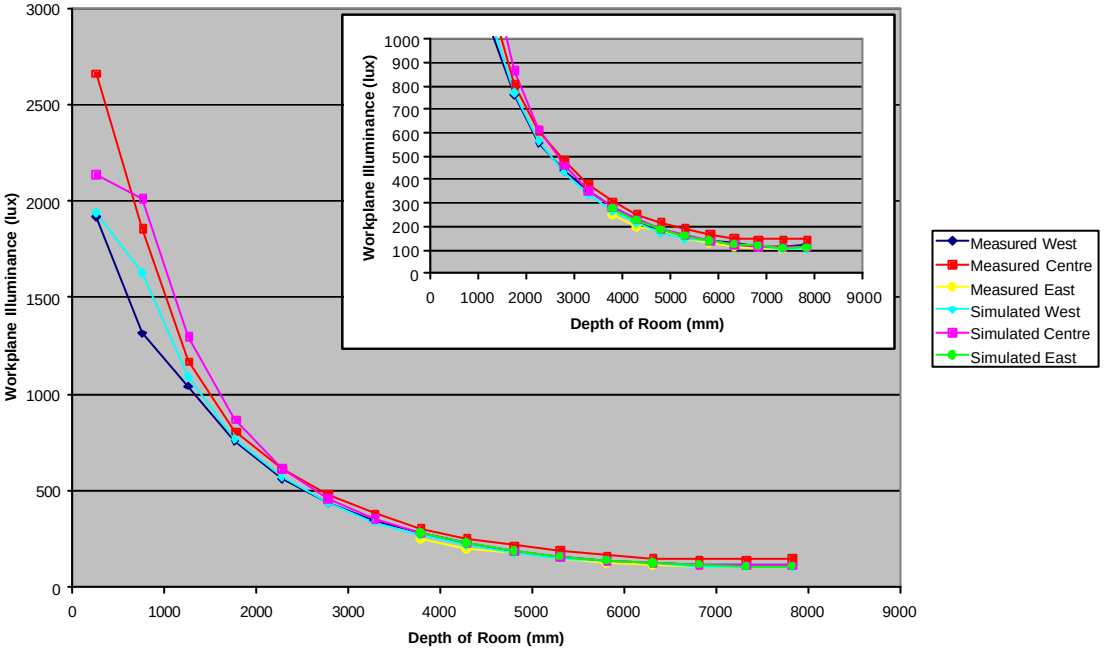

Figure 6.25 - Comparison of Predicted and Measured Illuminances in the Test Building with Tilted Micro-Light Guiding Shade Panels, Overcast Sky, Panels Uncovered (Insert Shows Scaled Up Version of Same Figure)

Room visualisations are shown in Figure 6.26. Clear reflections of the window and panels are again displayed in the walls and ceiling. These visualisations agree fairly well with perception, except for the sharp reflections of the window and panels.

a)  b) 

Figure 6.26 - Visualisations of the Test Building with Tilted Micro-Light Guiding Shade Panels, Overcast Sky: a) From Rear of Room; b) From Window

The Bland and Altman percentage differences plot is displayed in Figure 6.27, comparing illuminances displayed in Figure 6.25. Percentage differences were fairly well distributed, ranging from -24 and +19%. Underestimations were greater for the central profile, toward the rear of the room. Overestimations were more likely for the eastern profile. A bias between -5.4 and +0.3% indicated good agreement between measurement and simulation on average.

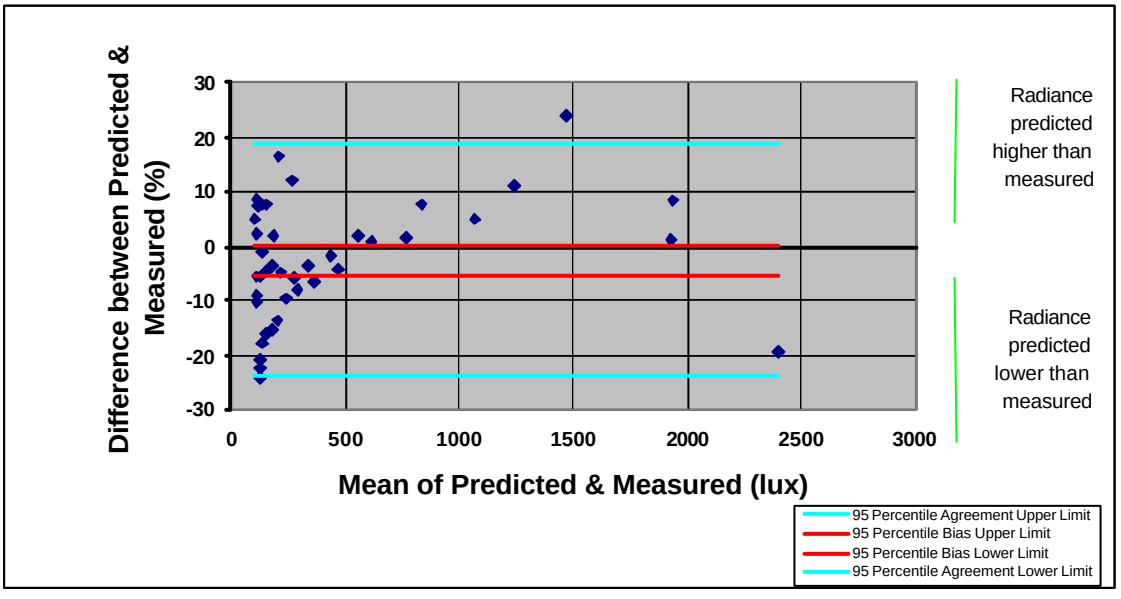

Figure 6.27 - Percentage Differences between Measurement and Simulation of Test Building with Tilted Micro-Light Guiding Shade Panels, Overcast Sky

Comparisons between measurement and simulation were made difficult by variable external conditions during measurement. The low bias is encouraging, as are the visualisations. Reflections in the walls and ceiling were again sharper than perceived.

6.4.2.3 Clear Sky, High Relative Solar Azimuth

Figures 6.28 to 6.30 compare measured and simulated illuminances in the test building under a clear sky with high relative solar azimuth.

Simulation significantly overestimated measurement in the window half of the room with the panels covered (Figure 6.28). Beyond 3m depth, agreement was improved, with simulations slightly underestimating measurement.

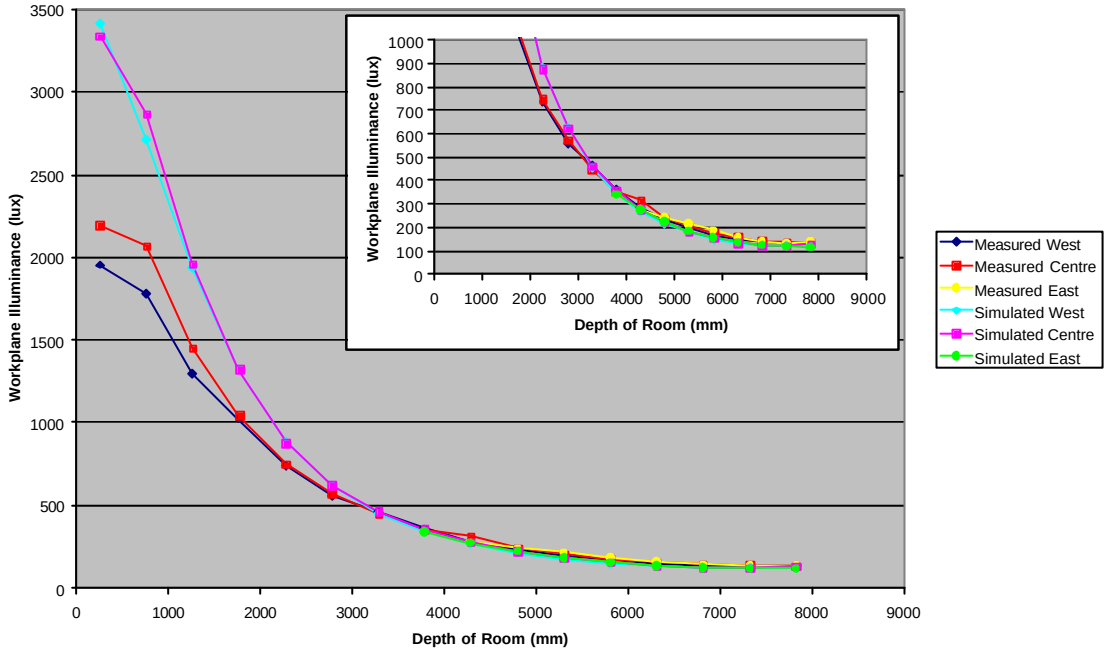

Figure 6.28 - Comparison of Predicted and Measured Illuminances in the Test Building with Tilted Micro-Light Guiding Shade Panels, Clear Sky, High Relative Azimuth, Panels Covered (Insert Shows Scaled Up Version of Same Figure)

In contrast to the above findings, simulated panel contributions underestimated measurements to around 5m depth (Figure 6.29). Measurements showed a raised western illuminance at 1.5m depth. This rise was caused by the directionally transmitted bright patch on the western wall. Simulations did not reflect this rise in illuminance, indicating an improperly modelled translucent material. Eastern illuminances were also underestimated. This is also related to the missing bright wall patch.

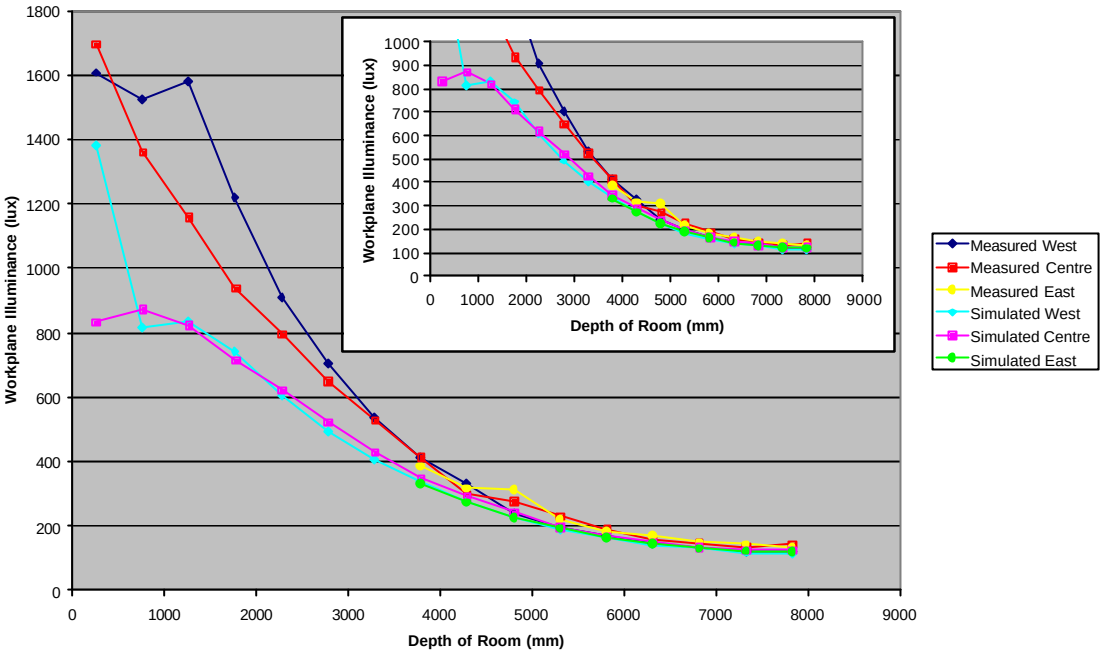

Figure 6.29 - Comparison of Predicted and Measured Illuminances in the Test Building with Tilted Micro-Light Guiding Shade Panels, Clear Sky, High Relative Azimuth, Panels Only (Insert Shows Scaled Up Version of Same Figure)

Better agreement was displayed in total room illuminance profiles (Figure 6.30). The overestimated view window component countered the underestimated panel component, providing better overall agreement. Eastern illuminances were still underestimated, due to the missing bright patch on the western wall.

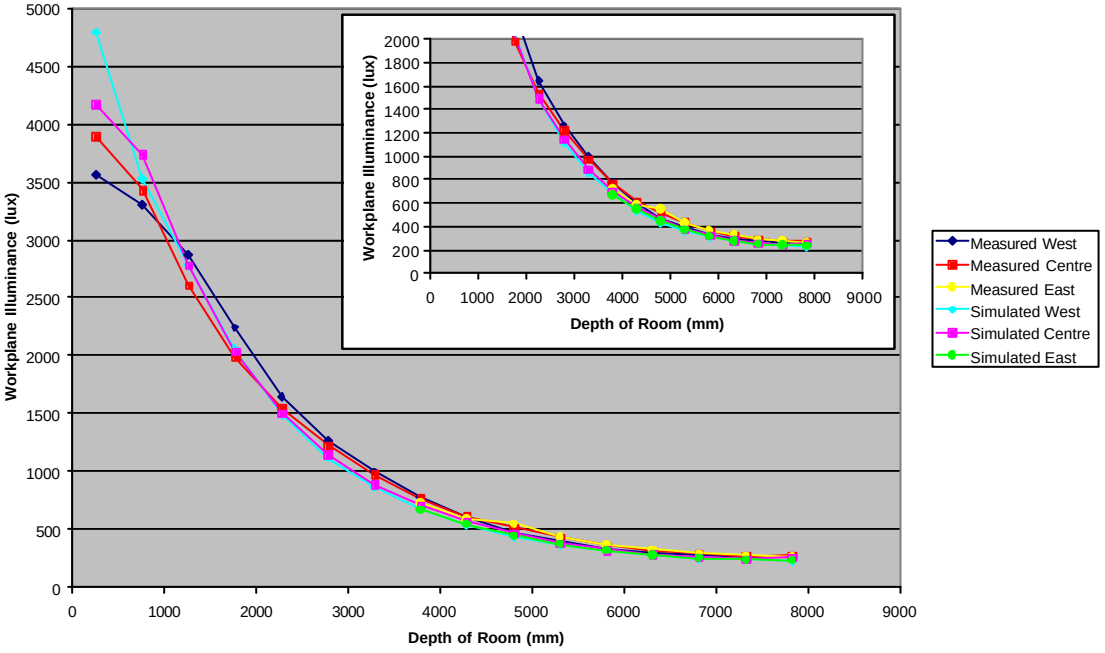

Figure 6.30 - Comparison of Predicted and Measured Illuminances in the Test Building with Tilted Micro-Light Guiding Shade Panels, Clear Sky, High Relative Azimuth, Panels Uncovered (Insert Shows Scaled Up Version of Same Figure)

Simulated vertical illuminances generally agreed well with measurements. That on the west wall near the window was underestimated due to the absent directionally transmitted bright patch. The location of underestimations (near the window on the west wall, near the rear wall on the east) concurs with underestimated horizontal illuminances in Figure 6.29.

Simulated room visualisations are displayed in Figure 6.31. Similar to Figures 6.21 and 6.26, clear reflections of the window and panels appeared in the walls and ceiling. The directionally transmitted bright patch on the west wall near the window is not shown. This again indicates an incorrectly modelled translucent material.

a)  b) 

Figure 6.31 - Visualisations of the Test Building with Tilted Micro-Light Guiding Shade Panels, Clear Sky, High Relative Solar Azimuth: a) From Rear of Room; b) From Window

The Bland and Altman test was applied to the data shown in Figure 6.30. The resulting plot is displayed in Figure 6.32. Simulations generally underestimated measurements. These differences appear more consistent than those shown in Figures 6.22 and 6.27. A bias between -9.1 and -4.3% was found, with differences ranging between -24 and +11%. This bias is more negative than those reported above, but is still acceptable. Overestimations were provided near the window, and could indicate a problem with the external model. This concurs with some disagreement with measured external illuminances (Table 6.9).

Predicted illuminances were more consistently close to measured illuminances under this sky condition than under the overcast sky or other clear sky. The translucent material model again appeared incorrect, causing discrepancy near the window on the west and in the depth of the room on the east. Visualisations

again showed clearer reflections of the window and the panels than were perceived. Several sky models were tested, with illuminance results quite sensitive to the selected sky luminance distribution.

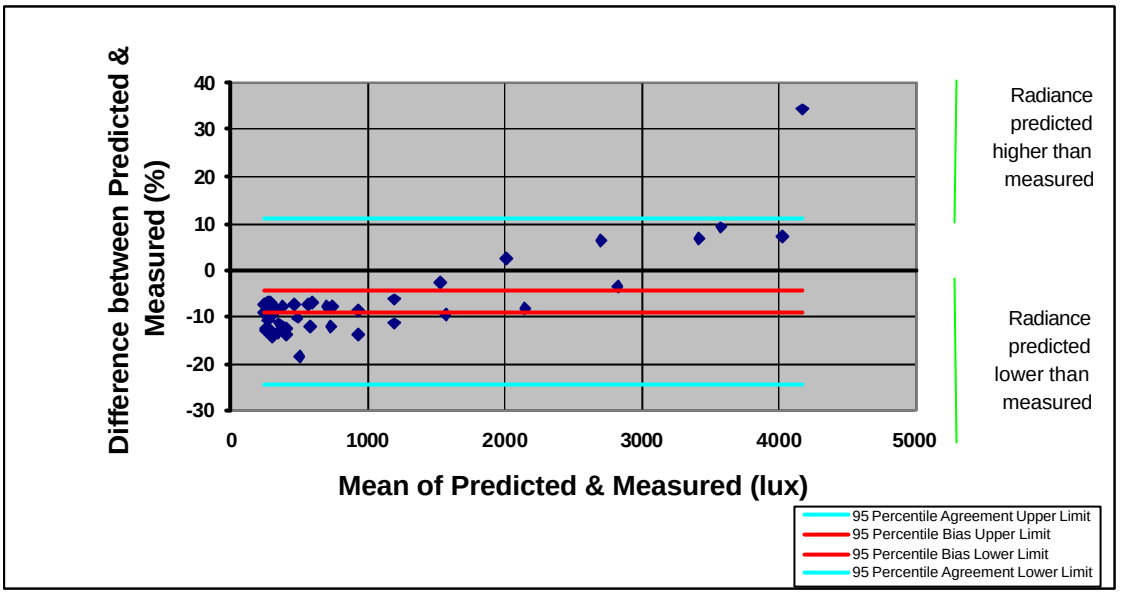

Figure 6.32 - Percentage Differences between Measurement and Simulation of Test Building with Tilted Micro-Light Guiding Shade Panels, Clear Sky, High Relative Solar Azimuth

6.4.2.4 Opalescent Translucent

Difficulties were encountered modelling the directionally transmitting translucent material. This provided significant errors in internal illuminance predictions and visualisations. This material also increased visual discomfort for building occupants. Thus, future micro-light guiding shade panels should employ more diffusing translucent materials. This should allow more accurate simulation of these panels. For this reason, the opalescent panels described in section 5.5.2.4 were simulated on the test building. The view window was covered for all internal measurements, such that all internal illumination was contributed by the micro-light guiding shade panels.

Figure 6.33 displays measured and simulated illuminances provided by the panels covered with opalescent sheeting. The low level of delivered illumination is caused by the covered view window and the two translucent sheets on top of one another. Agreement between measurement and simulation is clearly excellent. Some variation was observed near the window and near the rear wall, but this level of variation was comparatively small.

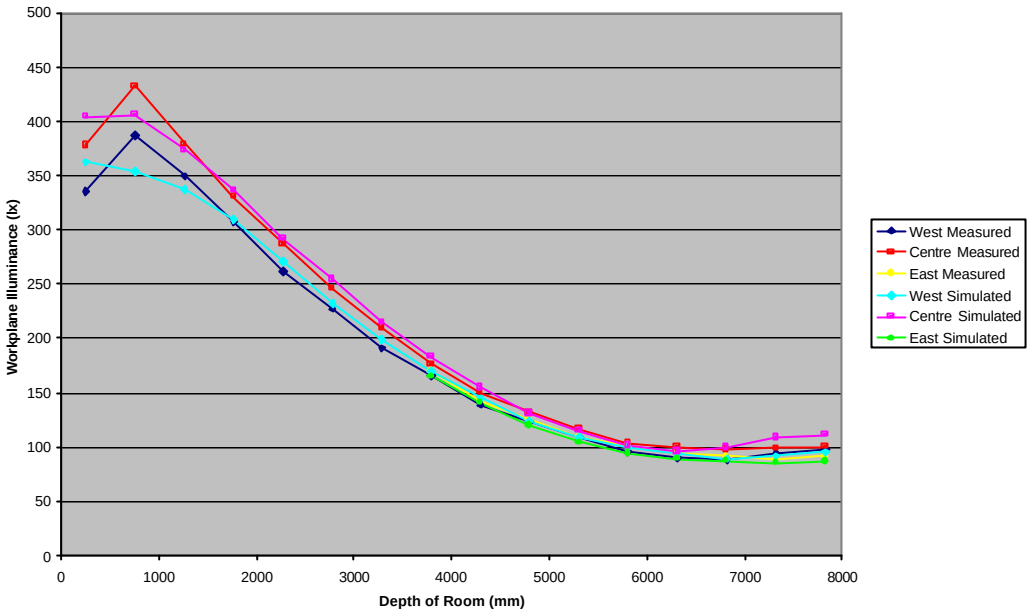

Figure 6.33 - Comparison of Predicted and Measured Illuminances in the Test Building with Tilted Micro-Light Guiding Shade Panels and Opalescent Sheeting, Panels Only

The test of Bland and Altman was applied to this comparison, as shown in Figure 6.34. Percentage differences between measurement and simulation were less than shown in Figures 6.22, 6.27 and 6.32. They were also somewhat more consistent. There was some spread in differences near the window and in the rear of the room, but most differences were less than 10%. A low bias of between -1.0 and +1.4% was found, and a range between ±9%. These results display excellent agreement between measurement and simulation where the translucent material is well understood and modelled.

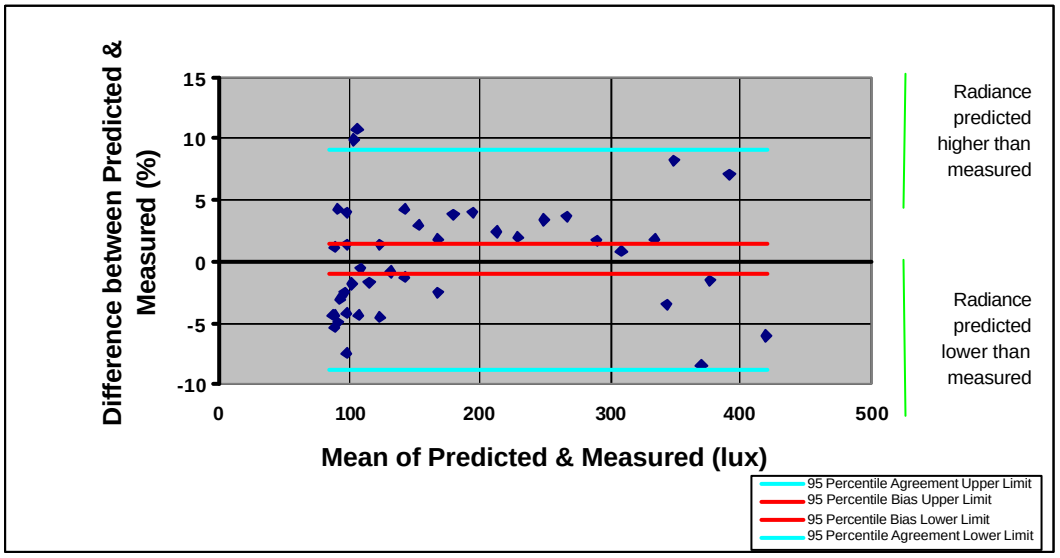

Figure 6.34 - Percentage Differences between Measurement and Simulation of Test Building with Tilted Micro-Light Guiding Shade Panels and Opalescent Sheeting, Panels Only

6.4.2.5 Summary

Simulations of the tilted micro-light guiding shade panels on the test building were sensitive to the translucent material model, sky conditions and the external environment. The installed translucent material has not been adequately modelled. Simulations of the panels with opalescent sheeting demonstrated that excellent agreement could be achieved between measurement and simulation with a well understood and modelled translucent. Visualisations showed sharper reflections of the window and panels than was perceived.

Comparisons with overcast sky measurements were made difficult by changing external conditions during measurement. Percentage differences between measured and simulated horizontal illuminances were fairly well distributed between ±20%. However, a relatively small negative bias was found on average. These comparisons were very good, despite the difficult measuring conditions.

The clear sky with low relative solar azimuth simulations provided a bias closer to zero, but a larger spread of differences. This larger spread was caused by the incorrectly modelled translucent material.

The clear sky with large relative solar azimuth proved difficult to model, with significant errors in external illuminances. Simulated internal illuminance levels provided a small negative bias and a smaller range of differences.

6.5 SUMMARY

The created micro-light guiding shade panels were simulated on the test building under various external conditions. Simulations were performed using various algorithms created for RADIANCE and described in Chapter 7. Simulation controlling parameters were set to high levels, providing accurate illuminance predictions and visualisations.

Two micro-light guiding shade panel models were created. The vertical panels required two models of different widths. An external light shelf completed this model. The tilted panels approximated the required parabolic section with seven flat sections. Two translucent materials were modelled with the tilted panels, one providing highly directional transmittance.

Measurements and modelling of test building geometry and materials was detailed and time-consuming. Extensive material measurements were completed. Particular attention was given to the important wall and ceiling materials. Two approaches were taken to modelling these materials. One involved the default angle-independent specular reflectance model implemented by RADIANCE. The other approach required a new material model, based on the work of He *et al.* (1991).

More accurate simulations were completed by creating a new sky model. This new model is based on the Standard Sky Luminance Distribution (SSLD) of Kittler *et al.* (1997). Five sky models matched those under which measurements were completed. Predicted external illuminances agreed well with measurements for most skies. Some variation was found for the clear sky with high relative solar azimuth. Objects exterior to the building were added, including a grass ground plane, a footpath and the façade of the Bureau of Meteorology building.

The micro-light guiding shade panels were demonstrated by simulation. Four visualisations showed the contributions to internal illumination of the view window and the vertical micro-light guiding shade panels. The panels and an external light shelf reduced the undesired transmission of direct sunlight without diminishing internal light levels in the rear of the room.

Both specular reflection models were applied to simulations of the vertical micro-light guiding shade panels. Visualisations and illuminance predictions agreed very well with perception and measurements. The He *et al*. material model provided sharper reflections of the window and panels in the walls and ceiling than were perceived. However, it provided more accurate reflections of

internal room objects than the default material model. Both models provided very low percentage differences between measurement and simulation. These provided high confidence in the models of the test building and micro-light guiding shade panels. The He *et al*. model was selected for further simulations, based on a slightly lower bias, more accurate reflections of interior objects, and its fundamentally correct basis.

The He *et al*. material model was applied to all simulations of the tilted micro-light guiding shade panels. These simulations revealed errors related to difficulties modelling the directionally transmitting translucent material. Visualisations again showed sharper reflections of the window and panels than were perceived. Despite these problems, predicted illuminances and visualisations agreed well with measurement and perception. Low biases were reported for all sky conditions. Results were sensitive to sky luminance distributions. This showed the importance of selecting more accurate sky models than provided by the current limited CIE standards.

Simulations of the tilted micro-light guiding shade panels were repeated with an opalescent translucent material. This form of translucent material is preferred for future micro-light guiding shade panels. These simulations displayed excellent agreement with measurement, with a very low bias, and a range of percentage differences between ±9%. This provides great confidence in future simulations of the micro-light guiding shade panels on other buildings.

Excellent agreement between measurement, perception and simulation were displayed for the micro-light guiding shade panels installed on the test building. Agreement was improved where the transmission properties of the employed translucent material were well understood and modelled. Since future micro-light guiding shade panels should employ highly diffusing translucent sheeting, these results provide confidence in simulation accuracy. Models of room materials and the external environment were important to accurate simulations. Thus, extensive material measurements were required, and a new sky model was created and implemented.

With confidence in simulation of the micro-light guiding shade panels on real buildings, designers can examine the effect of the panels on new and existing buildings. Highly accurate material models are not necessary for these projects if comparative analysis is employed. This form of analysis should demonstrate the benefit of the panels compared to other options including clear glazing and conventional tilted shades. Thus, the He *et al*. model of specular reflectance should not be required for these analyses. However, results were sensitive to selected sky luminance distributions. Therefore, the SSLD sky models are preferred over the existing limited CIE standards.

6.6 CONCLUSIONS

- Predicted illuminances and visualisations agreed well with measurement and perception. Agreements were improved where the transmission properties of the translucent material were well understood and accurately modelled. The provides confidence in RADIANCE simulations of the micro-light guiding shade panels.
- The Standard Sky Luminance Distribution of Kittler *et al.* (1997) improved the accuracy of test building simulations.
- The He *et al*. model of angle-dependent specular reflection provided some improvements over the default angle-independent model. Visualisations provided by the former model showed sharper interior reflections than were observed. The small degree of accuracy improvements may not justify use of this more complex and time-consuming model.

CHAPTER 7 - RADIANCE ALGORITHMS FOR IMPROVED DAYLIGHT SIMULATION

Several new algorithms were developed for improved RADIANCE daylight simulation. Developments include algorithms to accurately simulate two novel daylight redirecting devices. The developed models were tested by assessment of luminous angular throughputs. Once it was determined that the models worked as required, sensitivity tests were performed. These tests examined the sensitivity of light throughput distributions to materials, manufacture and design. Two new sky models were created and implemented. New algorithms were also developed to improve RADIANCE's simulation of specular reflection. Finally, a new statistical technique was utilised to compare measured and simulated results.

All algorithms were applied in simulation, improving simulation performance. Each of these algorithms and investigations is described separately in the following sections. Many sections make detailed reference to RADIANCE programs and terminology. For more information about RADIANCE, refer to the RADIANCE web-site (Erhlich, 2001) and Ward Larson and Shakespeare (1998). Applications of each algorithm were described in Chapters 4 and 6. The discussion presented in Chapter 8 demonstrates how all are combined in a complete daylight simulation.

7.1 MODELLING THE LASER CUT PANEL

7.1.1 THE LASER CUT PANEL MATERIAL

The laser cut panel (LCP) is a powerful light redirecting element that improves the distribution of daylight in rooms, whilst reducing unwanted solar heat gains. Its manufacture, performance and many applications were outlined in Chapter 2, and are not reproduced here.

The operation of the LCP is illustrated in Figure 7.1. Sunlight, incident from the left, may reflect off the surface or enter the panel. A fraction of the sunlight entering the panel is reflected at the laser cuts by total internal reflection. This deflected fraction exits the panel heading upwards. The remaining sunlight

passes through the panel undeflected. Thus, the optics of the material are characterised by a fraction reflected *R*, a fraction deflected *fd* and a fraction undeflected *fu*. The fractions *R*, *fd* and *fu* are related to the refractive index of the panel *n*, the cut-spacing to cut-depth ratio *D/W*, and the direction of incidence of light on the panel (Edmonds, 1993a).

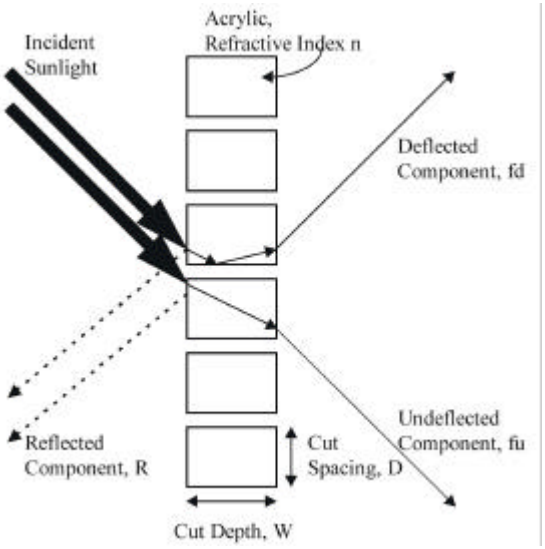

Figure 7.1 - Reflected, Deflected and Undeflected Light Components from the Laser Cut Panel

The fraction of incident light deflected *fd*, as a function of incidence angle, is illustrated in Figure 7.2. This displays the relatively complex angular performance of the LCP. It also shows the dependence of this relationship on the ratio of cut-spacing to cut-depth, *D/W*. Thus, the specification of the LCP can be altered to change its angular selectivity and the strength of redirected illumination.

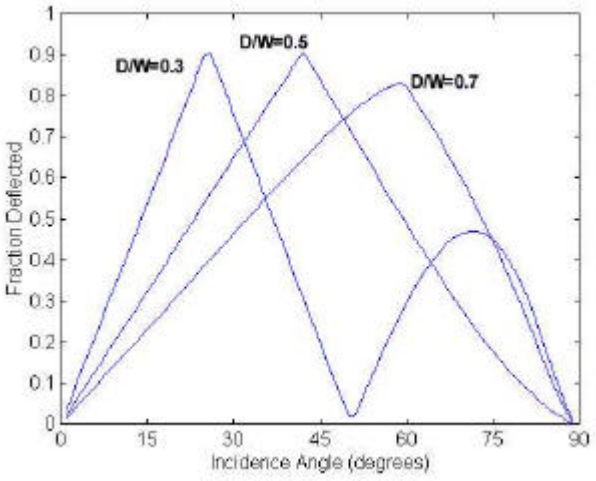

Figure 7.2 - Complex Angular Performance of the Laser Cut Panel

7.1.2 NEED FOR MODELLING ALGORITHM

The LCP provides powerful light deflection and complex angular selectivity. Such devices are difficult for lighting programs to effectively simulate (Apian-Bennewitz, Goller, Herkel, Kovach-Hebling & Wienold, 1998; Mischler, 2001). However, RADIANCE's excellent versatility provided a method by which to model the LCP. This required a calculation algorithm to adequately describe the action of the LCP.

7.1.3 BASIS OF THE LASER CUT PANEL MODEL

Materials are defined in RADIANCE using a set of inbuilt material primitives. RADIANCE allows for many forms of material, at various levels of generality. The *prism2* primitive is a material type of intermediate generality. This material is used to simulate light redirection from prismatic glazings. It may be used to describe reflectance or transmittance, and allows for two ray redirections. This primitive is used to model the LCP.

7.1.4 THE DEVELOPED LASER CUT PANEL ALGORITHM

The LCP transmits and reflects incident light rays, generating three possible emergent rays: the reflected, deflected and undeflected beams (Figure 7.1). For each ray incident upon an LCP, the linked function file calculates the fractions reflected, deflected and undeflected, and the directions of these emergent beams. The function file performing these calculations is listed in Appendix 4.

The *prism2* primitive allows for two ray redirections. However, the LCP generates three possible ray redirections. As RADIANCE cannot model all three ray redirections, only the two most important redirections for each incident ray are passed. The relative importance of each redirection is determined by the reflectivity *R*, and the fractions deflected *fd* and undeflected *fu*.

7.1.5 APPLICATION OF THE LASER CUT PANEL ALGORITHM

A typical application of the LCP is shown in Table 7.1. This application places the LCP vertically, replacing a conventional window glazing. The first line labels the material with the arbitrary name *lcp_material* and identifies it with the primitive type *prism2*. The second line lists eleven string elements. *f1* and *f2*

are the fractions of light that are directed by the panel into the directions (*dx1*,*dy1*,*dz1*) and (*dx2*,*dy2*,*dz2*) respectively. *lcp0.cal* is the function file in which all the necessary calculations occur. The end of the second line specifies a rotation of the material geometry through 90° around the *z*-axis. The third line contains zero integer variables, and the fourth line lists two real variables. The first of these is the specified cut-spacing to cut-depth ratio, *D/W=0.5*, and the second is the refractive index of acrylic, *n=1.5*.

Table 7.1: Definition of Laser Cut Panel Material

```
void prism2 lcp_material
11 f1 dx1 dy1 dz1 f2 dx2 dy2 dz2 lcp0.cal -rz 90
0
2 0.5 1.5
```

The beginning of the function file (Appendix 4) details the geometry of the panels. The panel is assumed to be oriented in the *y*-*z* plane, with cuts parallel to the *y*-direction (Figure 7.3). RADIANCE allows for shifting this orientation when defining the material. This is demonstrated in Table 7.1 where the material is rotated through 90° about the *z*-axis. The panel then faces the positive *y*-direction, with cuts parallel to the *x*-axis. Rotations about all axes are possible, allowing any geometric application of the material.

Following the material definition, a panel may be formed from the material using RADIANCE's surface primitives. Only the planar surfaces *polygon* and *ring* may be used in conjunction with the *prism2* material primitive.

Using this algorithm, it is possible to model any geometry involving the LCP with cuts normal to the panel surface. The model treats the LCP as a macroscopic entity of homogeneous light redirection properties, rather than a microscopic entity comprising several small air gaps. To treat the LCP in the latter manner would increase processing time by at least an order of magnitude. Multiple internal reflections and internal losses are considered. Two ray redirections are passed to the output, those being the most important of the three possible components.

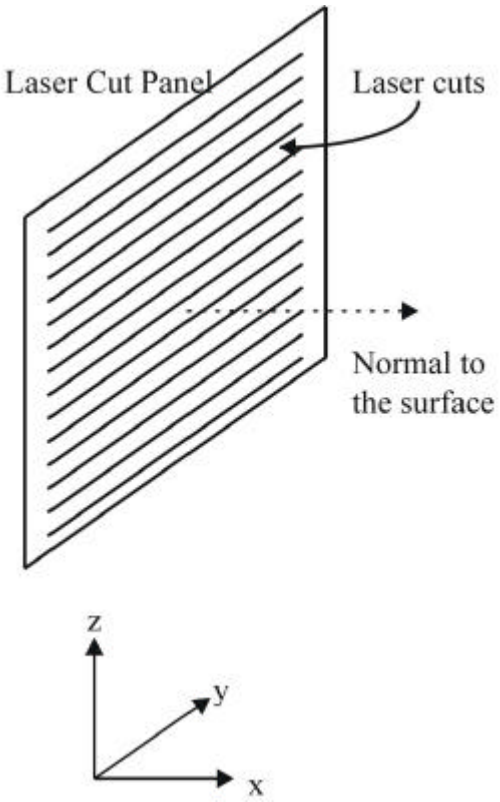

Figure 7.3 - Default Orientation of the Laser Cut Panel

7.1.6 TESTING THE LASER CUT PANEL ALGORITHM

7.1.6.1 Testing by Angular Throughput Distribution

The LCP algorithm was tested by simulating the angular throughput of an LCP exposed to a known sky condition. The simulation methodology is described in section 7.2. A sheet of clear glass and an LCP were exposed to the same CIE standard overcast sky.

The transmitted luminance distributions are shown in Figure 7.4. The shown distributions are inverted, with luminance displayed below horizontal indicating light passing through the window from above the horizontal. The clear glass profile is simply the exterior luminance distribution modified by the glass' angular transmittance. The LCP clearly redirects illumination into the upward direction. The simulated LCP had a *D/W* ratio of 0.5, providing maximum light deflection at 42° incidence (Figure 7.2). This maximum deflection appears as a minimum in the lower transmitted lobe and a maximum in the upper deflected lobe. Thus, all transmitted and redirected illumination passed through the panel in the expected directions with the expected magnitudes.

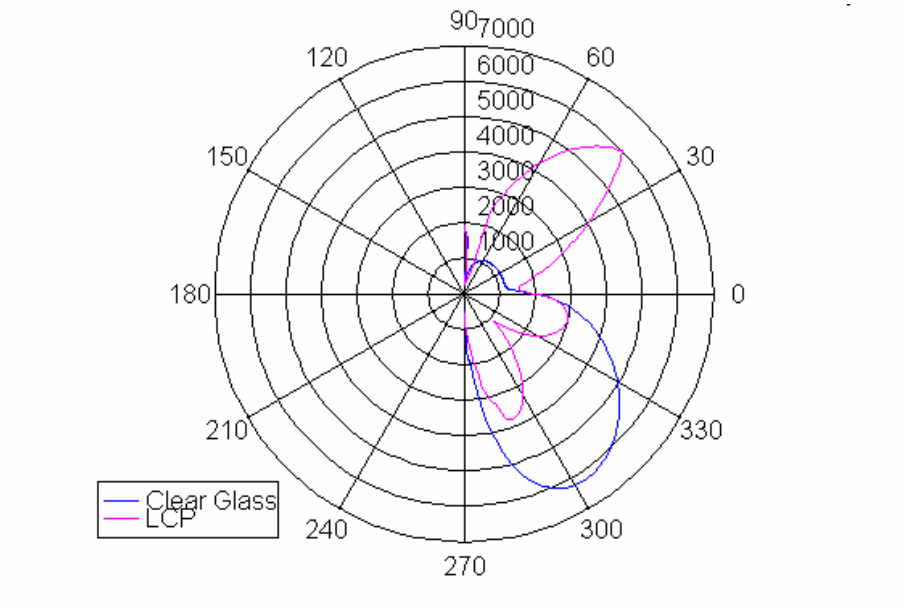

Figure 7.4 - Light Transmitted through Laser Cut Panel and Clear Glass Window under Overcast Sky

7.1.6.2 Comparison with Measured Transmission Data

More thorough tests of the LCP algorithm were performed in comparison with photogoniometer measurements of the bi-directional transmission distribution function (BTDF). The measurement process involved collimated incident light, transmitted through the sample onto triangular screens, imaged by a CCD camera. Andersen, Michel, Roecker and Scartezzini (2001) detail the measuring instrument and calculation technique. Light was incident from direction $(q_1, f_1) = (60°, 90°)$ on an LCP with $D/W=0.667$ (Figure 7.5). BTDFs were averaged over zones of angular dimensions $(Dq_2, Df_2) = (5°, 5°)$.

This figure is not available online.
Please consult the hardcopy thesis
available from the QUT Library

Figure 7.5 - Geometry of BTDF Assessment (Andersen *et al.*, 2001)

A simulated light source approximated that used in the photogoniometer, in terms of solid angular size subtended at the sample. A sample of LCP was surrounded by an opaque diaphragm. Illuminance incident upon the sample, E_1, was predicted at the sample centre. Luminances transmitted into each zone were simulated at 0.1° intervals in q_2 and f_2. Transmitted luminances were averaged over projected solid angles within each zone. Averaged BTDFs were then found within each zone as

$$\overline{BTDF} = \overline{L_2} \Big/ E_1 \qquad \textbf{Equation 7.1}$$

This simulation process revealed non-zero luminances only in the zone located around the direction $(q_2, f_2) = (120°, 90°)$. This is the direction into which the LCP deflects light that is incident from direction $(q_1, f_1) = (60°, 90°)$. No non-zero luminances were found around the undeflected direction $(q_2, f_2) = (120°, 270°)$, nor in any other direction. The non-zero luminances combined for an averaged BTDF in the deflected direction of 236.8sr^{-1}.

Photogoniometer measurements found many more non-zero BTDFs. The measured BTDF in the deflected direction (averaged within the zone surrounding the deflected direction) was substantially less than simulation at 24.3sr^{-1}. Measurements clearly revealed more spread of illumination than simulation. This probably resulted from panel imperfections that were not modelled.

Simulation did not predict the measured illumination in the undeflected direction. This was caused by use of the *prism2* material primitive that models only two ray redirections. For this combination of *D/W* ratio and incident direction, the fraction undeflected is less than the fraction reflected. Thus, the undeflected component was neglected in favour of the reflected component. For this simulation, no reflected component was present, and the undeflected component was needlessly ignored.

To further compare simulation and measurement, luminous transfer efficiencies were compared. These were found as the ratio of luminous exitance E_2 [units: lm m^{-2}] on the rear of the LCP and incident illuminance E_1 [units: lx]. The luminous transfer efficiency represents the portion of incident illumination that passes through the panel to emerge from its rear side. The measured transfer efficiency was calculated by integrating averaged BTDFs with respect to projected solid angles. Simulated luminance was integrated over projected solid angles to determine luminous exitance. The simulated transfer efficiency was then found by dividing the luminous exitance by the predicted incident illuminance.

These calculations returned luminous transfer efficiencies of 67.5 and 78.1% for measurement and simulation respectively. Simulation clearly overestimated measurement. This discrepancy was likely caused by the lack of modelled panel imperfections. These imperfections include surface blemishes and rounded corners to the laser cuts. Such imperfections rejected more light than was simulated. This reduced the measured luminous transfer efficiency from its ideal maximum. It is interesting to note that, for this panel and angle of incidence, the fraction deflected is 78.0%. The simulated luminous transfer efficiency is clearly determined by this value.

7.1.6.3 Problem under Sunny Conditions

Further LCP simulations in rooms under sunny conditions revealed further problems involving the selection of the two most important components. The problem is illustrated in Figure 7.6.

Sunlight enters the room through the view window and strikes the floor. The floor then becomes a secondary source of illumination within the room. In the course of backward raytracing, a light ray strikes the LCP in the clerestory window from above at approximately 60° incidence. At this incidence, the fraction reflected is less than both the fractions deflected and undeflected. Thus, rays are traced in the deflected and undeflected directions, hitting the sky and ground respectively. If a reflected ray had been traced, it would have hit the bright floor. This ray would have returned a greater luminance than both the

deflected and undeflected rays. However, as the fraction reflected was less than the fractions deflected and undeflected, this important source of illumination was ignored.

This should not pose a large problem in most situations, but can cause discrepancies. The problem is not easily fixed by material definitions or function files.

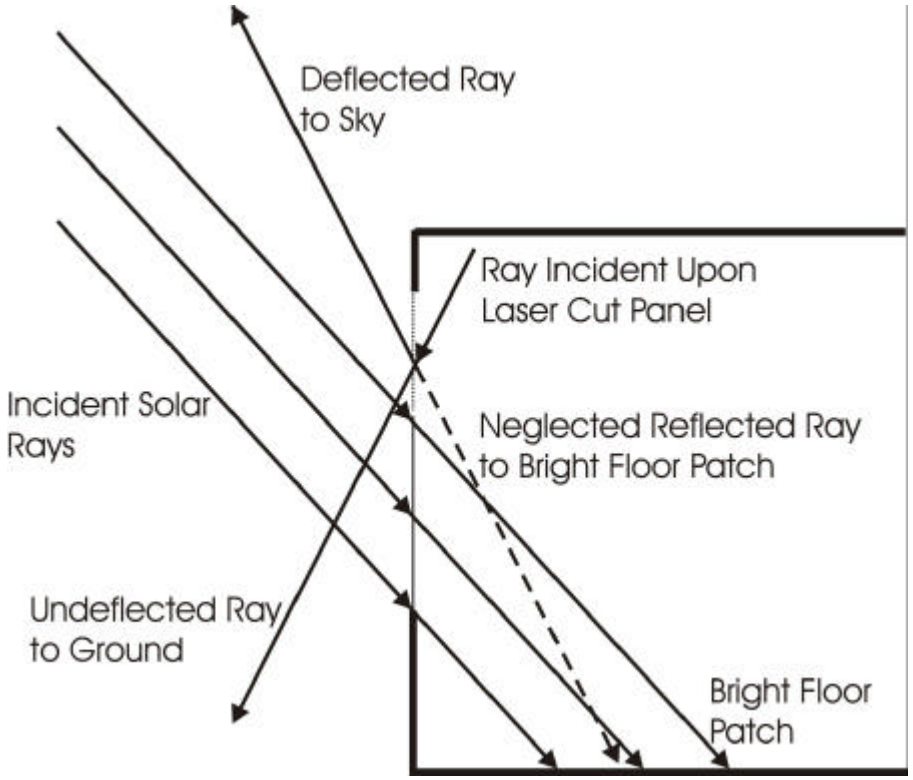

Figure 7.6 - Neglected Reflected Component under Sunny Sky Conditions

7.1.7 DISCUSSION AND FURTHER APPLICATIONS

The LCP algorithm works according to theory. For the particular combination of measured LCP and incidence direction, the undeflected component was needlessly ignored by the *prism2* material primitive. This problem of important but ignored components was also present under sunny sky conditions. Generally, however, this should not provide large discrepancies under most circumstances.

Panel imperfections that can be observed and measured are not considered by the simulation algorithm. Thus, predicted luminances in the deflected and undeflected directions will generally be higher and less spread than measured.

This should not significantly affect illuminance predictions, but may provide errors in visualisations and glare analysis. Further development of the algorithm may be required.

The above comparison of simulations with BTDF measurements is important new work in the investigation of complex fenestration systems (Andersen, Rubin & Scartezzini, 2002). Photogoniometers for the assessment of complex fenestration systems are becoming more common (Andersen, 2002; Andersen *et al.*, 2001; Apian-Bennewitz, 1994; Apian-Bennewitz & von der Hardt, 1998; Mitanchey, Periole & Fontoynont, 1995; Smith, Green, McCredie, Hossain, Swift & Luther, 2001; van Dijk, 2001). Further work is progressing on comparing computational models with measurements, for the validation of both, and greater understanding of the complex systems involved.

One question arising from the above comparison involves the definition of BTDF for specularly transmitting materials. It was necessary to precisely model the source geometry in these comparisons, as the BTDF was dependent on the solid angular size of the source subtended at the sample. Thus, BTDF measurements of specular samples will give average BTDF assessments, with resolution similar to the angular size of the source subtended at the sample. This would not occur for diffusely transmitting materials (Andersen, 2002). If the BTDF is intended to be a fundamental property of a material or system, the dependence of BTDF on source geometry is a fundamental problem with the definition of BTDF for specular samples.

Two other products described in Chapter 2 perform the same function as the LCP, but are made in different ways. These two products are Serraglaze (Milner & Wiggington, 2001) and Inglas-Y (Inglas, 2002). Although direct comparisons have not been completed, there should be little difference in the performance of these three devices. Thus, the developed LCP algorithm should also readily model both of these materials.

7.2 SIMULATING ANGULAR THROUGHPUT DISTRIBUTIONS

7.2.1 NEED FOR ALGORITHM

When modelling light redirecting devices, it is helpful to examine their light throughput distributions. Simulated distributions can be compared with measurable quantities (ie. luminance, luminous intensity) for validation purposes.

This technique can be useful to glazing manufacturers and designers of façade components. Such groups may wish to investigate new concepts in the early design stage, without considering manufacturing difficulties (Mitanchey *et al.*, 1995). If the concept can be accurately simulated, design options can be assessed at a rapid pace.

7.2.2 DESCRIPTION OF THE ALGORITHM

7.2.2.1 *Rtrace* Process

To obtain light throughput distributions, first create the appropriate model, including geometry, materials and light sources. Light sources can be known sky luminance distributions, or defined angular sources such as the sun. An *rtrace* input file contains rays aimed at the device from a range of directions. For instance, to obtain the vertical luminous throughput distribution of an LCP, a set of rays focus on the centre of the panel. These rays are located in the vertical plane, evenly spaced between 90° below and 90° above the horizontal (Figure 7.7). Rtrace then determines the radiance associated with each of these rays.

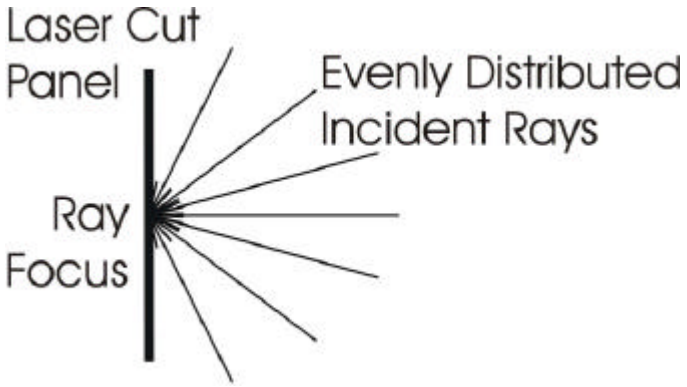

Figure 7.7 - Determining the Luminous Throughput Distribution of a Laser Cut Panel

An example use of rtrace to calculate a luminance output distribution is shown below (Table 7.2). The rtrace input file contains the rays described above. Spectral radiances calculated by rtrace are converted to luminances by *rcalc*, with the resulting luminance profile sent to an output file. This process can be simplified by the use of *rlux* where this program is available.

Table 7.2: Calculating a Vertical Light Output Distribution using *Rtrace*

```
rtrace -h- [rtrace options] octree < input | rcalc -e $1=47.1*$1+117.2*$2+14.7*$3 > output
```

7.2.2.2 *Mkillum* Process

For devices similar to the micro-light guiding shade panel, mkillum may pre-calculate the device's throughput distribution. This is applicable to the micro-light guiding shade panel, as all light exiting the device participates in RADIANCE's indirect calculation. Mkillum directs a large number of rays at the device's output surface and pre-calculates the resulting luminous output distribution. The result is a surface of pre-calculated, area-averaged luminous output distribution.

This form of simulation was used to assess the vertical luminous output distributions of various micro-light guiding shade panels. For these assessments, the region around horizontal was particularly important. These assessments revealed potential difficulties with the use of mkillum.

Mkillum creates luminous output distributions as pre-calculated radiances in a large number of three-dimensional directions. The number of directions is defined by mkillum's *d* parameter. For flat surfaces, the output hemisphere is divided into approximately *dp* regions of equal projected solid angle. This implies that the region around 45° incidence is more densely sampled than regions around the surface normal and grazing incidence. When a ray strikes a surface with a pre-calculated luminous output distribution, a radiance is interpolated between the nearest pre-calculated radiances. Errors are greater where directions are less densely sampled. This occurs around the surface normal and grazing incidence. So, where a vertical output distribution is created for a vertical surface (Figure 7.7), errors are greatest in the important region near the horizontal. Table 7.3 displays values of *d* required to obtain

acceptable resolution in the horizontal direction. The effect of significantly increasing *d* on the predicted luminous output distribution around the horizontal direction is illustrated in Figure 7.8.

Table 7.3: *Mkillum d* Parameter Required to Obtain a Given Angular Resolution in the Horizontal Direction

Resolution, Dq **(degrees)**	**d**
1	10 779 006
5	17 331
10	1 100
15	223

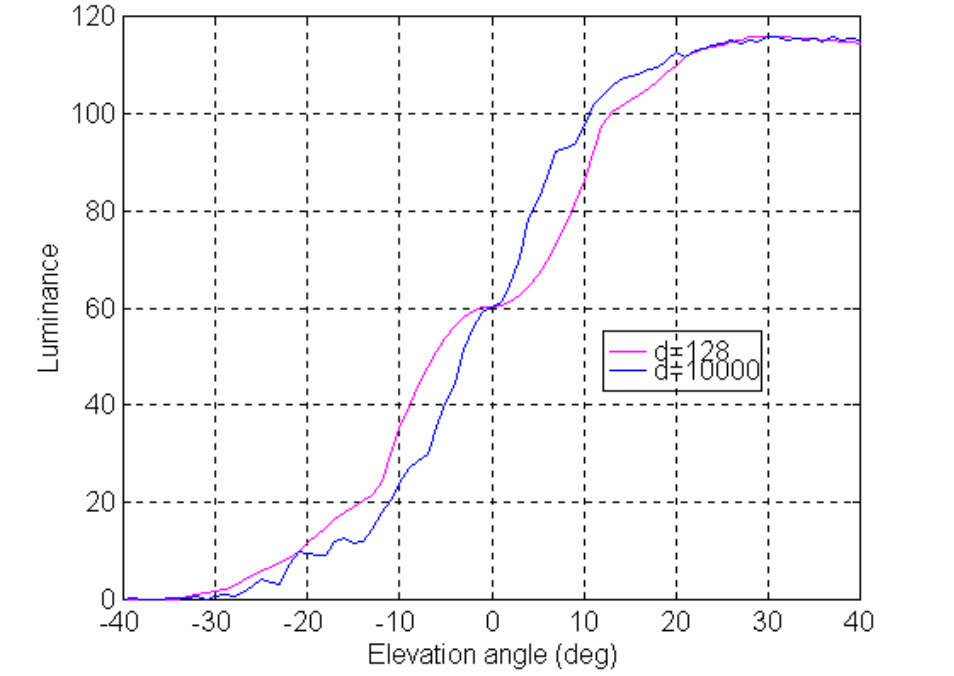

Figure 7.8 - Improved Resolution in Horizontal Direction by Significantly Increasing *Mkillum* d Parameter

Where a one degree resolution is desired in the horizontal direction, *d* must be set at a very high level. This very high level of *d* creates long simulations and very large data files. This problem can be circumvented by replacing the single vertical mkillum surface with two non-vertical surfaces. Mkillum and rtrace are run separately for each surface, creating two luminous output distributions which are then combined.

Figure 7.9 shows a single vertical surface replaced by two surfaces, each oriented 45° from vertical. In this orientation, the horizontal direction will be strongly sampled by mkillum. Two output files contain the luminance output distributions for each surface. With knowledge of the length *l* and height *h* of the original surface and the luminance output distributions of the two surfaces, L_{top} and L_{bot}, the luminous intensity *I* and luminance *L* outputs of the vertical surface are found as

$$I(q) = \frac{lh}{\sqrt{2}}\left[L_{top}(q_{top})\cos(q_{top}) + L_{bot}(q_{bot})\cos(q_{bot})\right] \qquad \textbf{Equation 7.2}$$

$$L(q) = \frac{I(q)}{lh\cos(q)} \qquad \textbf{Equation 7.3}$$

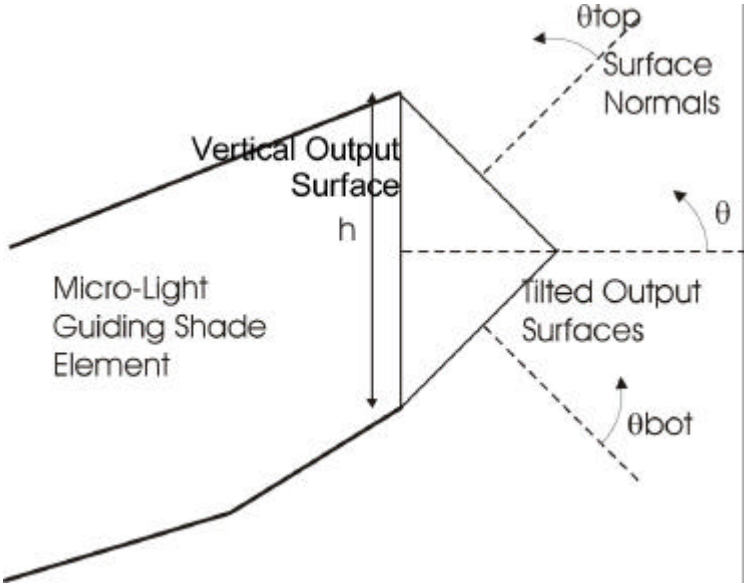

Figure 7.9 - Creating Vertical Output Distributions with Multiple *Mkillum* Surfaces

Multiple mkillum surfaces can also be applied to surfaces of any orientation. Any output distributions can be obtained, including full three-dimensional output visualisations. Some corrections must be made to Equations 7.2 and 7.3 for surfaces and output distributions of different orientations.

Mkillum's *s* parameter must also be set to a high level. This parameter determines the number of ray samples sent to the tested surface for each tested direction. By setting this parameter to a high level, aliasing introduced by non-uniform area sampling will be reduced.

7.2.3 APPLICATION OF THE ALGORITHM

Simulated distributions must be post-processed to compare with experimental measurements. Informative comparisons are easily made of *relative* light output distributions, without consideration of magnitude. Direct comparisons between experiment and simulation require greater knowledge of experimental conditions. Section 4.3.1 demonstrates the post-processing of simulated luminances for comparison with measurement. This involved simulations and measurements of the luminous intensity output of the light guiding shade.

7.2.4 TESTING THE ALGORITHM

The rtrace process for determination of luminous output distributions was frequently applied in Chapter 4. Obtained distributions displayed excellent agreement with expectation and with measurement. This indicates that the algorithm for prediction of luminous output distributions works correctly.

The effect of increasing mkillum's *d* parameter on luminance prediction in the horizontal region is shown in Figure 7.8. This shows luminance delivered by the vertical micro-light guiding shade panel. This device's output angular range was bounded by the horizontal direction. The magenta curve displays the luminance output distribution obtained with *d=128*. This corresponds to an angular resolution of around 17° in the horizontal region. The blue curve was provided by setting *d=10000*. This implies an angular resolution in the horizontal region of around 5.7°. Interpolation between discrete radiance values is displayed as the smoothly varying, anti-symmetric shape around the horizontal. The greater resolution provided by *d=10000* required less interpolation, and thus displayed smaller errors in resolving this important region of the luminance output distribution.

Multiple mkillum surfaces were applied to the light guiding shade simulations. The resulting luminous intensity distributions are displayed in Figure 7.10. All distributions were obtained with *d=10000*. Excellent agreement was displayed between the luminous intensity distributions for one and two surfaces. This shows that the multiple surface approach worked as desired.

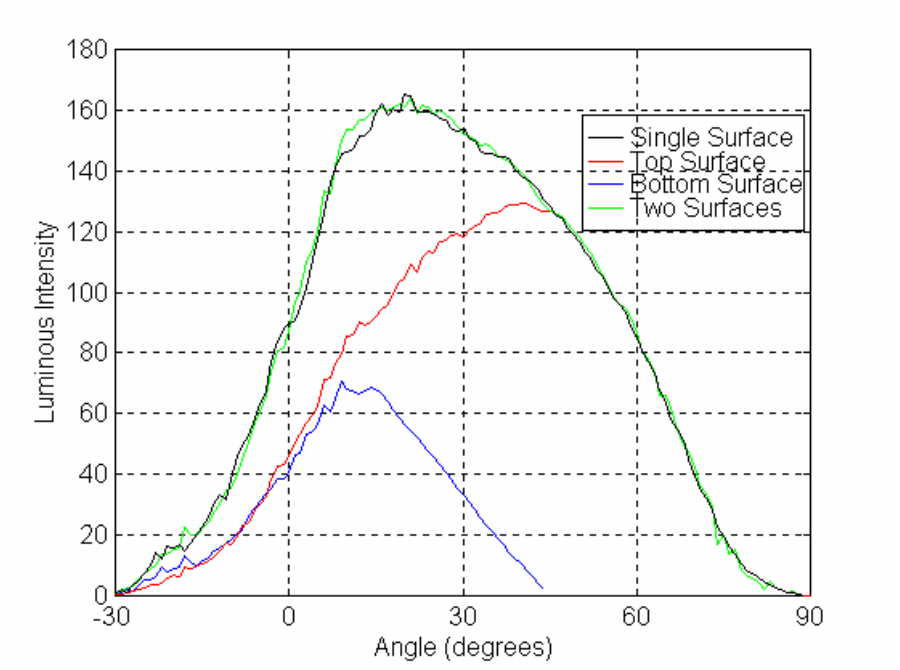

Figure 7.10 - Prediction of Luminous Intensity Output Distributions using Multiple *Mkillum* Surfaces

The effect of using multiple surfaces on the simulated luminance output distribution in the horizontal region is shown in Figure 7.11. Some improvement was provided by the multiple surface approach, although it is difficult to tell with *d=10000*. Improvement is clearest in the region within five degrees of horizontal. In this region, radiance interpolation is clear when derived from one mkillum surface, and not apparent when derived from two surfaces.

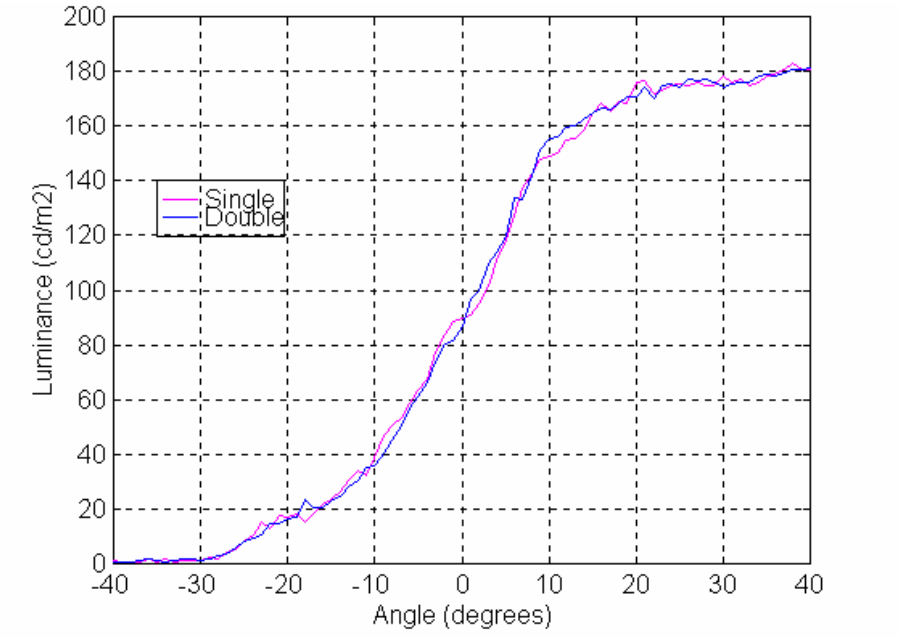

Figure 7.11 - Luminance Outputs in the Horizontal Region with Multiple *Mkillum* Surfaces

7.2.5 DISCUSSION AND FURTHER APPLICATIONS

This algorithm can be applied to many forms of glazing and façade devices. The LCP algorithm validation was an example of such an application (section 7.1.6.2). Similar comparisons with BTDF measurements have been performed with the Genelux lighting simulator (Mitanchey *et al.*, 1995). Genelux requires further development and the implementation of more advanced optical phenomena including Rayleigh scattering and polarisation. Some similar developments may be required for RADIANCE.

The simulation of luminous output distributions can be applied in sensitivity studies. Numerous such studies were applied to the micro-light guiding shade panel. These applications are described in section 7.3.

7.3 SENSITIVITY STUDIES

7.3.1 NEED FOR SENSITIVITY STUDIES

Sensitivity studies assist in choosing appropriate materials and manufacturing techniques. They also help with designing the best device for each application. For the micro-light guiding shade panels, sensitivity studies examined the sensitivity of light throughput distributions to device manufacture and material specification. The aim of these studies was to determine how accurate the device construction must be to achieve the desired performance.

7.3.2 DESCRIPTION OF THE ALGORITHM

Sensitivity studies involved the prediction of angular throughput distributions. Following the creation of a base model, such factors as surface reflectivity, surface roughness and degree of smoothing of geometrical elements were altered. For each change made, a new light throughput distribution was obtained and examined for the effect of the alteration.

7.3.3 APPLICATION OF SENSITIVITY STUDIES

7.3.3.1 Manufacture of Micro-Light Guiding Shade Elements

Tests regarding the manufacture of the micro-light guiding shade elements were described in sections 4.3.5 and 5.3.2.2. For these tests, the definition of the parabolic section was altered within gensurf, creating ideal parabolic sections,

circular arcs and approximations comprising several flat reflectors. Luminous output distributions were created for each form of reflector, for both the vertical and tilted micro-light guiding shade panels.

7.3.3.2 Reflector Material Roughness

The simulated roughness of the reflector materials was determined by a sensitivity study, and application of the test of Bland and Altman (1986) (section 4.3.4). Different roughness values were applied to the reflectors, and luminous output distributions were obtained for each. These distributions were investigated using the Bland and Altman test.

7.3.3.3 Truncation of Micro-Light Guiding Shade Elements

Truncation of the reflector elements was dismissed by a final sensitivity study (section 4.3.6). Several elements of a vertical micro-light guiding shade panel were created with different degrees of truncation. Both the upper flat reflector and lower curved reflector were truncated. This required some alteration to the gensurf command in creating the lower reflector. Luminous throughput distributions were generated for each degree of truncation.

7.3.4 DISCUSSION AND FURTHER APPLICATIONS

Sensitivity studies aided the development of the micro-light guiding shade panel. They demonstrated that the micro-light guiding shade panel can be constructed with ease by replacing the parabolic reflector with several flat sections. It is also important to specify reflector materials that provide smooth, specular reflectance. Finally, truncation of the micro-light guiding shade elements was dismissed.

Sensitivity tests, involving the simulation of angular throughput distributions (section 7.2), can be applied to many new glazing and façade elements. The design and manufacture of new elements can be optimised using sensitivity studies similar to those described.

7.4 NEW SKY MODELS

7.4.1 NEED FOR NEW SKY MODELS

To accurately simulate novel daylighting devices on buildings, it is necessary to have an appropriate range of representative sky models (Bellia, Cesarano & Sibilio, 1994). The standard distribution of RADIANCE provides a uniform sky, and CIE standard clear, intermediate and overcast skies. This range of skies is not broad enough to accurately represent all sky conditions (Igawa & Nakamura, 2001; Kittler, Perez & Darula, 1997; Littlefair, 1994; Mardaljevic, 2000a; Perez, Seals & Michalsky, 1993).

7.4.2 BASIS OF NEW SKY MODELS

Several alternative sky models were created. These include Kittler's Standard Sky Luminance Distribution (SSLD) (Kittler *et al.*, 1997), and Igawa and Nakamura's all sky model (Igawa & Nakamura, 2001). Many of these skies can be interactively examined on the SDF Sky Modelling web-site (Roy, 2001).

Kittler's SSLD is based on more than a hundred measured sky luminance distributions from Berkeley, Tokyo and Sydney (Kittler *et al.*, 1997). 15 new representative sky types were determined. These distributions may shortly be implemented as the new CIE standard general sky.

The all sky model is based on 115 sky luminance distributions measured in Tokyo (Igawa & Nakamura, 2001). This sky model has the same fundamental basis as the SSLD. The coefficients of this model vary continuously with solar altitude and horizontal global illuminance.

7.4.3 THE DEVELOPED SKY MODELS

Sky models were created for both Kittler's SSLD and Igawa and Nakamura's all sky model. Both required new RADIANCE calculation files containing equations describing the sky luminance distributions. The sky models are applied through the *brightfunc* pattern modifier on *glow* sky and ground hemispheres.

7.4.3.1 Kittler's Standard Sky Luminance Distribution

The 15 SSLD types cover skies from heavily overcast with steep gradation and azimuthal independence, to very clear with a clear solar corona (Kittler *et al.*, 1997). The sun is not generated by the sky model. The different sky types are described by five model coefficients, as reported by Kittler *et al.* (1997). The five model coefficients, as well as zenith radiance, ground brightness and the sun's direction cosines, are included in the brightfunc definition. The calculation file *ssldlum.cal* (Appendix 5) creates the required sky luminance distribution, based on the equations of Kittler *et al.* (1997).

7.4.3.2 Igawa and Nakamura's All Sky Model

The all sky model is a continuous sky model described only by solar position and horizontal global illuminance (Igawa & Nakamura, 2001). The fundamental equations of the all sky model are identical to those of the SSLD. However, the five model coefficients are continuous functions of solar altitude and horizontal global illuminance. Thus, the brightfunc definition requires only the horizontal global illuminance, ground brightness and sun direction cosines. The calculation file *asm_new.cal* (Appendix 5) determines the five model coefficients, and generates the zenith luminance and sky luminance distribution.

7.4.4 APPLICATION OF THE NEW SKY MODELS

When performing daylight simulation, an appropriate sky model must be determined. A set of representative skies allows performance assessment under varying external conditions. The SDF Sky Modelling web-site (Roy, 2001) allows interactive comparison of many different sky models. This provides comparison of current CIE standard clear, intermediate and overcast skies with other models including the SSLD. Unfortunately, the all sky model is not available. Such examination can show the benefit of applying the more widely applicable SSLD, and will aid in determining the most appropriate sky types. The all sky model is easier to apply than the SSLD, as it requires knowledge of only the solar position and horizontal global illuminance. However, it is not as versatile as the SSLD.

7.4.4.1 Kittler's Standard Sky Luminance Distribution

For each selected sky, the five model coefficients are found by reference to Kittler *et al.* (1997). The sun direction cosines can be found by running *gensky* and sending the results to a temporary scene file. If the zenith luminance is known, the zenith radiance is determined by dividing the luminance by RADIANCE's luminous efficacy *K=179 lm/W*. If the horizontal global illuminance *HGI* (units: lx) and ground reflectance ρ are known, the ground brightness R_g (units: $Wm^{-2}sr^{-1}$) (assumed isotropic) is found as

$$R_g = \frac{rHGI}{Kp}$$ **Equation 7.4**

If the zenith luminance or radiance are not known, an arbitrary initial estimate must be made. A sun description, and ground and sky glows and *source*s are then added to the scene file. The photopic reflectance of the sky and ground glows must be 100%. The solar radiance is determined from the direct normal or direct horizontal illuminance.

The zenith radiance must be corrected to provide the desired diffuse horizontal illuminance. This is achieved by first creating a test octree containing only the sky scene file. Determine the global (*-ab 1*) and direct (*-ab 0*) horizontal illuminances using *rillum* or rtrace. If the diffuse horizontal illuminance (the difference between global and direct horizontal illuminances) does not meet expectation, the zenith radiance should be scaled accordingly.

The step-by-step process of sky creation, an example completed sky scene file and a process by which to visualise the resulting sky luminance distribution are provided in Appendix 5.

7.4.4.2 Igawa and Nakamura's All Sky Model

Application of the all sky model is more simple than application of the SSLD. Only the horizontal global illuminance, the ground brightness and sun direction cosines are required. The sun direction cosines can be found by generating a temporary scene file with gensky. The ground brightness can be determined

using Equation 7.4. An example brightfunc definition is displayed in Appendix 5. The sun, and sky and ground glows and sources must complete the sky definition.

7.4.5 TESTING THE NEW SKY MODELS

Created sky luminance distributions can be visualised using hemispherical fish-eye views overlaid with iso-luminance contours. Figures 6.8 to 6.12 show such views for five SSLD sky models. These images display the expected sky luminance distributions, indicating that the algorithm works as expected. Table 6.9 compares measured and predicted external illuminances. In most cases, measured and simulated illuminances were very similar. This provides further confidence in the SSLD sky model.

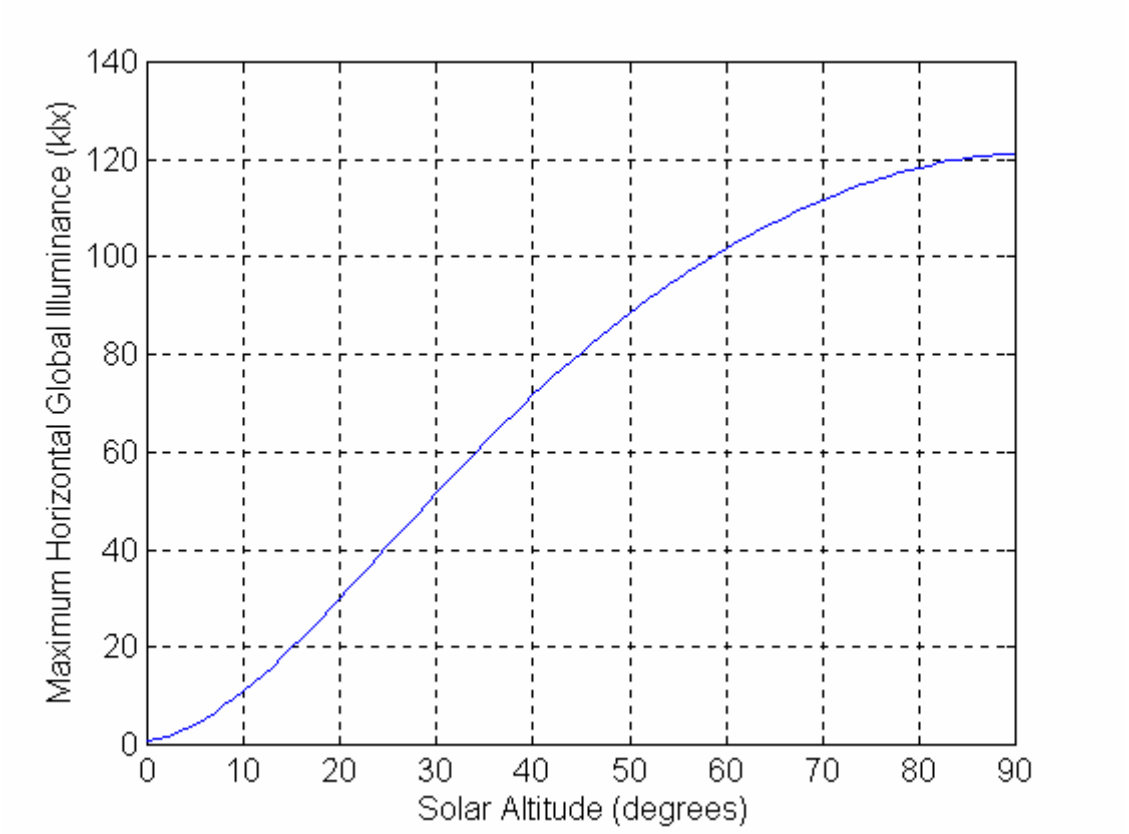

Figure 7.12 - Maximum Horizontal Global Illuminance Allowed by the All Sky Model

The all sky model was not applied to simulations of the micro-light guiding shade panels. However, fish-eye views of generated skies indicate excellent agreement with expectation. One problem that has arisen is the circumstance in which the specified horizontal global illuminance is greater than the standard global illuminance. The standard global illuminance is the expected horizontal

global illuminance under a perfectly clear sky (Figure 7.12). If this value is exceeded, the specified horizontal global illuminance is considered higher than possible, and a sky luminance distribution is not produced. The cause of such discrepancy is likely incorrect specification by the user. Regardless, an error capture process should be added to account for such circumstances.

7.4.6 DISCUSSION AND FURTHER DEVELOPMENTS

The SSLD sky models significantly improved simulations of the micro-light guiding shade panels on the test building. They provide excellent versatility to model a much greater range of realistic sky conditions than provided by the current CIE standards.

A similar RADIANCE application is the *gendaylit* program. This program creates sky models based on Perez's all-weather model (Perez *et al.*, 1993). Similar to the all sky model, the few necessary inputs are solar position, diffuse horizontal and direct normal irradiance. The program is easy to use and provides great versatility in sky types. The program was created for the UNIX version of RADIANCE, and as such was not available for the present simulations.

Despite the already available *gendaylit* program, the SSLD sky models are important as these may become the new CIE standard skies. Also, the ability to simulate numerous sky models can only add to RADIANCE's daylight simulation versatility. With this consideration, the all sky model was created as part of a collaboration within the International Energy Agency Task 31 - Daylighting Buildings in the 21st Century. Further sky models would easily be modelled in similar fashions to the SSLD and the all sky model.

7.5 MATERIAL REFLECTION MODELLING

7.5.1 NEED FOR MATERIAL MODELLING ALGORITHM

Attention must be given to specular reflections in daylight simulations. The assumption of perfectly diffusing surfaces may cause illuminance underestimation at a distance from the window (Ashmore & Richens, 2001; Fontoynont, Laforgue, Mitanchey, Aizlewood, Butt, Carroll, Hitchcock, Erhorn,

De Boer, Michel, Paule, Scartezzini, Bodart & Roy, 1999). This is because materials that are not perfectly diffusing tend to reflect more light in the direction opposite the light source. Incorrect modelling of specular reflections adversely affects illuminance estimates, glare analysis and visualisations.

As described previously in Section 6.2.2.2, light reflection can be difficult to model. Ideal and spread specular reflection (Figure 6.7) vary with both direction and microscopic material properties (He, Torrance, Sillion & Greenberg, 1991). However, angle-dependent specular reflection was removed from RADIANCE due to difficulty modelling reflections of light sources (Ward, 1997).

In most cases, RADIANCE's incomplete specular reflection model will not cause large errors. However, errors may appear in simulations involving materials with large specular components, such as the walls and ceiling of the test building. These surfaces were clearly important to simulations of the test building. As such, particular attention was given to the correct modelling of these surfaces.

7.5.2 BASIS OF THE ALGORITHM

He *et al.* (1991) presented a comprehensive model of light reflection. Light reflection was divided into three components: specular, spread specular and uniform diffuse. The specular and spread specular components were well described and fundamentally derived.

Predicted bi-directional reflectance distribution functions (BRDFs) compared well with measured profiles. The BRDF for unpolarised incident light is given as

$$r_{bd} = r_{bd,sp} + r_{bd,ss} + r_{bd,ud} \qquad \textbf{Equation 7.5}$$

where $r_{bd,sp}$, $r_{bd,ss}$ and $r_{bd,ud}$ represent the specular, spread specular and uniform diffuse components of reflection, respectively. These components are given as

$$r_{bd,ud} = a(l)$$

$$r_{bd,sp} = \frac{r_s}{\cos q_i dw_i}\Delta \qquad \textbf{Equation 7.6}$$

$$r_{bd,ss} = \frac{R}{p}\frac{GSD}{\cos q_i \cos q_r}$$

The uniform diffuse component is constant with respect to incident and reflected directions, q_l and q_r, varying only with wavelength λ. The specular component is zero outside the cone of reflection (D function), with r_s varying as

$$r_s = RSe^{-g} \qquad \textbf{Equation 7.7}$$

where R, S and g represent Fresnel reflectivity, shadowing and apparent roughness functions respectively. The spread specular component incorporates Fresnel reflectivity and shadowing, as well as a geometrical factor G and distribution function D.

The model is defined in terms of two parameters describing the microscopic form of the surface. s_0 is the standard deviation in surface height, and t is the surface autocorrelation length. Together, these parameters describe the microscopic roughness of the surface, with large t/s_0 describing a smooth surface. The various parameters and reflection components combine for a complex, but physically meaningful model of surface reflectance.

7.5.3 DESCRIPTION OF THE ALGORITHM

Two approaches were taken to modelling the test building walls and ceiling. Both involved the He *et al*. surface reflection model. The first approach adopted RADIANCE's default angle-independent specular reflection model. The second approach allowed specular reflection to vary according to the model of He *et al.* (1991).

7.5.3.1 Angle-Independent Specular Reflection Model

To apply RADIANCE's default angle-independent specular reflection model, an average specular reflectance was required. The calculation of average specular reflectance occurred in two parts.

Firstly, the measured specular reflectances were fitted to the He *et al*. model. This required solution of Equation 7.7 for surface parameters s_0 and t. A maximum surface height deviation s_0 was determined from knowledge of the measured specular reflectance r_s and Fresnel reflectivity at 45° incidence *R(45°)*. A value of s_0 less than the calculated maximum was then chosen. This allowed subsequent calculation of g, S and t.

Determination of s_0 and t provided the remaining angular dependence of specular reflectance. Specular reflectance was then averaged over projected solid angles,

$$\overline{r_s} = \frac{\int_{q=0}^{p/2} r_s(q_i)\cos q_i \, dw_i}{\int_{q=0}^{p/2} \cos q_i \, dw_i} \qquad \textbf{Equation 7.8}$$

This form of averaging was most closely related to average light flux reflection over all angles of incidence.

Numerous combinations (s_0, t) were calculated and applied in simulation of the test building. Different material parameters made little difference to internal illuminances, and the final selection of parameters was based on qualitative examination of visualisations.

7.5.3.2 He *et al.* (1991) Specular Reflection Model

The He *et al*. model of angle-dependent specular reflectance was implemented by adapting an existing RADIANCE calculation file. The resulting calculation file, *Her.cal*, is shown in Appendix 6.

Selection of material parameters (s_0, t) followed the same procedure as outlined above. s_0 was set below a calculated maximum, and t was determined from measured specular reflectance at 45° incidence. Several combinations (s_0, t) were assessed. Different combinations made little difference to room illumination. A final determination of parameters was found by qualitative examination of visualisations.

7.5.4 APPLICATION OF THE ALGORITHM

7.5.4.1 Angle-Independent Specular Reflection Model

For *plastic* material primitives, parameter *A4* equals the averaged specular reflectance. The relative values of parameters *A1*, *A2* and *A3* determine the colour of the material. The required photopically averaged combination *C* of parameters *A1*, *A2* and *A3* is found from diffuse reflectance r_d and parameter *A4*.

$$C = \frac{r_d}{1 - A4}$$ **Equation 7.9**

The photopic average *C* is calculated from *A1*, *A2* and *A3* as

$$C = 0.263A1 + 0.655A2 + 0.082A3$$ **Equation 7.10**

(RADIANCE version 2.4, coefficients altered in later versions). Parameters *A1*, *A2* and *A3* are scaled to provide the required photopic average *C*.

7.5.4.2 He *et al.* (1991) Specular Reflection Model

Implementation of the angle-dependent specular reflection model requires use of RADIANCE's *BRTDfunc* material primitive. This material primitive provides maximum flexibility over surface reflectance and transmittance (Ward, 1996). The He *et al*. model is implemented by defining a material as shown in Table 7.4.

Table 7.4: Material Definition using He *et al.* (1991) Material Reflectance Model

```
void BRTDfunc name
10
        s s s
        0 0 0
        dd dd dd
        Her.cal
0
12
        amb_r amb_g amb_b
        amb_r amb_g amb_b
        0 0 0
        sigma0 tau
        n_real
```

Real variables *amb_r*, *amb_g* and *amb_b* should be replaced by the material's coloured diffuse reflectance, assumed the same on both sides of the material. Variables *sigma0*, *tau* and *n_real* should be replaced by values of s_0, t [units: μm] and the material's real index of refraction.

7.5.5 TESTING THE ALGORITHM

7.5.5.1 Uniform Diffuse Component

The individual components of reflection (specular, spread specular and uniform diffuse) were tested by turning off various parts of the material model. This was achieved by individually setting to zero the parameters *s*, *dd* and *amb_r,g,b* in Table 7.4. For instance, when modelling only the uniform diffuse component of reflection, each instance of *s* and *dd* in Table 7.4 was replaced by zero. For each combination, illuminance profiles were predicted in the test building.

The specular and spread specular components contributed very little to illuminance levels within the building. However, illuminances rose unexpectedly within three metres of the building's rear wall. This indicated problems either in the developed He *et al*. model or in RADIANCE's BRTDfunc primitive.

The problem was investigated by creating a pair of test surfaces, one above the other, illuminated by a uniform sky (Figure 7.13). Both surfaces were modified by a BRTDfunc material. No specular or spread specular components were included in the material definition. Rays were traced through these surfaces to investigate the light reflected by and transmitted through the two surfaces.

Although the transmission component of the BRTDfunc material definition was set at zero, light appeared to pass through the two surfaces and emerge from underneath them.

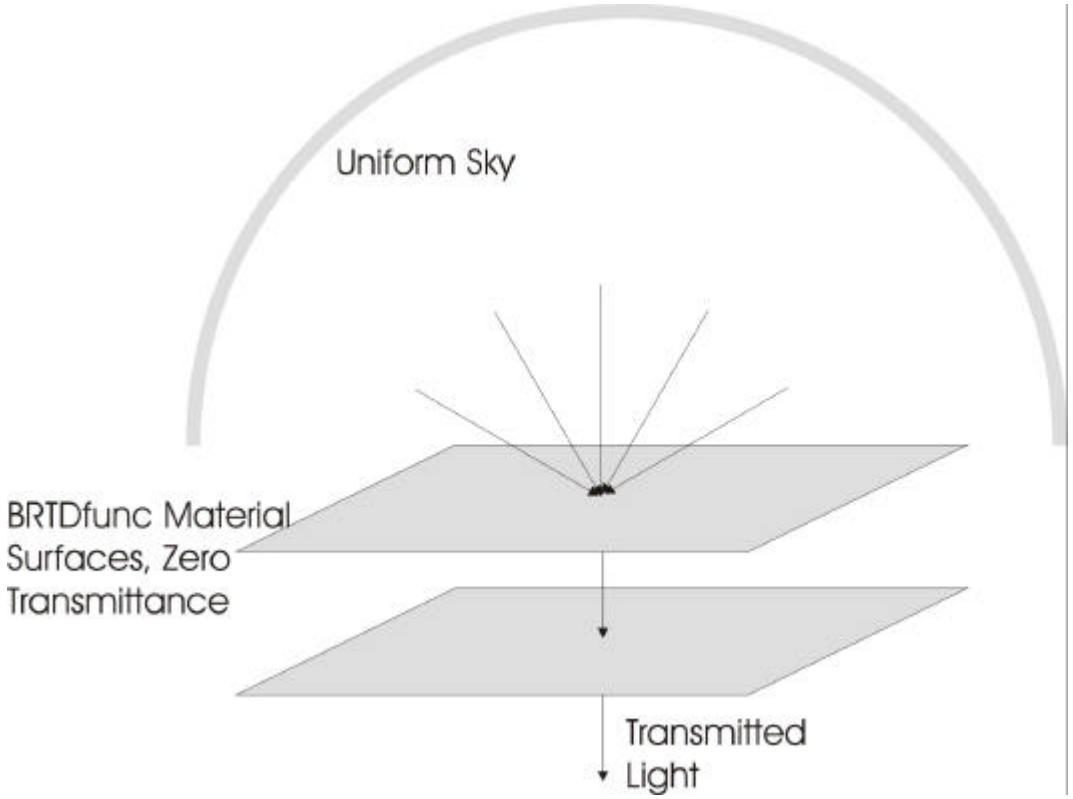

Figure 7.13 - Unexpected Transmission of Light Through *BRTDfunc* Surfaces

A similar test was applied to the test building simulation. An opaque box was created around the east, south and west walls and roof of the test building. Illuminances within the building were again simulated. If no illumination were able to pass through the test building walls and ceiling, this external box should make no difference to results. However, the resulting illuminance profile displayed no unexpected rise in the rear of the room. Thus, the unexpected illuminance rise was attributed to spurious light transmission through the BRTDfunc materials. Further test building simulations with these materials included the external opaque box.

7.5.5.2 Material Primitive Comparison

Illuminance profiles and visualisations obtained with both the angle-dependent and angle-independent models of specular reflection were presented in section 6.4.1. Excellent agreement was achieved between illuminance predictions and visualisations of the two models. This reveals firstly that the

He *et al*. model algorithm worked as required. It also showed that the more complex model of He *et al*. provided little performance improvement for this simulation. However, the He *et al*. model was selected for further modelling of the test building, based on slightly more accurate illuminance predictions, more realistic reflections of interior objects, and its more fundamentally correct formulation.

7.5.6 DISCUSSION AND FURTHER APPLICATIONS

The benefit of the new algorithm is questionable; it provided modest improvements in quality and substantially longer simulation times. The existing RADIANCE material model was greatly optimised by considering such benefits versus extra simulation times (Ward, 1992). Thus, the lack of angle-dependent specular reflection model indicates that RADIANCE's creator considered the extra calculation time outweighed possible improvements in accuracy.

Further analysis can be performed as a sensitivity study. This study could analyse the sensitivity of RADIANCE illuminance predictions to surface specularity and roughness. If this study revealed great sensitivity to surface specularity, consideration should be given to application of the model of He *et al.* (1991) in one of the forms described above.

7.6 STATISTICAL SIMULATION VALIDATION

7.6.1 NEED FOR STATISTICAL VALIDATION TECHNIQUE

To provide designers with confidence that simulations work as desired, statistical validations must be completed. These involve comparisons of measured and simulated parameters of interest. In statistical terms, it is necessary to compare two non-normal distributions for locational data, gathered as matched pairs. There is no standard method of performing such comparisons (Murdoch & Barnes, 1986; Selvanathan, Selvanathan, Keller, Warrack & Bartel, 1994). Thus, non-parametric methods must be employed. The test of Bland and Altman (1986) is an ideal test to perform the required comparisons.

7.6.2 BASIS OF THE TECHNIQUE

The test of Bland and Altman (1986) was created for statistical comparison between two methods of clinical assessment. This form of comparison is closely related to the statistical validation of simulations. Thus, the test of Bland and Altman was easily adapted to this purpose.

When applied to simulation validation, the test provides graphical comparison between simulated and measured data. The test plots the difference between measured and simulated results against the mean of the two. 95% confidence intervals for the difference and bias (mean difference) are overlaid on the same plots. Thus, the plot clearly represents the bias between experiment and simulation, and demonstrates locations at which simulations disagree with measurements. This test can be applied to absolute or percentage differences.

7.6.3 DESCRIPTION OF THE TECHNIQUE

For each matched pair of simulated and measured data, the difference and mean are calculated. The calculated differences can be either absolute or percentage. The mean, standard deviation and standard error of the differences are then calculated. 95% confidence intervals are generated for the difference and the bias. The confidence interval for the bias gives a good estimate of the mean difference between measurement and simulation.

The calculated differences and means of matched pairs are plotted against each other. The upper and lower limits of the bias and range are overlaid on the same plot. Thus, the test provides estimates and graphical representation of the bias between measurement and simulation, the range of differences, and any trends or outliers.

7.6.4 APPLICATION OF THE TECHNIQUE

The test of Bland and Altman was applied to many simulations described in Chapters 4 and 6. Spreadsheets were created to perform the calculations and graphical representation. An example spreadsheet is shown in Appendix 7. For these comparisons, analyses of absolute differences were of little utility compared to analyses of percentage differences. This is likely to occur for most simulation validations of this form.

7.6.5 DISCUSSION AND FURTHER APPLICATIONS

Validation is essential to simulation work. This is exemplified in the simulation research of the International Energy Agency Tasks 21 and 31, and Technical Committee 3.33 of the CIE - Test Cases for Assessment of Accuracy of Interior Lighting Computer Programs. Each body continues to produce and validate new simulation programs and algorithms. It is essential that appropriate statistical techniques be applied to this validation work. The test of Bland and Altman (1986) may fulfil this requirement.

7.7 SUMMARY

Numerous new simulation algorithms were created to improve RADIANCE's simulation of daylight and daylighting devices. Each of the techniques were applied in various simulations described throughout this thesis. Simulation of the micro-light guiding shade panel, in particular, has been aided by these new algorithms.

The laser cut panel (LCP) is a powerful light deflecting device with many daylighting applications. Its powerful light deflection properties required the development of a new RADIANCE algorithm. This involved the prism2 material primitive, allowing the propagation of two redirected rays for each incident ray. The function file chooses the two most important of three possible ray redirections, and generates two new rays in the required directions. The algorithm is applied by the creation of an LCP material, and its application to a flat surface. The algorithm was tested by simulation of angular throughput distributions, and comparisons with measured bi-directional transmission distribution functions. The algorithm generally performed well, agreeing well with theory. Problems were discovered in simulating light spreading from imperfectly manufactured elements, and in the disregard of potentially important light redirections. The algorithm and testing techniques can be readily applied to other complex light redirecting devices, including Serraglaze and Inglas-Y.

Simulated angular light throughput distributions are useful for testing new façade and glazing elements. Mkillum can pre-process the light output distributions of devices such as the micro-light guiding shade panel. For high

resolution in the horizontal region, it was helpful to create two dummy output surfaces tilted 45° from vertical. Light throughput distributions are then predicted using rtrace or rlux. Resulting throughput distributions should then be post-processed to compare with measurement and expectation.

Sensitivity studies can aid in optimising device design, material specification and manufacture. Several sensitivity studies were completed by investigating angular light throughput distributions and their changes with device parameters. The techniques described can be easily applied to various new façade and glazing elements.

Two new sky models have improved RADIANCE's versatility in daylight simulation. The Standard Sky Luminance Distribution (SSLD) and the all sky model provided greater ability to model a representative range of skies. The SSLD may become the new CIE standard sky distributions. The all sky model requires only solar position and horizontal global illuminance. Both models were implemented by creating new calculation files, and applied with the brightfunc pattern modifier. Several SSLDs were implemented in modelling the micro-light guiding shade panels on the test building. Predicted external illuminances agreed well with measurements, and simulation performance was improved. More sky models could easily be implemented in RADIANCE.

A new material modelling algorithm was developed, based on the work of He *et al.* (1991). The model of He *et al.* (1991) describes angle-dependent specular and spread specular reflected components in terms of two microscopic material parameters. This angle-dependent specular reflection was not present in the default RADIANCE calculation (Ward, 1997). It was considered that, with large semi-specular reflectors, such as those in the test building, rear room illuminances would be underpredicted by the default model. Two approaches were applied to modelling the test building walls and ceiling. One approach involved the default angle-independent model with an averaged specular reflectance. The other approach implemented the full model of He *et al*. A problem was discovered with unexpected transmission through surfaces modified by the BRTDfunc material primitive. This was corrected by covering

the offending surfaces with an opaque box. Following this correction, simulation results obtained using the new algorithm compared well with simulations completed with RADIANCE's default material model. Thus, the algorithm worked as desired, but results were quite insensitive to the new model. The benefit of the new, more complex and time-consuming algorithm may not be justified by simulation results of sufficiently greater accuracy.

The statistical test of Bland and Altman (1986) was applied to validation of RADIANCE simulations. Such a statistical process is required to provide practitioners with confidence in their simulations. The test provides graphical representations of differences between measurement and simulation, bias, ranges of differences, trends and outliers. The test can be applied to either absolute or percentage differences; the latter appears best suited to the validation of simulation results. The technique has great potential for future validations of simulation tools and algorithms, such as those performed by the International Energy Agency and the CIE.

7.8 CONCLUSIONS

- Numerous new simulation algorithms have improved RADIANCE's daylight simulation, and aided development of the micro-light guiding shade panel.
- The laser cut panel algorithm performs according to theory, but does not model inherent surface imperfections.
- Simulation of angular light throughput distributions is useful for investigation of new devices and their simulation.
- Sensitivity studies can aid in optimising device design, specification and manufacture.
- The Standard Sky Luminance Distribution model improved test building simulations under various external conditions.
- The He *et al*. material model may improve daylight simulations, at the expense of substantially longer simulation times.
- The statistical test of Bland and Altman (1986) is well suited to the validation of simulation tools and algorithms.

CHAPTER 8 - DISCUSSION AND CONCLUSION

Successful daylighting of high rise buildings in the sub-tropics is a difficult task. Windows are traditionally heavily shaded or tinted, severely reducing daylight levels. This occurs despite abundant direct sunlight and high ambient illumination. The micro-light guiding shade panel was developed as a solution to this problem. The device combines solar shading and daylight redirection in a panel looking outwardly similar to conventional tilted shades.

The work presented in this thesis is summarised in section 8.1. The findings are then applied such that readers may extract information useful to them. Conclusions drawn from this research are then presented and related to the aims of Chapter 1. This is followed by directions for future research.

8.1 SUMMARY

8.1.1 THE MICRO-LIGHT GUIDING SHADE PANEL

Successful daylighting of commercial buildings can provide many benefits to building owners and occupiers, and the environment. Severe shading of sub-tropical buildings challenges the designer endeavouring to improve natural lighting. The frequency and intensity of available sunlight provides great potential if it can be effectively utilised while avoiding glare and excessive heat gain.

The solution to the problem of successfully daylighting sub-tropical commercial buildings must combine efficient daylight redirection with effective solar shading. The micro-light guiding shade panel achieves these objectives. It also achieves myriad other objectives including: deep and constant daylight penetration, low glare, low space intrusion, easy installation, acceptable aesthetics (in the opinion of all that viewed the tilted panels), and applicability to new buildings and retrofits.

Constructed micro-light guiding shade panels performed largely as expected. Light was delivered into the desired directions, providing deep, comfortable, natural illumination while reducing excessive illumination near the window.

Some glare was delivered by the tilted panels, due to the poorly diffusing nature of the installed translucent material. This glare was eliminated by replacing the installed translucent material with opalescent sheeting. The room on which the panels were installed was consistently preferred over the room shaded by conventional tilted shades. Artificial lighting was also less likely switched on due to installation of the panels.

Micro-light guiding shade panel designs are determined by the size, orientation and tilt of the panel, and the upper and lower directions into which light is directed. In terms of annual luminous transfer, panels are most effective on façades facing north to north-west (southern hemisphere, sub-tropical climate). Optimal panel tilt is determined by geographic location, orientation and local climate. The lower direction into which light is directed should be on or slightly above horizontal. Optimal light capture and throughput is achieved by setting the upper bound of the output angular range parallel to the panel's surface.

Construction of the micro-light guiding shade panels proved difficult and time-consuming. Industrial pressing of the micro-light guiding shade elements should be considered for future constructions. This requires greater initial cost outlay, but provides substantial benefit in manufacturing time and effort. Care must be taken to specify smooth reflector materials and highly diffusing translucent materials, and to produce appropriately curved reflectors. If such care is not taken, some light can be spilt into undesirable directions, increasing chances of glare. Future implementations of the micro-light guiding shade panels would be improved by a translucent material with greater light spreading ability yet higher transmittance.

Material costs increase as accuracy of construction and aesthetic considerations are improved. Construction costs would be reduced, for significant volumes of panels, by introducing an industrial manufacturing process such as metal pressing.

8.1.2 DAYLIGHT SIMULATION

For daylighting strategies and devices to be used to their full potential, designers must understand their impact on building performance early in the design process. Thus, these strategies and devices must be modelled with available lighting simulation software.

The performance of lighting simulators varies widely, with some being more effective for artificial illumination, and some being very accurate in simulating natural lighting. For the simulation of natural lighting in architectural designs, RADIANCE is a superior lighting simulator. RADIANCE provides high capabilities, high accuracy and high quality results, if used by an experienced user, and appropriate simulation parameters are employed. RADIANCE performs advanced lighting simulation and provides convincing visualisations, all in reasonable computation times. It also successfully models complex light redirecting devices. For these reasons, RADIANCE was chosen to perform advanced lighting simulations involving the micro-light guiding shade panel.

RADIANCE simulations were validated against experimental assessments of light throughput distributions and internal illuminances. Visualisations and predictions agreed very well with perception and measurements. The employed material model provided accurate reflections of internal room objects, but sharper reflections of the window and panels than were perceived. The bias between simulation and measurement was generally less than 10%. Some discrepancies were revealed, related to difficulties modelling the poorly diffusing translucent material. These errors were eliminated where the translucent material was well understood and correctly modelled. Since future implementations of the micro-light guiding shade panel should employ a highly diffusing translucent material, the reported errors should not pose a problem for future simulations.

Several new simulation algorithms have improved RADIANCE's simulation of daylight and daylighting devices. These algorithms include: the laser cut light redirecting panel, simulation of angular light throughput distributions, sensitivity

studies, new sky models, a new material model, and a statistical test for simulation validation. Each algorithm was tested and applied to daylight simulation and development of the micro-light guiding shade panel. The main findings of these studies are discussed below, and applications of the algorithms are demonstrated in section 8.2.2.

Simulations helped to determine optimal device design, material specification and manufacture. This was achieved through several sensitivity studies, based on predicted angular throughput distributions. These techniques can be easily applied to various new façade and glazing elements.

Simulation results were sensitive to sky luminance distributions. This sensitivity demonstrated the importance of selecting more representative sky models than provided by the current limited CIE standards. Accurate simulations were completed by creating a new sky model, based on the forthcoming CIE Standard Sky Luminance Distribution. The new sky model provided greater ability to model a representative range of real skies.

The walls and ceiling of the test building were modelled with a new material modelling algorithm. This allowed for angle-dependent specular reflection not provided by the default RADIANCE calculation. However, simulation results were quite insensitive to the new model. As such, the benefit of employing the new, more complex and time-consuming algorithm was not justified by simulation results of sufficiently greater accuracy.

The statistical test of Bland and Altman (1986) was applied to simulation validation. The statistical test greatly aided simulations of the micro-light guiding shade panels. The technique has great potential for future validations of simulation tools and algorithms.

8.2 APPLYING THESE FINDINGS

8.2.1 THE MICRO-LIGHT GUIDING SHADE PANEL

The micro-light guiding shade panel is an effective daylighting device, successfully combining direct solar shading and daylight redirection. The device meets all of the objectives of an optimal daylighting device for sub-tropical commercial buildings.

The most appropriate method of manufacture has not yet been found, although industrial metal pressing appears as a favourable technique. The device will be demonstrated to practitioners of daylighting design. These practitioners will have greater knowledge of and access to suitable manufacturing processes. If sufficient interest is aroused, a collaboration will ensue to further develop and commercially implement the micro-light guiding shade panel on sub-tropical high rise office buildings.

Many commercial building developers build and subsequently sell their buildings. If they are to implement new designs or devices on their buildings, they must pay extra initial capital. To quickly regain this extra capital, they must charge a greater selling price, or raise rents. However, they must strive to keep their prices in line with current market levels. The major economic incentive of daylighting is not reduced running costs, but increased occupant productivity. Therefore, developers must market this advantage to building purchasers and tenants. This must first be marketed to developers, architects and builders.

Public awareness of environmental issues is growing. The importance of these issues must move up the purchasing chain, from consumers to providers to owners to developers. This can be a slow process. Various government initiatives are encouraging consumers, providers, owners and developers to search for readily available, acceptable solutions. Designs and devices of daylighting practitioners are well placed and easily marketed in this situation. This provides incentive for the further development and commercialisation of the micro-light guiding shade panel.

Future developments of the micro-light guiding shade panel could include a venetian blind style vertical configuration, and older style aesthetics for retrofitting onto existing residences. Elements could be scaled down in thickness to fit within double glazing units, appearing as conventional venetian louvres. This would be placed in a clerestory window, with the outer glazing comprising a translucent material. Altering the outward aesthetics of the panels could expand the market to residential, institutional, industrial and other commercial buildings.

The micro-light guiding shade panel can also be combined with internal light pipes. The panel would then act as a light collector and collimator. The panel's light output would be coupled to the input of the light guide, to be delivered deep within the building. This concept is similar to the anidolic ceiling of Courret, Scartezzini, Francioli and Meyer (1998) (section 2.1.6.3). Coupling must be optimised to efficiently deliver light into the light guide. The panel must deliver light output centred on the horizontal, with a low spread of output directions. Efficient artificial light sources may be included to provide a complete lighting solution. These sources can maintain acceptable internal illumination at times when insufficient daylight is available. Considerations of flexibility in office buildings may restrain the use of this combination to feature spaces.

8.2.2 DAYLIGHT SIMULATION

Simulation validations revealed that the micro-light guiding shade panel model is highly accurate. This provides confidence that simulations involving the device will accurately demonstrate the effects of the panel on interior illumination. With confidence in these simulations, building designers can examine the effect of the panels on new and existing buildings.

The most informative simulation analyses for these applications involves comparisons of various design options. For these analyses, material models must be representative, but do not need to be perfectly accurate. However, results can be sensitive to sky luminance distributions. Therefore, the SSLD

sky model is preferred over the existing limited CIE standard skies. This form of analysis should demonstrate the benefit of the panels compared to other options including clear glazing and conventional tilted shades.

Numerous new algorithms have improved RADIANCE's capability for accurate daylight simulation. The following demonstrates how all of the algorithms combine for a complete daylight simulation.

A model must first be defined in terms of the objects, geometries and materials involved. Any new devices should be modelled in a manner similar to the micro-light guiding shade panel and the laser cut panel. This may require the creation of new geometries or new calculation files.

The next step is to define an appropriate sky model. A set of representative skies should be considered to examine performance under varying external conditions. The SDF Sky Modelling web-site (Roy, 2001) may be consulted at this stage. For each selected sky, the necessary coefficients are determined and the new sky is defined.

The angular throughput of glazing and façade elements can be found using rtrace and mkillum. If elements are not correctly modelled, their definitions must be altered accordingly. Sensitivity analyses can then aid in optimising the design. Sensitivity analysis can also test for sensitivity to specular reflectance of important surfaces within the model. If high sensitivity is discovered, the specular reflection model of He, Torrance, Sillion and Greenberg (1991) should be considered.

Following selection of appropriate simulation parameters, full simulations can proceed. The mkillum pre-processor may be invoked for important façade and glazing elements. Visualisations, luminance contour maps, false-colour images and illuminance maps may be created. If practical, simulation results should be validated against experimental measurements. The test of Bland and Altman (1986) is well suited to such comparisons.

8.3 CONCLUSIONS

The work presented in this thesis has contributed to the improved daylighting of high rise sub-tropical office buildings. Specific conclusions are:

- The micro-light guiding shade panel successfully combines efficient daylight redirection and effective solar shading.
- The device achieves all the objectives of a daylighting device on a high rise sub-tropical building. These objectives include: deep, constant, comfortable daylight penetration, low glare to occupants, low space intrusion, easy installation, aesthetically acceptable, applicable to new buildings and retrofits.
- Panel design may be optimised for different locations, climates, orientations and aesthetic requirements.
- Optimal manufacturing techniques and cost-effectiveness must yet be determined.
- RADIANCE simulations of the device compared very well with experimental results. Low bias was revealed between simulation and measurement, generally less than 10%.
- RADIANCE simulation of the micro-light guiding shade panel greatly aided its development.
- Several new simulation algorithms have improved RADIANCE's simulation of daylight. Algorithms providing most benefit include: the laser cut light redirecting panel, sensitivity studies, new sky models, a statistical test for simulation validation.

All of the aims of this research were achieved. Application of these research findings will achieve the underlying purpose of this research:

THE DAYLIGHTING OF HIGH RISE SUB-TROPICAL BUILDINGS HAS BEEN IMPROVED.

8.4 FUTURE RESEARCH DIRECTIONS

For the micro-light guiding shade panel to be successfully applied on high rise sub-tropical buildings, a mass-manufacturing technique must be determined. This will be pursued with members of the building industry. These individuals

will preferably have an interest in daylight design, and will imagine many applications of the device. Further applications implies greater levels of manufacture, and reduced unit costs.

Marketing of the device will benefit from growing consumer awareness of environmental issues, and greater promotion of energy efficiency by government and institutional bodies. Should a market be developed for the micro-light guiding shade panel, further alternative design options may be investigated to expand this market.

The developed simulation algorithms are being distributed to RADIANCE users through publications, conference presentations and email discussion groups. These findings will also be distributed to the International Energy Agency Task 31 - Daylighting Buildings in the 21st Century, and to the CIE Technical Committee 3.33 - Test Cases for Assessment of Accuracy of Interior Lighting Computer Programs. The laser cut panel simulation algorithm is already to be included in future official releases of ADELINE.

The IEA Task 31 and CIE TC 3.33 are developing several new simulation techniques. The IEA group is developing methods of simulating complex fenestration systems, including the micro-light guiding shade panel and the laser cut panel, in numerous lighting simulators. Thus, the results of this research may then be applied in many other lighting simulators.

Further application of the micro-light guiding shade panel and other daylighting technologies may be aided by annual daylight simulation. Several approaches to this already exist for RADIANCE. Inclusion of the micro-light guiding shade panel and laser cut panel in these programs will also aid in their greater implementation.

Many alternative sky models are available that may be incorporated into RADIANCE and other daylight simulators. This work is being implemented within IEA Task 31.

Sensitivity studies relating to the roughness and specularity of important room surfaces would reveal the potential importance of angle-dependent specular reflectivity. This work may then lead to further implementation of the He *et al.* (1991) model within RADIANCE.

The statistical test of Bland and Altman (1986) is highly suitable to validating simulation programs and algorithms. This technique will be described to the members of CIE TC 3.33, potentially improving their validation efforts.

APPENDIX 1 - MATLAB SCRIPTS INVESTIGATING THE MICRO-LIGHT GUIDING SHADE PANEL

Several Matlab scripts aided investigation of micro-light guiding shade panel designs and performance. Five of these scripts were described in section 4.2, and are listed below. Several sections of code are shared amongst the different scripts. To simplify presentation, where a stanza has been displayed in a previous script, reference is made to the previous script, and that stanza is not again presented in full. References are indicated by italics.

A1.1 LGS2.M - MICRO-LIGHT GUIDING SHADE GENERATOR

```
% Program to design micro-light guiding shade panel
% Various system performance parameters are also calculated

% Set beta, theta, gamma and the panel width
beta=25;            betarad=beta*pi/180;
theta=65;           thetarad=theta*pi/180;
gamma=-10;          gammarad=gamma*pi/180;
width=64;
if beta>=((180-theta-gamma)/2)
        error('Sheet not possible with these settings.  Set beta<(180-theta-gamma)/2')
end

% Which curves are needed?
uppercurve=beta<(90-theta);
lowercircle=beta>(90-theta);

% To find aperture width a
flower=width*(sin((thetarad-gammarad)/2))^2/cos(betarad+gammarad);
if lowercircle
        a=flower;
else
        a=flower/((sin((thetarad+pi/2+betarad)/2))^2);
end

% Set the input aperture
ox=0;
oy=0;
ax=-a*sin(betarad);
ay=-a*cos(betarad);
inaperturex=[ox ax];
inaperturey=[oy ay];
plot(inaperturex,inaperturey,'y')
grid on
hold on
```

```
% Set the lower circle section, if required, and the range of the lower parabola
if lowercircle
        ex= -a*cos(thetarad);
        ey=-a*sin(thetarad);
        phicirclerad=(-pi/2-betarad):.01:(thetarad-pi);
        circlex=[ax a*cos(phicirclerad) ex];
        circley=[ay a*sin(phicirclerad) ey];
        philowerrad=pi:-.01:(thetarad-gammarad);
        flower=a;
else
        circlex=ax;
        circley=ay;
        ex=ax;
        ey=ay;
        philowerrad=(thetarad+pi/2+betarad):-.01:(thetarad-gammarad);
end
plot(circlex,circley,'r')

% Set the lower parabola
rlower=flower./((sin(philowerrad/2)).^2);
br=flower/((sin((thetarad-gammarad)/2))^2);
bx=ox+br*cos(gammarad);
by=oy+br*sin(gammarad);
lowerx=[ex rlower.*cos(philowerrad-thetarad) bx];
lowery=[ey -rlower.*sin(philowerrad-thetarad) by];
plot(lowerx,lowery,'m')

% Set curved upper surface, if required
if uppercurve
        fupper=a/2*(1-sin(betarad+gammarad));
        dr=fupper/((sin((thetarad-gammarad)/2))^2);
        dx=dr*cos(thetarad)+ax;
        dy=dr*sin(thetarad)+ay;
        phiuppercurve=(thetarad-gammarad):.01:(pi/2-betarad-gammarad);
        rupper=fupper./((sin(phiuppercurve/2)).^2);
        uppercurvex=[dx rupper.*cos(phiuppercurve+gammarad)+ax ox];
        uppercurvey=[dy rupper.*sin(phiuppercurve+gammarad)+ay oy];
else
        uppercurvex=ox;
        uppercurvey=oy;
        dx=ox;
        dy=oy;
end
plot(uppercurvex,uppercurvey,'r')

% Set flat upper surface
if beta==0
        cx=bx;
else
        cx=(dy-by+bx*cot(betarad)-dx*tan((thetarad+gammarad)/2))/(cot(betarad)-
tan((thetarad+gammarad)/2));
end
cy=dy+(cx-dx)*tan((thetarad+gammarad)/2);
upperx=[cx dx];
uppery=[cy dy];
plot(upperx,uppery,'m')
```

```
% Set up the exit aperture
exitx=[bx cx];
exity=[by cy];
plot(exitx,exity,'b')

% Make a complete unit
lgsx=[upperx uppercurvex inaperturex circlex lowerx exitx];
lgsy=[uppery uppercurvey inaperturey circley lowery exity];

% Set up two displaced complete units
deltay=cy-by;
deltax=cx-bx;
displacement=sqrt(deltax^2+deltay^2);
lgsupx=lgsx+deltax;
lgsupy=lgsy+deltay;
lgsdownx=lgsx-deltax;
lgsdowny=lgsy-deltay;
plot(lgsupx,lgsupy,'m',lgsdownx,lgsdowny,'m')
toppanelx=[ax-deltax ox+deltax];
toppanely=[ay-deltay oy+deltay];
plot(toppanelx,toppanely,'b')

% Set up a square scaled diagram
breadth=cx-ax+2*deltax;
height=cy-ey+2*deltay;
maxdim=max([breadth height]);
midx=(cx+ax)/2;
midy=(cy+ey)/2;
axis('square')
axis([midx-maxdim/2 midx+maxdim/2 midy-maxdim/2 midy+maxdim/2])
hold off

% Parameters describing the performance of the system
input_aperture=a
lgs_length=displacement
percent_in=a/displacement*100
panel_width=width

% Find the length of material required per light guiding shade section
if lowercircle
        lengthae=a*(thetarad-pi/2+betarad);
        maxlowerphi=pi;
else
        lengthae=0;
        maxlowerphi=thetarad+pi/2+betarad;
end
lengthdc=sqrt((cx-dx)^2+(cy-dy)^2);
intstr='log((1-cos(phi/2))/sin(phi/2))-cos(phi/2)/(sin(phi/2))^2';
lengtheb=flower*(eval(subs(intstr,'maxlowerphi','phi'))-eval(subs(intstr,'(thetarad-gammarad)','phi')));
if uppercurve
        lengthod=fupper*(eval(subs(intstr,'(pi/2-betarad-gammarad)','phi'))-eval(subs(intstr,'(thetarad-
gammarad)','phi')));
else
        lengthod=0;
end
length_tot=lengthdc+lengthod+lengthae+lengtheb

tit=['Micro LGS Panel, theta = ' num2str(theta) ' , gamma = ' num2str(gamma)];
title(tit)
```

A1.2 LGS3.M - VARIATION IN PANEL PERFORMANCE WITH INPUT PARAMETERS

```
% Program to investigate different micro-light guiding shade panel parameters
% Set beta and investigate performance for a range of theta and gamma angles

% Set beta and the panel width and length
beta=30;            betarad=beta*pi/180;
width=80;
panel_length=1000;

% Run through various settings of theta and gamma
theta_in=5:5:85;
gamma_in=0:-5:-45;
for i=1:length(theta_in)
for j=1:length(gamma_in)
theta=theta_in(i);  thetarad=theta*pi/180;
gamma=gamma_in(j);      gammarad=gamma*pi/180;

% Which curves are needed?
Refer to script lgs2.m

% To find aperture width a
Refer to script lgs2.m

% Set the points A and O
ox=0;
oy=0;
ax=-a*sin(betarad);
ay=-a*cos(betarad);

% Set the point E, and the lower focal length
if lowercircle==1
        ex=-a*cos(thetarad);
        ey=-a*sin(thetarad);
        flower=a;
else
        ex=ax;
        ey=ay;
        flower=a/2*(1+sin(thetarad+betarad));
end

% Set the point B
br=flower/((sin((thetarad-gammarad)/2))^2);
bx=ox+br*cos(gammarad);
by=oy+br*sin(gammarad);

% Set the point D
if uppercurve==1
        fupper=a/2*(1-sin(betarad+gammarad));
        dr=fupper/((sin((thetarad-gammarad)/2))^2);
        dx=dr*cos(thetarad)+ax;
        dy=dr*sin(thetarad)+ay;
else
        dx=ox;
        dy=oy;
end
```

```
% Set the point C
if beta==0
        cx=bx;
else
        cx=((dy-by)+bx*cot(betarad)-dx*tan((thetarad+gammarad)/2))/(cot(betarad)-
tan((thetarad+gammarad)/2));
end
cy=dy+(cx-dx)*tan((thetarad+gammarad)/2);

% Find parameters describing the performance of the system
deltay=cy-by;
deltax=cx-bx;
displacement=sqrt(deltax^2+deltay^2);
input_aperture=a;
lgs_length=displacement;
percent_in=a/displacement*100;
number=panel_length/lgs_length;

% Find the length of material required per light guiding shade section
Refer to script lgs2.m

% Output performance parameters for each combination (theta, gamma)
theta_out(i,j)=theta;
gamma_out(i,j)=gamma;
aperture_out(i,j)=input_aperture;
lgs_length_out(i,j)=lgs_length;
percent_out(i,j)=percent_in;
length_out(i,j)=length_tot;
number_out(i,j)=number;
total_length_out(i,j)=total_length;

end
end

% Find theta for maximum percentage throughput
[maxpc,opt_theta_ndx]=max(percent_out);
opt_theta=theta_in(opt_theta_ndx)
```

A1.3 LGS4.M - DESIGN OF OPTIMAL MICRO-LIGHT GUIDING SHADE PANELS

```
% Program to design optimum micro-light guiding shade panel
% Various system performance parameters are calculated
% Set only beta, gamma and width of panel

% Set beta, theta, gamma and the panel width
beta=30;          betarad=beta*pi/180;
theta=90-beta;    thetarad=theta*pi/180;
gamma=0;          gammarad=gamma*pi/180;
width=80;
panel_length=1200;

% To find aperture width a
flower=width*(sin((thetarad-gammarad)/2))^2/cos(betarad+gammarad);
a=flower/((sin((thetarad+pi/2+betarad)/2))^2);

% Set the input aperture
Refer to script lgs2.m
```

```
% Set the lower parabola
philowerrad=(thetarad+pi/2+betarad):-.04:(thetarad-gammarad);
flower=a/2*(1+sin(thetarad+betarad));
rlower=flower./((sin(philowerrad/2)).^2);
br=flower/((sin((thetarad-gammarad)/2))^2);
bx=ox+br*cos(gammarad);
by=oy+br*sin(gammarad);
lowerx=[ax rlower.*cos(philowerrad-thetarad) bx];
lowery=[ay -rlower.*sin(philowerrad-thetarad) by];
plot(lowerx,lowery,'m')

% Set flat upper surface
Refer to script lgs2.m

% Set up the exit aperture
Refer to script lgs2.m

% Make a complete unit
Refer to script lgs2.m

% Set up two displaced complete units
Refer to script lgs2.m

% Set up a square scaled diagram
Refer to script lgs2.m

% Parameters describing the performance of the system
input_aperture=a
lgs_length=displacement
percent_in=a/displacement*100
panel_width=width;
number=panel_length/lgs_length

% Find the length of material required per lgs section
maxlowerphi=thetarad+pi/2+betarad;
lengthoc=sqrt((cx-ox)^2+(cy-oy)^2);
intstr='log((1-cos(phi/2))/sin(phi/2))-cos(phi/2)/(sin(phi/2))^2';
lengthab=flower*(eval(subs(intstr,'maxlowerphi','phi'))-eval(subs(intstr,'(thetarad-gammarad)','phi')));
length_tot=lengthoc+lengthab;
total_length=number*length

tit=['Optimum Micro LGS Panel, beta = ' num2str(beta) ' , gamma = ' num2str(gamma)];
title(tit)
```

A1.4 LGS6.M - PANEL PERFORMANCE VARIATION WITH PANEL TILT, COURSE OF A DAY

```
% Program to determine optimum micro-light guiding shade panel
% Considers orientation of the panel
% Set only gamma and width, orientation and length of panel
% Beta varied for optimal luminous throughput
% Allows for attenuation of sunlight

% To set the panel orientation and parameters, and gamma
orientation=-45;
gamma=-10;        gammarad=gamma*pi/180;
width=80;
panel_length=1000;
```

```
% Time of day and year
time=9:.2:17;
day=173;                    % mid-winter

% Geographical location
lat=-27.5*pi/180;
rlong=150;
slong=153;

% Solar position
et1=0.17*sin(4*pi*(day-80)/373);
et2=0.129*sin(2*pi*(day-8)/355);
et=et1-et2;
dec=0.4093*sin(2*pi*(day-81)/368);
stime=time+et+(slong-rlong)/15;
w=(stime-12)*pi/12;
alt=180/pi*asin(sin(lat)*sin(dec)+cos(lat)*cos(dec)*cos(w));
azi=180/pi*acos((cos(lat)*sin(dec)-cos(dec)*sin(lat)*cos(w))./cos(pi/180*alt));
arvo=stime>12;
azi=azi-2*arvo.*azi;
Rsol=[sin(azi'*pi/180).*cos(alt'*pi/180) cos(azi'*pi/180).*cos(alt'*pi/180) sin(alt'*pi/180)];
sunup=Rsol(:,3)>0;
Rsol=Rsol.*(sunup*ones(1,3));
zen=pi/180*(90-alt);
m=sqrt((626.08.*cos(zen)).^2+1253.16)-626.08.*cos(zen);
e0=100;             % unattenuated normal illuminance of 100 klx
tau=0.08;           % dry optical depth
e=e0*exp(-tau*m);           % attenuated normal illuminance
% X faces East, Y faces North, Z faces the zenith

% Let beta vary and determine transmission and total length of material
beta_in=0:5:85;
for i=1:length(beta_in);
        beta=beta_in(i);    betarad=beta*pi/180;

% Set theta and find normal to the panel
theta=90-beta;      thetarad=theta*pi/180;
normal=[sin(orientation*pi/180)*cos(beta*pi/180) cos(orientation*pi/180)*cos(beta*pi/180)
sin(beta*pi/180)];
if gamma>theta
        error('Beta set too high, set beta below 90-gamma')
end

% To find aperture width a
Refer to script lgs4.m

% Set the points O, B and C
ox=0;
oy=0;
br=flower/((sin((thetarad-gammarad)/2))^2);
bx=ox+br*cos(gammarad);
by=oy+br*sin(gammarad);
if beta==0
        cx=bx;
else
        cx=((oy-by)+bx*cot(betarad)-ox*tan((thetarad+gammarad)/2))/(cot(betarad)-
tan((thetarad+gammarad)/2));
end
cy=oy+(cx-ox)*tan((thetarad+gammarad)/2);
```

```
% Find parameters describing the system
deltay=cy-by;
deltax=cx-bx;
displacement=sqrt(deltax^2+deltay^2);
percent_in=a/displacement;
number=panel_length/displacement;

% Find the length of material required per lgs section
Refer to script lgs4.m

% Find cosine of angle of incidence on panel, if panel is hit by sunlight
cosine=Rsol*normal';
front1=cosine>0;
front2=abs(azi'-orientation)<90;
front=front1.*front2;
new_cos=cosine.*front;
if nnz(new_cos)==0
        average_inc=0;
else
        average_inc=sum(new_cos.*e')/nnz(new_cos);          % klx
end
transmission=panel_length*average_inc*percent_in/1e3;
        % Assumes panel breadth 1 m
integrated=panel_length*sum(new_cos.*e')*percent_in/5000;

% Outputs of beta angle, transmission, material length and sunlight hours
beta_out(i)=beta;
transmission_out(i)=transmission;
max_trans(i)=panel_length*max(new_cos.*e')*percent_in/1000;
min_trans(i)=panel_length*min(new_cos.*e')*percent_in/1000;
length_out(i)=total_length;
integrated_out(i)=integrated;
end
sunon=time(min(find(new_cos)))
sunoff=time(max(find(new_cos)))

% Plot out transmission and luminous throughput
plot(beta_out,transmission_out,beta_out,max_trans,beta_out,min_trans)
grid on
set(gca,'XTick',[0:6]*15)
axis([0 90 get(gca,'YLim')])
title(['Luminous Throughput, Working Hours, Orientation = ' num2str(orientation) ', Gamma = '
num2str(gamma)])
xlabel('Beta (degrees)')
ylabel('Luminous Flux (klm)')
pause
plot(beta_out,integrated_out)
grid on
set(gca,'XTick',[0:6]*15)
axis([0 90 get(gca,'YLim')])
title(['Integrated Luminous Throughput, Working Hours, Orientation = ' num2str(orientation) ', Gamma =
' num2str(gamma)])
xlabel('Beta (degrees)')
ylabel('Luminous Throughput (klm hr)')
```

A1.5 LGS7.M - PANEL PERFORMANCE VARIATION WITH PANEL TILT, ANNUAL VARIATION

```
% Program to determine optimum micro LGS device
% Considers orientation of the panel
% Set only gamma and width, orientation and length of panel
% Beta varied for optimal luminous throughput
% Integrates luminous throughput over the course of the year
% Allows for attenuation of sunlight, and for sunshine probabilities

% To set the panel orientation and parameters, and gamma
Refer to script lgs6.m

% Time of day and year
time=9:.2:17;
days=[15 46 74 105 135 166 196 227 258 288 319 349];
declin=0.4093*sin(2*pi*(days-81)/368);
for i=1:12
        day=days(i);

% Geographical location
Refer to script lgs6.m

% Solar position
Refer to script lgs6.m

% Let beta vary and determine transmission and total length of material
Refer to script lgs6.m

% Set theta and find normal to the panel
Refer to script lgs6.m

% To find aperture width a
Refer to script lgs4.m

% Set the points O, B and C
Refer to script lgs6.m

% Find parameters describing the system
Refer to script lgs6.m

% Find cosine of angle of incidence on panel, if panel is hit by sunlight
cosine=Rsol*normal';
front1=cosine>0;
front2=abs(azi'-orientation)<90;
front=front1.*front2;
new_cos=cosine.*front;
integrated=panel_length*sum(new_cos.*e')*percent_in/5000;
        % Assumes panel breadth 1 m

% Output of transmission for each month(i) and beta(j)
integrated_out(i,j)=integrated;
end
end

% Calculation of sunshine probabilities
daily_sunshine=[8.4 7.5 7.6 7.4 6.4 7.3 7.5 8.5 9.0 8.5 8.5 8.8]; % Brisbane
sun_duration=2*acos(-tan(declin)*tan(lat))/(pi/12);
sunshine_prob=daily_sunshine./sun_duration;
```

```
% Integration of luminous flux across the course of the year
month_days=[31 28 31 30 31 30 31 31 30 31 30 31];
sunny_days=month_days.*sunshine_prob;
flux_total=sunny_days*integrated_out/1000;

% Plot out luminous throughput
plot(beta_in,integrated_out)
grid on
set(gca,'XTick',[0:6]*15)
axis([0 90 get(gca,'YLim')])
title(['Integrated Luminous Throughput, Working Hours, Orientation = ' num2str(orientation) ', Gamma =
' num2str(gamma)])
xlabel('Beta (degrees)')
ylabel('Luminous Throughput (klm hr)')
pause
plot(beta_in,flux_total)
grid on
set(gca,'XTick',[0:6]*15)
axis([0 90 get(gca,'YLim')])
title(['Integrated Lu minous Flux over the Year, Orientation = ' num2str(orientation) ', Gamma = '
num2str(gamma)])
xlabel('Beta (degrees)')
ylabel('Luminous Flux (Mlm hr)')
```

APPENDIX 2 - DELIVERY OF LOW LEVEL ILLUMINATION BELOW HORIZONTAL

Low level illumination was directed below horizontal by the tilted micro-light guiding shade panel. This unexpected illumination could present a problem for implementation of the tilted micro-light guiding shade panel. The cause of this discrepancy was revealed by basic raytracing with the modelled device, and is described below with reference to Figure A 2.1.

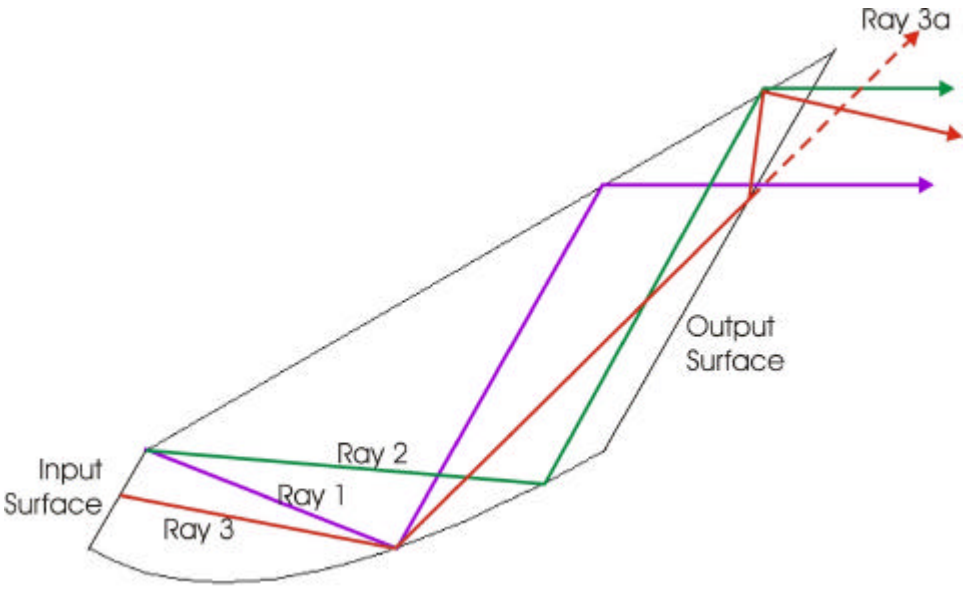

Figure A 2.1 - Light Directed Below Horizontal by Interior Reflections off the Transparent Output Surface

Rays 1 and 2 enter the device from the focus of the parabolic section. They are reflected by the parabola into directions parallel to the parabola's axis (parallel to the panel's front and rear surfaces). The upper reflector then sends these rays into the horizontal direction. Ray 3 enters the device below rays 1 and 2. It intercepts the parabola at the same location as ray 1, and is reflected into a lower direction. It then strikes the panel's plastic output surface at a high angle of incidence. Ray 3a is transmitted through the plastic, exiting the device in the expected direction. However, a large portion of the ray is reflected at the plastic surface and continues upward inside the device. This ray intercepts the upper surface at the same location as ray 2. It is then reflected into a lower direction than ray 2. This direction is necessarily below horizontal.

This is a typical path for a ray intercepting the parabolic reflector toward the panel's output surface. Thus, there will be significant reflections off the output panel's inner surface, delivering significant luminance below horizontal. The same process reduced luminances in directions above 30° above horizontal.

APPENDIX 3 - MICRO-LIGHT GUIDING SHADE PANEL RADIANCE MODEL

RADIANCE simulation of the micro-light guiding shade panel proceeds in four parts. First, the reflective surfaces of a micro-light guiding shade element are created. Second, the reflecting elements are arrayed and surrounded by a supporting frame and a translucent input panel. Thirdly, the created panels are placed into a RADIANCE model. With all geometry and materials defined, the RADIANCE simulation finally proceeds.

A3.1 CREATING A MICRO-LIGHT GUIDING SHADE ELEMENT

Material definitions are not required in the scene file containing the geometry of the micro-light guiding shade element. However, materials used in this scene file must be defined elsewhere.

Two surfaces are created as in Figure A 3.1. The upper surface is a flat polygon reflector. The lower surface is a parabolic section, defined using gensurf.

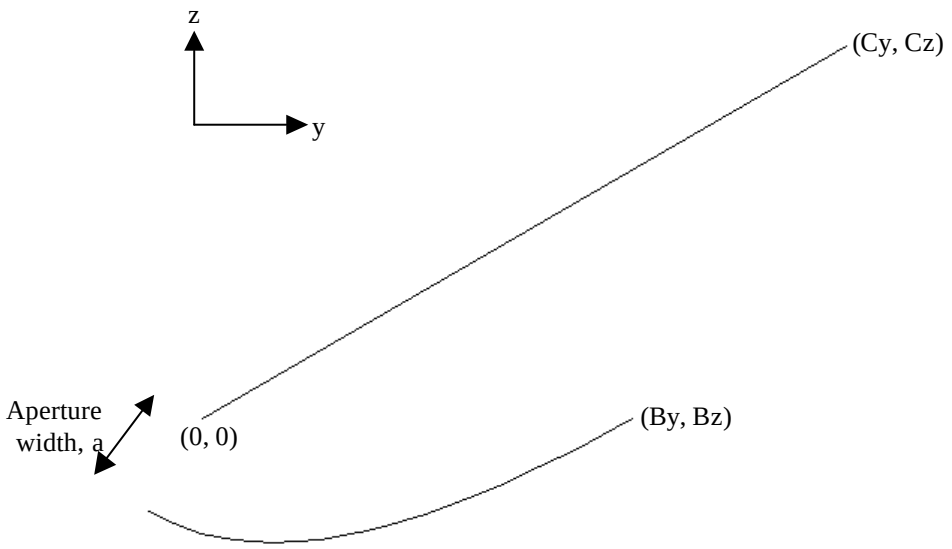

Figure A 3.1 - Geometry of Micro-Light Guiding Shade Element

The upper surface is a rectangular polygon. The rectangle extends in the *yz* plane from (*0*, *0*) to (*Cy*, *Cz*), and has width in the *x*-direction the same as that of the panel. The coordinates (*Cy*, *Cz*) are calculated from the panel's thickness *t* and tilt from vertical *b*.

$$Cy = \frac{t\cos b}{1-\sin b}$$

$$Cz = t$$

Equation A 3.1

The lower parabolic section is created using *gensurf*, as shown below.

Table A 3.1 - Parabolic Section Definition, from Scene File *Element.rad*

```
!gensurf reflector lower_surface 'width * s' \
'a / sq (sin (PI / 360 * (180 - t * (90 + beta)))) * cos (PI / 180 * ((t - 1) * (90 + beta)))' \
'a / sq (sin (PI / 360 * (180 - t * (90 + beta)))) * sin (PI / 180 * ((t - 1) * (90 + beta)))' \
1 10 -e 'a = 19.63; beta = 30; width = 1200; sq (v) = v * v' -s
```

The aperture width *a* is first calculated as

$$a = \frac{t(1-\sin b)}{2\cos b}$$

Equation A 3.2

The calculated aperture width should be placed after '*a* = ' in the fourth line of Table A 3.1. The panel tilt and width should also be placed in this line, following '*beta* = ' and '*width* = ' respectively.

A completed scene file, containing definitions of both reflectors, is shown below (Table A 3.2). This shows an element of a panel with tilt 30°, thickness 68mm and width 1200mm. The reflector material, defined in the panel scene file (section A3.2), is named '*reflector*'. The calculated coordinates of point C were (*117.78*, *68*), and the aperture width was calculated as 19.63mm.

Table A 3.2 - Micro-Light Guiding Shade Element Scene File *Element.rad*

```
##############################################
# Micro-light guiding shade panel element
# Panel tilt 30 degrees, thickness 68mm, width 1200mm
# Orientated such that x is long direction, z is up, y toward output aperture.
# Origin upper edge of input aperture, minimum x.

# reflective surfaces
reflector polygon upper_surface
0
0
12
        0       0       0
        1200    0       0
        1200    117.78  68
        0       117.78  68
```

```
!gensurf reflector lower_surface 'width * s' \
'a / sq (sin (PI / 360 * (180 - t * (90 + beta)))) * cos (PI / 180 * ((t - 1) * (90 + beta)))' \
'a / sq (sin (PI / 360 * (180 - t * (90 + beta)))) * sin (PI / 180 * ((t - 1) * (90 + beta)))' \
        1 10 -e 'a = 19.63; beta = 30; width = 1200; sq (v) = v * v' -s
```

A3.2 MICRO-LIGHT GUIDING SHADE PANEL SCENE FILE

All materials must be defined in the micro-light guiding shade panel scene file. The reflector material is a highly reflective metal with large specular component. An example of a suitable material is silver coated aluminium, with 95% specular reflectivity. A translucent material must be defined for the diffusing input sheet, and a transparent material must be defined for the clear output sheet. Finally, all materials required for the panel's supporting frame must be defined. Example definitions for the reflective, translucent and transparent materials are shown below.

Table A 3.3 - Micro-Light Guiding Shade Panel Material Definitions, from Scene File *MLGSpnl.rad*

```
void metal reflector
0
0
5 .95 .95 .95 1 0.04
# 95% specular reflectance only

void trans translucent
0
0
7 .941 .941 .941 0 0 .847 0
# 79.7% diffuse transmittance, 14.4% diffuse reflectance

void glass transparent
0
0
3 0.989889 1 0.984464
# 91.4% normal transmittance
```

The reflectors defined in the previous scene file are arrayed in the panel using xform. The first reflector is rotated, mirrored and/or transformed into place using xform's *-r*, *-m* and *-t* options. The origin point (*0*, *0*) in the previous scene file represents the lower edge of the upper reflector. Numerous elements are then created using xform's *-a* and *-t* options. The separation between elements is found from the panel's tilt b and thickness t as

$$Vertical\_Separation = t$$
$$Horizontal\_Separation = t \tan b$$

Equation A 3.3

An example application of xform to create the array of elements is shown in Table A 3.4. The top element is placed first by applying a mirror in the *y*-direction and then translating it into position. A set of nine elements is then created, each separated from the previous by 68mm in the vertical direction and 39.260mm in the horizontal direction. The created panel is shown in Figure A 3.2.

Table A 3.4 - Array of Micro-Light Guiding Shade Elements, from Scene File *MLGSpnl.rad*

```
!xform -my -t 0 117.68 -68 -a 9 -t 0 39.260 -68 element.rad
```

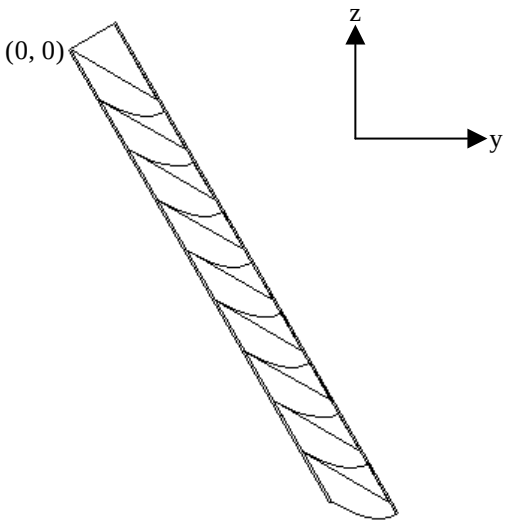

Figure A 3.2 - Generated Array of Micro-Light Guiding Shade Elements

A rectangular polygon of translucent material is placed on the outer surface of the panel. The translucent sheet for the above-shown panel is defined in Table A 3.5. The transparent output sheet is created separately as it will serve as input to mkillum. These surfaces are described below. Finally, a support frame is created around the panel.

Table A 3.5 - Translucent Input Sheet, from Scene File *MLGSpnl.rad*

```
# Translucent input sheet
translucent polygon input
0
0
12
        0       58.890          34
        0       441.673 -629
        1200    441.673 -629
        1200    58.890          34
```

A3.3 PLACING THE PANEL IN THE SCENE AND CREATING OUTPUT SURFACES

The panel is now added to the rest of the RADIANCE model. This is achieved simply through another scene file calling xform, as shown below.

Table A 3.6 - Placing the Micro-Light Guiding Shade Panel Into the Scene, Scene File *Panel.rad*

```
# Micro-light guiding shade panel placed in scene
!xform -t 400 8000 2430 mlgspnl.rad
```

This example moves into place the panel defined in the scene file *mlgspnl.rad*. The top corner of the panel is moved to the coordinates (*400*, *8000*, *2430*).

Each output of the micro-light guiding shade elements is an important source of natural illumination. As such, the luminous output of each surface is pre-calculated using mkillum. To perform the mkillum process, the output surfaces are contained in separate scene files. A single output polygon is written to a scene file. This surface is then arrayed in a second file.

The single output polygon is a rectangle extending in the *yz* plane from (*By*, *Bz*) to (*Cy*, *Cz*) (Figure A 3.1), with width in the *x*-direction the same as that of the panel. The coordinates (*Cy*, *Cz*) are shown above (Equation A3.1), and the coordinates (*By*, *Bz*) are calculated as

$$By = \frac{t}{\cos b}$$

$$Bz = 0$$

Equation A 3.4

An example surface is defined in Table A 3.7. The panel is 1200mm wide, and the coordinates (*By*, *Bz*) = (*78.52*, *0*) and (*Cy*, *Cz*) = (*117.78*, *68*). It is important that the surface normal points out of the panel.

Table A 3.7 - Micro-Light Guiding Shade Element Output, Scene File *Outsurf.rad*

```
# Output surface of MLGS element in panel MLGSpnl.rad
transparent polygon output_surface
0
0
12
        0       78.52   0
        0       117.78  68
        1200    117.78  68
        1200    78.52   0
```

This output surface is then transformed into position, arrayed, and finally moved into the scene. The transformations are the same as those used for the micro-light guiding shade elements. All transformations can be applied in one command line, as shown below (Table A 3.8). In this example, the surface is first mirrored in the *y*-direction, then translated to align with the top micro-light guiding shade element. An array of nine surfaces is then created, each separated by 39.260mm in the horizontal direction and 68mm in the vertical direction. Finally, the nine surfaces are moved into the scene.

Table A 3.8 - Micro-Light Guiding Shade Output Surfaces, Scene File *Outpnl.rad*

```
#@mkillum d=128 s=192

# Nine output surfaces for the micro-light guiding shade panel placed in the scene
!xform -my -t 0 117.68 -68 -a 9 -t 0 39.260 -68 -i 1 -t 400 8000 2430 outsurf.rad
```

Mkillum options are placed at the beginning of the output surface geometry file. These parameters determine the accuracy of the pre-calculated luminous output distributions.

A3.4 SIMULATION PROCESS

Simulation of the micro-light guiding shade panel involves use of the mkillum pre-processor. This proceeds as demonstrated below (Table A 3.9). The remainder of the RADIANCE model is contained in the files *material.rad*, *sky.rad* and *geom.rad*. Any number of other scene files can replace these. The file *rtopts.vp* contains rtrace options settings.

Table A 3.9 - Batch File for Creation of *Octree* Containing Micro-Light Guiding Shade Panel

```
oconv material.rad sky.rad geom.rad panel.rad > model.oct
oconv -i model.oct outpnl.rad > model0.oct
mkillum @rtopts.vp model0.oct < outpnl.rad > ilpnl.rad
oconv -f -i model.oct ilpnl.rad > model1.oct
```

The first oconv command creates the base octree, *model.oct*, containing all scene files except the panel output surfaces. The second oconv command adds the panel outputs to the previous octree, creating the new octree *model0.oct*. Mkillum then pre-calculates the luminous output distributions of the surfaces contained in *outpnl.rad*, using the rtrace options contained in rtopts.vp. This process creates the new scene file *ilpnl.rad*, containing the output surfaces and their luminous output distributions. Finally, this new scene file is added to the base octree, model.oct, creating a frozen final octree *model1.oct*.

The octree model1.oct contains a complete description of the RADIANCE model, with pre-calculated light output distributions from the micro-light guiding shade panel. RADIANCE simulation processes, including rpict, rillum, rtrace and *rview*, can then continue as usual.

APPENDIX 4 - LASER CUT PANEL FUNCTION FILE *LCP0.CAL*

```
{
        The laser cut panel (LCP) with cuts normal to the surface

        A1 = D/W ratio (cut spacing divided by cut depth)
        A2 = n, refractive index of panel material (1.5 for acrylic)

        The panel is oriented in the yz plane with normal to the
        front face in the x direction.  Cuts are parallel to the y direction.
        Deflection is restricted to the z direction.

        The effects of multiple internal reflections and
        reflection losses are considered.
        The two strongest components (of undeflected, deflected and reflected
        components) are displayed.

        Example material definition (LCP turned with outward normal in y direction,
        D/W=0.5, n=1.5):

        void prism2 lcpmat
        11 f1 dx1 dy2 dz1 f2 dx2 dy2 dz2 lcp0.cal -rz 90
        0
        2 0.5 1.5

        Phillip Greenup             3/9/98

}

{ Fresnel calculations of transmission and reflection }
cos_i=abs(Rdot);
rte=(cos_i-sqrt(A2*A2-1+cos_i*cos_i))/(cos_i+sqrt(A2*A2-1+cos_i*cos_i));
rtm=(A2*A2*cos_i-sqrt(A2*A2-1+cos_i*cos_i))/(A2*A2*cos_i+sqrt(A2*A2-1+cos_i*cos_i));
R=(rte*rte+rtm*rtm)/2;
T=1-R;

{ Fractions deflected and undeflected }
tan_rp=abs(Dz)/(sqrt(A2*A2-1+Dx*Dx));
m=floor(tan_rp/A1);
fd0=(tan_rp/A1)*(-1)^m+2*floor((m+1)/2)*(-1)^(m+1);
fu0=1-fd0;
fd=fd0*T*T;
fu=fu0*T*T;

{ Selection of two strongest components }
N1=if(fu-fd,if(fu-R,1,3),if(fd-R,2,3));
N2=if(fu-fd,if(fu-R,if(fd-R,2,3),1),if(fd-R,if(fu-R,1,3),2));

f1=select(N1,fu,fd,R);
dx1=select(N1,Dx,Dx,-Dx);
dy1=Dy;
dz1=select(N1,Dz,-Dz,Dz);

f2=select(N2,fu,fd,R);
dx2=select(N2,Dx,Dx,-Dx);
dy2=Dy;
dz2=select(N2,Dz,-Dz,Dz);
```

APPENDIX 5 - NEW SKY MODELS

A5.1 STANDARD SKY LUMINANCE DISTRIBUTION

A5.1.1 CALCULATION FILE *SSLDLUM.CAL*

```
{
        Standard Sky Luminance Distribution of Kittler, Perez and Darula (1997)

        Corrected by Phillip Greenup Nov 2000

        Additional arguments required for calculation of skybright:

        A1                      - zenith radiance
        A2                      - ground brightness
        A3,A4,A5,A6,A7          - coefficients for SSLD
        A8,A9,A10               - sun direction

}

skybright = wmean((Dz+1.01)^10, intersky, (Dz+1.01)^-10, A2 );
wmean(a, x, b, y) = (a*x+b*y)/(a+b);
intersky = if( (Dz-0.01),
                A1 * phi(Dz) / phi(1) * f(gamma) / f(zt) ,
                A1 * phi(0.01) / phi(1)      * f(gamma) / f(zt) ) ;

phi(v) = 1 + A3*Exp(A4/v);          { gradation function }
f(v) = 1 + A5 * ( Exp(A6*v) - Exp(A6*1.5708) ) + A7*cos(v)*cos(v) ;
                                    { indicatrix function }

cosgamma = Dx* A8 + Dy*A9 + Dz*A10;
gamma = Acos(cosgamma);                 { angle from sun to this point in sky }
zt = Acos(A10);                     { angle from zenith to sun }
eta = Acos(Dz);                     { angle from zenith to this point in sky }
```

A5.1.2 STEPS FOR USE OF SSLD SKY LUMINANCE DISTRIBUTION ALGORITHM

A5.1.2.1 Creation of Sky Definition Scene File

1. Select appropriate sky model from SSLD table and SDF web site. Find coefficients (*a*, *b*, *c*, *d*, *e*).
2. Generate scene file using gensky or gendaylit for sun coordinates (*SX*, *SY*, *SZ*).
3. Calculate ground brightness from horizontal global illuminance and mean ground reflectivity as:

$$R = \frac{rHGI}{pK}$$ **Equation A 5.1**

where R = ground brightness [W/m2/sr]

ρ = mean ground reflectivity

HGI = horizontal global illuminance [lx]

K = luminous efficacy = 179 [lm/W]

4. Select an arbitrary zenith radiance *Z* (eg. 100 W/m2/sr).
5. Open generated scene file in text editor. The sky luminance distribution is created as:

```
void brightfunc skyfunc
2 skybright ssldlum.cal
0
10 Z R a b c d e SX SY SZ
```

where Z = zenith radiance [W/m2/sr] (step 4)

R = ground brightness [W/m2/sr] (step 3)

a, b, c, d, e = SSLD coefficients (step 1)

SX, SY, SZ = sun coordinates (step 2)

An example of a completed sky luminance definition is shown below.

6. If the sun is required, and the direct normal or horizontal illuminance is known, the solar brightness is calculated as:

$$r = \frac{DHI}{wSZK}$$ **Equation A 5.2**

or $$r = \frac{DNI}{wK}$$ **Equation A 5.3**

where r = solar brightness [W/m2/sr]

DHI = direct horizontal illuminance [lx]

DNI = direct normal illuminance [lx]

ω = solar solid angle = 5.981e-5 [sr]

SZ = z-component of solar coordinates (step 2)

K = luminous efficacy = 179 [lm/W]

The sun is created in the scene file as:

```
void light solar
0
0
3 r r r

solar source sun
0
0
4 SX SY SZ 0.5
```

An example of a completed sun definition is shown below.

7. If the sun is not required, remove it.
8. Create ground material (glow primitive), source (source primitive) and groundsheet (plastic material and polygon or disc geometry). Create sky material (glow primitive and skyfunc modifier) and source (source primitive). The colour averaged reflectivities of the ground and sky glows must be unity (ie. 0.263 * *R* + 0.655 * *G* + 0.082 * *B* = 1). An example of a complete set of material definitions is shown below.
9. Save edited scene file in appropriate directory.
10. Create a test octree containing the created sky scene file only.
11. Calculate the direct horizontal illuminance (DHI) using rillum as:

    ```
    echo 0 0 0 0 0 1 | rillum -ab 0 test.oct
    ```

    Calculate the horizontal global illuminance (HGI) using rillum as:

    ```
    echo 0 0 0 0 0 1 | rillum -ab 1 test.oct
    ```

    The diffuse horizontal illuminance (FHI) is found as the difference between the global and direct horizontal illuminances (FHI=HGI-DHI).
12. If the diffuse horizontal illuminance is not as expected, the arbitrarily selected zenith radiance (step 4) must be scaled. The corrected zenith radiance is calculated as:

$$Z(corrected) = Z(incorrect)\frac{FHI(correct)}{FHI(incorrect)}$$ **Equation A 5.4**

    The previous zenith radiance is replaced with the corrected value. This can be tested by repeating steps 9 through 11.
13. Save the completed sky definition file.

A5.1.2.2 Example of a Completed Sky Definition File

```
# Sky at 1pm on 24 Oct, in Brisbane Australia.
# Overcast moderately gradated and slightly brightening toward dull sun.
# SSLD code II.2, generated by ssldlum.cal
# Direct horizontal illuminance 15 klx
# Diffuse horizontal illuminance 70 klx
# Global horizontal illuminance 85 klx
# Ground reflectance 20%

void light solar
0
0
3 1.55e+006 1.55e+006 1.55e+006

solar source sun
0
0
4 -0.365584 0.231372 0.901563 0.5

void brightfunc skyfunc
2 skybright ssldlum.cal
0
10 177 30.2 1.1 -0.8 2 -1.5 .15 -0.365584 0.231372 0.901563

skyfunc glow ground_glow
0
0
4 .983 1.078 .429 0

ground_glow source ground
0
0
4 0 0 -1 180

skyfunc glow sky_glow
0
0
4 .991 .991 1.101 0

sky_glow source sky
0
0
4 0 0 1 180

# 7k714 : green paint : LESO91
# 0.20
void plastic grass
0
0
5 0.197 0.216 0.086 0 0

grass polygon ground_sheet
0
0
12
      -10000  -10000  -10
      13000   -10000  -10
      13000   18400   -10
      -10000  18400   -10
```

A5.1.2.3 To Visualise the Created Sky Definition

1. Create a test octree containing only the sky definition scene file.
2. Make an initial check using rview, as:

   rview -vth -vp 0 0 0 -vd 0 0 1 -vu 0 1 0 -vv 180 -vh 180 test.oct

3. Re-expose the image for optimum viewing, as *exp 1* .
4. Find the exposure level for filtering a created visualisation, as *exp* =.
5. Make a visualisation with rpict, as:

   rpict -vth -vp 0 0 0 -vd 0 0 1 -vu 0 1 0 -vv 180 -vh 180 test.oct

6. Re-expose the created visualisation, as:

   pfilt -e 1 test1.pic > test2.pic

7. Find the exposure level of the new visualisation, as:

   getinfo test2.pic

8. Re-expose this image to the same level as found in step 4, using *pfilt*, creating a new visualisation *test3.pic*.
9. Run *falsecol* to create contour lines on the sky-map, as:

   falsecol -ip test3.pic -cl -s ? -l cd/m2 -n ? > test4.pic

The scale and contours set using -s ? -n ? can be found by trial and error.

A5.2 ALL SKY MODEL

A5.2.1 CALCULATION FILE *ASM_NEW.CAL* AND EXAMPLE OF APPLICATION

```
{
      Sky brightness function for all sky model distribution

      Additional arguments required for calculation of skybright

      A1 - horizontal global illuminance (klx)
      A2 - ground plane brightness (W/m2/sr)
      A3 , A4 , A5 - sun direction (normalised)

      Programmed by Phil Greenup 7/6/02

      Example of application:

      void brightfunc skyfunc
      2 skybr asm_new.cal
      0
      5 65 24.9 -0.365584 0.231372 0.901563
}

skybr = wmean ( ( Dz + 1.01 )^10 , allsky , ( Dz + 1.01 )^-10 , A2 ) ;
wmean ( m , i , n , j ) = ( m * i + n * j ) / ( m + n ) ;
```

```
allsky = lz * allsky_rel * 1000 / 179 ;
                  { absolute sky radiance (W/m2/sr) }
allsky_rel = phi(Dz) / phi(1) * func(zt) / func(PI/2-sh) ;
                  { relative sky luminance (-) }

phi(v) = 1 / ( 1 + 5.5 / exp( a * v ) ) ;       { gradation function }
func(v) = 1 + b * ( exp( c * v ) - exp( c * PI / 2 ) ) +
      d*cos(v)*cos(v) ;                  { indicatrix function }

{ Coefficients for gradation and indicatrix functions }
a = 2.26 + ne * ( -5.82 + 1.82 * ne ) ;
b = 24.3 * ( 1.6 * ne )^5.9 * exp ( -0.20 * ne ) * ( 1.1 - ne )^1.5 ;
c = -3.05 / ( 1 + 24 * exp ( -7.7 * ne ) ) ;
d = 0.46 / ( 1 + 630 * exp ( -9.9 * ne ) ) ;

lz = e * (sin ( 0.7 * sh ))^1.3 + f * (tan ( 0.7 * sh ))^1.3 + g ;
                  { zenith luminance (kcd/m2) }

{ Coefficients for zenith luminance function }
e = ne*(4.821+ne*(-114.78+ne*(160.55+ne*(1121.5+
      ne*(-2123.2+ne*962.58))))) ;
f = ne*(63.044+ne*(188.91+ne*(-440.19+ne*(-1302.3+
      ne*(2713.8-ne*1231.9))))) ;
g = ne*(0.04+ne*(2.43-ne*1.86)) ;

ne = A1 / sevg ;     { normal global illuminance }
sevg = 0.83+sh*(15.47+sh*(306.20+sh*(-375.95+sh*(188.79-sh*36.78)))) ;
                  { standard global illuminance (klx) }

coszt= Dx * A3 + Dy * A4 + Dz * A5 ;
zt = Acos (coszt) ;     { angle from sun to this point in sky (rad) }
sh = Asin (A5) ;        { solar altitude (rad) }
```

APPENDIX 6 - ADAPTED CALCULATION FILE FOR MATERIAL MODEL OF HE *ET AL*. (1991) *HER.CAL*

```
{
      He-Torrance Reflectance Model (Siggraph 1991)

      Modified by Phillip Greenup to remove imaginary refractive index
      (13/9/01)

      Modified by Phillip Greenup for quicker solution of z0 and easy
      exit of Dsum2 when tau/lambda is high.
      (7/2/02)

      This is the simplified version that doesn't account for
      changes in reflection due to changes in wavelength.  Also,
      specular and directional-diffuse highlights are left uncoloured
      because colouring them requires multiple evaluations of some
      very expensive functions.

      The primitive for this function should look something like:

      void BRTDfunc name
      10
            s s s
            0 0 0
            dd dd dd
            Her.cal
      0
      12    amb_r amb_g amb_b
            amb_r amb_g amb_b
            0 0 0
            sigma0 tau
            n_real

      For metals, the specular colour may be modified like so:

      void BRTDfunc name
      10
            s_r s_g s_b
            0 0 0
            dd dd dd
            Her.cal
      0
      12    amb_r amb_g amb_b
            amb_r amb_g amb_b
            0 0 0
            sigma0 tau
            n_real

      This doesn't work for the directional diffuse component,
      unfortunately.  A second set of functions dd_r, dd_g and dd_b
      may be used, but they cost three times as much to compute!

}
```

```
                { Constants }
lambda : .55;                { wavelength (microns) }
z0err : .0001;               { accepted error in value of z0 }
Dsumlim : .000001;           { last term of D summation }
Dsummax : 200;               { maximum terms in D summation }

                { Parameters }
sigma0 = arg(10);       { surface height deviation (microns) }
tau = arg(11);          { correlation distance (microns) }
n_real = arg(12);       { real part of index of refraction }

                { Constant functions }
Exp(x) : if(-x-400, 0, exp(x));
           { rayinit.cal version too timid for D() }

                { Repeated formulas }
cotexp(t) = tau/sigma0/2/tan(t);
shadowf2(et,erfcet) = (1-.5*erfcet) /
           ((1/sqrt(PI)/et - erfcet)/2 + 1);
shadowf1(t) = or(FTINY-sigma0, .01-abs(t));
shadowf0(t) = abs(t) - (PI/2-.0001);
shadowf(t) = if(shadowf0(t), 0, if(shadowf1(t), 1,
           shadowf2(cotexp(t), erfc(cotexp(t)))));
K(t) = if(abs(t)-FTINY, tan(t) * erfc(cotexp(t)), 0);
fuvA(ct) = sq(n_real) - 1 + sq(ct);
fperp2(ct) = sq(ct-sqrt(fuvA(ct))) /
           sq(ct+sqrt(fuvA(ct)));
fpara2(ct) = sq(sq(n_real)*ct - sqrt(fuvA(ct))) /
           sq(sq(n_real)*ct + sqrt(fuvA(ct)));
fresnel2(ct) = (fperp2(ct) + fpara2(ct))/2;

                { Formulas dependent only on reflected direction }
theta_r = acos(RdotP);
shadowf_r = shadowf(theta_r);
K_r = K(theta_r);
s = fresnel2(RdotP)*Exp(-g(RdotP))*sq(shadowf_r);
s_r = s*arg(1)*CrP;
s_g = s*arg(2)*CgP;
s_b = s*arg(3)*CbP;

                { Formulas dependent on incident direction }
           { z0 }
z0d(Ki,z) = -(Ki+K_r)/(4*sigma0)*z*Exp(-sq(z/sigma0)/2) - sqrt(PI/2);
z0lim(x) = if(x, max(x,z0err), min(x,-z0err));
z0off(Ki,z) = (sigma0/4*(Ki+K_r)*Exp(-sq(z/sigma0)/2)-sqrt(PI/2)*z)/
                z0lim(z0d(Ki,z));
           { Newton Raphson iteration for z0 }
z0root(Ki, x0, x1, i) = if(i,
                if(z0err-abs(x1-x0),
                x1,
                z0root(Ki,x1,x1-z0off(Ki,x1),i-1)),
                0);
z0(ti) = z0root(K(ti), z0init(ti), z0init(ti)-z0off(K(ti),z0init(ti)),
                100);
           { set initial value for Newton Raphson iteration to z0
                from first order Taylor approx to z0 function }
z0init(ti) = sigma0*(K(ti)+K_r)/sqrt(8*PI+sq(K(ti)+K_r));
           { sigma }
sigma(ti) = if( FTINY-sigma0, sigma0,
                sigma0/sqrt(1+sq(z0(ti)/sigma0)) );
```

```
            { g }
g(cti) = sq(2*PI/lambda*sigma(Acos(cti))*(cti+RdotP));
            { |F|^2 }
fresnel2dd(kix,kiy,kiz) = fresnel2(sqrt(sq(kix-Dx) + sq(kiy-Dy) +
                  sq(kiz-Dz))/2);
            { G }
G(kix,kiy,kiz) = sq( (sq(kix-Dx)+sq(kiy-Dy)+sq(kiz-Dz)) /
                  (NxP*(kix-Dx)+NyP*(kiy-Dy)+NzP*(kiz-Dz)) );
            { D }
            { Dsum2 loop exited if tau/lambda is too large }
Dsum2(m,lt,c,t,e,g) = if(e-400,0,if(or(m-Dsummax,and(lt-t,
                  Dsumlim-t)),t,
                  t+Dsum2(m+1,t,c*g/(m+1),
                  c*g/(m+1)*Exp(-g-e/(m+1))/(m+1),e,g)));
Dsum(e,g) = Dsum2(1,0,g,g*Exp(-g-e),e,g);
D(kix,kiy,kiz) = sq(PI)/4/sq(lambda)*sq(tau) *
                  Dsum(sq(2*PI/lambda)/4*sq(tau)*
                  (sq(kix-Dx)+sq(kiy-Dy)+sq(kiz-Dz) -
                  sq(NxP*(kix-Dx)+NyP*(kiy-Dy)+NzP*(kiz-Dz))),
                  g(kix*NxP+kiy*NyP+kiz*NzP));
            { rho_dd }
dd2(cti) = shadowf_r*shadowf(Acos(cti))/cti/RdotP;
dd(kix,kiy,kiz) = dd2(kix*NxP+kiy*NyP+kiz*NzP)*G(kix,kiy,kiz)*
                  fresnel2dd(kix,kiy,kiz)/PI*D(kix,kiy,kiz);

                                    { Color version 3x as slow! }
dd_r(kix,kiy,kiz) = dd(kix,kiy,kiz)*arg(1)*CrP;
dd_g(kix,kiy,kiz) = dd(kix,kiy,kiz)*arg(2)*CgP;
dd_b(kix,kiy,kiz) = dd(kix,kiy,kiz)*arg(3)*CbP;
```

APPENDIX 7 - SPREADSHEET FOR APPLICATION OF BLAND AND ALTMAN TEST

BLAND AND ALTMAN TEST

INSTRUCTIONS: Enter data in columns B and C.
Delete remaining place markers (****).

Title: Tilted Panels, Opalescent Sheeting

Number of pairs of values: 41

Index	Radiance X1	Measured X2	Delta	Mean
1	363	335	8.23	348.79
2	354	387	-8.51	370.05
3	337	350	-3.49	343.41
4	310	307	0.91	308.39
5	271	262	3.70	266.34
6	232	228	1.99	229.76
7	199	191	4.05	194.87
8	169	166	1.91	167.59
9	145	139	4.23	141.94
10	124	123	1.44	123.38
11	108	109	-0.47	108.74
12	99	96	4.02	97.42
13	93	90	4.26	91.41
14	89	88	1.21	88.53
15	91	94	-3.10	92.54
16	95	98	-2.57	96.25
17	404	378	7.10	390.90
18	406	433	-6.10	419.30
19	373	379	-1.47	376.22
20	337	331	1.86	333.57
21	292	287	1.69	289.43
22	254	246	3.38	249.65
23	215	210	2.43	212.56
24	183	176	3.82	179.36
25	155	150	3.04	152.28
26	131	132	-0.76	131.50
27	115	117	-1.70	115.51
28	101	103	-1.76	102.09
29	95	100	-4.22	97.40
30	99	98	1.45	98.21
31	108	99	9.85	103.35
32	111	100	10.79	105.39
33	165	170	-2.50	167.38
34	141	143	-1.28	141.58
35	120	126	-4.47	122.69
36	104	109	-4.40	106.60
37	94	102	-7.48	97.71
38	89	94	-4.88	91.22
39	87	91	-4.31	89.04
40	85	89	-4.36	87.06
41	87	92	-5.31	89.07

OUTPUT

	X1	X2	X1-X2
MEAN	181.22	180.66	0.20
SD(samp)	104.45	104.54	4.56
SE	16.31	16.33	0.71
CV	0.58	0.58	22.75
SSD	436366	437119	832

t VALUE =	1.684	for P of	0.050
		and df =	40.00

Mean difference (bias)		0.200
95% confidence interval of bias		
	from	1.40
	to	-1.00
Plot of lines		
Bias upper limit	87.1	1.40
	419.3	1.40
Bias lower limit	87.1	-1.00
	419.3	-1.00

Agreement limits (95% confidence of X2 to X1)		
	from	-8.74
	to	9.14
Plot of lines		
Agreement upper limit	87.1	9.14
	419.3	9.14
Agreement lower limit	87.1	-8.74
	419.3	-8.74

Plot Ranges	X axis	Y axis
Min	87.06	-8.51
Max	419.30	10.79

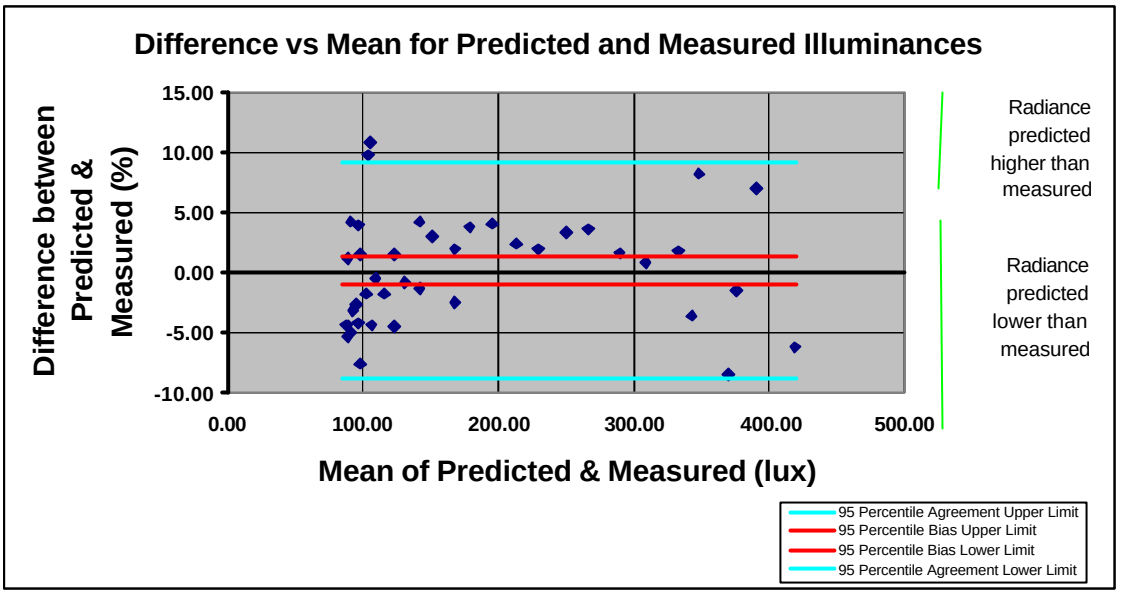
Difference vs Mean for Predicted and Measured Illuminances
Difference between Predicted & Measured (%)
15.00
10.00
5.00
0.00
-5.00
-10.00
0.00
100.00
200.00
300.00
400.00
500.00
Mean of Predicted & Measured (lux)
Radiance predicted higher than measured
Radiance predicted lower than measured
95 Percentile Agreement Upper Limit
95 Percentile Bias Upper Limit
95 Percentile Bias Lower Limit
95 Percentile Agreement Lower Limit

BIBLIOGRAPHY

- Abdou, O.A., 1997. Effects of Luminous Environment on Worker Productivity in Building Spaces. *Journal of Architectural Engineering*, 3 (3), 124-132.
- Aizlewood, M.E., 1993. Innovative Daylighting Systems: An Experimental Evaluation. *Lighting Res. Technol.*, 25 (4), 141-152.
- Alonso, C.L., 1998. A Simple Explanation of How Lighting Calculation Software Works Internally. *In*: *Lighting 98*. Illuminating Engineers Society. Brisbane, pp. 105-106.
- Andersen, M., 2002. Light Distribution through Advanced Fenestration Systems. *Building Research and Information*, 30 (4), 264-281.
- Andersen, M., L. Michel, C. Roecker and J.-L. Scartezzini, 2001. Experimental Assessment of Bi-Directional Transmission Distribution Functions Using Digital Imaging Techniques. *Energy and Buildings*, 33, 417-431.
- Andersen, M., M. Rubin and J.-L. Scartezzini, 2002. *Comparison between Ray-Tracing Simulations and Bi-Directional Transmission Measurements on Prismatic Glazing.* Lausanne, Switzerland: Solar Energy and Building Physics Laboratory LESO-PB, Swiss Federal Institute of Technology EPFL.
- Apian-Bennewitz, P., 1994. Designing an Apparatus for Measuring Bidirectional Reflection/Transmission. *In*: *Optical Materials Technology for Energy Efficiency and Solar Energy Conversion XIII*. International Society for Optical Engineering SPIE. Freiburg, 18-22 April, pp. 697-706.
- Apian-Bennewitz, P., 1995. *Messung Und Modellierung Von Lichtstreuenden Materialien Zur Computer-Simulation Von Tageslichtbeleuchtung.* Frieburg im Breisgau, Germany: Albert-Ludwigs-Universitat.
- Apian-Bennewitz, P., M. Goller, S. Herkel, A. Kovach-Hebling and J. Wienold, 1998. Computer-Oriented Building Design: Advances in Daylighting and Thermal Simulation Tools. *Renewable Energy*, 14 (1-4), 351-356.
- Apian-Bennewitz, P. and J. von der Hardt, 1998. Enhancing and Calibrating a Goniophotometer. *Solar Energy Materials and Solar Cells*, 54 (1-4), 309-322.

- Ashdown, I., 1995. *Validation of Radiative Flux Transfer (Radiosity) Predictions*. Aug 14. Ledalite Architectural Products Inc.
- Ashdown, I., 1996. Lighting for Architects. *Computer Graphics World*, 19 (8), 38.
- Ashmore, J. and P. Richens, 2001. Computer Simulation in Daylight Design: A Comparison. *Arch. Sci. Rev.*, 44 (1), 33-44.
- Australian Greenhouse Office, 1999. *Baseline Study of Greenhouse Gas Emissions from the Commercial Buildings Sector with Projections to Year 2010*. Canberra: Australian Greenhouse Office.
- Bartenbach, C., M. Moeller and R. Lanzenberger, 1986. *Window with Reflectors for Illuminating a Room* (Patent). No. AU-B-56802/86, Australia.
- Bartenbach, C., M. Moeller and R. Lanzenberger, 1987. *Arrangement for Illuminating a Room with Daylight* (Patent). No. 4699467, United States.
- Beck, A., W. Korner, O. Gross and J. Fricke, 1999. Making Better Use of Natural Light with a Light-Redirecting Double-Glazing System. *Solar Energy*, 66 (3), 215-221.
- Bellia, L., A. Cesarano and S. Sibilio, 1994. Daylighting Contribution in Interior Lighting: Experimental Verification of Software Simulation Results. *Lighting Res. Technol.*, 26 (2), 99-105.
- Bland, J.M. and D.G. Altman, 1986. Statistical Methods for Assessing Agreement between Two Methods of Clinical Measurement. *The Lancet* (Feb 8), 307-310.
- Bordenaro, M., 1993. Optimizing Energy Efficiency in Atrium Designs. *Building Design and Construction*, 34 (11), 50.
- Boubekri, M. and L.L. Boyer, 1992. Effect of Window Size and Sunlight Presence on Glare. *Lighting Res. Technol.*, 24 (2), 69-74.
- Centre for the Analysis and Dissemination of Demonstrated Energy Technologies, 1991. *Solar Light Pipe*. Report: Demo 16. Centre for the Analysis and Dissemination of Demonstrated Energy Technologies.
- Cannon-Brookes, S.W.A., 1997. Simple Scale Models for Daylighting Design: Analysis of Sources of Error in Illuminance Prediction. *Lighting Res. Technol.*, 29 (3), 135-142.
- Carter, D.J., 2002. The Measured and Predicted Performance of Passive Solar Light Pipe Systems. *Lighting Res. Technol.*, 34 (1), 39-52.

- Carvalho, M.J., M. Collares-Pereira, J.M. Gordon and A. Rabl, 1985. Truncation of CPC Solar Collectors and Its Effect on Energy Collection. *Solar Energy*, 35 (5), 393-399.
- Chauvel, P., J.B. Collins, R. Dogniaux and J. Longmore, 1982. Glare from Windows: Current Views of the Problem. *Lighting Res. Technol.*, 14 (1), 31-46.
- Clanton, N., 1996. Daylighting Increases Productivity While Cutting Costs. *Energy User News* , 21 (11), 34.
- Clanton, N., 1999. Lighting the School of the Future. *School Planning and Management*, 38 (12), 33.
- Clarke, J.A., M. Janak and P. Ruyssevelt, 1998. Assessing the Overall Performance of Advanced Glazing Systems. *Solar Energy*, 63 (4), 231-241.
- Close, J., 1996. Optimising Daylighting in High-Rise Commercial Developments in SE Asia and the Use of Computer Programmes as a Design Tool. *In*: *WREC 1996*. World Renewable Energy Congress. Perth.
- Cohen-Rosenthal, E., M. Schlarb, J. Thorne, A. Serchuk and D. Bradley, 2000. *Build It Right: Cleaner Energy for Better Buildings*. Report: No. 10. March. Washington D.C.: Renewable Energy Policy Project with American Council for an Energy-Efficient Economy.
- Compagnon, R., 1993. *Nonimaging Optics: A Short Introduction*. Solar Energy and Building Physics Laboratory LESO-PB, Swiss Federal Institute of Technology EPFL.
- Compagnon, R., J.-L. Scartezzini and B. Paule, 1993. *Application of Nonimaging Optics to the Development of New Daylighting Systems* (World Wide Web site). Solar Energy and Building Physics Laboratory LESO-PB, Swiss Federal Institute of Technology EPFL, url: http://lesowww.epfl.ch/anglais/daylighting/a_ises93.html, accessed: 18 June.
- Courret, G., B. Paule and J.-L. Scartezzini, 1996. Anidolic Zenithal Openings: Daylighting and Shading. *Lighting Res. Technol.*, 28 (1), 11-17.
- Courret, G. and J.-L. Scartezzini, 1998. Anidolic Solar Blinds: Sun Control with Three-Dimensional Optics. *In*: Goetzberger, A. and Krainer, A. (eds) *EuroSun 98*. ISES. Portoroz, Slovenia, Sept 14-17, pp. II.3.7.
- Courret, G., J.-L. Scartezzini, D. Francioli and J.-J. Meyer, 1998. Design and Assessment of an Anidolic Light-Duct. *Energy and Buildings*, 28, 79-99.

- Cowling, I.R., 1994. *Illuminating Apparatus* (Patent). No. 5295051, United States.
- Cowling, I., S. Coyne and G. Bradley, 1990. *Light in Brisbane Office Buildings - a Survey.* Brisbane: Centre for Medical and Health Physics, Queensland University of Technology.
- Cowling, I.R. and P. Veevers, 1990. The Design and Performance of a Permanently Mounted Daylighting Device. *Arch. Sci. Rev.*, 33 (4), 97-103.
- Cuttle, K., 2001. An Investigative Assessment of Visualisation. *In*: Bailey, R., Baird, G., Bromberek, Z., Brown, O., Burry, M., Cuttle, K., Dawson, A., Donn, M., Goldrick, A., Gray, J., Isaacs, N., Jaques, R., Kendrick, D., Luther, M.B., McIntosh, J., Osterhaus, W., Porteus, W., Skates, H., Stoecklein, A., Tippet, H. and Wood, P. (eds) *35th Annual Conference of the Australia and New Zealand Architectural Science Association - Computer-Mediated Reality: Crafting Design Quality*. Australian and New Zealand Architectural Science Association. Wellington, New Zealand, 21-23 Nov.
- Department of Employment and Industrial Relations, 1983. *Sunlight at Work.* Department of Employment and Industrial Relations.
- Digert, N.E., 2001. *Mini-Optical Light Shelf Daylighting System* (Patent). No. 6239910, United States.
- Edmonds, I., 1998. Post Occupancy Assessment of Innovative Daylighting Systems in Australian Buildings. *In*: *Lighting 98*. IES. Brisbane, pp. 155-160.
- Edmonds, I.R., 1988. *A Window Panel for Improved Daylighting of Room Interiors* (Patent). No. AU -B-24711/88, Australia.
- Edmonds, I.R., 1991. *Transparent Light Deflecting Panel for Daylighting Rooms* (Patent). No. 4989952, United States.
- Edmonds, I.R., 1992. *Permanently Fixed Collimation Devices Which Combine the Function of Shading and Daylighting Building Interiors* (Patent). No. AU-B-15055/92, Australia.
- Edmonds, I.R., 1993a. Performance of Laser Cut Light Deflecting Panels in Daylighting Applications. *Solar Energy Materials and Solar Cells*, 29, 1-26.
- Edmonds, I.R., 1993b. *Transparent Light Deflecting Panel for Daylighting Rooms* (Patent). No. 2240576, United Kingdom.

- Edmonds, I.R., 1994. Application of Laser Cut Panels, Collimating Shades and Mirror Light Pipes to Improve Daylighting in Buildings. *In*: *Workshop Lichtlenkende Bauteile*. 2-4 Nov.
- Edmonds, I.R., P.A. Jardine and G. Rutledge, 1996. Daylighting with Angular-Selective Skylights: Predicted Performance. *Lighting Res. Technol.*, 28 (3), 122-130.
- Edmonds, I.R., G.I. Moore, G.B. Smith and P.D. Swift, 1995. Daylighting Enhancement with Light Pipes Coupled to Laser-Cut Light-Deflecting Panels. *Lighting Res. Technol.*, 27 (1), 27-35.
- Edmonds, I.R., J. Reppel and P. Jardine, 1997. Extractors and Emitters for Light Distribution from Hollow Light Guides. *Lighting Res. Technol.*, 29 (1), 23-32.
- Edmonds, I.R., M.J. Travers and J. Reppel, 1997. High Latitude Application of Laser Cut Panels for Enhanced Daylighting of Commercial and Domestic Buildings Via Light Guides. *In*: Konttinen, P. and Lund, P.D. (eds) *North Sun '97 - 7th International Conference on Solar Energy at High Latitudes*. Helsinki University of Technology Advanced Energy Systems and Technologies. Espoo-Otaniemi, Finland, June 9-11, pp. 777-783.
- Elmer, W.B., 1980. *The Optical Design of Reflectors.* New York: John Wiley & Sons Inc.
- Erhlich, C., 2001. *RADIANCE WWW Server* (World Wide Web site). Lawrence Berkeley Laboratory, url: http://radsite.lbl.gov/radiance/framew.html, accessed: 19 Aug.
- Fontoynont, M., P. Laforgue, R. Mitanchey, M.E. Aizlewood, J. Butt, W. Carroll, R. Hitchcock, H. Erhorn, J. De Boer, L. Michel, B. Paule, J.-L. Scartezzini, M. Bodart and G.G. Roy, 1999. *Validation of Daylighting Simulation Programs*. November. Vaulx-en-Velin, France: International Energy Agency Solar Heating and Cooling Task 21 / Energy Conservation in Buildings and Community Systems Programme Annex 29.
- Gordon, J.M. and P. Kashin, 1994. Achieving Uniform Efficient Illumination with Multiple Asymmetric Compound Parabolic Luminaires. *Optical Engineering*, 33 (1), 267-272.
- Gordon, J.M., P. Kashin and A. Rabl, 1992. Nonimaging Reflectors for Efficient Uniform Illumination. *Appl. Opt.*, 31 (28), 6027-6035.

- Gordon, J.M. and A. Rabl, 1992. Nonimaging Compound Parabolic Concentrator-Type Reflectors with Variable Extreme Direction. *Appl. Opt.*, 31 (34), 7332-7338.
- Greenman, P., 1981. Geometrical Vector Flux Sinks and Ideal Flux Concentrators. *J. Opt. Soc. Am.*, 71 (6), 777-779.
- He, X.D., K.E. Torrance, F.X. Sillion and D.P. Greenberg, 1991. A Comprehensive Physical Model for Light Reflection. *Computer Graphics*, 25 (4), 175-186.
- Hopkinson, R.G., 1970a. Glare from Windows. *Construction Research and Development Journal*, 2 (3), 98-105.
- Hopkinson, R.G., 1970b. Glare from Windows 2 - What People Say. *Construction Research and Development Journal*, 2 (4), 169-175.
- Hopkinson, R.G., 1972. Glare from Daylighting in Buildings. *Appl. Ergonomics*, 206-215.
- Hughes, P.C., 1983. An Examination of the Beneficial Action of Natural Light on the Psychobiological System of Man. *In*: *CIE 20th Session*. International Commission on Illumination CIE. pp. D603.
- Igawa, N. and H. Nakamura, 2001. All Sky Model as a Standard Sky for the Simulation of Daylit Environment. *Building and Environment*, 36, 763-770.
- Inglas, 2002. *Inglas* (World Wide Web site). Inglas GmbH, url: www.inglas.de, accessed: June 11.
- Institution of Engineers Australia, 2001. *Sustainable Energy Innovation in the Commercial Buildings Sector.* Canberra: Institution of Engineers Australia.
- Jarvis, D. and M. Donn, 1997. Comparison of Computer and Model Simulations of a Daylit Interior with Reality. *In*: *Building Performance and Simulation Assoc. Conf.* Building Performance and Simulation Assoc. Prague, Czech Republic, 8-10 Sept.
- Khodulev, A.B. and E.A. Kopylov, 1996. *Physically Accurate Lighting Simulation in Computer Graphics Software* (World Wide Web site). url: rmp.kiam.ru/articles/pals, accessed: 22 Jan.
- Kittler, R., R. Perez and S. Darula, 1997. A New Generation of Sky Standards. *In*: *Conf. Lux Europa*. pp. 359-373.

- Koster, H., 1994. *Light Guidance System for the Illumination of an Interior Area* (Patent). No. 5293305, United States.
- Kristensen, P.E., 1994. Daylighting Technologies in Non-Domestic Buildings. *Int. J. Solar Energy*, 15, 55-67.
- Kumpers, H.R., 1989. *Products for Passive Solar Heat Gain Manufactured by Okalux Kapillarglas GMBH of West Germany*. Okalux Kappillarglas GMBH of West Germany.
- Laar, M., 2001. Light and Shadow - an Analysis of Daylighting and Shadowing Systems for the Tropics. *In*: Pereira (ed.) *PLEA.* Florianopolis, Brazil, Nov 7-9, pp. 209-213.
- Laar, M. and F.W. Grimme, 2002. German Developments in Daylight Guidance Systems: An Overview. *Building Research and Information*, 30 (4), 282-301.
- Leslie, R.P., 1994. What Makes Daylighting Successful? *CADDET Energy Efficiency Newsletter*, Vol. 4.
- Littlefair, P.J., 1992. Daylight Coefficients for Practical Computation of Internal Illuminances. *Lighting Res. Technol.*, 24 (3), 127-135.
- Littlefair, P.J., 1994. The Luminance Distributions of Clear and Quasi-Clear Skies. *In*: *CIBSE National Lighting Conference*. Chartered Institute of Building Services Engineers. pp. 267-279.
- Littlefair, P.J., M.E. Aizlewood and A.B. Birtles, 1994. The Performance of Innovative Daylighting Systems. *Renewable Energy*, 5 (II), 920-934.
- Lorenz, W., 1998. Design Guidelines for a Glazing with a Seasonally Dependent Solar Transmittance. *Solar Energy*, 63 (2), 79-96.
- Lorenz, W., 2001. A Glazing Unit for Solar Control, Daylighting and Energy Conservation. *Solar Energy*, 70 (2), 109-130.
- Maamari, F., M. Fontoynont and R. Mitanchey, 2002. Analytical References to Test Lighting Software Programs - Application to Lightscape 3.2. *submitted to Lighting Research and Technology*.
- Mardaljevic, J., 1995. Validation of a Lighting Simulation Program under Real Sky Conditions. *Lighting Res. Technol.*, 27 (4), 181-188.
- Mardaljevic, J., 2000a. *Daylight Simulation: Validation, Sky Models and Daylight Coefficients.* Leicester, UK: De Montfort University.

- Mardaljevic, J., 2000b. Simulation of Annual Daylighting Profiles for Internal Illuminance. *Lighting Res. Technol.*, 32 (3), 111-118.
- Mardaljevic, J., 2001. The BRE-IDMP Dataset: A New Benchmark for the Validation of Illuminance Prediction Techniques. *Lighting Res. Technol.*, 33 (2), 117-136.
- Milner, P. and M. Wiggington, 2001. *The Serraglaze Daylighting System - the Technology Behind It* (World Wide Web site). Redbus Serraglaze Limited, url: www.serraglaze.redbus.co.uk, accessed: 5 June.
- Mischler, G., 2001. *Lighting Simulation Knowledgebase - Daylight Redirection Systems* (World Wide Web site). Schorsch, url: http://www.schorsch.com/kbase/prod/redir/, accessed: 16 Aug.
- Mitanchey, R., G. Periole and M. Fontoynont, 1995. Goniophotometric Measurements: Numerical Simulation for Research and Development Applications. *Lighting Res. Technol.*, 27 (4), 189-196.
- Moeck, M., 1998. On Daylight Quality and Quantity and Its Application to Advanced Daylight Systems. *J. IES* (Winter), 3-21.
- Moeck, M. and S.E. Selkowitz, 1996. A Computer-Based Daylight Systems Design Tool. *Automation in Construction*, 5, 193-209.
- Muller, H.F.O., 1994. Application of Holographic Optical Elements in Buildings for Various Purposes Like Daylighting, Solar Shading and Photovoltaic Power Generation. *Renewable Energy*, 5 (II), 935-941.
- Murdoch, J. and J.A. Barnes, 1986. *Statistical Tables for Science, Engineering, Management and Business Students.* London: Macmillan Education Ltd.
- Nelson, K.L., 1997. Daylighting Benefits Extend Beyond Just Energy Savings. *Energy User News* , 22 (2), 30.
- Ng, E.Y.-Y., L.K. Poh, W. Wei and T. Nagakura, 2001. Advanced Lighting Simulation in Architectural Design in the Tropics. *Automation in Construction*, 10, 365-379.
- Nicklas, M. and G. Bailey, 1996. Daylit Students Shine Brighter. *SunWorld*, 20 (3), 13-15.
- Penney, T.R. and J. Althof, 1990. American Trends in Commercial Buildings. *In*: *Int. Conf. on Water and Energy Conservation in Commercial Buildings.* Brisbane, Oct 17-20, pp. 116-125.

- Perez, R., R. Seals and J. Michalsky, 1993. All-Weather Model for Sky Luminance Distribution - Preliminary Configuration and Validation. *Solar Energy*, 50 (3), 235-245.
- Productivity Commission, 1999. *The Environmental Performance of Commercial Buildings*. November. Canberra: Productivity Commission.
- Rabl, A., 1976. Comparison of Solar Concentrators. *Solar Energy*, 18 (2), 93-111.
- Rabl, A., 1994. Edge-Ray Method for Analysis of Radiation Transfer among Specular Reflectors. *Appl. Opt.*, 33 (7), 1248-1259.
- Rabl, A. and J.M. Gordon, 1994. Reflector Design for Illumination with Extended Sources: The Basic Solutions. *Appl. Opt.*, 33 (25), 6012-6021.
- Raiford, R. and J.J. Smith, 2000. Everything You Ever Wanted to Know About Lighting ... But Were Too Afraid to Ask. *Buildings*, 94 (4), 79-93.
- Randazzo, M., 1994. Envelope Is Critical Element in Efficient Design. *Energy User News* , 19 (11), 31.
- Rea, M., 1994. Daylighting. *In*: *IES Handbook*. Illuminating Engineers Society of North America.
- Reinhart, C.F., 2001. *Daylight Availability and Manual Lighting Control in Office Buildings - Simulation Studies and Analysis of Measurement.* Freiburg, Germany: Fraunhofer-Institut fur Solare Energiesysteme.
- Reinhart, C.F. and S. Herkel, 2000. The Simulation of Annual Daylight Illuminance Distributions - a State-of-the-Art Comparison of Six RADIANCE-Based Methods. *Energy and Buildings*, 32, 167-187.
- Reppel, J. and I.R. Edmonds, 1998. Angle-Selective Glazing for Radiant Heat Control in Buildings: Theory. *Solar Energy*, 62 (3), 245-253.
- Riegel, R.J., L.S. Windheim, K.V. Davy and M.D. Shanus, 1983. Case Study: Lockheed Building 157 - an Innovative Deep Daylighting Design for Reducing Energy Consumption. *In: Advances in Energy Cost Savings for Industry and Buildings*. Atlanta, Georgia: Fairmont Press Inc.
- Ries, H.R. and R. Winston, 1994. Tailored Edge-Ray Reflectors for Illumination. *J. Opt. Soc. Am.*, 11 (4), 1260-1264.
- Rodgers, N.C., J.A. Ballinger and C. Dunkerley, 1979. An Analysis of Innovative Methods in Natural Lighting. *Arch. Sci. Rev.*, 22 (2), 44-48.

- Ronnelid, M., M. Adsten, T. Lindstrom, P. Nostell and E. Wackelgard, 2001. Optical Scattering from Rough-Rolled Aluminum Surfaces. *Appl. Opt.*, 40 (13), 2148-2158.
- Rosenfeld, A.H. and S.E. Selkowitz, 1977. Beam Daylighting: An Alternative Illumination Technique. *Energy and Building*, 1, 43-50.
- Roy, G.G., 2000. *A Comparative Study of Lighting Simulation Packages Suitable for Use in Architectural Design*. Perth: School of Engineering, Murdoch University.
- Roy, G.G., 2001. *SDF Client* (World Wide Web site). Murdoch University, url: http://eng-sun3.murdoch.edu.au/~geoff/webpages/index.html, accessed: 17 Aug.
- Ruck, N., O. Aschehoug, S. Aydinli, J. Christoffersen, G. Courret, I.R. Edmonds, R. Jakobiak, M. Kischoweit-Lopin, M. Klinger, E. Lee, L. Michel, J.-L. Scartezzini and S. Selkowitz, 2000a. Daylighting Systems. *In*: Aschehoug, O., Christoffersen, J., Jakobiak, R., Johnsen, K., Lee, E., Ruck, N. and Selkowitz, S., *Daylight in Buildings*. Berkeley, California: Lawrence Berkeley National Laboratory, pp. 4.1-4.104.
- Ruck, N., O. Aschehoug, S. Aydinli, J. Christoffersen, G. Courret, I.R. Edmonds, R. Jakobiak, M. Kischoweit-Lopin, M. Klinger, E. Lee, L. Michel, J.-L. Scartezzini and S. Selkowitz, 2000b. Design Tools. *In*: Aschehoug, O., Christoffersen, J., Jakobiak, R., Johnsen, K., Lee, E., Ruck, N. and Selkowitz, S., *Daylight in Buildings*. Berkeley, California: Lawrence Berkeley National Laboratory, pp. 6.1-6.19.
- Ruck, N., O. Aschehoug, S. Aydinli, J. Christoffersen, G. Courret, I.R. Edmonds, R. Jakobiak, M. Kischoweit-Lopin, M. Klinger, E. Lee, L. Michel, J.-L. Scartezzini and S. Selkowitz, 2000c. Monitoring Procedures. *In*: Aschehoug, O., Christoffersen, J., Jakobiak, R., Johnsen, K., Lee, E., Ruck, N. and Selkowitz, S., *Daylight in Buildings*. Berkeley, California: Lawrence Berkeley National Laboratory, pp. 8.44-8.48.
- Scartezzini, J.-L. and G. Courret, 2002. Anidolic Daylighting Systems. *Solar Energy*, 73 (2), 123-135.
- Schuman, J., F. Rubinstein, K. Papamichael, L. Beltran, E.S. Lee and S. Selkowitz, 1992. *Technology Reviews: Daylighting Optical Systems*. Report: LBL-33203. Berkeley, California: Lawrence Berkeley National Laboratory.

- Selvanathan, A., S. Selvanathan, G. Keller, B. Warrack and H. Bartel, 1994. *Australian Business Statistics.* Melbourne: Thomas Nelson Australia.
- Sick, F., 1995. A Simulation Approach to Determine a Visual Comfort Index Including Daylight for Adequate Building Performance Evaluation. *In*: *Building Simulation '95*. pp. 295-300.
- Sit, A. and S. Aydinli, 1999. *Test Room Studies: Laser Cut Panels*. September. International Energy Agency Solar Heating and Cooling Task 21 Subtask A.
- Smith, G.B., D.C. Green, G. McCredie, M. Hossain, P.D. Swift and M.B. Luther, 2001. Optical Characterisation of Materials and Systems for Daylighting. *Renewable Energy*, 22, 85-90.
- Steemers, K., 1994. Daylighting Design: Enhancing Energy Efficiency and Visual Quality. *Renewable Energy*, 5 (II), 950-958.
- Ubbelohde, M.S. and C. Humann, 1998. A Comparative Evaluation of Daylighting Software: Superlite, Lumen Micro, Lightscape and Radiance. *In*: *Daylighting '98.* Ottawa, Canada, pp. 97-104.
- van Dijk, D., 2000. *Daylighting Products with Redirecting Visual Properties*. 31 Dec. Delft, the Netherlands: TNO Building and Construction Research.
- van Dijk, H.A.L., 2001. The European Project REVIS, Daylighting Products with Redirecting Visual Properties. *In*: *NorthSun 2001*.
- Ward, G., 1994. A Contrast-Based Scalefactor for Luminance Display. *In*: *Graphics Gems*. Boston: Academic Press, pp. 415-421.
- Ward, G., 1996. *Radiance Reference Manual.* Stuttgart: International Energy Agency Solar Heating and Cooling Task 12.
- Ward, G.J., 1992. Measuring and Modeling Anisotropic Reflection. *Computer Graphics*, 26 (2), 265-272.
- Ward, G.J., 1994. The RADIANCE Lighting Simulation and Rendering System. *In*: Cunnigham, S. (ed.) *SIGGRAPH 94 - Computer Graphics Annual Conference Series*. Association for Computing Machinery's Special Interest Group on Computer Graphics. Orlando, Florida, July 24-29, pp. 459-472.
- Ward, G.J., 1997. *Release Notes*. Berkeley, California: Lawrence Berkeley National Laboratory.

- Ward, G.J., 1998. Tools for Lighting Design and Analysis. *In*: *SIGGRAPH 98*. pp. 3.1-3.17.
- Ward Larson, G. and R. Shakespeare, 1998. *Rendering with Radiance: The Art and Science of Lighting Visualization.* San Francisco: Morgan Kaufman Publishers.
- Welford, W.T. and R. Winston, 1978. *The Optics of Nonimaging Concentrators.* London: Academic Press Inc. Ltd.
- Wienold, J., K. Beckinger, P. Apian-Bennewitz, C. Reetz and C. Reinhart, 1998. Stationary Virtual Reality (SVR) - a New Method for Predicting User Acceptance of Daylighting Systems. *In*: *First CIE Symposium on Lighting Quality*. pp. 178-182.
- Winston, R., 1991. Nonimaging Optics. *Sci. Am.*, 264 (March), 52-57.
- Winston, R. and H. Ries, 1993. Nonimaging Reflectors as Functionals of the Desired Irradiance. *J. Opt. Soc. Am. A.*, 10 (9), 1902-1908.
- Wotton, E. and B. Barkow, 1983. An Investigation of the Effects of Windows and Lighting in Offices. *In*: *Int. Daylighting Conf.* Phoenix.
- Wren, C., 2000. Solar Integration and Energy Conscious Design of Commercial Buildings. *In*: *Shaping the Sustainable Millenium Conf.* Queensland University of Technology. Brisbane, 5-7 July.
- Wren, C. and F. Barram, 2000. Solar Integration on Commercial Buildings. *In*: Yarlagadda, P., Bell, J., Stoynov, L.A. and Mills, D. (eds) *Solar 2000 - Renewable Energy Transforming Business*. Australia and New Zealand Solar Energy Society. Brisbane, 29 Nov - 1 Dec, pp. 605-612.
- York, B., J. de Vaal, C. DesBrisay, D. Eijadi, G. Harlow, B. Lee, S. Selkowitz and L. Whitehead, 1990. Development and Demonstration of a Self-Aligning, Multi-Storey Core Daylighting System. *In*: *Int. Daylighting Conf.* Moscow.
- Zacharopolous, A., P.C. Eames, D. McLarnon and B. Norton, 2000. Linear Dielectric Non-Imaging Concentrating Covers for PV Integrated Building Facades. *Solar Energy*, 68 (5), 439-451.